MOSCOW CENTER
FOR DIAGNOSTICS & TELEMEDICINE

ISSN 2712-8490 (Print)
ISSN 2712-8962 (Online)

DIGITAL DIAGNOSTICS

A peer-reviewed scientific medical journal

4 Volume 2 Issue

2023

ECO • VECTOR
https://journals.eco-vector.com/DD

УЧРЕДИТЕЛИ
- ГБУЗ «Научно-практический клинический центр диагностики и телемедицинских технологий ДЗМ»
- ООО «Эко-Вектор»

Свидетельство о регистрации СМИ ПИ
№ ФС 77 - 74099 от 19.10.2018

ИЗДАТЕЛЬ
ООО «Эко-Вектор»
Адрес: 191186, Санкт-Петербург, Аптекарский переулок, д. 3, литера А, помещение 1Н
E-mail: info@eco-vector.com
WEB: https://eco-vector.com

РЕКЛАМА
Отдел рекламы
Тел.: +7 (968) 545 78 20
E-mail: adv2@eco-vector.com

РЕДАКЦИЯ
Зав. редакцией
Елена Андреевна Филиппова
E-mail: ddjournal@eco-vector.com
Тел: +7 (965) 012 70 72
Адрес: 127051, Москва, ул. Петровка, д. 24, стр. 1

ПОДПИСКА
Подписка на печатную версию через интернет:
www.journals.eco-vector.com/
www.akc.ru
www.pressa-rf.ru

OPEN ACCESS
В электронном виде журнал распространяется бесплатно —
в режиме немедленного открытого доступа

ИНДЕКСАЦИЯ
- SCOPUS
- РИНЦ
- Google Scholar
- Ulrich's International Periodicals Directory
- WorldCat

Оригинал-макет
подготовлен в издательстве «Эко-Вектор».
подготовлен в издательстве «Эко-Вектор».
Литературный редактор: *М.Н. Шошина*
Корректор: *М.Н. Шошина*
Вёрстка: *Ф.А. Игнащенко*
Обложка: *Е.Д. Бугаенко*

16+

ISSN 2712-8490 (Print)
ISSN 2712-8962 (Online)

Digital Diagnostics

Том 4 | Выпуск 2 | 2023

ЕЖЕКВАРТАЛЬНЫЙ РЕЦЕНЗИРУЕМЫЙ НАУЧНЫЙ МЕДИЦИНСКИЙ ЖУРНАЛ

ЭКО • ВЕКТОР

FOUNDERS
- Moscow Center for Diagnostics and Telemedicine
- Eco-Vector

PUBLISHER
Eco-Vector
Address: 3 liter A, 1H, Aptekarsky pereulok, 191186, Saint Petersburg, Russian Federation
E-mail: info@eco-vector.com
WEB: https://eco-vector.com

ADVERTISE
Adv. department
Phone: +7 (968) 545 78 20
E-mail: adv2@eco-vector.com

EDITORIAL OFFICE
Executive editor
Elena A. Philippova
E-mail: ddjournal@eco-vector.com
Phone: +7 (965) 012 70 72

SUBSCRIPTION
For print version:
www.journals.eco-vector.com/

PUBLICATION ETHICS
Journal's ethic policies are based on:
- ICMJE
- COPE
- ORE
- CSE
- EASE

OPEN ACCESS
Immediate Open Access is mandatory for all published articles

INDEXATION
- SCOPUS
- Russian Science Citation Index
- Google Scholar
- Ulrich's International Periodicals Directory
- WorldCat

TYPESET
compleate in Eco-Vector
Copyeditor: *M.N. Shoshina*
Proofreader: *M.N. Shoshina*
Layout editor: *Ph. Ignashchenko*
Cover: *E. Bugaenko*

16+

ISSN 2712-8490 (Print)
ISSN 2712-8962 (Online)

Digital Diagnostics

Volume 4 | Issue 2 | 2023

QUARTERLY PEER-REVIEW MEDICAL JOURNAL

СОДЕРЖАНИЕ

CONTENTS

DOI: https://doi.org/10.17816/DD321423

Двойной просмотр результатов маммографии с применением технологий искусственного интеллекта: новая модель организации массовых профилактических исследований

Ю.А. Васильев[1], И.А. Тыров[2], А.В. Владзимирский[1], К.М. Арзамасов[1], И.М. Шулькин[1], Д.Д. Кожихина[1], Л.Д. Пестренин[1]

[1] Научно-практический клинический центр диагностики и телемедицинских технологий, Москва, Российская Федерация
[2] Департамент здравоохранения города Москвы, Москва, Российская Федерация

АННОТАЦИЯ

Обоснование. Доступность наборов медицинских данных и технологий разработки программного обеспечения на основе искусственного интеллекта в последние годы привела к увеличению количества решений для медицинской диагностики и маммографии в частности. Это программное обеспечение, зарегистрированное как медицинское изделие, может быть использовано для описания цифровых маммографий, что позволит в значительной мере сэкономить временные, материальные и кадровые ресурсы в здравоохранении при гарантированном сохранении качества профилактических исследований молочных желёз.

Цель — обосновать возможность и эффективность применения программного обеспечения на основе технологий искусственного интеллекта для первой интерпретации цифровых маммограмм при сохранении практики второго описания рентгеновских изображений врачом-рентгенологом.

Материалы и методы. Набор данных из 100 цифровых маммографических исследований, из них 50 — «Отсутствие целевой патологии», 50 — «Присутствие целевой патологии» (с признаками злокачественных новообразований), был обработан программным обеспечением на основе технологий искусственного интеллекта, зарегистрированным в Российской Федерации как медицинское изделие. Выполнен ROC-анализ. Ограничения исследования: значения метрик диагностической точности получены для версий программного обеспечения на основе технологий искусственного интеллекта, актуальных на конец 2022 года.

Результаты. При настройке на 80,0% чувствительность специфичность искусственного интеллекта составила 90,0% (95% ДИ 81,7–98,3), точность — 85,0% (95% ДИ 78,0–92,0). При настройке на 100% специфичность искусственный интеллект показал чувствительность 56,0% (95% ДИ 42,2–69,8), точность — 78,0% (95% ДИ 69,9–86,1). При настройке на 100% чувствительность специфичность искусственного интеллекта составила 54,0% (95% ДИ 40,2–67,8), точность — 77,0% (95% ДИ 68,8–85,2). Предложены два подхода, предусматривающие автономную первую интерпретацию цифровой маммографии посредством искусственного интеллекта. Первый подход заключается в оценке рентгеновского изображения с помощью искусственного интеллекта с более высокой чувствительностью, чем у двойного описания маммографии врачами-рентгенологами, при сопоставимом уровне специфичности. Второй подход подразумевает, что программное обеспечение на основе технологий искусственного интеллекта будет определять категорию маммографии («Отсутствие целевой патологии» или «Присутствие целевой патологии») с указанием степени своей «уверенности» в полученном результате в зависимости от «коридора», в который попадает предсказанное значение.

Заключение. Оба предложенных сценария использования программного обеспечения на основе технологий искусственного интеллекта с целью автономного первого описания цифровых маммограмм способны обеспечить качество диагностики, не уступающее двойному описанию снимков врачами-рентгенологами и даже превышающее его. Экономическая выгода от практической реализации данного подхода в масштабах страны может составлять от 0,6 до 5,5 млрд рублей ежегодно.

Ключевые слова: профилактические исследования; маммография; искусственный интеллект; диагностическая точность.

Как цитировать

Васильев Ю.А., Тыров И.А., Владзимирский А.В., Арзамасов К.М., Шулькин И.М., Кожихина Д.Д., Пестренин Л.Д. Двойной просмотр результатов маммографии с применением технологий искусственного интеллекта: новая модель организации массовых профилактических исследований // *Digital Diagnostics.* 2023. Т. 4, № 2. С. 93–104. DOI: https://doi.org/10.17816/DD321423

Рукопись получена: 17.03.2023 **Рукопись одобрена:** 25.04.2023 **Опубликована:** 25.05.2023

DOI: https://doi.org/10.17816/DD321423

Double-reading mammograms using artificial intelligence technologies: A new model of mass preventive examination organization

Yuriy A. Vasilev[1], Ilya A. Tyrov[2], Anton V. Vladzymyrskyy[1], Kirill M. Arzamasov[1], Igor M. Shulkin[1], Daria D. Kozhikhina[1], Lev D. Pestrenin[1]

[1] Moscow Center for Diagnostics and Telemedicine, Moscow, Russian Federation
[2] Moscow Health Care Department, Moscow, Russian Federation

ABSTRACT

BACKGROUND: In recent years, the availability of medical datasets and technologies for software development based on artificial intelligence technology has resulted in a growth in the number of solutions for medical diagnostics, particularly mammography. Registered as a medical device, this program can interpret digital mammography, significantly saving time, material, and human resources in healthcare while ensuring the quality of mammary gland preventive studies.

AIM: This study aims to justify the possibility and effectiveness of artificial intelligence-based software for the first interpretation of digital mammograms while maintaining the practice of a radiologist's second description of X-ray images.

MATERIALS AND METHODS: A dataset of 100 digital mammography studies (50 — "absence of target pathology" and 50 — "presence of target pathology," with signs of malignant neoplasms) was processed by software based on artificial intelligence technology that was registered as a medical device in the Russian Federation. Receiver operating characteristic analysis was performed. Limitations of the study include the values of diagnostic accuracy metrics obtained for software based on artificial intelligence technology versions, relevant at the end of 2022.

RESULTS: When set to 80.0% sensitivity, artificial intelligence specificity was 90.0% (95% CI, 81.7–98.3), and accuracy was 85.0% (95% CI, 78.0–92.0). When set to 100% specificity, artificial intelligence demonstrated 56.0% sensitivity (95% CI, 42.2–69.8) and 78.0% accuracy (95% CI, 69.9–86.1). When the sensitivity was set to 100%, the artificial intelligence specificity was 54.0% (95% CI, 40.2–67.8), and the accuracy was 77.0% (95% CI, 68.8–85.2). Two approaches have been proposed, providing an autonomous first interpretation of digital mammography using artificial intelligence. The first approach is to evaluate the X-ray image using artificial intelligence with a higher sensitivity than that of the double-reading mammogram by radiologists, with a comparable level of specificity. The second approach implies that artificial intelligence-based software will determine the mammogram category ("absence of target pathology" or "presence of target pathology"), indicating the degree of "confidence" in the obtained result, depending on the corridor into which the predicted value falls.

CONCLUSIONS: Both proposed approaches for using artificial intelligence-based software for the autonomous first interpretation of digital mammograms can provide diagnostic quality comparable to, if not superior to, double-image reading by radiologists. The economic benefit from the practical implementation of this approach nationwide can range from 0.6 to 5.5 billion rubles annually.

Keywords: artificial intelligence; diagnostic accuracy; mammography; preventive medicine.

To cite this article
Vasilev YuA, Tyrov IA, Vladzymyrskyy AV, Arzamasov KM, Shulkin IM, Kozhikhina DD, Pestrenin LD. Double-reading mammograms using artificial intelligence technologies: A new model of mass preventive examination organization. *Digital Diagnostics.* 2023;4(2):93–104. DOI: https://doi.org/10.17816/DD321423

Received: 17.03.2023 **Accepted:** 25.04.2023 **Published:** 25.05.2023

DOI: https://doi.org/10.17816/DD321423

使用人工智能对乳腺X线摄影结果进行两次查看：一种组织大规模预防性研究的新模式

Yuriy A. Vasilev[1], Ilya A. Tyrov[2], Anton V. Vladzymyrskyy[1], Kirill M. Arzamasov[1], Igor M. Shulkin[1], Daria D. Kozhikhina[1], Lev D. Pestrenin[1]

[1] Moscow Center for Diagnostics and Telemedicine, Moscow, Russian Federation
[2] Moscow Health Care Department, Moscow, Russian Federation

简评

论证。近年来，医疗数据集和人工智能软件技术开发的可达性，使得医疗诊断，特别是乳腺X线摄影的解决方案激增。这种登记为医疗设备的软件可被用于描述数乳腺X线摄影，这允许提供医疗服务时在很大程度上节省时间、物质和人力的资源，同时确保乳房预防性检查的质量。

该研究的目的是证明使用基于人工智能技术的软件对数字乳房X光照片进行第一次解读的可用性和有效性，同时保持放射科医生对X射线图像进行第二次描述的做法。

材料和方法。我们用在俄罗斯联邦登记为医疗设备的基于人工智能技术的软件处理了100张数字乳房X光照片的数据集，其中50张为“无目标病变”，50张为“存在目标病变”（有恶性肿瘤症状）。进行了ROC分析。研究局限性：诊断准确性度量值是基于人工智能技术的软件版本获得的，是在2022年底有效的。

结果。当设置为80.0%的灵敏度时，人工智能显示出90.0%的特异度（95% CI 81.7-98.3）和85.0%的准确性（95% CI 78.0-92.0）。当设置为100%的特异度时，人工智能显示出56.0%的灵敏度（95% CI 42.2-69.8）和78.0%的准确性（95% CI 69.9-86.1）。当设置为100%灵敏度时，人工智能的特异度为54.0%（95% CI 40.2-67.8），准确性为77.0%（95% CI 68.8-85.2）。提出了两种方法，涉及通过人工智能对数字乳腺X线摄影进行的第一次自主解读。第一种方法是利用人工智能评估X射线图像，其灵敏度高于放射科医生进行的双重乳腺X线摄影描述，特异度水平相当。第二种方法是基于人工智能技术的软件将对乳腺X线摄影进行分类（“无目标病变”或“存在目标病变”），表明其对结果的“信心”程度，取决于预测值所处的“走廊”。

结论。使用基于人工智能技术的软件对数字乳房X光照片进行第一次自主描述的两种提出方案都能提供与放射科医生对图像进行的双重描述相同甚至更高的诊断质量。在全国范围内在实践中实现这种方法的经济效益可能是每年6亿至55亿卢布。

关键词：预防性研究；乳腺X线摄影；人工智能；诊断准确性。

To cite this article
Vasilev YuA, Tyrov IA, Vladzymyrskyy AV, Arzamasov KM, Shulkin IM, Kozhikhina DD, Pestrenin LD. 使用人工智能对乳腺X线摄影结果进行两次查看：一种组织大规模预防性研究的新模式. *Digital Diagnostics.* 2023;4(2):93–104. DOI: https://doi.org/10.17816/DD321423

收到：17.03.2023 **接受：**25.04.2023 **发布日期：**25.05.2023

BACKGROUND

Breast malignancies are a significant problem from medical, socioeconomic, and demographic points of view, heading the list of cancers and leading the mortality causes of the female population. A steady increase in prevalence from 45.24 to 53.43 per 100,000 population was observed from 2011 to 2019; later, it sharply decrease to 47.39 per 100,000 population in 2020, with a renewed rise in 2021 [1]. Such a pattern is accounted for by the suspension of mass screening during the COVID-19 pandemic. Conversely, it was a completely substantiated decision, and the situation demonstrates how vulnerable the healthcare system is. The emergency-related resource re-allocation took its toll on the socially significant diseases. However, even outside the pandemic, breast malignancies are still underdiagnosed, and the rate of newly diagnosed advanced diseases is high: as much as 27.0% of new cases are classified as stage III–IV cancer. A remarkable positive trend is noteworthy: the prevalence-to-incidence ratio over the reporting period is increasing steadily. In 2011, it was 9.5, while in 2021, it increased to 11.9. It is indicative of gradual improvements in the quality and efficacy of breast malignancy treatment [2].

Thus, the optimization of mass screening is warranted to expand coverage and population compliance; increase capacity, quality, and cost-efficiency; and enable sustainability and continuous accessibility. Given the evident progress in anti-cancer therapies, accomplishing these goals will take breast malignancy treatment to the next level.

Currently, the most common type of screening for breast malignancies is mammography. Following effective regulations, screening mammograms are subject to double reading, i.e., the images obtained with each patient should be viewed and interpreted by two independent radiologists. Such practice has been proved expedient by domestic and foreign authors. The cumulative rate of pathologic change detection is higher with double reading. Single reading lowers the sensitivity for all categories of breast imaging reporting and data system (BI-RADS) compared with double reading. Moreover, single reading is associated with various negative consequences for the examined patients [3, 4], although double reading also has its downsides, such as resource-intensiveness, quality issues, and funding difficulties.

Resource-intensiveness. In primary healthcare, two radiologists are required to interpret every screening image, with the vast majority of them being "target changes not found." There is a risk for these positions to be filled in fictitiously to cover staff shortage, which would affect women's health badly. Meanwhile, given the actual need for screening mammograms and the rate of the equipment fleet growth, the shortage of staff for these purposes is expected.

Quality issues. Interpreting mammograms requires specific skills in a narrow subarea of modern radiology. This worsens the staff shortage: formally employing more radiologists will not contribute to timely precise detection of breast malignancies.

Funding difficulties. Double payment only applies if there is a separate service of mammography interpretation, and one payment is allocated for mammography scanning and its interpretation, whereas the other covers interpretation only. If this is not the case, funding difficulties arise: the payment is allocated only for combined mammography scanning and mammogram interpretation. Therefore, underfunding is common when only a single payment available, not covering the second mammogram reading.

The potential problems outlined can be solved with the use of artificial intelligence (AI) in interpreting mammograms.

High-quality readings obtained with such technology have been reported in the literature. Indeed, certain AI-based solutions have diagnostic precision similar to an average radiologist. The cumulative sensitivity, specificity, and area under the receiver operating curve (ROC) were 75.4, 90.6, and 0.89% for AI and 73.0, 88.6, and 0.85% for a radiologist, respectively, and no significant differences were found [5]. A meta-analysis [6] showed that the cumulative sensitivity, specificity, and area under the ROC for AI-based mammography interpretation were 91.4%, 91.6%, and 94.5%, respectively. The similarity coefficients for the intersection-over-union accuracy for abnormal change localizations segmented by AI and a radiologist were 0.86 and 0.96, respectively [7]. In our opinion, AI-based solutions should be implemented not just as discrete systems backing up the decisions made by doctors but as independent computerized processes.

This study aimed to justify a model for mass mammography screening using AI technology.

MATERIALS AND METHODS

The study was part of the Experiment for Computer Vision Innovations Used in Medical Image Analysis and its further use in the healthcare system of Moscow (hereinafter, the Moscow experiment), which took place in 2020 and was funded by the Government of Moscow (mosmed.ai). This study was feasible because of the accuracy of AI-based software demonstrated with 61,497 mammograms over the first year of the Moscow experiment [8].

Study design

This study has a mixed design, i.e., using a retrospective diagnostic study for the quantitative component and an analytical study for the qualitative component.

AI technology

AI-based software should be registered as a medical device to be used in routine clinical practice. AI-based software products by OOO "Medical Screening Systems" (Reg. No. RZN 2021/14449) and OOO "Third Opinion Platform" (Reg. No. RZN 2022/16534) intended for computerized

mammogram interpretation are registered as medical devices in the Russian Federation.

Such a product by one of the above companies was used for the study. As part of the Moscow experiment, the AI-based software was integrated into the Unified Radiology Information Service (ERIS) of the Unified Medical Information and Analytical System (EMIAS) of Moscow. Digital mammography images in the DICOM format were the input for the AI-based software. After the analysis, a text interpretation (DICOM SR) was generated, along with abnormal areas mapping (DICOM SC) and an overall disease probability. AI-generated results appeared on ERIS EMIAS along with the raw data. The overall probability values of cancer were used in the study. The correctness of BI-RADS rating and the precision of abnormal finding localization were not evaluated in this study.

Dataset

This study included 100 digital mammograms obtained as part of breast cancer screening, of which 50 demonstrated abnormalities. The mean age of the examined patients was 63 ± 6 years.

The images were categorized into "target changes not found" or "target changed detected" based on the consensus of two assessors (radiologists with >5 years of experience in mammography). The primary inclusion criterion for "target changed detected" was histological verification. Different opinions of assessors were an exclusion criterion for "target changes not found." The exclusion criteria for both categories were age <18 years and low-quality images (PGMI score 1) identified by the assessor at the mapping stage for dataset preparation.

Mammography abnormalities consistent with BI-RADS categories 3–5 were classified as "target changed detected." Mammography results consistent with BI-RADS categories 1 or 2, i.e., without any suspicion of breast malignancy, were classified as "target changes not found."

The distribution based on the American College of Radiology types was as follows: A, n = 26; B, n = 16; C, n = 5; and D, n = 3 in "target changes not found," and A, n = 15; B, n = 24; C, n = 11; and D, n = 0 in "target changed detected."

Images included in the dataset were obtained with FUJIFILM Corporation (Japan) mammography machines. The following healthcare providers contributed to the dataset: City Polyclinic (CP) No. 22 Branch No. 1, Diagnostic Clinical Center No. 1, CP No. 8, CP No. 36, CP No. 22, CP No. 209, Diagnostic Center No. 2 Branch No. 4, Consultation and Diagnostic Polyclinical No. 121, Clinical and Diagnostic Center No. 4, and M.P. Konchalovsky City Clinical Hospital with the Moscow Healthcare Department, Outpatient Department No. 3.

Ethics review

The study was based on the results of the Moscow experiment and was approved by the Ethics Committee (Protocol abstract No. 2 NEK MRO RORR dated February 20, 2020; ClinicalTrials ID: NCT04489992).

Statistical analysis

Receiver operating curve (ROC) analysis available from a web tool was used for statistical data processing (https://roc-analysis.mosmed.ai/) [9, 10]. The true values were binary (0 for "target changes not found"; 1 for "target changes detected"). The result was the probability of cancer determined by AI-based software. Data obtained in the CSV format were uploaded to an electronic form, after which the web tool plotted a ROC. Cutoff values corresponding to the leftmost point with 100% sensitivity and the rightmost point with 100% specificity were determined in the interactive mode. Later, other diagnostic accuracy parameters for the established cutoff value were analyzed. A classic 2 × 2 contingency table was used for the analysis. Correct classification of a mammogram as "target changed detected" was considered true positive, and correct classification of a mammogram as "target changes not found" was considered true negative. Incorrect classification of a normal mammogram as "target changed detected" was considered false positive, and incorrect classification of an abnormal mammogram as "target changes not found" was considered false negative.

All statistical parameters presented in the results were calculated using 95% confidence interval (CI) by bootstrapping with 1,000 iterations.

RESULTS

The following model was suggested: the attending physician refers the patient to mammography screening in accordance with the current regulations and clinical guidelines. The X-ray technologist performs the examination. The resulting digital mammograms are sent to the archive of medical images as part of the medical information system of a medical organization and/or a healthcare information system of a constituent entity of the Russian Federation. The first reading is performed by the software (an approved AI-based medical device). Following the first reading, an automatic electronic medical record[1] is formed in the information system, containing (a) the series of images with graphic marks and/or a temperature map of abnormal areas, if any; (b) a structured report, brief user guide, conclusion, details, and cancer probability. The second reading is performed by a radiologist. Based on the second reading, an electronic interpretation protocol and conclusion are provided in the information system.

[1] Medical records generated automatically by the approved medical devices that do not require the electronic signature of a healthcare professional (in accordance with Order of the Ministry of Health of the Russian Federation No. 947n dated September 7, 2020, On approval of the procedure for electronic documents turnover in healthcare).

A study was performed to establish whether AI-based software can provide the required level of diagnostic accuracy. The ROC for the studied AI-based software is shown in Fig. 1. The distribution of mammograms by groups (true positive, true negative, false negative, and false positive) depending on the selected cutoff value is presented in Table 1.

When setting a cutoff value of 0.93 corresponding to 100.0% specificity, AI correctly identified mammography from the "target changes detected" group, i.e., no false positives were recorded. Of the 50 mammograms in the "target changes detected" group, AI correctly identified 28 (56.0%) images at the specified threshold setting. With these settings of the AI-based software, sensitivity, specificity, and diagnostic accuracy were 56.0% (95% CI 42.2–69.8), 100.0% (95% CI 100.0–100.0), and 78.0% (95% CI 69.9–86.1), respectively.

When setting a cutoff value of 0.25 corresponding to 100.0% sensitivity, no false negatives were observed, and 27 true negatives were identified (54.0% of all images in the "target changes not found" group). With these settings of the AI-based software, the sensitivity, specificity, and diagnostic accuracy were 100.0% (95% CI 100.0–100.0), 54.0% (95% CI 40.2–67.8), and 77.0% (95% CI 68.8–85.2), respectively.

When setting a cutoff value of 0.82 to maximize the Youden index, the sensitivity was 80.0%, 45 were true-negative results (90.0% of all images in the "Target changes not found" group), and 40 were true-positive results (80.0%

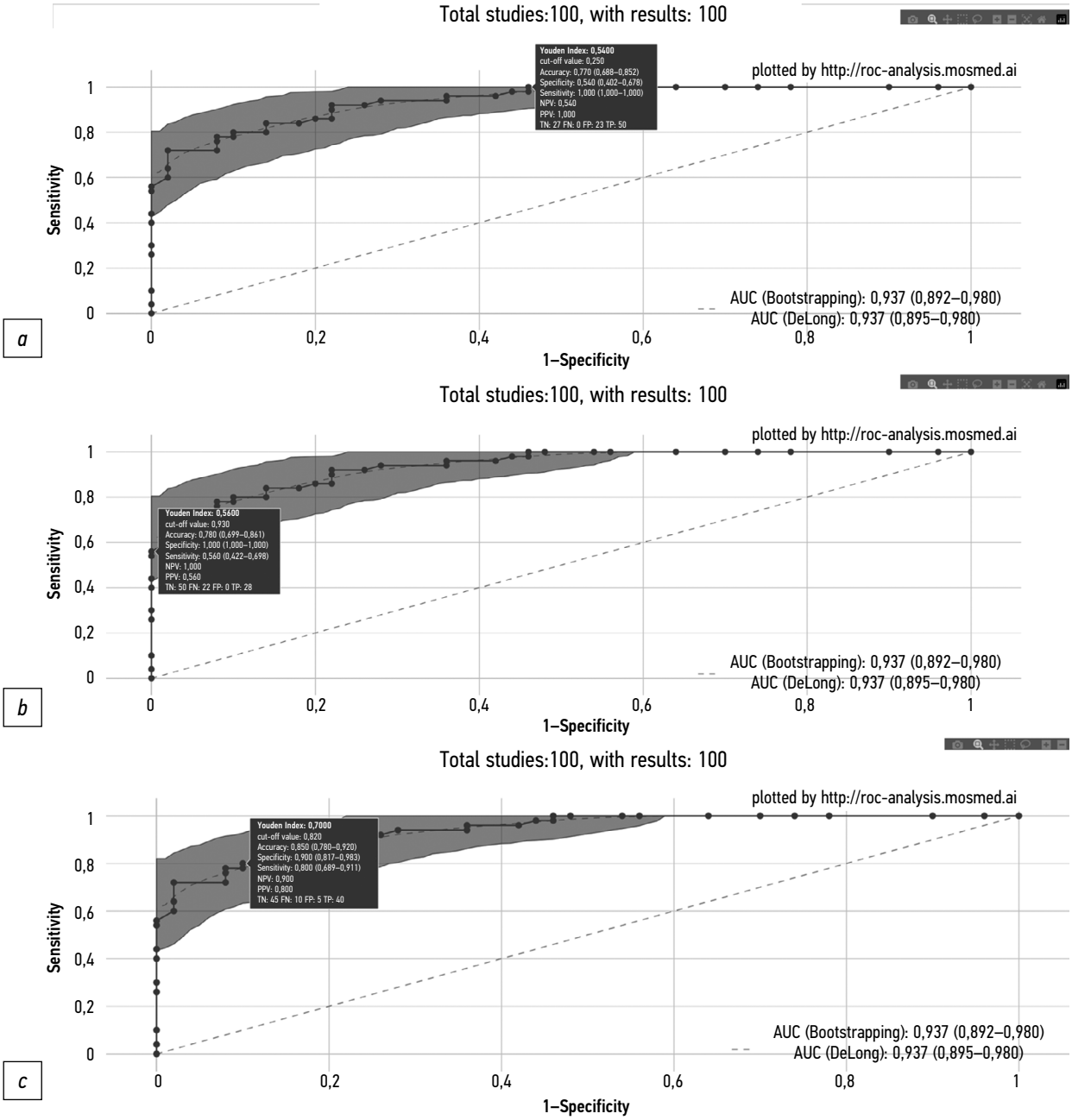

Fig. 1. ROC for AI-based software. The highlight shows the 95% confidence interval. Experimental values corresponding to 100.0% sensitivity (*a*), 100.0% specificity (*b*), and 80.0% sensitivity (*c*) are highlighted individually. For each experimental point, the rectangle shows the diagnostic accuracy metrics at the corresponding cutoff value.

Table 1. 2 × 2 contingency table for different threshold values

Group	No. of scans	Result	100% sensitivity	100% specificity	Balanced sensitivity and specificity
Target changes detected	50	True positive	50	28 56.0%**	40 80.0%**
		False positive	23	0	5
Target changes not found	50	True negative	27 54.0%*	50	45 90.0%*
		False negative	0	22	10

Note: * The percentage of true-negative results is calculated from the total "target changes not found" images. ** The percentage of true-positive results is calculated from the total "target changes detected" images.

of all images in the "target changes detected" group). With these settings of the AI-based software, the sensitivity, specificity, and diagnostic accuracy were 80.0% (95% CI 68.9–91.1), 90.0% (95% CI 81.7–98.3), and 85.0% (95% CI 78.0–92.0), respectively.

DISCUSSION

Summary of the primary outcome

Setting different cutoff values for AI-based software used for description and interpretation of mammography data allows achieving the sensitivity, specificity, and accuracy metrics that correspond to or exceed those for double reading of mammogram by radiologists.

Discussion of the primary outcome

In the Russian Federation, approximately 8.2 million mammographies[2] are performed annually as part of screening, and their double reading requires a significant amount of time, staff, and financial resources. The use of AI-based software for the first review of mammograms will reduce the above costs while maintaining or even improving diagnostic quality. Two approaches were proposed to setting up AI-based software for the first reading of mammograms.

The first approach involves the use of AI-based software with balanced values of sensitivity and specificity. In our case, the sensitivity was 80.0%, which exceeds the sensitivity of double reading of mammograms by radiologists determined in reviews (72.0%–73.0%) [5, 6]. In this study, the specificity of AI (90.0%) is not inferior to that of two radiologists (88.0%–98.0%) [5, 6]. AI-based software in combination with the assessment by one radiologist will have a higher overall accuracy of mammography interpretation than interpretation by only one radiologist, which is confirmed by a number of scientific publications [11–13]. An electronic medical record containing a conclusion on the category of the image ("target changes not found" or "Target changes detected") will be generated by AI-based software with this approach.

The second approach implies that the AI-based software will determine the category of the image ("target changes not found" or "target changes detected"), indicating the degree of its "confidence" in the result. The general concept of the method is shown in Fig. 2.

As mentioned in the Results, cutoff values were determined for the predicted values at 100% sensitivity and 100% specificity (0.25 and 0.93, respectively) when plotting the ROC for the AI-based software. Based on these data, it is proposed to contribute to the predicted value to one of three "corridors," which correspond to different classification results and different degrees of AI "confidence":

1) Green corridor: the predicted values are within the range of 0–0.25 and correspond to the category "target changes not found" with 100% confidence,
2) Red corridor: the predicted values are within the range of 0.93–1.0 and correspond to the category "target changes detected" with 100% confidence,
3) Yellow corridor: the predicted values are within the range of 0.25–0.93 inclusive and correspond to the "target changes not found" or "target changes detected" category; however, the probability of correct classification is <100%.

The predicted value and color of the corridor in which it falls are proposed to be added to the description of mammography by the AI-based software. With this information, the radiologist making the second reading after the AI step will know how much they can rely on the results. This will help the doctor stay alert when examining a mammogram from the yellow corridor. In the long term, this approach can increase the confidence of radiologists in the results of AI-based software because, despite the current high level of accuracy, AI is not yet able to correctly classify 100% of the analyzed images with a high degree of confidence.

The advantage of the second approach is not only the ability of AI to categorize some mammograms as "target changes not found" or "target changes detected" with a 100% degree of confidence (green and red corridors for the

[2] I.E. Tyurin. 2020 Report by the Chief Independent Expert of the Ministry of Health of Russia on radiation and instrumental diagnostics [electronic resource]. Accessed at: https://static-0.minzdrav.gov.ru/system/attachments/attaches/000/056/620/original/Отчет_за_2020_год_Тюрин.pdf?1624967722.

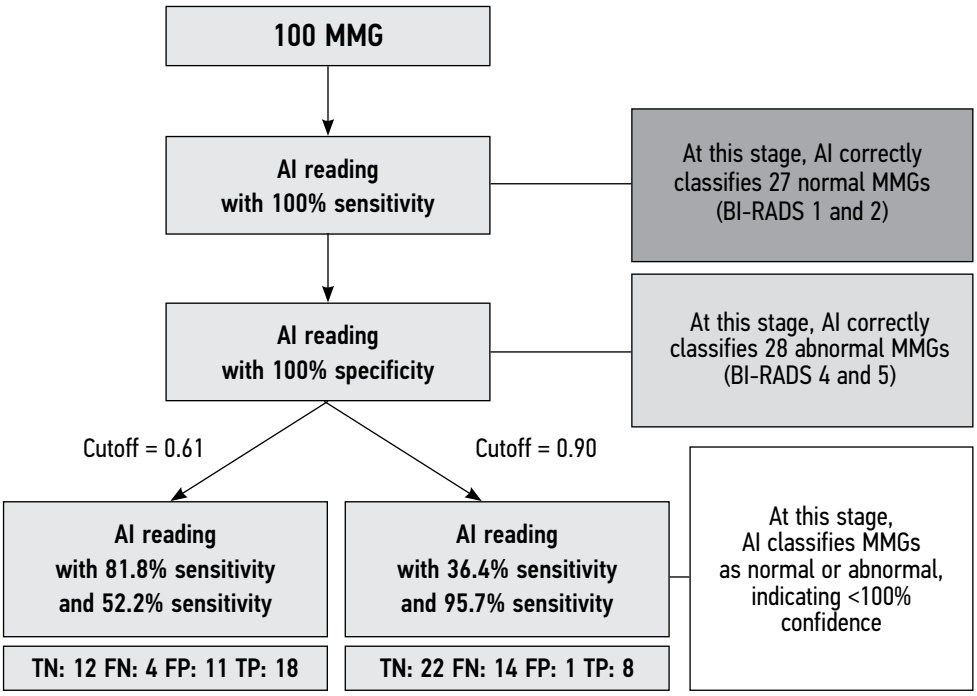

Resulting sensitivity	92.0%	72.0%
Resulting specificity	78.0%	98.0%

Fig. 2. Concept of an approach to the first mammogram reading using artificial intelligence involving binary image classification with an indication of the degree of confidence of the AI-based software in the results obtained.

Note: AI, artificial intelligence; FN, false negative; FP, false positive; MMG, mammogram; TN, true negative; TP, true positive.

predicted values) but also the ability to change the cutoff value to balance the sensitivity and specificity of AI-based software for the analysis of mammograms that fall into the yellow corridor. Depending on the clinical task, a higher sensitivity can be set, which will provide better detection of pathology with the lowest number of false-negative results or higher specificity to reduce the number of false-positive results (Table 2) [5, 6].

The results of this study demonstrate the possibility of using AI-based software for the first reading of mammograms; however, in the future, the software must be optimized to more effectively distinguish between "target changes not found" and "target changes detected." Only high-quality mammograms were initially selected for this study. However, modern AI-based software has the function of offline mammography quality control. When introduced into routine practice, AI-based software can perform technical assessment of image quality and clinical assessment [8].

Economic justification of AI-based double reading of mammograms

As part of the study, payment rates for medical care provided under the territorial program of compulsory medical insurance adopted in the constituent entities of the Russian Federation for 2023 were analyzed.

In 19 constituent entities (22.4% of all constituent entities of the Russian Federation), a separate payment for medical service A06.20.004 mammography (provided as

Table 2. Sensitivity and specificity with different approaches to mammogram reading

Screening mammography results	Sensitivity, %	Specificity, %
Double reading by two radiologists *	72.0–73.0	88.0–98.0
First approach to using AI for the first mammogram reading (binary classification)	80.0	90.0
Second approach to using AI for the first mammogram reading (binary classification with a degree of confidence) with a cutoff value of 0.61	92.0	78.0
Second approach to using AI for the first mammogram reading (binary classification with a degree of confidence) with a cutoff value of 0.90	72.0	98.0

Note: * Based on literature data [5, 6].

part of screening) is available. In 4 out of 19 constituent entities, a separate payment for medical service A06.30.002 description and interpretation of radiographic images (second reading of mammograms) is also available. In all other constituent entities of the Russian Federation, the payment for a comprehensive service (without specifying the mammography-related services included in it) is charged at the first stage of screening of the adult population.

The cost of mammogram description varies from 114.97 to 1034.93 rubles. As of March 1, 2023, the description and interpretation of mammography data using AI is available only as part of the Moscow experiment [8]. According to the rate agrees for medical care provided under the territorial program of compulsory medical insurance in Moscow, this medical service costs 239.00 rubles[3].

In this study, two approaches to determining the required amount of funding for screening mammograms in the Russian Federation were analyzed. The first approach was to perform calculations based on the cost of medical services in Moscow for 2023. A description of mammography by a radiologist costs 178.00 rubles. Therefore, a double reading of each mammogram by radiologists will cost 356.00 rubles. In turn, mammography description by AI and a radiologist, as mentioned above, costs 239.00 rubles. Thus, with an average number of annual mammograms of 8.2 million in Russia, double reading by two radiologists will cost 2.9 billion rubles, and double reading by AI and a radiologist will cost 1.9 billion rubles. Potential savings through the use of AI-based software may account to 1.0 billion rubles annually. The second approach was to perform calculations based on the cost of medical services in the constituent entities of the Russian Federation for 2023. The percentage of money saved was also considered, thanks to the interpretation of mammography by AI and a radiologist compared with double reading by two radiologists in Moscow, which amounted to the following:

$$\frac{178{,}00 \times 2 - 239{,}00}{178{,}00 \times 2} \times 100\% = 32{,}8\%.$$

Mammogram reading by a radiologist in the constituent entities of the Russian Federation costs 114.97–1034.93 rubles, which means that double reading by radiologists costs 229.94–2069.86 rubles. Assuming that the interpretation of mammography by AI and a radiologist in the constituent entities of the Russian Federation is cheaper than double reading by radiologists by 32.8% (as is the case in Moscow), the resulting cost of double mammogram reading by AI and a radiologist will range from 154.51 to 1390.94 rubles. Thus, with an average number of annual mammograms of 8.2 million in Russia, double reading by two radiologists will cost 1.8–16.9 billion rubles, whereas double reading by AI and a radiologist will cost 1.2–11.4 billion rubles. Potential savings due to the use of AI-based software at the national level may amount to 0.6–5.5 billion rubles annually.

Study limitations

The determined values of diagnostic accuracy metrics are valid for AI-based software versions as of the end of 2022. For patients in the "target changes not found" group, changes over time on the BI-RADS scale were not evaluated, which can be regarded as a study limitation.

CONCLUSION

The results of this study show the feasibility and prospects of using AI for the first reading of mammograms. AI-based software (registered as a medical device) has sensitivity and specificity non-inferior or superior to those of two radiologists. The model for using AI-based software for the first reading combined with the second reading by a radiologist allows for nationwide economic benefits amounting to 0.6–5.5 billion rubles annually.

ADDITIONAL INFORMATION

Funding source. This article was prepared by a group of authors as a part of the research and development effort titled "Evidence-based methodologies for sustainable development of artificial intelligence in medical imaging", registration number to EGISU: 123031500004-5.
Competing interests. The authors declare that they have no competing interests.

Authors' contribution. All authors made a substantial contribution to the conception of the work, acquisition, analysis, interpretation of data for the work, drafting and revising the work, final approval of the version to be published and agree to be accountable for all aspects of the work. Yu.A. Vasilev, I.A. Tyrov — research concept, final proofreading of the text; A.V. Vladzymyrskyy — research concept and design, writing and editing of the text; K.M. Arzamasov — research concept and design, analysis of the data obtained, writing and editing of the text; I.M. Shulkin — research design, collection and processing of materials, final proofreading the text; D.D. Kozhikhina — research design, collection and processing of materials; L.D. Pestrenin — analysis of the data obtained, writing the text.

REFERENCES

1. Malignant neoplasms in Russia in 2021 (morbidity and mortality). Ed by A.D. Kaprin, V.V. Starinsky, A.O. Shahzadova. Moscow; 2022. 252 p. (In Russ).

2. The state of oncological assistance to the population of Russia in 2021. Ed by A.D. Kaprin, V.V. Starinsky, A.O. Shahzadova. Moscow; 2022. 239 p. (In Russ).

[3] Rate agreement for medical care provided under the Territorial Program of Compulsory Medical Insurance for Moscow in 2023 (Concluded in Moscow on December 30, 2022). Accessed at: https://www.consultant.ru/law/review/208575247.html.

3. Chen Y, James JJ, Michalopoulou E, et al. Performance of radiologists and radiographers in double reading mammograms: The UK national health service breast screening program. *Radiology*. 2023;306(1):102–109. doi: 10.1148/radiol.212951
4. Euler-Chelpin MV, Lillholm M, Napolitano G, et al. Screening mammography: Benefit of double reading by breast density. *Breast Cancer Res Treat*. 2018;171(3):767–776. doi: 10.1007/s10549-018-4864-1
5. Hickman SE, Woitek R, Le EP, et al. Machine learning for workflow applications in screening mammography: Systematic review and meta-analysis. *Radiology*. 2022;302(1):88–104. doi: 10.1148/radiol.2021210391
6. Liu J, Lei J, Ou Y, et al. Mammography diagnosis of breast cancer screening through machine learning: A systematic review and meta-analysis. *Clin Exp Med*. 2022. doi: 10.1007/s10238-022-00895-0
7. Rozhkova NI, Rojtberg PG, Varfolomeeva AA, et al. Neural network-based segmentation model for breast cancer X-ray screening. *Sechenov medical journal*. 2020;11(3):4–14 (In Russ). doi: 10.47093/2218-7332.2020.11.3.4-14
8. Vasilev JA, Vladzimirskyy AV. Computer vision in radiology: The first stage of the Moscow experiment: Monograph. Moscow: Izdatel'skie resheniya; 2022. 388 p. (In Russ).
9. Patent RUS № 2022617324/05.04.2022. Byul. № 4. Morozov SP, Andreichenko AE, Chetverikov SF, et al. A web-based tool for performing ROC analysis of diagnostic test results. Available from: https://www.elibrary.ru/item.asp?id=48373757. Accessed: 10.03.2023. (In Russ).
10. Morozov SP, Vladzimirsky AV, Klyashtornyy VG, et al. Clinical acceptance of software based on artificial intelligence technologies (radiology). Moscow; 2019. 45 p. (Ser. Best practices in medical imaging).
11. Schaffter T, Buist DS, Lee CI, et al. Evaluation of combined artificial intelligence and radiologist assessment to interpret screening mammograms. *JAMA Netw Open*. 2020;3(3):e200265. doi: 10.1001/jamanetworkopen.2020.0265
12. Wan Y, Tong Y, Liu Y, et al. Evaluation of the combination of artificial intelligence and radiologist assessments to interpret malignant architectural distortion on mammography. *Front Oncol*. 2022;(12):880150. doi: 10.3389/fonc.2022.880150
13. Leibig C, Brehmer M, Bunk S, et al. Combining the strengths of radiologists and AI for breast cancer screening: A retrospective analysis. *Lancet Digit Health*. 2022;4(7):e507–e519. doi: 10.1016/S2589-7500(22)00070-X

СПИСОК ЛИТЕРАТУРЫ

1. Злокачественные новообразования в России в 2021 году (заболеваемость и смертность) / под ред. А.Д. Каприна, В.В. Старинского, А.О. Шахзадовой. Москва, 2022. 252 с.
2. Состояние онкологической помощи населению России в 2021 году / под ред. А.Д. Каприна, В.В. Старинского, А.О. Шахзадовой. Москва, 2022. 239 с.
3. Chen Y., James J.J., Michalopoulou E., et al. Performance of radiologists and radiographers in double reading mammograms: The UK national health service breast screening program // Radiology. 2023. Vol. 306, N 1. P. 102–109. doi: 10.1148/radiol.212951
4. Euler-Chelpin M.V., Lillholm M., Napolitano G., et al. Screening mammography: Benefit of double reading by breast density // Breast Cancer Res Treat. 2018. Vol. 171, N 3. P. 767–776. doi: 10.1007/s10549-018-4864-1
5. Hickman S.E., Woitek R., Le E.P., et al. Machine learning for workflow applications in screening mammography: Systematic review and meta-analysis // Radiology. 2022. Vol. 302, N 1. P. 88–104. doi: 10.1148/radiol.2021210391
6. Liu J., Lei J., Ou Y., et al. Mammography diagnosis of breast cancer screening through machine learning: A systematic review and meta-analysis // Clin Exp Med. 2022. doi: 10.1007/s10238-022-00895-0
7. Рожкова Н.И., Ройтберг П.Г., Варфоломеева А.А., и др. Сегментационная модель скрининга рака молочной железы на основе нейросетевого анализа рентгеновских изображений // Сеченовский вестник. 2020. Т. 11, № 3. С. 4–14. doi: 10.47093/2218-7332.2020.11.3.4-14
8. Компьютерное зрение в лучевой диагностике: первый этап Московского эксперимента. Монография / под ред. Ю.А. Васильева, А.В. Владзимирского. Москва: Издательские решения, 2022. 388 с.
9. Патент РФ на изобретение № 2022617324/05.04.2022. Бюл. № 4. Морозов С.П., Андрейченко А.Е., Четвериков С.Ф., и др. Веб-инструмент для выполнения ROC-анализа результатов диагностических тестов. Режим доступа: https://www.elibrary.ru/item.asp?id=48373757. Дата обращения: 10.03.2023.
10. Morozov S.P., Vladzimirsky A.V., Klyashtornyy V.G., et al. Clinical acceptance of software based on artificial intelligence technologies (radiology). Moscow, 2019. 45 p. (Сер. Best practices in medical imaging).
11. Schaffter T., Buist D.S., Lee C.I., et al. Evaluation of combined artificial intelligence and radiologist assessment to interpret screening mammograms // JAMA Netw Open. 2020. Vol. 3, N 3. P. e200265. doi: 10.1001/jamanetworkopen.2020.0265
12. Wan Y., Tong Y., Liu Y., et al. Evaluation of the combination of artificial intelligence and radiologist assessments to interpret malignant architectural distortion on mammography // Front Oncol. 2022. N 12. P. 880150. doi: 10.3389/fonc.2022.880150
13. Leibig C., Brehmer M., Bunk S., et al. Combining the strengths of radiologists and AI for breast cancer screening: A retrospective analysis // Lancet Digit Health. 2022. Vol. 4, N 7. P. e507–e519. doi: 10.1016/S2589-7500(22)00070-X

AUTHORS' INFO

*** Lev D. Pestrenin,** Junior Research Associate;
address: 24/1 Petrovka street, 127051 Moscow, Russia;
ORCID: 0000-0002-1786-4329;
eLibrary SPIN: 7193-7706;
e-mail: PestreninLD@zdrav.mos.ru

ОБ АВТОРАХ

*** Пестренин Лев Дмитриевич,** мл. науч. сотр.;
адрес: Россия, 127051, Москва, ул. Петровка, д. 24, стр. 1;
ORCID: 0000-0002-1786-4329;
eLibrary SPIN: 7193-7706;
e-mail: PestreninLD@zdrav.mos.ru

* Corresponding author / Автор, ответственный за переписку

Yuriy A. Vasilev, MD, Cand. Sci. (Med);
ORCID: 0000-0002-0208-5218;
eLibrary SPIN: 4458-5608;
e-mail: npcmr@zdrav.mos.ru

Ilya A. Tyrov;
ORCID: 0000-0001-9337-624X;
eLibrary SPIN: 8625-3458;
e-mail: npcmr@zdrav.mos.ru

Anton V. Vladzymyrskyy, MD, Dr. Sci. (Med), Professor;
ORCID: 0000-0002-2990-7736;
eLibrary SPIN: 3602-7120;
e-mail: npcmr@zdrav.mos.ru

Kirill M. Arzamasov, MD, Cand. Sci. (Med);
ORCID: 0000-0001-7786-0349;
eLibrary SPIN: 3160-8062;
e-mail: ArzamasovKM@zdrav.mos.ru

Igor M. Shulkin;
ORCID: 0000-0002-7613-5273;
eLibrary SPIN: 5266-0618;
e-mail: npcmr@zdrav.mos.ru

Daria D. Kozhikhina;
ORCID: 0000-0001-7690-8427;
eLibrary SPIN: 5869-3854;
e-mail: npcmr@zdrav.mos.ru

Васильев Юрий Александрович, канд. мед. наук;
ORCID: 0000-0002-0208-5218;
eLibrary SPIN: 4458-5608;
e-mail: npcmr@zdrav.mos.ru

Тыров Илья Александрович;
ORCID: 0000-0001-9337-624X;
eLibrary SPIN: 8625-3458;
e-mail: npcmr@zdrav.mos.ru

Владзимирский Антон Вячеславович, д-р мед. наук, профессор;
ORCID: 0000-0002-2990-7736;
eLibrary SPIN: 3602-7120;
e-mail: npcmr@zdrav.mos.ru

Арзамасов Кирилл Михайлович, канд. мед. наук;
ORCID: 0000-0001-7786-0349;
eLibrary SPIN: 3160-8062;
e-mail: ArzamasovKM@zdrav.mos.ru

Шулькин Игорь Михайлович;
ORCID: 0000-0002-7613-5273;
eLibrary SPIN: 5266-0618;
e-mail: npcmr@zdrav.mos.r

Кожихина Дарья Дмитриевна;
ORCID: 0000-0001-7690-8427;
eLibrary SPIN: 5869-3854;
e-mail: npcmr@zdrav.mos.ru

DOI: https://doi.org/10.17816/DD321963

Диагностическая и экономическая оценка применения комплексного алгоритма искусственного интеллекта, направленного на выявление десяти патологических находок по данным компьютерной томографии органов грудной клетки

В.Ю. Чернина[1], М.Г. Беляев[1], А.Ю. Силин[2], И.О. Аветисов[2], И.А. Пятницкий[1, 10], Е.А. Петраш[1, 3], М.В. Басова[1], В.Е. Синицын[4, 5], В.В. Омельяновский[6, 7, 8], В.А. Гомболевский[1, 9]

[1] АЙРА Лабс, Москва, Российская Федерация
[2] Клинический госпиталь на Яузе, Москва, Российская Федерация
[3] Национальный медицинский исследовательский центр онкологии имени Н.Н. Блохина, Москва, Российская Федерация
[4] Московский государственный университет имени М.В. Ломоносова, Москва, Российская Федерация
[5] Научно-практический клинический центр диагностики и телемедицинских технологий, Москва, Российская Федерация
[6] Центр экспертизы и контроля качества медицинской помощи, Москва, Российская Федерация
[7] Российская медицинская академия непрерывного профессионального образования, Москва, Российская Федерация
[8] Научно-исследовательский финансовый институт, Москва, Российская Федерация
[9] Институт искусственного интеллекта, Москва, Российская Федерация
[10] Техасский университет в Остине, Остин, США

АННОТАЦИЯ

Обоснование. Технологии искусственного интеллекта призваны помогать в решении проблемы пропуска находок при лучевых исследованиях. Важным вопросом является оценка экономической пользы от внедрения технологий искусственного интеллекта.

Цель — оценить частоту выявления патологических находок и экономический потенциал применения комплексного искусственного интеллекта для компьютерной томографии органов грудной клетки, валидированного экспертами, по сравнению с рентгенологами без доступа к технологиям в условиях частного медицинского центра.

Материалы и методы. Проведено обсервационное одноцентровое ретроспективное исследование. В исследование включались компьютерные томограммы органов грудной клетки без внутривенного контрастирования, выполненные в ООО «Клинический госпиталь на Яузе» (Москва) в период с 01.06.2022 по 31.07.2022. Компьютерные томограммы обработаны комплексным алгоритмом искусственного интеллекта для десяти патологий: инфильтративные изменения в лёгких, характерные для вирусной пневмонии (COVID-19 в условиях пандемии); лёгочные узлы; свободная жидкость в плевральных полостях; эмфизема лёгких; увеличение диаметра грудной аорты; увеличение диаметра ствола лёгочной артерии; коронарный кальциноз; оценка толщины надпочечников; оценка высоты и плотности тел позвонков. Два эксперта анализировали компьютерные томограммы и сравнивали результаты с анализом искусственного интеллекта. Для всех находок, выявленных и не выявленных врачами клиники, определили дальнейшую маршрутизацию в соответствии с клиническими рекомендациями. Для каждого пациента была рассчитана стоимость неоказанных медицинских услуг по прайс-листу клиники.

Результаты. Итоговую группу составили 160 компьютерных томограмм органов грудной клетки с описаниями. С помощью искусственного интеллекта выявлено 90 (56%) исследований с патологиями, из них в 81 (51%) протоколе была пропущена хотя бы одна патология. Общая стоимость неоказанных медицинских услуг «второго этапа» для всех патологий от 81 пациента была оценена в 2 847 760 руб. (37 250,99 долларов или 256 217,95 китайских юаней). Стоимость неоказанных медицинских услуг только для тех патологий, которые пропущены врачами, но выявлены искусственным интеллектом, составила 2 065 360 руб. (27 016,57 долларов или 185 824,05 китайских юаней).

Заключение. Применение искусственного интеллекта для анализа данных компьютерной томографии органов грудной клетки в качестве помощника рентгенолога позволяет существенно уменьшить число случаев пропуска патологий. Использование искусственного интеллекта может принести в 3,6 раза больше стоимости за медицинские услуги по сравнению со стандартной моделью работы рентгенологов без применения таких технологий, и, таким образом, быть рентабельным для применения в условиях частного медицинского центра.

Ключевые слова: компьютерная томография; искусственный интеллект; грудная клетка; случайные находки.

Как цитировать

Чернина В.Ю., Беляев М.Г., Силин А.Ю., Аветисов И.О., Пятницкий И.А., Петраш Е.А., Басова М.В., Синицын В.Е., Омельяновский В.В., Гомболевский В.А. Диагностическая и экономическая оценка применения комплексного алгоритма искусственного интеллекта, направленного на выявление десяти патологических находок по данным компьютерной томографии органов грудной клетки // *Digital Diagnostics.* 2023. Т. 4, № 2. С. 105–132. DOI: https://doi.org/10.17816/DD321963

Рукопись получена: 07.04.2023 **Рукопись одобрена:** 22.05.2023 **Опубликована:** 01.06.2023

DOI: https://doi.org/10.17816/DD321963

Analysis of the diagnostic and economic impact of the combined artificial intelligence algorithm for analysis of 10 pathological findings on chest computed tomography

Valeria Yu. Chernina[1], Mikhail G. Belyaev[1], Anton Yu. Silin[2], Ivan O. Avetisov[2], Ilya A. Pyatnitskiy[1, 10], Ekaterina A. Petrash[1, 3], Maria V. Basova[1], Valentin E. Sinitsyn[4, 5], Vitaly V. Omelyanovskiy[6, 7, 8], Victor A. Gombolevskiy[1, 9]

[1] IRA Labs, Moscow, Russian Federation
[2] Clinical Hospital on Yauza, Moscow, Russian Federation
[3] N.N. Blokhin National Medical Research Center of Oncology, Moscow, Russian Federation
[4] Lomonosov Moscow State University, Moscow, Russian Federation
[5] Research and Practical Clinical Center for Diagnostics and Telemedicine Technologies, Moscow, Russian Federation
[6] The Center for Healthcare Quality Assessment and Control, Moscow, Russian Federation
[7] Russian Medical Academy of Continuous Professional Education, Moscow, Russian Federation
[8] Scientific and research financial institute, Moscow, Russian Federation
[9] Artificial Intelligence Research Institute, Moscow, Russian Federation
[10] The University of Texas at Austin, Austin, Texas, USA

ABSTRACT

BACKGROUND: Artificial intelligence technology can help solve the significant problem of missed findings in radiology studies. An important issue is assessing the economic benefits of implementing artificial intelligence.

AIM: To evaluate the frequency of missed pathologies detection and the economic potential of artificial intelligence technology for chest computed tomography compared and validated by experienced radiologists.

MATERIALS AND METHODS: This was an observational, single-center retrospective study. The study included chest computed tomography without IV contrast from June 1 to July 31, 2022, in Clinical Hospital in Yauza, Moscow. The computed tomography was processed using a complex artificial intelligence algorithm for 10 pathologies: pulmonary infiltrates, typical for viral pneumonia (COVID-19 in pandemic conditions); lung nodules; pleural effusion; pulmonary emphysema; thoracic aortic dilatation; pulmonary trunk dilatation; coronary artery calcification; adrenal hyperplasia; and osteoporosis (vertebral body height and density changes). Two experts analyzed computed tomography and compared results with artificial intelligence. Further routing was determined according to clinical guidelines for all findings initially detected and missed by radiologists. The hospital price list determined the potential revenue loss for each patient.

RESULTS: From the final 160 computed tomographies, the artificial intelligence identified 90 studies (56%) with pathologies, of which 81 (51%) were missing at least one pathology in the report. The "second-stage" lost potential revenue for all pathologies from 81 patients was RUB 2,847,760 ($37,251 or CNY 256,218). Lost potential revenue only for those pathologies missed by radiologists but detected by artificial intelligence was RUB 2,065,360 ($27,017 or CNY 185,824).

CONCLUSION: Using artificial intelligence as an "assistant" to the radiologist for chest computed tomography can dramatically minimize the number of missed abnormalities. Compared with the normal model without artificial intelligence, using artificial intelligence can provide 3.6 times more benefits. Using advanced artificial intelligence for chest computed tomography can save money.

Keywords: artificial intelligence; chest; computed tomography; incidental findings.

To cite this article

Chernina VYu, Belyaev MG, Silin AYu, Avetisov IO, Pyatnitskiy IA, Petrash EA, Basova MV, Sinitsyn VE, Omelyanovskiy VV, Gombolevskiy VA. Analysis of the diagnostic and economic impact of the combined artificial intelligence algorithm for analysis of 10 pathological findings on chest computed tomography. *Digital Diagnostics.* 2023;4(2):105–132. DOI: https://doi.org/10.17816/DD321963

Received: 07.04.2023 **Accepted:** 22.05.2023 **Published:** 01.06.2023

DOI: https://doi.org/10.17816/DD321963

旨在从胸部电子计算机断层扫描中识别十种病理检查所见的综合人工智能算法使用的诊断和经济评估

Valeria Yu. Chernina[1], Mikhail G. Belyaev[1], Anton Yu. Silin[2], Ivan O. Avetisov[2], Ilya A. Pyatnitskiy[1, 10], Ekaterina A. Petrash[1, 3], Maria V. Basova[1], Valentin E. Sinitsyn[4, 5], Vitaly V. Omelyanovskiy[6, 7, 8], Victor A. Gombolevskiy[1, 9]

[1] IRA Labs, Moscow, Russian Federation
[2] Clinical Hospital on Yauza, Moscow, Russian Federation
[3] N.N. Blokhin National Medical Research Center of Oncology, Moscow, Russian Federation
[4] Lomonosov Moscow State University, Moscow, Russian Federation
[5] Research and Practical Clinical Center for Diagnostics and Telemedicine Technologies, Moscow, Russian Federation
[6] The Center for Healthcare Quality Assessment and Control, Moscow, Russian Federation
[7] Russian Medical Academy of Continuous Professional Education, Moscow, Russian Federation
[8] Scientific and research financial institute, Moscow, Russian Federation
[9] Artificial Intelligence Research Institute, Moscow, Russian Federation
[10] The University of Texas at Austin, Austin, Texas, USA

简评

论证。人工智能技术打算帮助解决射线检验中遗漏发现的问题。一个重要的问题是对采用人工智能技术的经济效益进行的评估。

该研究的目的是评估在私人医疗中心环境下，与不应用技术的放射科医生相比，使用全面的、经过专家验证的人工智能进行胸部电子计算机断层扫描的检测频率和经济潜力。

材料和方法。进行了一项观察性、单中心的回顾性研究。本研究包括2022年6月1日至2022年7月31日在“Clinical Hospital on Yauza”（莫斯科）进行的没有静脉注射对比剂的胸部器官电子计算机断层扫描图像。电子计算机断层扫描图像由人工智能的综合算法处理，用于10种病症：病毒性肺炎（大流行条件下的COVID-19）的肺部浸润性病变；肺结节；胸膜腔内的游离液体；肺气肿；胸主动脉增宽；肺动脉干增宽；冠状动脉钙化；肾上腺厚度的评估；椎体高度和密度的评估。两位专家分析了电子计算机断层扫描图像，并对结果与人工智能分析进行了比较。对于诊所医生检测到和未检测到的所有发现，根据临床指南确定了进一步路由。对于每个病人，根据诊所的价格表，计算出未提供的医疗服务费用。

结果。最后一组由160个带有描述的胸部器官电子计算机断层扫描图像组成。人工智能识别出90个（56%）有病变的研究，其中81个（51%）协议至少有一个遗漏的病变。81名患者的所有病变的未提供的“第二阶段”医疗服务的总成本估计为2,847,760卢布（37,250.99美元或256,217.95人民币）。只有那些被医生遗漏但被人工智能检测出来的病变的未提供医疗服务费用为2,065,360卢布（27,016.57美元或185,824.05人民币）。

结论。来为分析胸部电子计算机断层扫描数据而使用的作为放射科医生助手的人工智能允许大大减少遗漏病变的情况。与不应用这种技术放射科医生工作的标准模式相比，使用人工智能可以为每项医疗服务带来3.6倍的成本，因此，在私人医疗中心环境下的应用具有成本效益。

关键词：电子计算机断层扫描；人工智能；胸廓；偶然发现。

To cite this article

Chernina VYu, Belyaev MG, Silin AYu, Avetisov IO, Pyatnitskiy IA, Petrash EA, Basova MV, Sinitsyn VE, Omelyanovskiy VV, Gombolevskiy VA.旨在从胸部电子计算机断层扫描中识别十种病理检查所见的综合人工智能算法使用的诊断和经济评估. *Digital Diagnostics.* 2023;4(2):105–132. DOI: https://doi.org/10.17816/DD321963

收到：07.04.2023 **接受：**22.05.2023 **发布日期：**01.06.2023

List of abbreviations

DATA SET: a data set, a collection of logical records
CI: confidence interval
AI: artificial intelligence
CT: computed tomography
ICD-10: International Statistical Classification of Diseases and Related Health Problems, Tenth Edition
MRI: magnetic resonance imaging
CNMS: cost of non-provided medical services

BACKGROUND

According to the World Health Organization, most deaths are associated with cardiovascular diseases (CVDs), infections, lung diseases, and cancers.[1] Based on large randomized trials of lung cancer screening, the use of chest low-dose computed tomography in asymptomatic patients at risk resulted in a 6.7% decrease in mortality from lung cancer and from all causes in the National Lung Screening Trial (USA) and in a 39% decrease in mortality during follow-up in the Year 5–10 of a Multicentric Italian Lung Detection study (Italy) due to incidental detection of clinically significant findings and treatment and prevention of relevant diseases [1,2].

Lung cancer screening programs are cost effective in high-risk patients. This effect varies across healthcare systems in different countries [3]. Moreover, these programs have significant differences in lung cancer mortality and total mortality. In one of the lung cancer screening studies, 77.1% of patients died not from the disease itself but from other causes such as CVDs, lung diseases, other tumors, and infectious diseases [1]. By focusing on lung cancer searching, a radiologist may miss abnormal findings associated with other diseases. For example, during lung cancer screening, 58% of clinically significant findings are not reflected in the radiologist protocol texts [4].

During the coronavirus disease-2019 (COVID-19) pandemic, lung cancer screening programs were suspended because computed tomography (CT) scanners are required to perform mass chest CT to diagnose COVID-19. In half of the patients who underwent chest CT, incidental findings were detected, and 1/4 had clinically significant findings [5]. Chest CT data allow diagnosis of diseases in the lungs, other organs, and systems [6-8]. Medical personnel shortage, burnout, pandemic effects, and increased workload can lead to missing clinically significant findings.

Artificial intelligence (AI) is the most promising technology for solving this problem; thus, assessing economic benefits of such innovations is necessary. Numerous AI healthcare products were developed for diagnostic radiology, and the number of such solutions exceeds the number of other medical AI services in several times.[2] In Russia, the largest AI imaging project is related to an experiment on the use of innovative computer vision technologies for evaluating medical images and further use of the Moscow healthcare system (hereinafter referred to as the Moscow experiment). For this project, more than 7.5 million imaging examinations were performed, including X-ray imaging, mammography, and CT [9].[3]

Briefly, the use of AI single-pathology algorithms is of limited practical value for controlling diseases that are among the leading causes of death worldwide. Given the need for simultaneous detection of several pathologies using AI, the first software products have been developed for a comprehensive analysis of chest CT. They have passed all testing stages and have been approved for prospective use in 153 Moscow healthcare organizations.[4] One of these products is a multi-IRA combined AI service by IRA Labs, which can simultaneously search for 10 abnormal signs of various diseases during CT [10-13], including the following:

1) Infiltrative lung lesions typical for viral pneumonia (COVID-19 pandemic; U07 according to ICD-10), with calculation of the percentage of lung damage.
2) Lung nodules with assessing their size, volume, and density to detect lung malignancies (ICD-10 code C34).
3) Free pleural fluid (effusion) (ICD-10 code J94).
4) Pulmonary emphysema as a sign of chronic obstructive pulmonary disease (ICD-10 code J44).
5) Measuring thoracic aorta diameter to detect aorta dilatation and aneurysms (ICD-10 codes I70 and I71).
6) Measuring the diameter of the pulmonary artery trunk to detect potential causes of pulmonary hypertension (ICD-10 code I27).
7) Evaluating the extent of coronary calcification using the Agatston score to assess the severity of coronary

[1] who.int [Internet]. Top 10 death causes in the World [cited on December 08, 2020]. Available from: https://www.who.int/ru/news-room/fact-sheets/detail/the-top-10-causes-of-death.

[2] IQVIA [Internet]. FDA Publishes Approved List of AI/ML-enabled Medical Devices [cite 2021 Oct 29]. Michaela Miller, Technology & Analytics Practice Lead, U.S. MedTech, IQVIA. Available from: https://www.iqvia.com/locations/united-states/blogs/2021/10/fda-publishes-approved-list-of-ai-ml-enabled-medical-devices.

[3] Center for Diagnostics and Telemedicine [Internet]. Experiment (https://mosmed.ai/ai/); data sets (https://mosmed.ai/datasets/). Accessed on March 17, 2023.

[4] Center for Diagnostics and Telemedicine [Internet]. Chest-IRA. IRA Labs LLC. Available from: https://mosmed.ai/service_catalog/chestira/.

atherosclerosis and the risk of coronary heart disease (ICD-10 codes I20–I25).
8) Measuring the adrenal gland size to detect lesions and hyperplasia (ICD-10 code C74).
9) Measuring vertebral body heights for diagnosing compression fractures (ICD-10 codes M80–M85).
10) Analyzing the density of the vertebral bodies to detect signs of osteoporosis (ICD-10 codes M80–M85).

This study aimed to evaluate the frequency of significant abnormal findings and the economic potential of using combined AI technologies in the analysis of chest CT, validated by radiologists, compared with analysis performed radiologists without AI access in a private medical center.

MATERIALS AND METHODS

Study design

In this observational single-center retrospective study, patient informed consent was not required. The study was prepared in accordance with the CHEERS 2022 checklist for the economic evaluation of medical studies [14].[5] An economic analysis plan was developed for a private medical center. It included the assessment of the potential additional costs of non-provided medical services (CNMS) that should be provided to patients with certain abnormal findings according to clinical guidelines and best practices of evidence-based medicine. The use of combined AI services added to CNMS resulted from radiologist activities, through further diagnostic actions to clarify the nature and severity of CT findings.

Treatment cost was not assessed in this study. The study design is presented in Fig. 1.

Eligibility criteria

Inclusion and exclusion criteria were used to form the study group.

Inclusion criteria: Chest CT in men and women who got medical assistance in a primary and specialized care organization for adult population of Moscow; chest CT performed and interpreted by radiologists between June 01, 2022, and July 31, 2022; chest CT performed without intravenous contrast enhancement; patients aged >18 years; availability of CT scans in DICOM format and protocol texts prepared by radiologists in the clinic; and the patient's first visit to a clinic.

Exclusion criteria: age >85 years; previous chest CT within 1 year; AI could not process scans because of reasons out of its control (e.g., inappropriate modality, scan region other than the chest, insufficient number of slices, i.e., <30); AI could not process scans due to reasons related to algorithm features (e.g., incorrect work due to the presence of significant metal artifacts at the scan level).

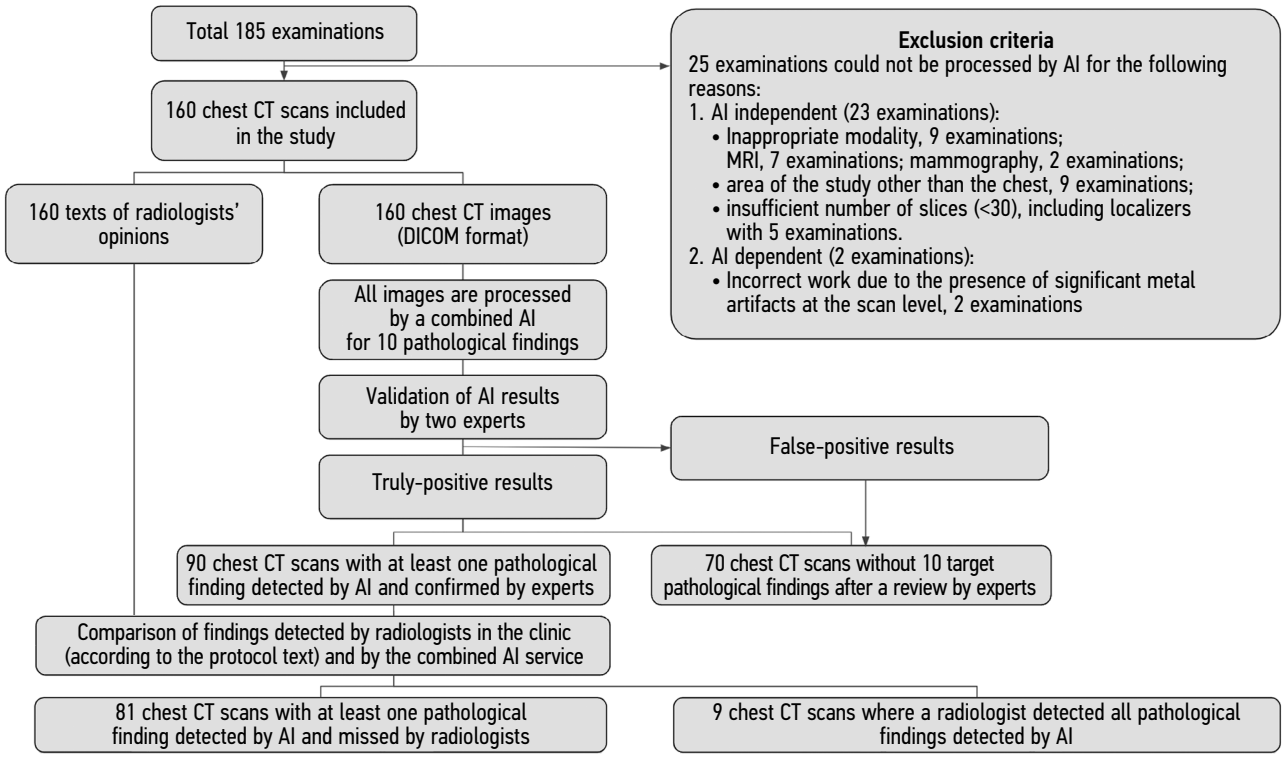

Fig. 1. Study design.

[5] EQUATOR Network [Internet]. Enhancing the QUAlity and Transparency Of health Research. Available from: https://www.equator-network.org/reporting-guidelines/cheers/.

Conditions of the study

CT was performed at the Clinical Hospital on Yauza LLC, which is a multidisciplinary private healthcare organization providing primary and specialized care to the adult population of Moscow.

Study duration

The study was conducted using CT performed between June 1, 2022, and July 31, 2022. Results were retrospectively analyzed using the AI algorithm and verified by experts between October 01, 2022, and November 30, 2022.

Description of the study

Chest CT was performed without intravenous contrast enhancement using a Philips Ingenuity CT scanner. This tomograph performed 128 slices per tube rotation. The chest CT protocol was performed in accordance with standard equipment manufacturer recommendations and national guidelines. CT findings were provided to experts and AI in two series reconstructed with a soft tissue kernel (60 HU for the center of the window, 360 HU for the width of the window) and a pulmonary kernel (–500 HU for the center of the window and 1,500 HU for the width of the window). The slice thickness was 1.0 mm. Iterative model reconstruction algorithms were used to improve image quality (reduce noise) and reduce the radiation dose to the patient.

All the included CT examinations were processed using multi-IRA combined AI software (IRA Labs) integrated into the clinic's picture archiving and communication system. The AI algorithms used in this study were previously tested on specially prepared calibration datasets as part of the Moscow AI experiment.[6]

The criterion for the possibility of AI use was algorithm accuracy not lower than the area under the ROC curve (ROC AUC) of 0.81 for each pathological finding, according to the guidelines for clinical trials of software based on intelligent technologies [15]. The diagnostic accuracy metrics for AI algorithms based on developer-independent closed datasets of the Moscow experiment are presented in Table 1 [9,10].

Primary study outcome

For all the findings detected and missed by physicians in the clinic, "second stages" were determined (consultations with specialists and various types of additional clinical, instrumental, and laboratory examinations), i.e., further routing of the patient in accordance with current clinical guidelines for each pathological finding.

Then, for each patient, the CNMS was calculated according to the price list of the clinic, which was determined based on non-provided medical services, required according to clinical guidelines for missed pathological findings. The CNMS was also calculated for the missed significant pathological findings, as shown in Table 2 [16-31]. For radiologists, abnormal findings

Table 1. Diagnostic accuracy metrics for a combined AI solution for chest CT, based on the datasets of the Moscow experiment

Name of the multi-IRA AI algorithm for certain pathologies	ROC AUC	Sensitivity	Specificity	Accuracy
COVID-IRA (detection of lung infiltrative lesions)	0.98	0.95	0.94	0.94
LungNodule-IRA (detection of lung nodules)	0.932	0.86	0.9	0.88
PleuralEffusion-IRA (detection of pleural effusion)	0.999	0.98	1	0.99
Aorta-IRA (chest) (evaluation of the thoracic aorta diameter)	0.997	0.96	1	0.98
Aorta-IRA (chest + abdomen) (evaluation of the thoracic and abdominal aorta diameters)	1	0.98	1	0.99
PulmTrunk-IRA (evaluation of the pulmonary trunk diameter)	1	1	0.98	0.99
Agatston-IRA (evaluation of the Agatston coronary calcification score)	0.986	0.96	0.96	0.96
Genant-IRA (evaluation of the height of vertebral bodies)	0.995	1	0.98	0.99
Emphysema-IRA (detection of emphysema)	0.989	0.94	0.98	0.96
Adrenal-IRA (assessment of the adrenal size for masses and hyperplasia)	0.96	1	0.96	0.98

[6] Center for Diagnostics and Telemedicine [Internet]. IRA Labs LLC: Chest-IRA (https://mosmed.ai/service_catalog/chestira/); Adrenal-IRA Abd (https://mosmed.ai/service_catalog/adrenalira/); Aorta-IRA Abd (https://mosmed.ai/service_catalog/aortaira/); Genant-IRA Abd (https://mosmed.ai/service_catalog/genant-ira/). Accessed on March 17, 2023.

Table 2. Criteria for abnormal findings and omissions

Health condition	Criteria for pathological findings	Criteria for skipping significant pathological findings	Criteria for skipping non-significant pathological findings
Lung nodules	At least one solid or subsolid (only the solid component is measured) nodule with an average size of ⩾6 mm (volume ⩾100 mm3) [16]	All findings for this condition that met the described criteria were considered significant, excluding perifissural lung nodules. Nodules along the pleura are benign and do not require further observations.	
Infiltrative lung changes typical for viral pneumonia (COVID-19) in a pandemic	1. Bilateral frosted glass infiltration of the lung parenchyma with peripheral predominance, with, or without consolidation infiltration of the lung parenchyma with a positive sign of an air bronchogram. 2. Bilateral cobblestone infiltration of the lung parenchyma (thickening of the interlobular interstitium with frosted glass), with peripheral predominance, with, or without consolidation infiltration of the lung parenchyma with a positive sign of an air bronchogram [17, 18]	Lung involvement >50%	Lung involvement <50%
Lung emphysema	In total ⩾6% (by volume) of areas in both lungs (excluding bronchial lumen) with CT density ⩽-950 HU [19,20]	All findings for this condition that met the described criteria were considered significant.	
Free pleural fluid (effusion)	A crescentic liquid accumulation (effusion) in the pleural cavity with a density of 0–30 HU in the gravity-dependent chest regions [21]	Maximum layer thickness >10 mm	Maximum layer thickness <10mm
Aneurysm / aorta dilatation	1. Dilatation of the ascending thoracic aorta: on native scans, the largest axial diameter of the ascending thoracic aorta is 40 to ⩽49 mm. 2. Aneurysm of the ascending thoracic aorta: on native scans, the largest axial diameter of the ascending thoracic aorta is ⩾50 mm. 3. Dilatation of the descending thoracic aorta: on native scans, the largest axial diameter of the descending thoracic aorta ranges from 31 to 39 mm. 4. Aneurysm of the descending thoracic aorta: on native scans, the largest axial diameter of the descending thoracic aorta is ⩾40 mm.[#] [22] 5. Dilatation of the abdominal aorta: the largest diameter is 25–⩽29 mm. 6. Aneurysm of abdominal aorta: the largest diameter ⩾30 mm [23,24]	Aneurysm of the ascending thoracic aorta (diameter ⩾50 mm) and descending thoracic aorta (diameter ⩾40 mm). Aneurysm of the abdominal aorta (diameter ⩾30 mm).	Dilatation of the ascending thoracic aorta (diameter of 40–49 mm) and descending thoracic aorta (diameter of 31–39 mm). Dilatation of the abdominal aorta (diameter ⩾30 mm).
Dilatation of the pulmonary trunk	Diameter of the pulmonary trunk ⩾29 mm[##] [25]	>29 mm	29 mm
Coronary calcification by Agatston score	On native scans, the Agatston score (the sum of areas in the projection of coronary vessels, multiplied by individual density factors*) is ⩾1, or CAC-DRS class A1–A3. [26,27] * Factor 1: 130–199 HU Factor 2: 200–299 HU Factor 3: 300–399 HU Factor 4: ⩾400 HU	Agatston score >10	Agatston score 1–10
Measurement of the adrenal size for masses and hyperplasia	Nodular formations of the adrenal body or pedicles with a short-axial diameter measuring⩾10 mm [28]	All findings for this condition that met the described criteria are considered significant.	

[#] The Task Force for the Diagnosis and Treatment of Aortic Diseases of the European Society of Cardiology (ESC). ESC Guidelines on the diagnosis and treatment of aortic diseases, 2014. Available from: https://scardio.ru/content/Guidelines/Recom%20po%20aorte%207_rkj_15.pdf.

[##] The Task Force for the diagnosis and treatment of pulmonary hypertension of the European Society of Cardiology (ESC) and the European Respiratory Society (ERS). ESC/ERS Guidelines for the diagnosis and treatment of pulmonary hypertension, 2015. Available from: https://scardio.ru/content/Guidelines/ESC%20_L_hypert_2015.pdf.

Table 2. Ending

Health condition	Criteria for pathological findings	Criteria for skipping significant pathological findings	Criteria for skipping non-significant pathological findings
Evaluation of the density of the spongy substance of vertebral bodies for the detection of osteoporosis/ osteopenia	Decrease in bone mineral density in Th11–L3 (optimally L1–L2) vertebral bodies according to ACR 2018 criteria, ISCD 2019 statement [29]	Density <+100 HU	Density +100 to +150 HU
Vertebral compression fractures related to osteoporosis	Vertebrae with compressive body deformity ⩾25% according to the Genant semi-quantitative scale, grades II–III [30, 31]. The deformation grade (DG) is calculated by the following formula: DG = (ratio of the maximum vertebral body size - minimum/maximum size) × 100%	All findings for this condition that met the described criteria were considered significant.	

were considered missed if it was not reported in the final CT descriptions in the electronic medical information system of the clinic provided that such information was available according to true-positive results (ground truth) after reviewing CT data by an expert and AI analysis. Findings were true positive if they were detected by the AI algorithm and confirmed by two medical experts analyzing CT.

Additional study outcomes

The number of protocols with significant and insignificant missed pathological findings and the percentage of erroneous protocols were calculated for each clinic radiologist.

Subgroup analysis

To eliminate erroneous program triggering, two experts (radiologists with 10 and 13 years of experience, respectively, who are not employees of the clinic that provided data for the study) reviewed CT scans with results of AI processing. In the case of controversial opinions, a single option was selected after a collective discussion. As a result of this analysis, the true-positive results of the AI analysis, confirmed by two experts, were selected. Then, AI findings were compared with the final chest CT descriptions prepared by radiologists in the clinic without using AI, and some cases of missed pathological findings were identified. All pathological findings missed by radiologists in the clinic were divided into significant and insignificant. The significance criteria for pathological findings were evaluated in accordance with basic diagnostic requirements for AI analysis in the Moscow experiment, agreed by the Commission for Scientific Problems of the Scientific and Practical Clinical Center for Diagnostics and Telemedicine Technologies of the Department of Healthcare of Moscow (Protocol No. 9/2021 dated December 10, 2021, No. 1/2022 dated February 28, 2022, No. 7/2022 dated December 06, 2022, No. 1/2023 dated January 13, 2023). These requirements are based on clinical guidelines and evidence-based best practices.

In this study, protocol texts were not evaluated for the presence or absence of the "epicardial fat" term because the radiologists in the clinic did not have tools to measure the volume of adipose tissue. The criteria for pathological findings and distribution by the missed pathological finding significance are presented in Table 2.

Ethical review

The Independent Ethical Committee of the Moscow Regional Branch of the Russian Society of Radiologists was notified about this this retrospective study (minutes dated March 01, 2023).

Statistical analysis

Results were presented using descriptive statistics methods, and the absolute number (*n*) and percentage (%) of observations were indicated for each category. Frequencies of pathological finding detection by different methods were compared using the Z-test for proportions. The *p*-values obtained for each of the nine pathological findings were adjusted for multiple testing (for general hypothesis of the absence of a statistically significant difference in diagnostic results) by the Bonferroni correction. Financial parameters were analyzed using a paired t-test. The level of statistical significance for *p* was 0.05. The statistical analysis was performed using the R program, version 4.1.3.

RESULTS

Study subjects

A total of 185 examinations were selected (male-to-female ratio: 47%:53%; age, 19–83 years; mean age, 49.5 years) in accordance with established criteria. Of them, 25 examinations were not processed by AI for the following reasons:

1) AI-independent (23 examinations).
   - Inappropriate modality (9 examinations: 7 MRIs; 2 mammographies).

- Scan region other than the chest (9 examinations).
- Insufficient number of slices (<30), including localizers (5 examinations).

2) AI-dependent (2 examinations)
   - Incorrect operation due to the presence of significant metal artifacts at the scan level (2 examinations).

The final group for analysis consisted of 160 chest CT scans with descriptions prepared by radiologists. Additional information on the presence of oncological, cardiovascular, and other chronic diseases in patients was not collected because patients visited this clinic only under compulsory or voluntary medical insurance policies and were on a paid basis to consult specialists. The medical information system about established diagnoses highly likely contained incomplete information.

Primary study outcomes

Automatic processes were set up to anonymize and transfer CT scans from the clinic to the developer of combined AI for chest CT and return the analysis results to the clinic and experts for AI validation. For quality control, experts provided a list of all discrepancies between the verified AI results and the text protocols to the clinic staff (Fig 2). No claims were obtained from the clinic. The largest number of clinically significant omissions in the protocol texts was found for osteoporosis and adrenal masses (n = 14 each). The largest number of insignificant omissions was recorded in aortic dilatation (n = 36) and osteopenia (n = 40). Detailed data on number of findings are presented in Fig. 3.

With AI, 90 (56%) examinations with pathological findings were identified, and at least one pathological finding was missed in 81 (51%) radiologist protocols. In 70 studies, the AI algorithm did not detect any pathological findings. In this study, examinations presented could have other abnormal findings that were not included into the AI validation program. Analysis results are summarized in Table 3.

A CT could reveal several pathological findings; some were detected by a radiologist in the clinic (and they were described in the protocol), and some were detected only by AI (potential benefit of AI).

A detailed CNMS analysis for missed pathological findings in every 90 patients is presented in Fig. 4. When comparing two diagnostic approaches (algorithm + expert verification vs. expert without AI), some statistically significant differences were obtained for the following abnormal findings: aortic aneurysms/dilatations, increased diameter of the pulmonary trunk, Agatston score, vertebral compression fractures, decreased density of the vertebral bodies, and adrenal gland thickening (Table 4).

The total estimated "second step" CNMS for all missed pathological findings in 81 patients was RUB 2,847,760 ($ 37,250.99 or CNY 256,217.95) with RUB 17,799 ($232.83 or CNY 1601.41) per patient. The cost of the total "second step" CNMS for pathological findings missed by radiologists in the clinic, but detected by AI, and confirmed by experts, was RUB 2,065,360 ($ 27,016.57 or CNY 185,824.05) with RUB 12,909 ($168.86 or CNY 1,161.45) per patient. The results of CNMS calculations for all findings are presented in Table 5.

The total estimated CNMS for significant missed pathological findings was RUB 770,855 ($ 10,083.4 or CNY 69,355.17) with RUB 4,818 ($63.02 or CNY 433.48) per patient. Results are presented in Table 6.

Costs were compared using a paired t-test with calculated average difference per patient and using 95% confidence interval (CI). Therefore, 160×12908.5 [160×9833.5; 160×15,983.5] correspond to the total CNMS for analyzing the population with own CIs. Results are presented in Table 7.

The final cost-effectiveness for the AI used in healthcare organizations is shown in Fig. 5.

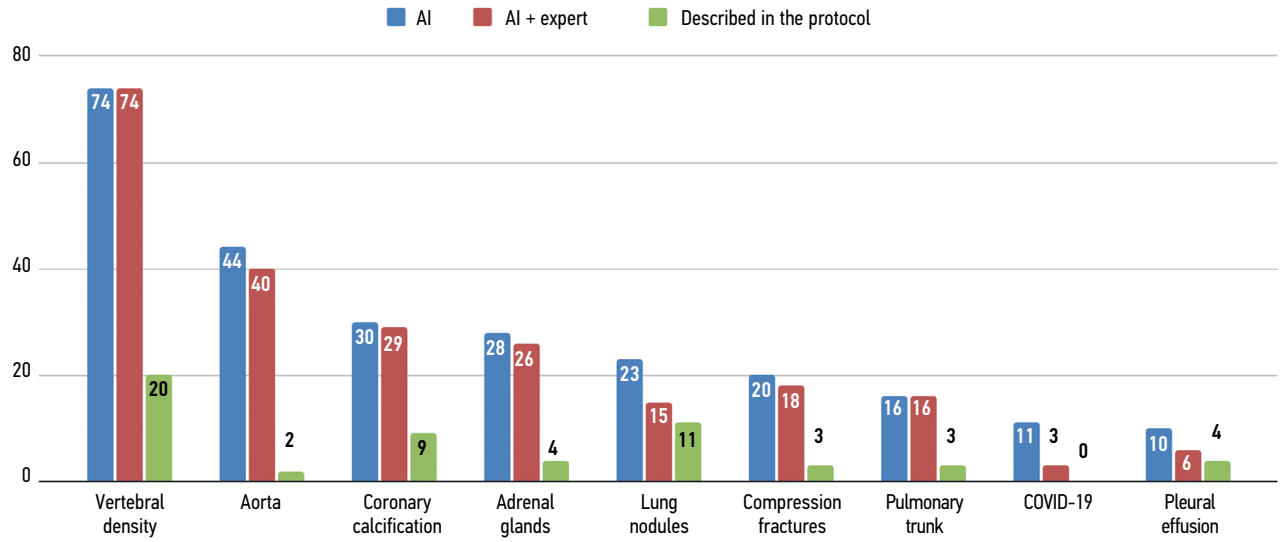

Fig. 2. Study result by the number of findings detected with and without AI.

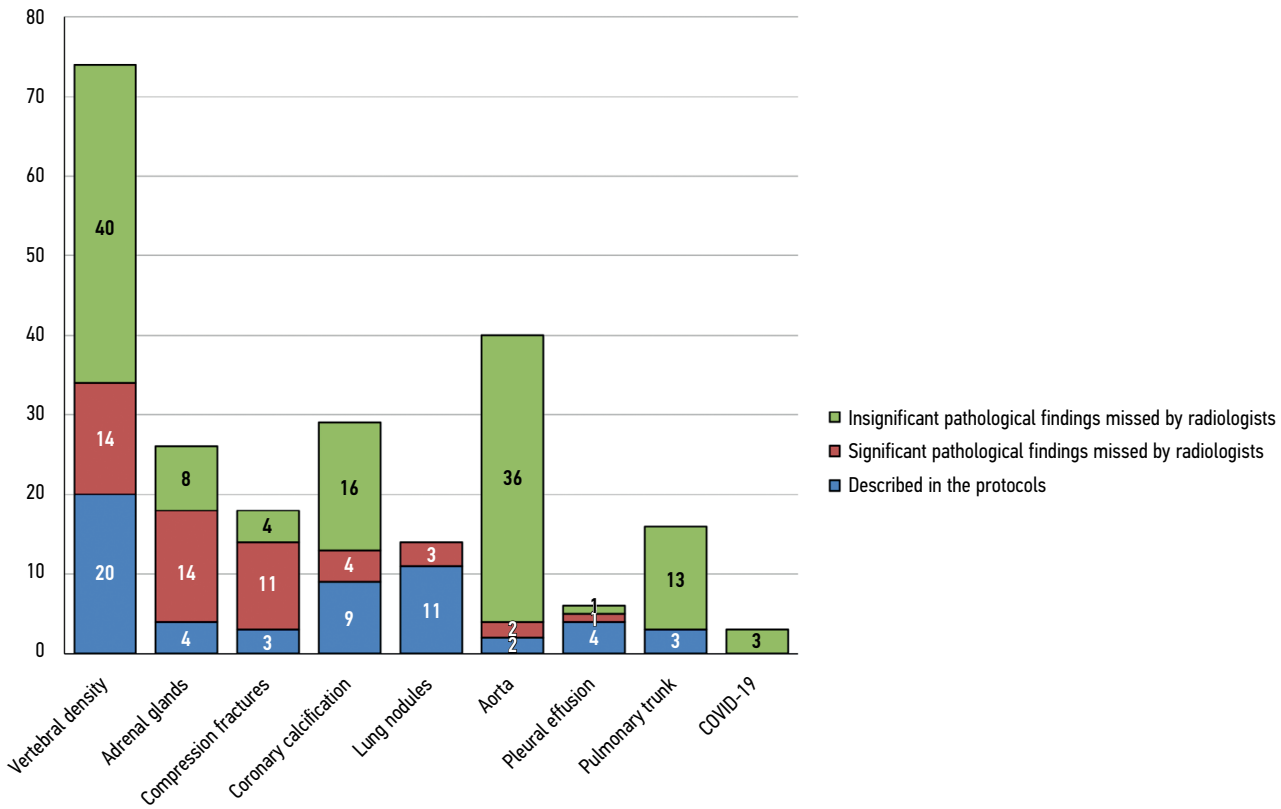

Fig. 3. Number of findings (ranked by the number of significant missed pathological findings).

Table 3. Summary data on the number of patients with detected and missed pathological findings

Parameter	Number	Total cases, %	Pathological findings assessment, %
Total patients	160	100	-
Without pathological findings	70	44	-
With pathological findings	90	56	100
A radiologist in the clinic has detected at least one pathological finding of those detected by AI.	35	22	39
A radiologist in the clinic has missed at least one pathological finding of those detected by AI.	81	51	90
Computed tomography examinations in which abnormal changes were detected only by an AI algorithm.	55	34	61

An example of calculating the CNMS

A radiologist in the clinic correctly described the pulmonary trunk dilation up to 34 mm, an increased Agatston score up to 350, and decreased density of the vertebrae to a maximum of +90 HU. The AI algorithm also detected these pathological findings. The AI algorithm also detected pathological findings that were not described in the radiologist's protocol, such as a lung nodule up to 10 × 9 mm, thoracic aorta dilatation up to 45 mm, and adrenal gland thickening up to 14 mm. An example of CNMS calculation for this case is presented in Table 8.

Additional data

Final data on the number of protocols with significant and insignificant missed pathological findings and the percentage of erroneous protocols are presented in Table 9. For the protocol, both significant, and insignificant missed pathological findings could be found. Of the 160 analyzed protocols, significant, and insignificant pathological findings were missed in 81 protocols, i.e., 50.6% of the total number of CT scans. The average percentage of protocols was 28.1% with significant missed pathological findings (max, 56.9; min, 5) and 27.2% with insignificant missed pathological findings (max, 74.1; min, 5).

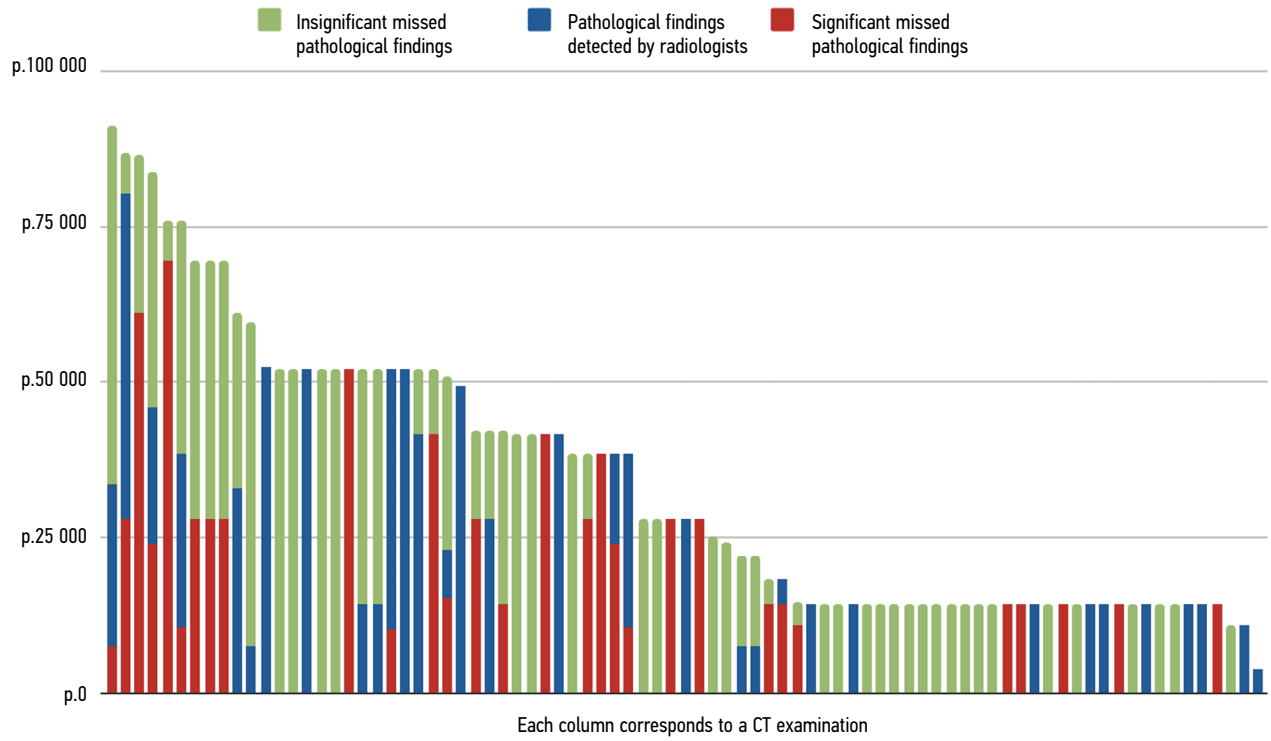

Fig. 4. Analysis of the cost of medical services not provided because of missed pathological findings, and all CT scans performed.

Table 4. Comparison of two diagnostic approaches to detect pathological findings

Parameters	Number of cases detected	Percentage [95% CI]	95% CI for proportion difference	*p* Z-test H0: proportions are equal (Bonferonni adjustment)
Signs of COVID-19 according to CT				
Algorithm + Expert	3	0,016 [0,003; 0,047]	[-0,008; 0,04]	0,246 (1)
Protocol	0	0 [0; 0,02]	-	-
Lung nodules				
Algorithm + Expert	15	0,082 [0,047; 0,132]	[-0,036; 0,08]	0,542 (1)
Protocol	11	0,06 [0,031; 0,106]	-	-
Effusion				
Algorithm + Expert	6	0,033 [0,012; 0,07]	[-0,028; 0,05]	0,749 (1)
Protocol	4	0,022 [0,006; 0,055]	-	-
Aorta				
Algorithm + Expert	40	0,22 [0,162; 0,287]	[0,141; 0,276]	<0,001 (<0,001)
Protocol	2	0,011 [0,001; 0,039]	-	-
Pulmonary trunk				
Algorithm + Expert	16	0,088 [0,051; 0,139]	[0,021; 0,122]	0,005 (0,042)
Protocol	3	0,016 [0,003; 0,047]	-	-

Table 4. Ending

Parameters	Number of cases detected	Percentage [95% CI]	95% CI for proportion difference	*p* Z-test H0: proportions are equal (Bonferonni adjustment)
Coronary calcification				
Algorithm + Expert	29	0,159 [0,109; 0,221]	[0,043; 0,177]	0,001 (0,01)
Protocol	9	0,049 [0,023; 0,092]	-	-
Vertebral compression fractures				
Algorithm + Expert	18	0,1 [0,06; 0,152]	[0,03; 0,135]	0,002 (0,015)
Protocol	3	0,016 [0,003; 0,047]	-	-
Assessment of the mineral density of the vertebral bodies				
Algorithm + Expert	74	0,407 [0,335; 0,482]	[0,207; 0,387]	<0,001 (<0,001)
Protocol	20	0,11 [0,068; 0,165]	-	-
Thickening of adrenal glands				
Algorithm + Expert	26	0,143 [0,095; 0,202]	[0,06; 0,181]	<0,001 (0,001)
Protocol	4	0,022 [0,006; 0,055]	-	-

Table 5. Analysis of the estimated cost of non-provided medical services from all missed CT findings

Parameter	Calculation for all patients of the pilot project (rubles/US dollars/renminbi)				Calculation per one patient (rubles/US dollars/renminbi)			
	Cost							
	Total (all)	Consultations (all)	Additional examinations (all)	Follow-up (all)	Total (all)	Consultations (all)	Additional examinations (all)	Follow-up (all)
Cost of the "second step" of diagnostics for all pathological findings	2 847 760/ 37 250,99/ 256 217,95	463 300/ 6060,34/ 41 683,91	2 049 760/ 26 812,51/ 184 420,49	334 700/ 4378,15/ 30 113,54	17 799/ 232,83/ 1601,41	2896/ 37,88/ 260,56	12 811/ 167,58/ 1152,63	2092/ 27,37/ 188,22
Cost of the second step only for those pathological findings that were missed by a radiologist and detected by the AI algorithm	2 065 360/ 27 016,57/ 185 824,05	326 800/ 4274,81/ 29 402,77	1 519 460/ 19 875,76/ 136 708,47	219 100/ 2866/ 19 712,81	12 909/ 168,86/ 1161,45	2043/ 26,72/ 183,81	9497/ 124,23/ 854,46	1369/ 17,91/ 123,17
Cost of the second step for pathological findings detected by radiologists	782 400/ 10 234,42/ 70 393,9	136 500/ 1785,53/ 12 281,14	530 300/ 6936,75/ 47 712,02	115 600/ 1512,14/ 10 400,73	4890/ 63,97/ 439,96	853/ 11,16/ 76,75	3314/ 43,35/ 298,17	723/ 9,46/ 65,05

The total number of protocols was associated with statistically significant increase in the number of errors. The total work experience in radiology (excluding residency) and thoracic radiology (including residency) was associated with a decrease in the number of errors. However, these data are not representative because of the small sample of radiologists and the presence of a dominant case. Detailed data on the experience of specialists are presented in

Table 6. Cons of medical services not provided due to missed significant pathological findings

Parameter	Calculations for all patients of the pilot project (RUB / $ / CNY)				Calculations per one patient (RUB/$/CNY)			
	Cost							
	Total (all)	Consultations (all)	Additional examinations (all)	Follow-up (all)	Total (all)	Consultations (all)	Additional examinations (all)	Follow-up (all)
Cost of the second step for significant pathological findings missed by radiologists	770 855/ 10 083,4/ 69 355,17	113 100/ 1479,44/ 10 175,8	584 255/ 7642,53/ 52 566,44	73 500/ 961,44/ 6612,92	4818/ 63,02/ 433,48	707/ 9,25/ 63,61	3652/ 47,77/ 328,58	459/ 6/ 41,3
Cost of the second step for pathological findings detected by radiologists	782 400/ 10 234,42/ 70 393,9	136 500/ 1785,53/ 12 281,14	530 300/ 6936,75/ 47 712,02	115 600/ 1512,14/ 10 400,73	4890/ 63,97/ 439,96	853/ 11,16/ 76,75	3314/ 43,35/ 298,17	723/ 9,46/ 65,05

Table 7. Cost-effectiveness

Cohort	Statistics	Cost			*p* (paired t-test)
		Total (all)	Total (findings by radiologists)	Mean difference with 95% CI	
Full cohort	*n*	160	160	12 908,5	<0,001
	Mean	17 798,5	4890	[9833,5; 15 983,5]	
	SD	23 304,74	11 945	-	
	Minimum	0	0	-	
	First quartile	0	0	-	
	Median	12 635	0	-	
	Third quartile	27 900	0	-	
	Maximum	91 095	52 420	-	
	Percentage of zero values	46,88	79,38	-	
Cohort with all detected pathological findings	*n*	81	81	24 298,4 [19 701,9; 28 894,8]	<0,001
	Mean	33 503,06	9204,71		
	SD	22 262,46	15 162,13	-	
	Minimum	3900	0	-	
	First quartile	14 395	0	-	
	Median	27 900	0	-	
	Third quartile	51 995	14 395	-	
	Maximum	91 095	52 420	-	
	Percentage of zero values	-	61,18	-	
Cohort with significant pathological findings	*n*	32	32	17 104,7	<0,001
	Mean	24 089,22	6984,53	[8726,8; 25 482,6]	
	SD	15 568,37	13 799,84	-	
	Minimum	7600	0	-	
	First quartile	14 395	0	-	
	Median	19 700	0	-	
	Third quartile	27 900	4825	-	
	Maximum	69 500	52 420	-	
	Percentage of zero values	-	71,88	-	

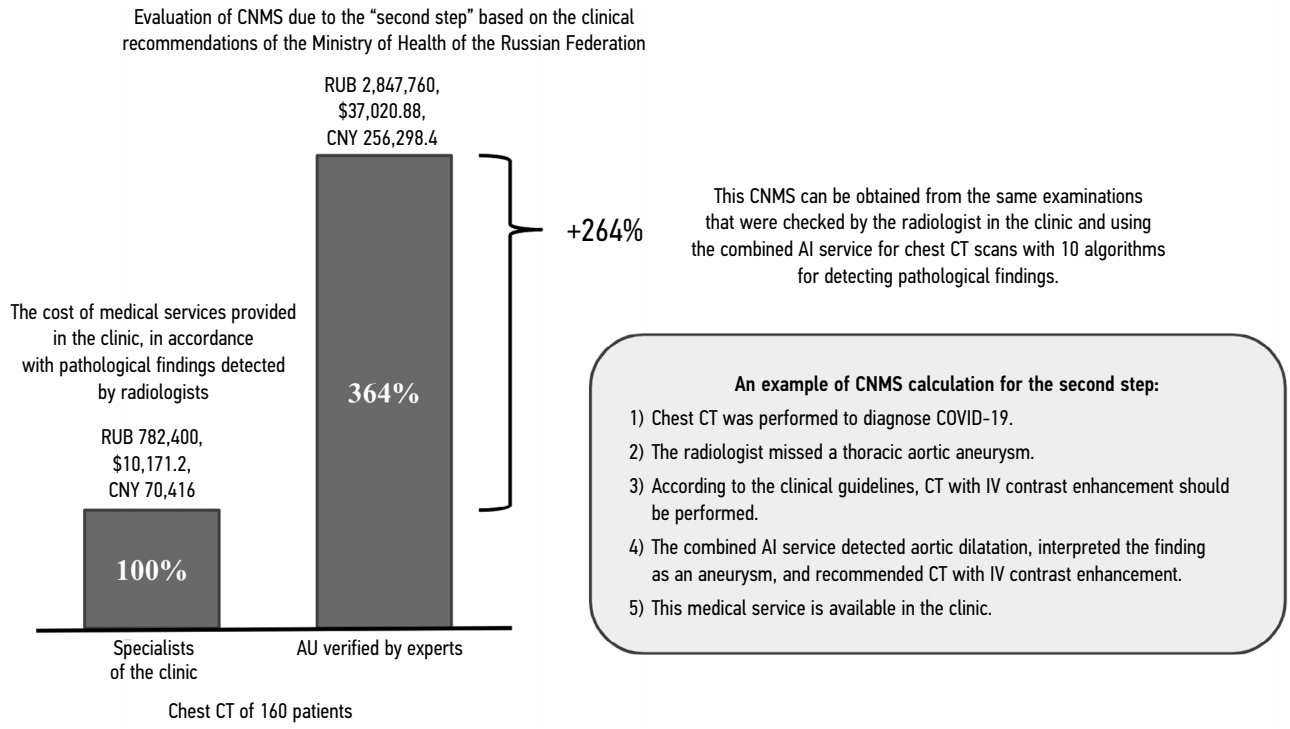

Fig. 5. Range of costs of medical services not provided due to the use of the combined AI service for chest CT scans in a clinic. AI, artificial intelligence; CT, computed tomography; CNMS, cost of non-provided medical services.

supplementary materials (Tables 10, 11). Examples of AI algorithm use are presented in Fig. 6, 7.

Adverse events

In this study, no adverse events were noted.

DISCUSSION

Summary of the primary study outcome

For the first time, this study showed the expected economic effect of using a combined AI-based software product for the analysis of chest CT data. The estimated economic effect is based on CNMS assessment.

Medical services should be provided to patients in accordance with current clinical guidelines. The total CNMS of the "second step" of the necessary diagnostics for pathological findings missed by radiologists and detected by AI was just over 2 million rubles, or 3.6 times more than the cost of medical services that could be provided by the clinic based on CT findings detected by radiologists in 160 patients. According to the calculation model used, only the CNMS, as significant missed pathological findings were slightly more than 770 thousand rubles, according to the price list of the clinic, or 98% more than the CNMS that the clinic could provide based on incidental findings.

In addition, the possibility of using combined AI-based software was proven for auditing CT description protocols.

Discussion of primary study outcome

An analysis of socioeconomic burden of the COVID-19 pandemic can show an example of significant social and economic consequences of a mass disease for the Russian healthcare system and society, and this require focusing attention not only on the clinical aspects but also on the economic importance of investing in disease control strategies [32]. According to experts, the social, and economic burden of COVID-19 in the Russian Federation in 2020 was approximately 5.4 trillion rubles (5% of the nominal GDP in 2020), which corresponds to 2486.30 years of life lost due to premature mortality (YLL) in men and 1378.22 YLL in women [32]. In 2020, the economic burden of non-communicable diseases in the Russian Federation was four trillion rubles, whereas the damage from chronic diseases is comparable to the entire healthcare budget of the Russian Federation, and funds saved through effective prevention could become a huge additional resource for the development of the country.[7]

In the available literature, no studies have evaluated the effect of combined AI analysis of chest CT on the economic aspects of clinic activities.

[7] Medvestnik [Internet]. The economic burden of non-communicable diseases in Russia has grown by a trillion rubles in two years [Ekonomicheskoye bremya neinfektsionnykh zabolevaniy v Rossii vyroslo za dva goda na trillion rubley] (cited: June 04, 2021). Available from: https://medvestnik.ru/content/news/Ekonomicheskoe-bremya-neinfekcionnyh-zabolevanii-v-Rossii-vyroslo-za-dva-goda-na-trillion-rublei.html.

Table 8. An example of calculating the cost of non-provided medical services based on data of one chest CT

Recommendations and cost for all pathological findings detected in patients						
Consultations (all)	**Additional examinations (all)**	**Over time monitoring findings (all)**	**Стоимость**			
			Total (all)	**Consultations (all)**	**Additional examinations (all)**	**Over time monitoring findings (all)**
Consultation by cardiologists orendocrinologists	Stress ECG, AP activity, CBC, calcium, abdomen ultrasonography, coronary CT angiography, stress echocardiography, hormonal activity of an adrenal tumor, echocardiography, blood biochemistry, CT with intravenous contrast enhancement	CT over time, consultations of the endocrinologist	**RUB 91,095 $1,191.6 CNY 8,195.98**	RUB 7,800 $102.03 CNY 701.78	RUB 71,795 $939.14 CNY 6,459.52	RUB 11,500 $150.43 CNY 1,034.68
Recommendations and costs for pathological findings missed by radiologists and detected by AI						
Consultations	**Additional examinations**	**Follow-up monitoring**	**Cost**			
			Total	**Consultations**	**Additional examinations**	**Follow-up monitoring**
-	Stress ECG, coronary CT angiography, stress echocardiography, hormonal activity of the adrenal tumor, echocardiography, and CT with intravenous contrast enhancement	CT over time	**RUB 65,300 $854.18 CNY 5,875.16**	0	RUB 57,700 $754.76 CNY 5,191.37	RUB 7,600 $99.41 CNY 683.79
Recommendations and cost for pathological findings detected by radiologists						
Consultation by cardiologist, endocrinologist	AP activity, CBC, calcium, abdomen ultrasound, and blood biochemistry	Consultation of an endocrinologist	**RUB 25,795 $337.42 CNY 2,320.82**	RUB 7,800 $102.03 CNY 701.78	RUB 14,095 $184.37 CNY 1,268.15	RUB 3,900 $51.02 CNY 350.89

Note. AP, alkaline phosphatase; CBC, complete blood count; CT, computed tomography; EchoCG, echocardiography.

Table 9. Results by the number of protocols with significant and non-significant missed pathological findings

No. of the radiologist	Total number of protocols prepared	Number of protocols with insignificant missed pathological findings (%)	Number of protocols with significant missed pathological findings (%)	Total number of protocols with significant and insignificant missed pathological findings (%)
Physician 2	58	33 (56,9)	28 (48,3)	47 (81)
Physician 5	23	7 (30,4)	9 (39,1)	11 (39,1)
Physician 3	23	7 (30,4)	7 (30,4)	13 (56,5)
Physician 1	16	2 (12,5)	3 (18,7)	5 (31)
Physician 6	20	1 (5)	1 (5)	2 (10)
Physician 7	18	1 (5,5)	1 (5,5)	2 (11,1)
Physician 4	2	1 (50)	1 (50)	1 (50)
Total	160	52 (32,5)	50 (31,2)	81 (50,6)

Pickhardt et al. [33] built a model of the cost and clinical effectiveness of combined AI screening with abdomen CT. Based on the expected disease prevalence, probability of transition between health conditions, associated healthcare costs, and treatment effectiveness in three diseases (CVD, osteoporosis, and sarcopenia), three mutually exclusive screening models were evaluated: (1) ignoring outcomes ("do not treat"; no intervention regardless of CT findings),

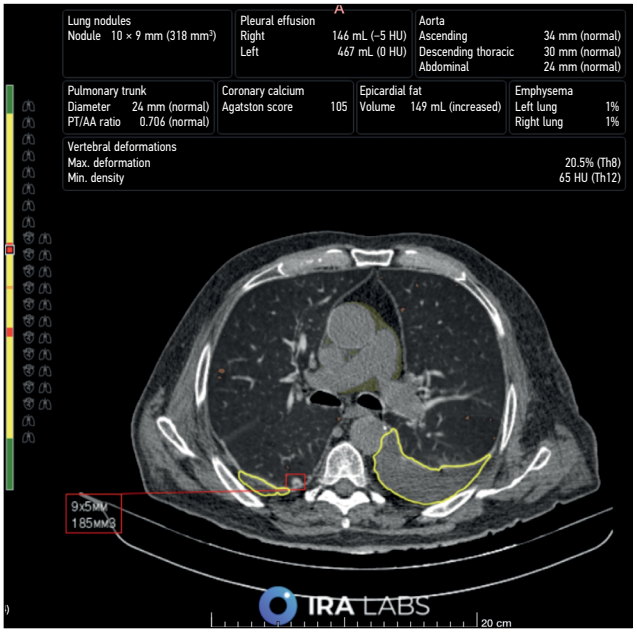

Fig. 6. An example of AI use. Patient B, 76 years old. A radiologist correctly identified bilateral hydrothorax and emphysematous changes but did not describe the lung nodule in the right lung. An AI algorithm revealed all three pathological findings: hydrothorax is highlighted with a yellow line, emphysematous changes are highlighted in orange, and the lung nodule is indicated by a red square.

(2) statin therapy for all ("treat all" for the prevention of CVD without considering CT findings), and (3) opportunistic screening for CVD, osteoporosis, and sarcopenia with AI-based abdomen CT (targeted treatment for at-risk individuals). For baseline scenarios in simulated in 10-year groups of 55-year-old men and women, AI-based opportunistic CT screening proved to be a cost effective and more clinically effective strategy the than "ignoring" and "treating all" approaches. Thus, AI-based opportunistic CT screening appears to be a highly cost effective and clinically effective strategy with a wide range of input assumptions and cost savings in most scenarios. However, compared with our study, a really working combined AI service was not presented. In addition, our study used the combined AI service for 10 target pathological findings, whereas the mentioned paper reviewed three diseases. In this regard, there are reasons to expect an increase in the potential cost-effectiveness of using AI, combined with its positive effect on diagnostics.

Few publications have examined the economic effect of such programs using an integrated approach for several pathological findings without using AI systems. For example, in the Netherlands, a comprehensive low-dose CT screening of three diseases, such as lung cancer, chronic obstructive pulmonary disease, and CVD in people aged 50–75, could be cost effective if its cost is <971 euros per patient [34]. In a 5-year study of nearly 7,500 low-dose CT scans, extrapulmonary malignant tumors incidentally detected during lung cancer screening were on early stages and had favorable outcomes, and additional examinations required much less cost than in cases with later stages [35]. Thus, the analysis of the costs of additional diagnostic and therapeutic measures associated with extrapulmonary changes detected during low-dose CT of lung cancer is

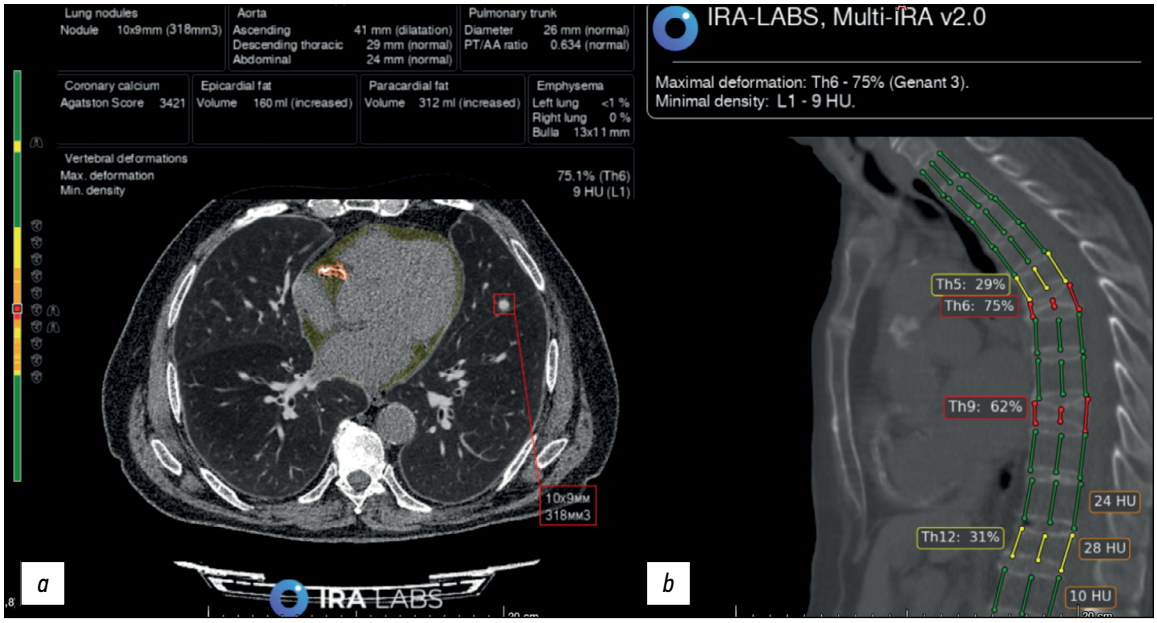

Fig. 7. An example of AI use. Patient B., 79 years old. Chest CT scans: *a*) axial section: a radiologist and an algorithm correctly identified a lung nodule in the left lung (indicated by a red square) and coronary calcification (outlined by an orange line). In addition, the algorithm indicated an increase in the volume of epicardial fat (filled in yellow; this pathological finding was not considered in the study); *b*) sagittal section: a radiologist and an algorithm correctly identified compression fractures of Th6 and Th9 vertebral bodies, Genant 3 (three columns are marked with red lines); however, the radiologist did not indicate deformities of Th5 and Th12 vertebral bodies, Genant 2 (three columns are marked with yellow lines) in the protocol.

one of the main steps in proving the cost-effectiveness of such measures. This approach (despite the limited lung cancer screening using chest CT) allows proposing the use of combined AI services to improve the diagnostic effectiveness and cost-effectiveness of examinations.

This study also used the combined AI service to detect 10 pathological findings. Such reserve analysis techniques are useful in making informed decisions about further research [36-38]. These analysis techniques are recommended for diagnostic intervention and evidence development to optimize data collection and more accurately estimate long-term economic health effect as a large amount of clinical data become available.

Before the COVID-19 pandemic, AI algorithms were used to detect radiologic symptoms for disease detection, classification, image optimization, radiation dose reduction, and workflow improvement [39]. Medical studies on the effectiveness of AI make such programs more understandable, more efficient, safer, and more integrated into medical staff workflows [40]. Currently, studies are ongoing in the IMALife project, which evaluates the decrease in mortality not only from lung cancer but also from the consequences of emphysema (a biomarker of chronic obstructive pulmonary disease) and coronary calcification (a biomarker of atherosclerosis) [41].

At present, AI effectiveness was evaluated for the detected target pathological finding. Ziegelmayer et al. [42] showed a negative incremental cost-effectiveness ratio (ICER) in the baseline CT+AI scenario compared with CT, demonstrating lower costs, and higher efficiency. To support the use of AI, threshold analysis showed that ICER remained negative until the $68 threshold. Therefore, the use of a monosystem for the analysis of low-dose CT data using AI for lung cancer screening is a reasonable diagnostic strategy in terms of cost-effectiveness.

The constantly growing volume of radiological examinations provides additional burden on radiologists [43]. Excessive workload can increase the likelihood of errors and deteriorate the quality of care [44]. An audit system with a retrospective double review of studies is widely used in radiology. A RADPEER system of the American Society of Radiology is the best-known system [45]. However, according to Lauritzen et al. [46], double reading of the 1/3 of examinations performed at their clinic takes 20%–25% of the working time of HCPs. AI algorithms can significantly reduce the time for examination review and increase audit volume and quality. However, the algorithm used should have the minimum number of false-positive errors. The use of AI had some effects on the quality of work of radiologists such as a change in the lung lesion severities in the case of suspected COVID-19 toward a decrease in the proportion of severe and critical lung lesions [47].

Our study also demonstrated the feasibility of using combined AI services for study description audit and identified >28% of protocols with significant missed pathological findings and 27% of protocols with non-significant missed pathological findings. For CT, radiologists in the clinic provide information on the main diagnostic tasks for which patients were referred to scan. In the clinic where our study was conducted, radiologists did not have tools at all workstations for quick measurement of the Agatston score, and the measurement of the density of the vertebral bodies was not included in the standard description of examinations performed in this radiology department. In addition, the average error rate was comparable between radiologists; thus, by dismissing 1–2 radiologists with the worst results according to audits, the clinic will not solve the problem of missing pathological findings.

In this study, the economic effect was calculated without considering AI costs and cost of AI validation by experts. These expenses are variable and depend on the number of algorithms, level of experts involved, and other factors. Any rate for the AI-based service will be cost effective, provided that the total expenses are lower than the profit obtained by a clinic using AI (Fig. 8). However, such an analysis is beyond the scope of this study.

Study Limitations

This pilot study has several limitations. The study has a retrospective design and evaluates the maximum potential CNMS of a private healthcare organization in accordance with recommendations for abnormal findings. In practice, not all patients tend to comply with doctor's recommendations, particularly when additional paid examinations and consultations are required. In addition, each clinic has its conversion that is not evaluated in this study.

This study aimed to estimate the cost of the "second step" without the cost of the "third" and subsequent steps, i.e., the cost of treatment and rehabilitation was not considered. However, for nearly all pathologies that the combined AI service can detect, the cost of treatment significantly exceeds the cost of the "second stage." Every clinic has many factors that affect the quality of medical personnel work. The quality of work parameter (number of missed clinically significant radiographic findings) can vary depending on the experience of the radiologists, number of examinations per day, time of day, day of the week, and many other additional factors that can affect knowledge level, attentiveness, and readiness of the radiologist to include in the protocol all abnormal findings and reasonable recommendations for the "second step."

This study did not evaluate the potential for false-negative AI findings because the combined AI service used was validated during independent testing by employing closed datasets of the Moscow experiment, and the selected AI settings were found to be acceptable and calibrated for subsequent use.

The aim of this study was not to assess the economic effect at the level of city and federal healthcare systems. However, each clinic in the Russian Federation has some

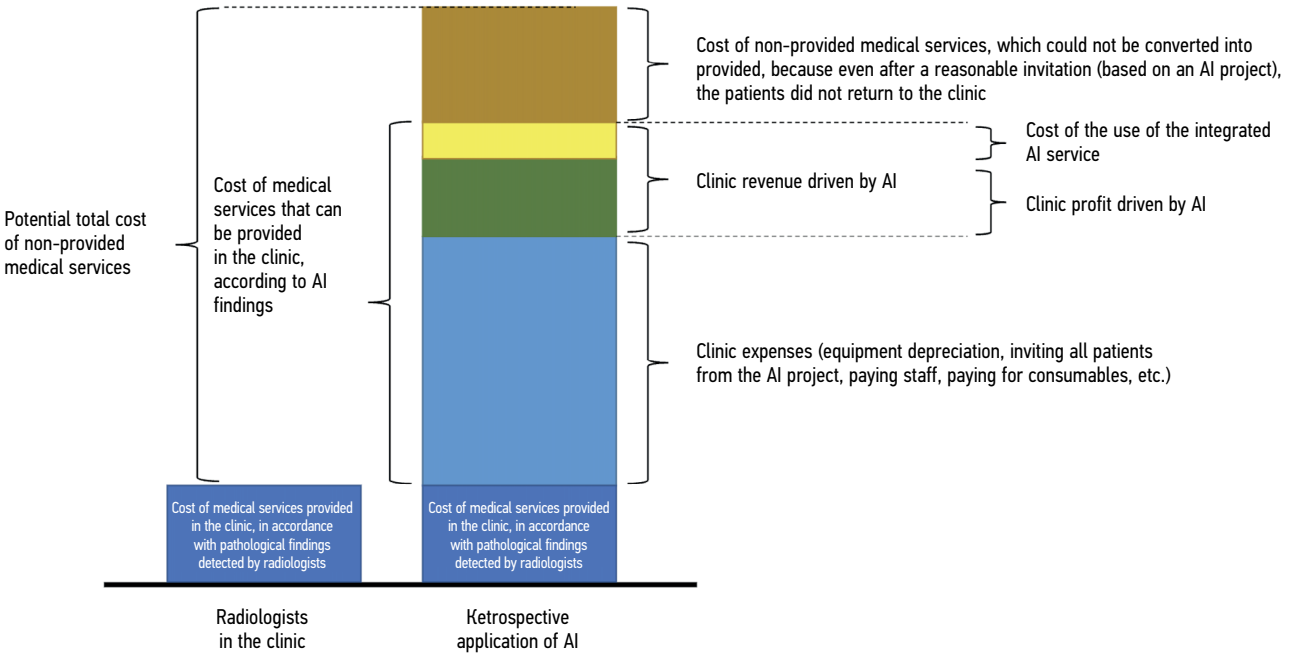

Fig. 8. Potential cost of medical services not provided because a combined AI service was not used for chest CT scans in a clinic, considering the cost of using AI.

opportunities to provide paid medical services supported by evidence-based medicine principles. This study did not evaluate compliance of patients according to invitations based on a retrospective analysis, whereas the findings are closely related to the time intervals between CT and the "second step."

CONCLUSION

A combined AI service can be used as an additional tool for radiologists when analyzing chest CT data to better detect 10 common and significant types of abnormal findings. When using such an approach, CNMS is 3.6 times larger than the standard operation model of radiologists not using AI.

Opportunistic screening of multiple diseases requires a detailed investigation of comorbidities to determine the optimal target group for diagnostic intervention using combined AI services. Combined AI solutions for chest CT are highly likely to be cost effective because such an approach allows the detection of various significant abnormal changes that require additional healthcare services.

ADDITIONAL INFORMATION

Funding source. This article was not supported by any external sources of funding.

Competing interests. The authors declare that they have no competing interests.

Authors' contribution. The authors confirm that their authorship complies with the international ICMJE criteria (all authors contributed significantly to developing the concept, research, and preparation of the article and read and approved the final version before publication).

Chernina V.Yu. — search for publications on the article's topic, formation of a data set, writing the text of the manuscript; Belyaev M.G. — expert evaluation of the data, manuscript's text editing; Silin A.Yu. — the concept of the study; Pyatnitskiy I.A. — manuscript's text editing; English text translation; Avetisov I.O., Petrash E.A. — manuscript's text editing; Basova M.V. — formation of a data set, processing of research results; Sinitsyn V.E. — expert evaluation of the data, manuscript's text editing; Omelyanovsky V.V. — expert evaluation data; Gombolevsky V.A. — the concept of the study, expert evaluation of data, manuscript's text writing, approval of the final version.

Acknowledgments. The authors' team would like to gratefully acknowledge Maksim E. Pisov, Technical Director of IRA Labs, and the development team (Proskurov V.A., Samoilenko A.I., Borzov A.S., Bukharaev A.N., Goncharov M.Y., Shirokikh B.N., Kurmukova A.I., Nachinkin I.A., Telepov A.Y., Shimovolos S.A., Donskova M.A., Samokhin V.Y., Shevtsova A.E., Yaushev F., Tkachenko S.M, Zakharov A.A., Saparov T.N., Filipenko V.K. Tomin V.D., Tomin J.D., Samoilenko A.I., Malevannu V.M., Leonov A.Yu, Nogova D.S., Bazarova A.I., Marakhovsky K.V., Belkov A.S., Vasin A.A., Berezhnaya D.S., Musikhin M.M.); Maria N. Dugova, Medical Director, and the team of medical experts (Ilyicheva D.V., Sevrukov D.D., Shchipakhina Y.A, Lyubimaya Y.O., Aleshina O.O., Tsybulskaya Y.A.); Mikhail S. Lamzin, Chief Operating Officer; Regina R. Gareeva, Product Manager, and Elena V. Panina, Deputy Director for Business Development.

REFERENCES

1. Aberle DR, Adams AM, Berg CD, et al.; National Lung Screening Trial Research Team. Reduced lung-cancer mortality with low-dose computed tomographic screening. *N Engl J Med*. 2011;365(5):395–409. doi: 10.1056/NEJMoa1102873

2. Pastorino U, Silva M, Sestini S, et al. Prolonged lung cancer screening reduced 10-year mortality in the MILD trial: new confirmation of lung cancer screening efficacy. *Ann Oncol*. 2019;30(7):1162–1169. doi: 10.1093/annonc/mdz117

3. Grover H, King W, Bhattarai N, et al. Systematic review of the cost-effectiveness of screening for lung cancer with low dose computed tomography. *Lung Cancer*. 2022;170:20–33. doi: 10.1016/j.lungcan.2022.05.005

4. Nikolaev AE, Gombolevskiy VA, Gonchar AP, et al. Incidental findings during lung cancer screening by low-dose computed tomography. *Tuberculosis Lung Dis*. 2018;96(11):60–67. (In Russ). doi: 10.21292/2075-1230-2018-96-11-60-67

5. Kilsdonk ID, de Roos MP, Bresser P, et al. Frequency and spectrum of incidental findings when using chest CT as a primary triage tool for COVID-19. *Eur J Radiol Open*. 2021;(8):100366. doi: 10.1016/j.ejro.2021.100366

6. Beltsevich DG, Melnichenko GA, Kuznetsov NS, et al. Russian Association of Endocrinologists clinical practice guideline for adrenal incidentalomas differential diagnosis. *Endocrine Sur*. 2016;10(4):31–42. (In Russ). doi: 10.14341/serg2016431-42

7. Emphysema of the lungs. Clinical recommendations (approved by the Ministry of Health of the Russian Federation, 2021). (In Russ). Available from: https://www.garant.ru/products/ipo/prime/doc/402775957/. Accessed: 25.08.2021.

8. Thoracic and thoracoabdominal aortic aneurysms. Clinical recommendations (approved by the Ministry of Health of the Russian Federation, 2023). (In Russ). Available from: https://www.angiolsurgery.org/library/recommendations/2022/aneurysms_thoracic_thoracoabdominal_aorta/recommendation.pdf. Accessed: 25.08.2021.

9. Vasiliev YuA, Vladzimirsky AV, Arzamasov KM, et al. Computer vision in radiation diagnostics: the first stage of the Moscow experiment. Monograph. 2nd ed., revised and updated. Ed. by Yu.A. Vasiliev, A.V. Vladzimirsky. Moscow: Izdatel'skie resheniya; 2023. 376 p. (In Russ).

10. Zakharov A, Pisov M, Bukharaev A, et al. Interpretable vertebral fracture quantification via anchor-free landmarks localization. *Med Image Anal*. 2023;(83):102646. doi: 10.1016/j.media.2022.102646

11. Goncharov M, Pisov M, Shevtsov A, et al. CT-Based COVID-19 triage: Deep multitask learning improves joint identification and severity quantification. *Med Image Anal*. 2021;(71):102054. doi: 10.1016/j.media.2021.102054

12. Shirokikh B, Shevtsov A, Dalechina A, et al. Accelerating 3D medical image segmentation by adaptive small-scale target localization. *J Imaging*. 2021;7(2):35. doi: 10.3390/jimaging7020035

13. Goncharov M, Pisov M, Belyaev M, et al. Quantification of epicardial adipose tissue in low-dose computed tomography images. *Lecture Notes Electrical Engineering*. 2022;784(1):98–107. doi: 10.1007/978-981-16-3880-0_11

14. Husereau D, Drummond M, Augustovski F, et al.; CHEERS 2022 ISPOR Good Research Practices Task Force. Consolidated health economic evaluation reporting standards 2022 (cheers 2022) statement: Updated reporting guidance for health economic evaluations. *Value Health*. 2022;25(1):3–9. doi: 10.1016/j.jval.2021.11.1351

15. Morozov SP, Vladzimirsky AV, Kljashtorny VG, et al. Clinical trials of software based on intelligent technologies (radiology diagnostics). Preprint № CDT-2019-1. Best Practice in Radiation Oncology and Instrumental Diagnostics. Vol. 23. Moscow: Center for Diagnostics and Telemedicine; 2019. 33 p. (In Russ).

16. Gombolevskiy VA, Blokhin IA, Laipan AS, et al. Methodological guidelines for lung cancer screening. Best Practice in Radiation and Instrumental Diagnostics. Vol. 56. Moscow: Center for Diagnostics and Telemedicine; 2020. 57 p. (In Russ).

17. Morozov SP, Protsenko DN, Smetanina SV, et al. Radiation diagnosis of coronavirus disease (COVID-19): Organization, methodology, interpretation of results: Guidelines. Best Practices in Radiation and Instrumental Diagnostics Series. Vol. 65. Moscow: Center for Diagnostics and Telemedicine; 2020. 78 p. (In Russ).

18. Temporary methodological recommendations. Prevention, diagnosis and treatment of new coronavirus infection (COVID-19). Ministry of Health of the Russian Federation. Version 17 (12/14/2022). (In Russ). Available from: https://static-0.minzdrav.gov.ru/system/attachments/attaches/000/061/254/original/%D0%92%D0%9C%D0%A0_COVID-19_V17.pdf?1671088207. Accessed: 17.03.2023.

19. Lynch DA, Austin JH, Hogg JC, et al. CT-definable subtypes of chronic obstructive pulmonary disease: A statement of the Fleischner Society. *Radiology*. 2015;277(1):192–205. doi: 10.1148/radiol.2015141579

20. Hersh CP, Washko GR, Estépar RS, et al. Paired inspiratory-expiratory chest CT scans to assess for small airways disease in COPD. *Respir Res*. 2013;146(1):42. doi: 10.1186/1465-9921-14-42

21. Walker C, Chung JH. Muller's imaging of the chest e-book: Expert radiology series. Elsevier Health Sciences; 2018.1104 p.

22. Erbel R, Aboyans V, Boileau C et al. ESC Committee for Practice Guidelines. 2014 ESC Guidelines on the diagnosis and treatment of aortic diseases: Document covering acute and chronic aortic diseases of the thoracic and abdominal aorta of the adult. The task force for the diagnosis and treatment of aortic diseases of the European society of cardiology (ESC). *Eur Heart J*. 2014;35(41):2873–2926. doi: 10.1093/eurheartj/ehu281

23. Wanhainen A, Verzini F, Van Herzeele I, et al. Clinical practice guidelines on the management of abdominal aorto-iliac artery aneurysms. *Eur J Vascul Endovascul Sur*. 2019;57(1):8–93. doi: 10.1016/j.ejvs.2018.09.020

24. Jurgens PT, Carr JJ, Terry JG, et al. Association of abdominal aorta calcium and coronary artery calcium with incident cardiovascular and coronary heart disease events in black and white middle-aged people: The coronary artery risk development in young adults study. *J Am Heart Assoc*. 2021;10(24):23–37. doi: 10.1161/JAHA.121.023037

25. Galiè N, Humbert M, Vachiery JL, et al. 2015 ESC/ERS Guidelines for the diagnosis and treatment of pulmonary hypertension: The joint task force for the diagnosis and treatment of pulmonary hypertension of the European society of cardiology (ESC) and the European respiratory society (ERS): Endorsed by: Association for European paediatric and congenital cardiology (AEPC), international society for heart and lung transplantation (ISHLT). *Eur Respir J*. 2015;46(4):903–975. doi: 10.1183/13993003.01032-2015

26. Agatston AS, Janowitz WR, Hildner FJ et al. Quantification of coronary artery calcium using ultrafast computed tomography. *J Am Coll Cardiol*. 1990;15(4):827–832. doi: 10.1016/0735-1097(90)90282-t

27. Zhuravlev KN. Coronary CT angiography. Best practices in radiation and instrumental diagnostics series. Vol. 65. Moscow: Center for Diagnostics and Telemedicine; 2020. 35 p. (In Russ).

28. Mayo-Smith WW, Song JH, Boland GL, et al. Management of incidental adrenal masses: A white paper of the ACR incidental findings committee. *J Am Coll Radiol*. 2017;14(8):1038–1044. doi: 10.1016/j.jacr.2017.05.001
29. Belaya ZE, Belova KYu, Biryukova EV, et al. Federal clinical guidelines for diagnosis, treatment and prevention of osteoporosis. *Osteoporosis Bone Diseases*. 2021;24(2):4–47. (In Russ). doi: 10.14341/osteo12930
30. Genant HK, Jergas M. Assessment of prevalent and incident vertebral fractures in osteoporosis research. *Osteoporosis Int*. 2003;14(3):43–55. doi: 10.1007/S00198-002-1348-1
31. Pathological fractures complicating osteoporosis. Clinical recommendations. Moscow; 2018. 90 p. (In Russ). Available from: https://neirodoc.ru/wp-content/uploads/2019/10/patologicheskie-perelomy-oslozhnyayuschie-osteoporoz-2018.pdf. Accessed: 17.03.2023.
32. Kolbin AS, Gomon YuM, Balykina YuE, et al. Socioeconomic and global burden of COVID-19. *Good Clin Pract*. 2021;(1):24–34. (In Russ). doi: 10.37489/2588-0519-2021-1-24-34
33. Pickhardt PJ, Correale L, Hassan C. AI-based opportunistic CT screening of incidental cardiovascular disease, osteoporosis, and sarcopenia: Cost-effectiveness analysis. *Abdom Radiol (NY).* 2023;(3):1181–1198. doi: 10.1007/s00261-023-03800-9
34. Behr CM, Koffijberg H, Degeling K, et al. Can we increase efficiency of CT lung cancer screening by combining with CVD and COPD screening? Results of an early economic evaluation. *Eur Radiol*. 2022;32(5):3067–3075. doi: 10.1007/s00330-021-08422-7
35. Chintanapakdee W, Mendoza DP, Zhang EW, et al. Detection of extrapulmonary malignancy during lung cancer screening: 5-year analysis at a tertiary hospital. *J Am Coll Radiol*. 2020;17(12):1609–1620. doi: 10.1016/j.jacr.2020.09.032
36. Girling A, Lilford R, Cole A, et al. Headroom approach to device development: Current and future directions. *Int J Technol Assess Health Care*. 2015;31(5):331–338. doi: 10.1017/S0266462315000501
37. Ijzerman MJ, Steuten LM. Early assessment of medical technologies to inform product development and market access: A review of methods and applications. *Appl Health Econ Health Policy*. 2011;9(5):331–347. doi: 10.2165/11593380-000000000-00000
38. Izerman MJ, Koffijberg H, Fenwick E, et al. Emerging use of early health technology assessment in medical product development: A scoping review of the literature. *Pharmacoeconomics*. 2017;35(7):727–740. doi: 10.1007/s40273-017-0509-1
39. Sahiner B, Pezeshk A, Hadjiiski LM, et al. Deep learning in medical imaging and radiation therapy. *Med Phys*. 2019;46(1):1–36. doi: 10.1002/mp.13264
40. Allen BJ, Seltzer SE, Langlotz CP, et al. A road map for translational research on artificial intelligence in medical imaging: From the 2018 national institutes of health/RSNA/ACR/The academy workshop. *J Am Coll Radiol*. 2019;16(9):1179–1189. doi: 10.1016/j.jacr.2019.04.014
41. Xia C, Rook M, Pelgrim GJ, et al. Early imaging biomarkers of lung cancer, COPD and coronary artery disease in the general population: rationale and design of the ImaLife (Imaging in Lifelines) Study. *Eur J Epidemiol*. 2020;35(1):75–86. doi: 10.1007/s10654-019-00519-0
42. Ziegelmayer S, Graf M, Makowski M, et al. Cost-Effectiveness of artificial intelligence support in computed tomography-based lung cancer screening. *Cancers (Basel).* 2022;14(7):1729. doi: 10.3390/cancers14071729
43. McDonald RJ, Schwartz KM, Eckel LJ, et al. The effects of changes in utilization and technological advancements of cross-sectional imaging on radiologist workload. *Acad Radiol*. 2015;22(9):1191–1198. doi: 10.1016/j.acra.2015.05.007
44. Sokolovskaya E, Shinde T, Ruchman RB, et al. The effect of faster reporting speed for imaging studies on the number of misses and interpretation errors: A pilot study. *J Am Coll Radiol*. 2015;12(7):683–688. doi: 10.1016/j.jacr.2015.03.040
45. Geijer H, Geijer M. Added value of double reading in diagnostic radiology, a systematic review. *Insights Imaging*. 2018;9(3):287–301. doi: 10.1007/s13244-018-0599-0
46. Lauritzen PM, Hurlen P, Sandbæk G, et al. Double reading rates and quality assurance practices in Norwegian hospital radiology departments: Two parallel national surveys. *Acta Radiol*. 2015;56(1):78–86. doi: 10.1177/0284185113519988
47. Morozov SP, Chernina VYu, Andreychenko AE, et al. How does artificial intelligence effect on the assessment of lung damage in COVID-19 on chest CT scan? *Digital Diagnostics*. 2020;2(1):27–38. (In Russ). doi: 10.17816/DD60040

СПИСОК ЛИТЕРАТУРЫ

1. Aberle D.R., Adams A.M., Berg C.D., et al.; National Lung Screening Trial Research Team. Reduced lung-cancer mortality with low-dose computed tomographic screening // N Engl J Med. 2011. Vol. 365, N 5. P. 395–409. doi: 10.1056/NEJMoa1102873
2. Pastorino U., Silva M., Sestini S., et al. Prolonged lung cancer screening reduced 10-year mortality in the MILD trial: New confirmation of lung cancer screening efficacy // Ann Oncol. 2019. Vol. 30, N 7. P. 1162–1169. doi: 10.1093/annonc/mdz117
3. Grover H., King W., Bhattarai N., et al. Systematic review of the cost-effectiveness of screening for lung cancer with low dose computed tomography // Lung Cancer. 2022. N 170. P. 20–33. doi: 10.1016/j.lungcan.2022.05.005
4. Николаев А.Е., Гомболевский В.А., Гончар А.П., и др. Случайные находки при скрининге рака легкого методом низкодозной компьютерной томографии // Туберкулез и болезни лёгких. 2018. Т. 96, № 11. С. 60–67. doi: 10.21292/2075-1230-2018-96-11-60-67
5. Kilsdonk I.D., de Roos M.P., Bresser P., et al. Frequency and spectrum of incidental findings when using chest CT as a primary triage tool for COVID-19 // Eur J Radiol Open. 2021. N 8. P. 100366. doi: 10.1016/j.ejro.2021.100366
6. Бельцевич Д.Г., Мельниченко Г.А., Кузнецов Н.С., и др. Клинические рекомендации Российской ассоциации эндокринологов по дифференциальной диагностике инциденталом надпочечников // Эндокринная хирургия. 2016. Т. 10, № 4. С. 31–42. doi: 10.14341/serg2016431-42
7. Эмфизема легких. Клинические рекомендации (утв. Министерством здравоохранения РФ, 2021). Режим доступа: https://www.garant.ru/products/ipo/prime/doc/402775957/. Дата обращения: 17.03.2023.
8. Аневризмы грудной и торакоабдоминальной аорты. Клинические рекомендации (утв. Министерством здравоохранения РФ, 2023). Режим доступа: https://www.angiolsurgery.org/library/recommendations/2022/aneurysms_thoracic_thoracoabdominal_aorta/recommendation.pdf. Дата обращения: 17.03.2023.
9. Васильев Ю.А., Владзимирский А.В., Арзамасов К.М., и др. Компьютерное зрение в лучевой диагностике: первый этап Московского эксперимента. Монография. 2-е изд., перераб.

и доп. / под ред. Ю.А. Васильева, А.В. Владзимирского. Москва: Издательские решения, 2023. 376 с.
10. Zakharov A., Pisov M., Bukharaev A., et al. Interpretable vertebral fracture quantification via anchor-free landmarks localization // Med Image Anal. 2023. N 83. P. 102646. doi: 10.1016/j.media.2022.102646
11. Goncharov M., Pisov M., Shevtsov A., et al. CT-Based COVID-19 triage: Deep multitask learning improves joint identification and severity quantification // Med Image Anal // 2021. N 71. P. 102054. doi: 10.1016/j.media.2021.102054
12. Shirokikh B., Shevtsov A., Dalechina A., et al. Accelerating 3D medical image segmentation by adaptive small-scale target localization // J Imaging. 2021. Vol. 13, N 7. P. 35. doi: 10.3390/jimaging7020035
13. Goncharov M., Pisov M., Belyaev M., et al. Quantification of epicardial adipose tissue in low-dose computed tomography images // Lecture Notes in Electrical Engineering. 2022. Vol. 784, N 1. P. 98–107. doi: 10.1007/978-981-16-3880-0_11
14. Husereau D., Drummond M., Augustovski F., et al.; CHEERS 2022 ISPOR Good Research Practices Task Force. Consolidated health economic evaluation reporting standards 2022 (cheers 2022) statement: Updated reporting guidance for health economic evaluations // Value Health. 2022. Vol. 25, N 1. P. 3–9. doi: 10.1016/j.jval.2021.11.1351
15. Морозов С.П., Владзимирский А.В., Кляшторный В.Г., и др. Клинические испытания программного обеспечения на основе интеллектуальных технологий (лучевая диагностика). Препринт № ЦДТ-2019-1. Серия «Лучшие практики лучевой и инструментальной диагностики». Вып. 23. Москва: ГБУЗ НПКЦ ДиТ ДЗМ, 2019. 33 с.
16. Гомболевский В.А., Блохин И.А., Лайпан А.Ш., и др. Методические рекомендации по скринингу рака легкого. Серия «Лучшие практики лучевой и инструментальной диагностики». Вып. 56. Москва: ГБУЗ НПКЦ ДиТ ДЗМ, 2020. 57 с.
17. Морозов С.П., Проценко Д.Н., Сметанина С.В., и др. Лучевая диагностика коронавирусной болезни (COVID-19): организация, методология, интерпретация результатов: методические рекомендации. Серия «Лучшие практики лучевой и инструментальной диагностики». Вып. 65. Москва: ГБУЗ НПКЦ ДиТ ДЗМ, 2020. 78 с.
18. Временные методические рекомендации. Профилактика, диагностика и лечение новой коронавирусной инфекции (COVID-19). Министерство здравоохранения Российской Федерации. Версия 17 (14.12.2022). Режим доступа: https://static-0.minzdrav.gov.ru/system/attachments/attaches/000/061/254/original/%D0%92%D0%9C%D0%A0_COVID-19_V17.pdf?1671088207. Дата обращения: 17.03.2023.
19. Lynch D.A., Austin J.H., Hogg J.C., et al. CT-definable subtypes of chronic obstructive pulmonary disease: A statement of the Fleischner Society // Radiology. 2015. Vol. 277, N 1. P. 192–205. doi: 10.1148/radiol.2015141579
20. Hersh C.P., Washko G.R., Estépar R.S., et al. Paired inspiratory-expiratory chest CT scans to assess for small airways disease in COPD // Respir Res. 2013. Vol. 146, N 1. P. 42. doi: 10.1186/1465-9921-14-42
21. Walker C., Chung J.H. Muller's imaging of the chest e-book: Expert radiology series. Elsevier Health Sciences, 2018. 1104 p.
22. Erbel R., Aboyans V., Boileau C., et al.; ESC Committee for Practice Guidelines. 2014 ESC Guidelines on the diagnosis and treatment of aortic diseases: Document covering acute and chronic aortic diseases of the thoracic and abdominal aorta of the adult. The Task Force for the Diagnosis and Treatment of Aortic Diseases of the European Society of Cardiology (ESC) // Eur Heart J. 2014. Vol. 35, N 41. P. 2873–2926. doi: 10.1093/eurheartj/ehu281
23. Wanhainen A., Verzini F., Van Herzeele I., et al. Clinical practice guidelines on the management of abdominal aorto-iliac artery aneurysms6 // Eur J Vascul Endovascul Sur. 2019. Vol. 57, N 1. P. 8–93. doi: 10.1016/j.ejvs.2018.09.020
24. Jurgens P.T., Carr J.J., Terry J.G., et al. Association of abdominal aorta calcium and coronary artery calcium with incident cardiovascular and coronary heart disease events in black and white middle-aged people: The coronary artery risk development in young adults study // J Am Heart Assoc. 2021. Vol. 10, N 24. P. 23–37. doi: 10.1161/JAHA.121.023037
25. Galiè N., Humbert M., Vachiery J.L., et al. 2015 ESC/ERS Guidelines for the diagnosis and treatment of pulmonary hypertension: The joint task force for the diagnosis and treatment of pulmonary hypertension of the European society of cardiology (ESC) and the European respiratory society (ERS): Endorsed by: Association for European paediatric and congenital cardiology (AEPC), international society for heart and lung transplantation (ISHLT) // Eur Respir J. 2015. Vol. 46, N 4. P. 903–975. doi: 10.1183/13993003.01032-2015
26. Agatston A.S., Janowitz W.R., Hildner F.J., et al. Quantification of coronary artery calcium using ultrafast computed tomography // J Am Coll Cardiol. 1990. Vol. 15, N 4. P. 827–832. doi: 10.1016/0735-1097(90)90282-t
27. Журавлев К.Н. КТ-коронарография. Серия «Лучшие практики лучевой и инструментальной диагностики». Вып. 65. Москва: ГБУЗ НПК ЦДиТ ДЗМ, 2020. 35 с.
28. Mayo-Smith W.W., Song J.H., Boland G.L., et al. Management of incidental adrenal masses: A white paper of the ACR incidental findings committee // J Am Coll Radiol. 2017. Vol. 14, N 8. P. 1038–1044. doi: 10.1016/j.jacr.2017.05.001
29. Белая Ж.Е., Белова К.Ю., Бирюкова Е.В., и др. Федеральные клинические рекомендации по диагностике, лечению и профилактике остеопороза // Остеопороз и остеопатии. 2021. Т. 24, № 2. С. 4–47. doi: 10.14341/osteo12930
30. Genant H.K., Jergas M. Assessment of prevalent and incident vertebral fractures in osteoporosis research // Osteoporosis Int. 2003. Vol. 14, N 3. P. 43–55. doi: 10.1007/S00198-002-1348-1
31. Патологические переломы, осложняющие остеопороз. Клинические рекомендации. Москва, 2018. 90 с. Режим доступа: https://neirodoc.ru/wp-content/uploads/2019/10/patologicheskie-perelomy-oslozhnyayuschie-osteoporoz-2018.pdf. Дата обращения: 17.03.2023.
32. Колбин А.С., Гомон Ю.М., Балыкина Ю.Е., и др. Социально-экономическое и глобальное бремя COVID-19 // Качественная клиническая практика. 2021. № 1. С. 24–34. doi: 10.37489/2588-0519-2021-1-24-34
33. Pickhardt P.J., Correale L., Hassan C. AI-based opportunistic CT screening of incidental cardiovascular disease, osteoporosis, and sarcopenia: Cost-effectiveness analysis // Abdom Radiol (NY). 2023. N 3. P. 1181–1198. doi: 10.1007/s00261-023-03800-9
34. Behr C.M., Koffijberg H., Degeling K., et al. Can we increase efficiency of CT lung cancer screening by combining with CVD and COPD screening? Results of an early economic evaluation // Eur Radiol. 2022. Vol. 32, N 5. P. 3067–3075. doi: 10.1007/s00330-021-08422-7
35. Chintanapakdee W., Mendoza D.P., Zhang E.W., et al. Detection of extrapulmonary malignancy during lung cancer screening: 5-year analysis at a tertiary hospital // J Am Coll Radiol. 2020. Vol. 17, N 12. P. 1609–1620. doi: 10.1016/j.jacr.2020.09.032
36. Girling A., Lilford R., Cole A., et al. Headroom approach to device development: Current and future directions // Int J

Technol Assess Health Care. 2015. Vol. 31, N 5. P. 331–338. doi: 10.1017/S0266462315000501
37. Ijzerman M.J., Steuten L.M. Early assessment of medical technologies to inform product development and market access: A review of methods and applications // Appl Health Econ Health Policy. 2011. Vol. 9, N 5. P. 331–347. doi: 10.2165/11593380-000000000-00000
38. Izerman M.J., Koffijberg H., Fenwick E., et al. Emerging use of early health technology assessment in medical product development: A scoping review of the literature // Pharmacoeconomics. 2017. Vol. 35, N 7. P. 727–740. doi: 10.1007/s40273-017-0509-1
39. Sahiner B., Pezeshk A., Hadjiiski L.M., et al. Deep learning in medical imaging and radiation therapy // Med Phys. 2019. Vol. 46, N 1. P. 1–36. doi: 10.1002/mp.13264
40. Allen B.J., Seltzer S.E., Langlotz C.P., et al. A road map for translational research on artificial intelligence in medical imaging: From the 2018 national institutes of health/RSNA/ACR/ The academy workshop // J Am Coll Radiol. 2019. Vol. 16, N 9. P. 1179–1189. doi: 10.1016/j.jacr.2019.04.014
41. Xia C., Rook M., Pelgrim G.J., et al. Early imaging biomarkers of lung cancer, COPD and coronary artery disease in the general population: Rationale and design of the ImaLife (Imaging in Lifelines) Study // Eur J Epidemiol. 2020. Vol. 35, N 1. P. 75–86. doi: 10.1007/s10654-019-00519-0
42. Ziegelmayer S., Graf M., Makowski M., et al. Cost-effectiveness of artificial intelligence support in computed tomography-based lung cancer screening // Cancers (Basel). 2022. Vol. 14, N 7. P. 1729. doi: 10.3390/cancers14071729
43. McDonald R.J., Schwartz K.M., Eckel L.J., et al. The effects of changes in utilization and technological advancements of cross-sectional imaging on radiologist workload // Acad Radiol. 2015. Vol. 22, N 9. P. 1191–1198. doi: 10.1016/j.acra.2015.05.007
44. Sokolovskaya E., Shinde T., Ruchman R.B., et al. The effect of faster reporting speed for imaging studies on the number of misses and interpretation errors: A pilot study // J Am Coll Radiol. 2015. Vol. 12, N 7. P. 683–688. doi: 10.1016/j.jacr.2015.03.040
45. Geijer H., Geijer M. Added value of double reading in diagnostic radiology, a systematic review // Insights Imaging. 2018. Vol. 9, N 3. P. 287–301. doi: 10.1007/s13244-018-0599-0
46. Lauritzen P.M., Hurlen P., Sandbæk G., et al. Double reading rates and quality assurance practices in Norwegian hospital radiology departments: Two parallel national surveys // Acta Radiol. 2015. Vol. 56, N 1. P. 78–86. doi: 10.1177/0284185113519988
47. Морозов С.П., Чернина В.Ю., Андрейченко А.Е., и др. Как искусственный интеллект влияет на оценку поражения лёгких при COVID-19 по данным КТ грудной клетки? // Digital Diagnostics. 2021. Т. 2, № 1. С. 27–38. doi: 10.17816/DD60040

AUTHORS' INFO

*** Valeria Yu. Chernina;**
address: 30/1 Bolshoy Boulevard, 121205 Moscow, Skolkovo, Russia;
ORCID: 0000-0002-0302-293X;
eLibrary SPIN: 8896-8051;
e-mail: v.chernina@ira-labs.com

Mikhail G. Belyaev, Cand. Sci. (Phys.-Math.), Professor;
ORCID: 0000-0001-9906-6453;
eLibrary SPIN: 2406-1772;
e-mail: belyaevmichel@gmail.com

Anton Yu. Silin;
ORCID: 0000-0003-4952-2347;
eLibrary SPIN: 4411-8745;
e-mail: silin@yamed.ru

Ivan O. Avetisov;
ORCID: 0009-0007-3550-7556;
e-mail: avetisov@yamed.ru

Ilya A. Pyatnitskiy;
ORCID: 0000-0002-2827-1473;
eLibrary SPIN: 6150-4961;
e-mail: i.pyatnitskiy@ira-labs.com

Ekaterina A. Petrash, MD, Cand. Sci. (Med.);
ORCID: 0000-0001-6572-5369;
eLibrary SPIN: 6910-8890;
e-mail: e.a.petrash@gmail.com

Maria V. Basova;
ORCID: 0009-0000-3325-8452;
e-mail: m.basova@ira-labs.com

Valentin E. Sinitsyn, MD, Dr. Sci. (Med.), Professor;
ORCID: 0000-0002-5649-2193;
eLibrary SPIN: 8449-6590;
e-mail: vsini@mail.ru

ОБ АВТОРАХ

*** Чернина Валерия Юрьевна;**
адрес: Россия, 121205, Москва, Сколково, Большой б-р, д. 30, стр. 1;
ORCID: 0000-0002-0302-293X;
eLibrary SPIN: 8896-8051;
e-mail: v.chernina@ira-labs.com

Беляев Михаил Геннадьевич, канд. физ.-мат. наук, профессор;
ORCID: 0000-0001-9906-6453;
eLibrary SPIN: 2406-1772;
e-mail: belyaevmichel@gmail.com

Силин Антон Юрьевич;
ORCID: 0000-0003-4952-2347;
eLibrary SPIN: 4411-8745;
e-mail: silin@yamed.ru

Аветисов Иван Олегович;
ORCID: 0009-0007-3550-7556;
e-mail: avetisov@yamed.ru

Пятницкий Илья Аркадьевич;
ORCID: 0000-0002-2827-1473;
eLibrary SPIN: 6150-4961;
e-mail: i.pyatnitskiy@ira-labs.com

Петраш Екатерина Александровна, канд. мед. наук;
ORCID: 0000-0001-6572-5369;
eLibrary SPIN: 6910-8890;
e-mail: e.a.petrash@gmail.com

Басова Мария Васильевна;
ORCID: 0009-0000-3325-8452;
e-mail: m.basova@ira-labs.com

Синицын Валентин Евгеньевич, д-р мед. наук, профессор;
ORCID: 0000-0002-5649-2193;
eLibrary SPIN: 8449-6590;
e-mail: vsini@mail.ru

* Corresponding author / Автор, ответственный за переписку

Vitaly V. Omelyanovskiy, MD, Dr. Sci. (Med.), Professor;
ORCID: 0000-0003-1581-0703;
eLibrary SPIN: 1776-4270;
e-mail: vvo@rosmedex.ru
Victor A. Gombolevskiy, MD, Cand. Sci. (Med.);
ORCID: 0000-0003-1816-1315;
eLibrary SPIN: 6810-3279;
e-mail: gombolevskii@gmail.com

Омельяновский Виталий Владимирович, д-р мед. наук,
ORCID: 0000-0003-1581-0703;
eLibrary SPIN: 1776-4270;
e-mail: vvo@rosmedex.ru
Гомболевский Виктор Александрович, канд. мед. наук;
ORCID: 0000-0003-1816-1315;
eLibrary SPIN: 6810-3279;
e-mail: gombolevskii@gmail.com

SUPPLEMENTARY MATERIALS

Table 10. Recommendations for additional methods

Health condition	Clinical guidelines	Consultation/additional examinations/follow-up monitoring
Lung nodules	Gombolevsky V.A., Blokhin I.A., Laipan A.Sh., etc. Guidelines for lung cancer screening. [Metodicheskiye rekomendatsii po skriningu raka logkogo.] Series: "Best practices of radiological and instrumental diagnostics." [Luchshiye praktiki luchevoy i instrumental'noy diagnostiki.] Issue 56. Moscow: Scientific and Practical Clinical Center for Diagnostics and Telemedicine Technologies of the Department of Healthcare of Moscow. 2020. 57 pp.	*Consultations:* oncologist. *Additional examinations:* biopsy, bronchoscopy under CT/ultrasound control, cytology, blood test (HIV, syphilis, and hepatitis), PFT, spirometry, CBC, ECG, PET/CT, and brain MRI with an intravenous contrast-enhancement *Follow-up monitoring:* depending on the number and size of lung nodules. Chest CT is recommended after 3–6 months.
Infiltrative lung changes typical for viral pneumonia (COVID-19 in a pandemic)	Interim Guidelines. Prevention, Diagnosis and Treatment of Novel Coronavirus Infection (COVID-19). The Ministry of Health of the Russian Federation. Version 17 (December 14, 2022). Available from: https://static-0.minzdrav.gov.ru/system/attachments/attaches/000/061/254/original/%D0%92%D0%9C%D0%A0_COVID-19_V17.pdf?1671088207	*Consultations:* primary care doctor. *Additional examinations:* pulse oximetry; ECG; SARS-CoV-2 RNA by nucleic acid amplification techniques; SARS-CoV-2 antigens by immunochromatographic techniques; CBC with erythrocytes, hemoglobin, hematocrit, leukocytes, platelets, and leukogram; blood biochemistry (urea, creatinine, electrolytes, glucose, ALT, AST, bilirubin, albumin, lactate, and lactate dehydrogenase, as well as troponin as a marker of myocardial damage and ferritin as a protein of acute inflammation phase to assess the disease severity and prognosis); CRP; hormonal testing (procalcitonin and NT-proBNP); coagulogram (activated partial thromboplastin time, prothrombin time, prothrombin ratio and/or quick prothrombin %, fibrinogen, and D-dimer by the quantitative method). *Follow-up monitoring:* 8 weeks after discharge, a visit to a doctor and imaging studies (if indicated) are recommended: chest X-ray*, spirography*, blood oxygen saturation at rest and during exercise (it is possible to conduct a 6-min walk test and determining saturation before and after the test)*, echocardiography, and other techniques (diffusion test, arterial blood gases, etc.) * If abnormalities are detected, lung CT is indicated.

Table 10. Continuation

Health condition	Clinical guidelines	Consultation/additional examinations/follow-up monitoring
Lung emphysema	Lung emphysema. Clinical guidelines (approved by the Ministry of Health of the Russian Federation, 2021). Available from: https://www.garant.ru/products/ipo/prime/doc/402775957/	*Consultations:* pulmonologist/primary care doctor. *Additional examinations:* blood gas test. If a hereditary A1AT deficiency of A1AT is suspected, determine the blood activity of A1AT, spirometry with a bronchodilator test, body plethysmography, and lung diffusion test. For all patients with clinical signs of A1AT deficiency and/or decreased serum A1AT, phenotype, and genotype testing is recommended. *Follow-up monitoring:* for all patients with A1AT deficiency, annual blood biochemistry for albumin, total bilirubin, AST, ALT, GGT, and platelets is recommended. For patients with pulmonary A1AT deficiency, spirometry is initially recommended every 6–12 months to rule out rapid disease progression, followed up with less frequent examinations. For patients with A1AT deficiency, an annual abdomen ultrasound is recommended to exclude liver manifestations of the disease.
Free pleural fluid (effusion)	Maskell N., Butland R. British Thoracic Society (BTS) guidelines for the investigation of adult patients with unilateral pleural effusion [Rekomendatsii Britanskogo torakal'nogo obshchestva (BTS) po obsledovaniyu vzroslykh bol'nykh s odnostoronnim plevral'nym vypotom]. Pulmonology [Pul'monologiya]. 2006. No. 2. P. 13–26. doi: 10.18093/0869-0189-2006-2-13-26	*Consultations:* pulmonologist. If tuberculosis is detected, a TB specialist should be consulted. If a malignant lesion is detected, an oncologist should be consulted. *Additional examinations:* consider pleural aspiration (ASAP, "as soon as possible"), cytology, protein, LDH, pH, Gram staining, culture, and sensitivity determination, staining for acid-resistant rods, and culture for *Mycobacterium tuberculosis.* Later, if necessary, chest CT with intravenous contrast enhancement and pleural biopsy. If no underlying cause is found after all investigations, consider thoracoscopy.
Aneurysm/dilatation of the aorta	Clinical guidelines. Recommendations for the diagnosis and treatment of aortic diseases [Rekomendatsii po diagnostike i lecheniyu zabolevaniy aorty] (2017) // Cardiology and Cardiovascular Surgery [Kardiologiya i serdechno-sosudistaya khirurgiya]. 2018. No. 1. P. 7–67	*Consultations:* cardiologist/vascular surgeon. *Additional examinations:* CT aortography with intravenous contrast enhancement. *Follow-up monitoring:* transthoracic echocardiography and abdominal ultrasound.
Dilatation of pulmonary trunk	Clinical guidelines. Pulmonary hypertension, including chronic thromboembolic pulmonary hypertension, 2020 (June 03, 2021). Approved by the Ministry of Health of the Russian Federation. Available from: http://disuria.ru/_ld/10/1026_kr20I27MZ.pdf	*Consultations:* cardiologist. *Additional examinations:* echocardiography; ECG; blood gas tests; perfusion scintigraphy with ventilation scintigraphy; CBC with hemoglobin and hematocrit, erythrocyte, leukocyte, platelets, and ESR; blood biochemistry (creatinine, sodium, potassium, glucose, total protein, CRP, AST, ALT, total bilirubin, and uric acid); blood antibodies to cardiolipin, phospholipids, beta-2-glycoprotein in the case of suspected chronic thromboembolic pulmonary hypertension to identify risk factors; content of antibodies to cell nucleus and DNA antigens to exclude association with systemic diseases of the connective tissue; NT-proBNP; IgM, IgG antibodies to HIV-1, and HIV-2 in blood; HBV antigen, anti-HCV, anti-treponema pallidum; clinical urinalysis; thyroid function test (free triiodothyronine, free thyroxine, and thyroid-stimulating hormone); abdominal ultrasound (complex) to exclude liver disease and/or portal hypertension.

Table 10. Ending

Health condition	Clinical guidelines	Consultation/additional examinations/follow-up monitoring
Coronary calcification	Clinical guidelines. Stable coronary heart disease, 2020 (Approved by the Scientific and Practical Council of the Ministry of Health of the Russian Federation). Available from: https://cr.minzdrav.gov.ru/schema/155_1	*Consultations:* cardiologist. *Additional examinations:* CBC (clinical) with hemoglobin, erythrocytes, and leukocytes; blood creatinine and estimated GFR or creatinine clearance for kidney function assessment; blood biochemistry, including total blood cholesterol, low-density lipoprotein cholesterol, and triglycerides; blood NT-proBNP; ECG at rest; ambulatory ECG monitoring; echocardiography; heart MRI when receiving non-conclusive echocardiography results (including with contrast enhancement); duplex scanning of the extracranial carotid arteries to detect atherosclerotic plaques; coronary CT angiography; stress ECG, stress echocardiography, stress MRI, and SPECT. *Follow-up:* in the case of repeated examinations, in all patients with a diagnosed stable coronary heart disease, annual monitoring of the clinical CBC, blood biochemistry, blood test for lipid metabolism abnormalities, blood creatinine, fasting blood glucose for timely therapy adjustment, if necessary, is recommended.
Measurement of adrenal size for masses and hyperplasia	Clinical guidelines. Adrenocortical cancer, 2020 (Approved by the Scientific and Practical Council of the Ministry of Health of the Russian Federation). Available from: https://cr.minzdrav.gov.ru/schema/341_1	*Consultations:* endocrinologist and oncologist. *Additional examinations:* test for the hormonal activity of the adrenal tumor (cortisol, ACTH, free plasma metanephrines, or 24-h urinary fractionated metanephrines, aldosterone, plasma renin, and serum potassium), abdominal CT with intravenous contrast enhancement (in the case of contraindications for CT with contrast enhancement, perform an abdominal MRI with the involved retroperitoneal space). In the case of adrenal gland lesion with an indeterminate CT phenotype and without hormonal hypersecretion, the situation with a multidisciplinary team is recommended. Three options are possible: (1) additional imaging studies (PET/CT with fluorodeoxyglucose), (2) watchful waiting with repeat non-contrast CT (or MRI) 3–6 months later, and (3) surgical treatment. *Follow-up:* in the case of lesions with an indeterminate CT phenotype, to assess changes in the tumor size over time (if observation was chosen based on the primary diagnosis), a repeat CT/MRI is recommended after 3–6 months. Surgical treatment in the case of a 20% increase in the lesion size (or an increase in the maximum diameter >5 mm) during a short follow-up period.
Evaluation of the density of the spongy substance of vertebral bodies for detection of osteoporosis/ osteopenia	Clinical guidelines. Osteoporosis, 2022 (Approved by the Scientific and Practical Council of the Ministry of Health of the Russian Federation). Available from: https://cr.minzdrav.gov.ru/recomend/87_4	*Consultations:* endocrinologist. *Additional examinations:* CBC (clinical); blood biochemistry (total calcium, creatinine with GFR, inorganic phosphorus, AP activity, and glucose); blood test for C-terminal telopeptide and/or N-terminal propeptide of type 1 procollagen (P1NP, a resorption marker for prescribing antiresorptive therapy and a bone formation marker for prescribing anabolic therapy) in patients receiving self-therapy for osteoporosis, initially, and after 3 months from the start of therapy for early assessment of therapy effectiveness and adherence; dual-energy X-ray densitometry (DXA) of the lumbar spine and proximal femur; 3D measurement of maximum oxygen consumption by quantitative CT (optional).
Vertebral compression fractures related to osteoporosis	Clinical guidelines. Pathologic fractures in osteoporosis, 2022 (Approved by the Scientific and Practical Council of the Ministry of Health of the Russian Federation). Available from: https://cr.minzdrav.gov.ru/recomend/614_2	*Consultations:* endocrinologist. *Additional examinations:* CBC (clinical); urinalysis; blood biochemistry with total and/or ionized calcium, inorganic phosphorus, total AP, and blood creatinine with GFR; blood level of parathyroid hormones, calcium, and phosphorus in 24-h urine; dual-energy X-ray densitometry. In the case of a low-energy fracture of the vertebral body in people aged >50 years, blood, and urine tests for paraproteins and M-gradient are required to exclude multiple myeloma.

Note. A1AT, alpha-1 antitrypsin; ACTH, adrenocorticotropic hormone; ALT, alanine aminotransferase; AST, aspartate aminotransferase; CBC, complete blood count; CRP, C-reactive protein; CT, computed tomography; ECG, electrocardiogram; EchoCG, echocardiography; ESR, erythrocyte sedimentation rate; GFR, glomerular filtration rate; GGT, gamma-glutamyl transferase; HBV, hepatitis B virus; HCV, hepatitis C virus; HIV, human immunodeficiency virus; LDH, lactate dehydrogenase; MRI, magnetic resonance imaging; NT-proBNP, aminoterminal pro B-type natriuretic peptide; AP, alkaline phosphatase; PET/CT, positron emission tomography with computed tomography; PFT, pulmonary function test; SPECT, single-photon emission computed tomography

Table 11. Employment history of physicians

Physician	Work experience			Employment	Academic degree
	in radiology (including residency)	in thoracic radiology (excluding residency)	in CT		
Physician 1	15	13	13	Part-time	Yes
Physician 2	17	5	5	Part-time	No
Physician 3	7	5	5	Full-time	No
Physician 4	16	14	14	Part-time	No
Physician 5	7	5	5	Part-time	No
Physician 6	5	3	3	Part-time	Yes
Physician 7	14	10	10	Part-time	No

Generalized linear model

The generalized linear model assumes that each finding Y_i has linear relationship with variables X_{ip}, $p=1,2,...m$:

$$Y_i=b_{i0}+b_1X_{i1}+b_2X_{i2}+...+b_mX_{im}+\varepsilon_i,$$

where X variables can be either categorical (considering groups, classes, and categories) or continuous. In the generalized linear model, coefficients $\{bj, j=0,1,2,...,m\}$ are estimated for the model of Y parameter dependence on factors $\{Xj, j=1,2,...,m\}$. For these coefficients, their statistical significance is determined (calculation of p-values for testing hypotheses H_{j0}: $b_j=0$, $j=0,1,2,...,m$), which shows the significance of the corresponding factors' effect on the target parameter.

In our case, some parameters have a lognormal distribution; thus, a logarithmic transformation was used for them. The final model is as follows:

Y = log (total number of protocols with critical and non-critical errors)

X1 = all protocols

X2 = log (work experience in thoracic radiology [excluding residency])

X3 = log (length of experience in CT)

Categorical parameter X4 = academic degree.

Results of estimating coefficients for the generalized linear model and their statistical significance are presented in the table:

Thus, the total number of protocols statistically significantly increases the number of errors. The total work experience in radiology and thoracic radiology decreases the number of errors. However, these data are not representative because of the small sample of HCPs and presence of a dominant case.

Partially similar results (for statistical significance and effects of one experience types) are also considered in the correlation analysis:

- ρ (log (total number of protocols with critical and non-critical errors), all protocols) = 0.88 with 95% CI [0.39; 0.98] and *p*-value of 0.008 (statistically significant correlation),
- ρ (log (total number of protocols with critical and non-critical errors), log (work experience in thoracic radiology [excluding residency]) = -0.45 with 95% CI [-0.9; 0.46] and *p*-value of 0.31 (statistically insignificant correlation),
- ρ (log (total number of protocols with critical and non-critical errors), log (work experience in thoracic radiology (excluding residency)) = -0.27 with 95% CI [-0.85; 0.61] and *p*-value of 0.56 (statistically insignificant correlation).
- However, the absence of statistical significate correlations does not allow establishing any trends.

	Estimate	Std. Error	t.value	Pr...t..
(Intercept)	0,132922	0,352989	0,37656	0,742697
bd_lr$"All protocols"	0,037246	0,006111	6,094863	0,025879
log(bd_lr$"Work experience in thoracic radiology/r/n(excluding residency)/r/n")	-7,96969	1,009013	-7,8985	0,015654
factor(bd_lr$"Academic degree")no	-0,92975	0,229399	-4,05297	0,055828

DOI: https://doi.org/10.17816/DD201870

Создание набора данных с диспозицией и транспозицией наложения электрокардиографических электродов при записи электрокардиограммы в 12 отведениях

Т.М. Газашвили[1], Д.В. Дроздов[2], Д.В. Шутов[3], А.С. Шкода[1]

[1] Городская клиническая больница № 67 имени Л.А. Ворохобова, Москва, Российская Федерация
[2] Национальный медицинский исследовательский центр кардиологии имени академика Е.И. Чазова, Москва, Российская Федерация
[3] Научно-практический клинический центр диагностики и телемедицинских технологий, Москва, Российская Федерация

АННОТАЦИЯ

Обоснование. Электрокардиография — одна из наиболее простых, широко распространённых, недорогих и информативных методик в функциональной диагностике, однако её диагностическая ценность резко снижается при неправильном проведении. Предпринимались попытки систематизировать ошибки и отклонения при наложении электродов, но все они касались наиболее частых вариантов (перестановка электродов красного и жёлтого, жёлтого и зелёного, грудных — выше или ниже стандартной схемы.

Цель — создать набор данных электрокардиограмм с разными вариантами транспозиций и диспозиций электродов при регистрации электрокардиограммы для обучения и тестирования систем машинного обучения.

Материалы и методы. В исследование включены пациенты в возрасте от 18 до 75 лет, 27 мужчин и 22 женщины. Все пациенты давали добровольное информированное согласие на проведение регистрации электрокардиограммы. Кардиограмму регистрировали на приборе «Модульная система для регистрации и дистанционной передачи электрокардиограммы «EASY ECG»». Каждому пациенту во время одного визита последовательно регистрировали электрокардиограммы с корректным наложением электродов и различными вариантами дис- и транспозиций.

Результаты. Всего зарегистрировано 488 электрокардиограмм у 49 пациентов. Полученные результаты свидетельствуют о значительной вариативности картины электрокардиограммы. При визуальном анализе зарегистрированных электрокардиограмм определение транспозиции, связанной с перестановкой отведений на руках и в грудных электродах C1–C2, не вызывало затруднений. Реже надёжно определялась установка грудных электродов в контакте друг с другом, диспозиции с переносом грудных отведений выше или ниже на 2 межреберья по сравнению со схемой Wilson. Транспозиции жёлтого и зелёного конечностных электродов, изменение положения грудных электродов, когда их «выстраивают» по прямой линии, «задирают» по межреберью, путают местами C5–C6, затруднительно определять даже при сопоставлении рядом двух кардиограмм — с правильным и транспозиционным наложением электродов. Вероятно, это зависит как от исходных изменений на электрокардиограмме, так и от типа телосложения, размеров молочной железы или наличия имплантата.

Заключение. Получен набор данных электрокардиограмм с различными вариантами дислокаций электродов. Набор данных состоит из серий электрокардиограмм, зарегистрированных у каждого пациента с различными вариантами наложения электродов (в наборе представлены не только нормальные электрокардиограммы, но и различные варианты электрокардиографических отклонений).

Ключевые слова: электрокардиограмма; ЭКГ; дефекты регистрации электрокардиограммы; искусственный интеллект; алгоритмы; функциональная диагностика.

Как цитировать

Газашвили Т.М., Дроздов Д.В., Шутов Д.В., Шкода А.С. Создание набора данных с диспозицией и транспозицией наложения электрокардиографических электродов при записи электрокардиограммы в 12 отведениях // *Digital Diagnostics*. 2023. Т. 4, № 2. С. 133–141. DOI: https://doi.org/10.17816/DD201870

Рукопись получена: 04.04.2023 **Рукопись одобрена:** 15.05.2023 **Опубликована:** 15.06.2023

DOI: https://doi.org/10.17816/DD201870

Creation of a training and test dataset with the disposition and transposition of overlaying electrocardiographic electrodes when recording electrocardiograms-12

Tamara M. Gazashvili[1], Dmitry V. Drozdov[2], Dmitry V. Shutov[3], Andrey S. Shkoda[1]

[1] City Clinical Hospital No. 67 named after L.A. Vorokhobov, Moscow, Russian Federation
[2] National Medical Research Centre of Cardiology Named After Academician E.I. Chazov, Moscow, Russian Federation
[3] Research and Practical Clinical Center for Diagnostics and Telemedicine Technologies, Moscow, Russian Federation

ABSTRACT

BACKGROUND: Electrocardiography is one of the simplest, most widely used, inexpensive, and informative methods in functional diagnostics; yet, if performed poorly, its diagnostic value is sharply reduced. Several attempts were made to systematize errors and deviations in electrode application, but all concerned the most common options (rearrangement of red and yellow electrodes, yellow and green electrodes, and chest electrodes — above or below the standard scheme).

AIM: To create an electrocardiogram dataset with different options for transpositions and dispositions of electrodes during electrocardiogram recording.

MATERIALS AND METHODS: The study included patients aged 18–75 years (27 males and 22 females). All patients provided informed consent for electrocardiogram registration. During one visit, the cardiogram was recorded on the device "Modular system for recording and remote transmission of electrocardiograms (EASY ECG)" for each patient.

RESULTS: In all, 488 electrocardiograms were recorded in 49 patients. The results obtained indicate a significant variability of the electrocardiogram pattern. Visual analysis of the electrocardiograms revealed no difficulties in determining the transposition associated with rearranging the leads on the arms (RY) in the thoracic C1–C2. The placement of thoracic electrodes in contact cheek-to-cheek dispositions with the transfer of thoracic leads above or below two intercostals was reliably determined compared with the Wilson scheme. The transpositions of the yellow and green limb electrodes and the change in the position of the thoracic ones when they are "lined up" in a straight line, "bullied" between the ribs (curved), and confused in places C5 and C6 are difficult to determine even when comparing two cardiograms next to each other, with the correct and transpositional superposition of the electrodes. The initial changes on the electrocardiograms, physique type, breast size, or the presence of an implant most likely determine it.

CONCLUSION: An electrocardiography dataset was obtained using various electrode dislocation variants. The dataset consists of a series of electrocardiograms obtained for each patient with several electrode placement options and contains both normal and pathological electrocardiograms.

Keywords: electrocardiogram; ECG; defects in the registration of the electrocardiogram; artificial intelligence; algorithms; functional diagnostics.

To cite this article

Gazashvili TM, Drozdov DV, Shutov DV, Shkoda AS. Creation of a training and test dataset with the disposition and transposition of overlaying electrocardiographic electrodes when recording electrocardiograms-12. *Digital Diagnostics.* 2023;4(2):133–141. DOI: https://doi.org/10.17816/DD201870

Received: 04.04.2023 **Accepted:** 15.05.2023 **Published:** 15.06.2023

DOI: https://doi.org/10.17816/DD201870

在记录12导联心电图时，创建一个具有心电图电极应用配置和转置的数据集

Tamara M. Gazashvili[1], Dmitry V. Drozdov[2], Dmitry V. Shutov[3], Andrey S. Shkoda[1]

[1] City Clinical Hospital No. 67 named after L.A. Vorokhobov, Moscow, Russian Federation
[2] National Medical Research Centre of Cardiology Named After Academician E.I. Chazov, Moscow, Russian Federation
[3] Research and Practical Clinical Center for Diagnostics and Telemedicine Technologies, Moscow, Russian Federation

简评

论证。心电图是功能诊断中最简单、最常见、最便宜和最有信息量的方法之一，然而它的诊断价值在错误操作中急剧下降。试图使电极应用时的错误和偏差系统化，但这些错误和偏差都涉及到最常见的变体（把红色和黄色、黄色和绿色、胸腔的电极移动到高于或低于标准方案的位置）。

该研究的目的是在记录心电图时创建一个具有不同电极配置和转置的心电图数据集，以训练和测试机器学习系统。

材料和方法。年龄在18至75岁的患者被纳入本研究，其中男性27人，女性22人。所有患者都自愿知情同意记录心电图。心电图是在《记录和远程传输心电图的模块化系统“EASY ECG”》设备上记录的。每位患者在一次就诊中都依次接受心电图检查，其中有正确的电极应用及不同的配置和转置的变体。

结果。一共有49名患者，记录了488张心电图。研究结果表明，心电图模式有很大的变异性。在对记录的心电图进行目测分析时，发现与手臂和胸腔C1-C2电极移动有关的转置并不困难。很少有胸腔电极相互接触的情况，与Wilson方案相比，胸腔导联移高或移低2个肋间的配置被可靠地发现。黄色和绿色肢体电极的转置，当“排成”一条直线，沿肋间隙“乱”，以及混入C5-C6时，胸廓电极的改变，即使并排比较两张心电图，有正确和转置的电极应用，也很难确定。这可能既取决于基线心电图的变化，也取决于体型、乳房大小或是否有植入物。

结论。我们获得了一个具有不同电极脱位变体的心电图数据集。该数据集由一系列记录在每个病人身上的不同电极应用变体的心电图组成（数据集中不仅有正常的心电图，还有不同的心电图异常变体）。

关键词：心电图；ECG；心电图记录失误；人工智能；算法；功能诊断。

To cite this article
Gazashvili TM, Drozdov DV, Shutov DV, Shkoda AS. 在记录12导联心电图时，创建一个具有心电图电极应用配置和转置的数据集. *Digital Diagnostics.* 2023;4(2):133–141. DOI: https://doi.org/10.17816/DD201870

收到：04.04.2023 **接受：**15.05.2023 **发布日期：**15.06.2023

BACKGROUND

Electrocardiography (ECG) is one of the simplest, most widespread, inexpensive, and informative techniques in cardiology; however, its diagnostic value is dramatically reduced if it is not performed correctly. The most common change in the recording technique is electrode displacement (dislocation). A disposition (a deliberate and necessary change in electrode placement) should be distinguished from a transposition (an erroneous change in electrode placement compared with the standard overlay pattern).

Several studies have attempted to systematize errors and deviations in electrode placement; however, all of them concerned the most frequent variants, such as relocation of red and yellow, yellow and green, and precordial electrodes above or below the standard pattern. [1-7] To avoid errors in the interpretation of ECG recordings, algorithms capable of detecting such errors are developed. Machine algorithms stably recognize right–left (RL) transposition.

To assess the quality and determine the criteria for the possibility of using such algorithms, ECG datasets should be created for training and testing both algorithms for automatic ECG analysis and by healthcare specialists, i.e., doctors and nursing staff.

This study aimed to create an ECG dataset with different electrode transpositions and dispositions during ECG recording for training and testing machine-learning systems.

MATERIALS AND METHODS

Inclusion criteria

Patients aged 18–75 years (27 men and 22 women) were included in the study. All patients gave voluntary informed consent for ECG recording.

Settings

The study was performed in the Moscow State Budgetary Institution City Clinical Hospital No. 67 named after L.A. Vorokhobov of Moscow Healthcare Department.

Description of treatment

The patients were divided into the following six arms:

1) Patients with normal ECG (recordings starting with 101, 102, 103, 104, 105, 106, 107, 108, 109, and 110).
2) Patients with ECG signs of left ventricular hypertrophy or complete left bundle branch block (recordings starting with 201, 202, 203, 204, 205, 206, 207, 208, and 209).
3) Patients with ECG signs of right bundle branch block (recordings starting with 301, 302, 303, 304, 305, and 306).
4) Patients with recorded ST (–) depression (recordings starting with 401, 402, 403, 404, 405, 406, 407, 408, and 409).
5) Patients with recorded ST(+) elevation, including the phenomenon of early ventricular repolarization (recordings starting with 501, 502, 503, 504, 505, 506, and 507).
6) Patients with any nonsinus rhythm that are preferably characterized by negative *P* waves in I, II, V1, and V2 leads (recordings starting with 601, 602, 603, 604, 605, 606, 607, and 608).

Cardiograms were recorded using EASY ECG Modular System for Recording and Remote Transmitting of ECGs according to TU 9441-001-42447560-2012 with Accessories (ATES MEDICA SOFT LTD, Russia, Registration Certificate No. RZN 2018/7062).

For ECG recording, operating silver/silver chloride electrodes were used with 26 × 47-mm plates (for limb ones) and 22-mm cups (for precordial ones).

Digitized cardiac signals were recorded in the European data format. [8] Recordings were made in 12 common leads with a sample rate of 500 Hz, the recording lasted for 10 s, and the signal magnitude was 10 mV. No signal filtering was performed, and the bandwidth was from 0.05 to 150 Hz.

Ethical review

The study was approved by the independent ethical committee of the Moscow Regional Branch of the Russian Society of Roentgenologists and Radiologists (RSRR MRB IEC).

RESULTS

Each patient underwent sequential ECG recording during one visit with correct electrode placement and different variants of dis- and transpositions. The coding and description of overlay patterns are provided in Table 1.

In total, 486 ECGs were recorded in 49 patients. The structure of the recorded ECGs is shown in Table 2.

After recording, all results were anonymized and pseudonymized[1], placed, and annotated on the ECG.RU platform using a unified thesaurus. [9] Each ECG file was named according to the following principles: the first three digits referred to the patient subgroup number and serial number, and subsequent letters referred to the coding of electrode placement.

For example, the file name "101_dis_st" meant that this ECG was recorded in a patient with an unchanged ECG, and the electrodes were placed correctly. The file name "203_trns_crv" contains the ECG of a patient with left ventricular hypertrophy, and the C4, C5, and C6 electrodes are placed along the intercostal line (not along the horizontal line, but curved upward). The file name "602_trns_yg" contains the ECG of a patient with nonsinus rhythm, and the yellow and green electrodes are reversed. Examples of recorded

[1] GOST R 55036-2012/ISO/TS 25237:2008. P85 Group. National Standard of the Russian Federation. Health Informatics. Pseudonymization. Access: https://docs.cntd.ru/document/1200100339.

Table 1. Electrode placement variants and their coding

Russian wording	English equivalent	Part of the ECG filename	Comment	Incorrectly displayed leads
Стандартное расположение электродов	Standard electrodes' arrangement	dis_st	Correctly applied electrodes	All leads are correct
Грудные электроды: на 2 межреберья выше стандартной схемы	Precordial electrodes' misplacement: up to 2 intercostal spaces above the standard arrangement	dis_u2	Occasionally required for clinical indications, but in general, it is the most common electrode misplacement	Correct: I, II, III, aVR, aVL, and aVF. Dislocated: V1, V2, V3, V4, V5, and V6
Грудные электроды: на 2 межреберья ниже стандартной схемы	Precordial electrodes' misplacement: below to 2 intercostal spaces down the standard arrangement	dis_d2	Occasionally required for clinical indications, but in general, it is electrode misplacement	Correct: I, II, III, aVR, aVL, and aVF. Dislocated: V1, V2, V3, V4, V5, and V6
Перепутаны красный (R) и жёлтый (L) электроды	Reversal of the two arm electrodes	trns_ry	Misplacement	Incorrect: I, II, III, aVR, aVL, and aVF. Correct: V1, V2, V3, V4, V5, and V6
Перепутаны жёлтый (L) и зелёный (F) электроды	Reversal of the left arm and left leg electrodes	trns_yg	Misplacement	Incorrect: I, II, III, aVR, aVL, and aVF. Correct: V1, V2, V3, V4, V5, and V6
Все грудные электроды расположены на прямой линии от C1–C6	All chest electrodes are placed at the same line	trns_ln	Misplacement	Correct: I, II, III, aVR, aVL, aVF, and V1. Incorrect: V2, V3, V4, V5, and V6
Перепутаны C1–C2	Reversal of the C1 and C2 electrodes	trns_12c	Misplacement	Correct: I, II, III, aVR, aVL, aVF, V3, V4, V5, and V6. Incorrect: V1 and V2
Перепутаны C5–C6	Reversal of the C5 and C6 electrodes	trns-56c	Misplacement	Correct: I, II, III, aVR, aVL, aVF, V1, V2, V3, and V4. Incorrect: V5 and V6
Электроды C4, C5, C6 расположены очень близко друг к другу (соприкасаются)	The C4, C5, C6 electrodes are placed too close to each other (cheek to cheek)	trns_cls	Misplacement	Correct: I, II, III, aVR, aVL, aVF, V1, V2, and V3. Incorrect: V4, V5, and V6
Электроды C4, C5, C6 расположены по межреберью (не по горизонтальной линии, а искривляются вверх)	The C4, C5, C6 electrodes are misplaced along the intercostal space (not at a horizontal line, but curved upwards)	trns_crv	Misplacement	Correct: I, II, III, aVR, aVL, aVF, V1, V2, and V3. Incorrect: V4, V5, and V6

ECGs are shown in pairs in Figures 1–3 (overlay pattern and corresponding ECG).

DISCUSSION

The obtained results indicate a significant variability of ECG patterns depending on the initial changes and, probably, the patient's body type and state of mammary glands. Despite sufficient studies on the variability of normal ECG changes, [6–8] the variability of changes in the initial abnormal ECG is yet to be examined, which we will do in our next paper.

In the visual evaluation of the recorded ECGs, transposition was determined based on the relocation of the arm leads (red and yellow—RL) and precordial C1–C2 was not complicated. The placement of precordial cheek-to-cheek electrodes, in disposition with the transfer of the precordial leads higher or lower by two intercostal spaces than the Wilson scheme (upper2 and lower2), was less often reliably determined.

Table 2. Allocation of cardiograms recorded in patients

Placement type / Subgroup of ECG changes	Standard ECG placement	Dislocation of precordial electrodes	Transposition of limb electrodes	Transposition of precordial electrodes	Total
Normal ECG	10	20	20	49	99
ECG with LVH and CLBBB	9	18	18	45	90
ECG with RBBB	6	12	12	30	60
ECG with ST(–) depression	9	18	18	43	88
ECG with ST(+) elevation	7	14	14	35	70
ECG with any nonsinus rhythm	8	15	16	40	79
Total	49	97	98	242	486

Notes. ECG, electrocardiogram; CLBBB, complete left bundle branch block; LVH, left ventricular hypertrophy; RBBB, right bundle branch block.

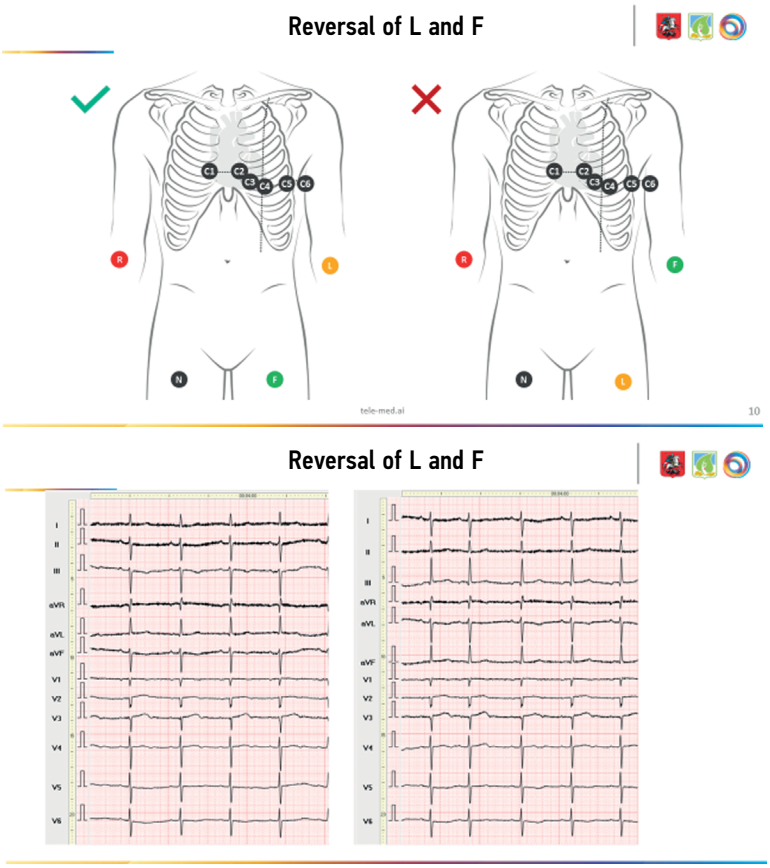

Fig. 1. Misplacement of L and F electrodes.

Transpositions of yellow and green limb electrodes (LF), changes in the position of precordial electrodes, when they are in line, curved, or C5–C6 electrodes are reversed, are difficult to determine even when directly comparing two cardiograms, with correct placement and transposition of electrodes. This probably depends on baseline ECG changes, body type (normosthenic, hypersthenic, or asthenic), breast size, or presence of an implant. Certainly, issues such as the consideration of the built, presence of a transplant, possible detailing of the initial ECG changes according to the reduced thesaurus, and comparison of the efficiency of recognition by a specialist and automatic analysis algorithms, require further evaluations.

Despite the known disadvantages, considering the high importance of the issue and difficulty of obtaining qualitatively recorded data and annotated ECGs, the obtained set of ECGs was published under an open license and used for both verification of algorithms of automatic ECG analysis and training of doctors and nursing staff.

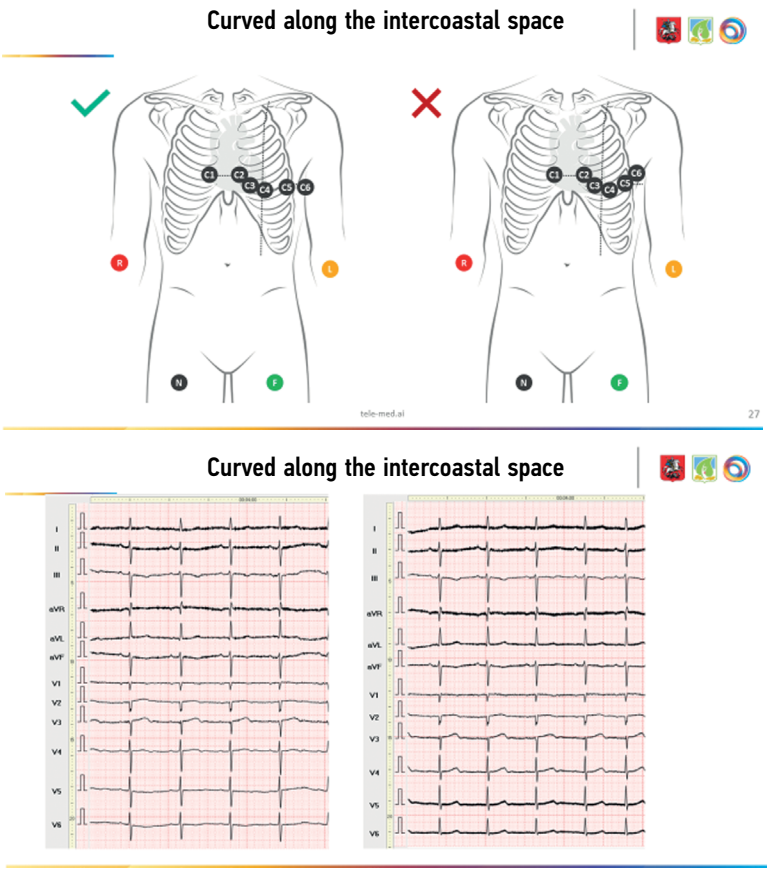

Fig. 2. Misplacement of C4–C6 electrodes.

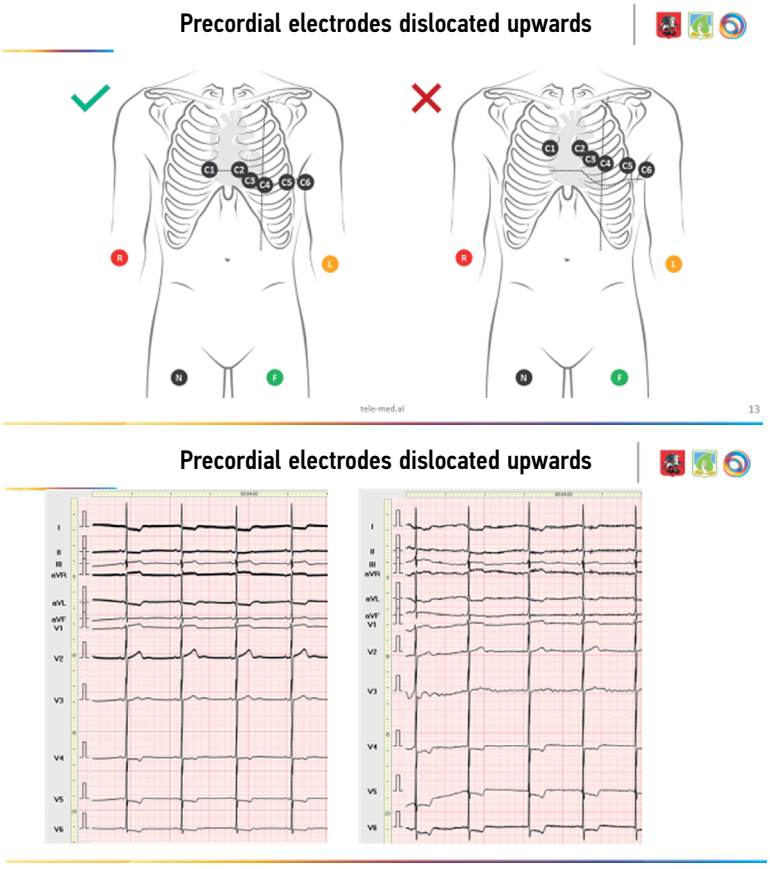

Fig. 3. Dislocation of C4–C6 electrodes.

Study limitations

On patient examination, their height, weight, and built (somatotypes) were not always considered. Taking these factors into account will probably increase the accuracy of determining the type of electrode dislocation.

CONCLUSION

In this study, an ECG dataset with different electrode dislocation variants was obtained. The dataset consists of ECG series recorded in each patient with different electrode overlap variants. The set includes not only normal ECGs but also different variants of abnormal ECGs.

ADDITIONAL INFORMATION

Funding source. This article was not supported by any external sources of funding.

Competing interests. The authors declare that they have no competing interests.

Authors' contribution. All authors made a substantial contribution to the conception of the work, acquisition, analysis, interpretation of data for the work, drafting and revising the work, final approval of the version to be published and agree to be accountable for all aspects of the work. D.V. Drozdov — concept development, organization of annotation process, thesaurus development, author supervision; T.M. Gazashvili — organization of ECG registration, depersonalization and transfer of records; D.V. Shutov — concept development, organization of depersonalization, transfer, annotation, author supervision; A.S. Skoda — general management, organization of the work of the center for instrumental diagnostics.

Acknowledgments. The authors express their gratitude to Medical Computer Systems LLC, personally to the director of the company Prilutsky Dmitry Anatolyevich and all employees of the platform ECG.ru. Meshcherina Tatiana Evgenievna and Shalmonova Elena Gennadievna for highly qualified ECG registration.

REFERENCES

1. Rosen AV, Koppikar S, Shaw C, Baranchuk A. Common ECG lead placement errors. Part I: Limb lead reversals. *Int J Med Students*. 2014;2(3):92–98. doi: 10.5195/ijms.2014.95

2. Rosen AV, Koppikar S, Shaw C, Baranchuk A. Common ECG lead placement errors. Part II: precordial misplacements. *Int J Med Students*. 2014;2(3):99–103. doi: 10.5195/ijms.2014.96

3. Jekova I, Krasteva V, Leberet R, et al. Inter-lead correlation analysis for automated detection of cable reversals in 12/16-lead ECG. *Comput Methods Programs Biomed*. 2016;(134):31–41. doi: 10.1016/j.cmpb.2016.06.003

4. Kania M, Rix H, Fereniec M, et al. The effect of precordial lead displacement on ECG morphology. *Med Biological Engineering Computing*. 2014;52(2):109–119. doi: 10.1007/s11517-013-1115-9.

5. Wenger W, Kligfield P. Variability of precordial electrode placement during routine electrocardiography. *J Electrocardiol*. 1996;29(3):179–184. doi: 10.1016/s0022-0736(96)80080-x

6. García-Niebla J, Llontop-García P, Valle-Racero JI, et al. Technical mistakes during the acquisition of the electrocardiogram. *Ann Noninvasive Electrocardiol*. 2009;14(4):389–403. doi: 10.1111/j.1542-474X.2009.00328.x

7. Peberdy MA, Ornato JP. Recognition of electrocardiographic lead misplacements. *Am J Emergency Med*. 1993;11(4):403–405. doi: 10.1016/0735-6757(93)90177-d

8. Kemp B, Olivan J. European data format 'plus' (EDF+), an EDF alike standard format for the exchange of physiological data. *Clin Neurophysiol*. 2003;114(9):1755–1761. doi: 10.1016/s1388-2457(03)00123-8

9. Drozdov DV, Shutov DV, Gazashvili TM, et al. Coordination of medical ECG descriptions using a thesaurus (list of standard phrases) of conclusions. *Medical Alphabet*. 2022;(10):19–26. (In Russ). doi: 10.33667/2078-5631-2022-11-19-26

СПИСОК ЛИТЕРАТУРЫ

1. Rosen A.V., Koppikar S., Shaw C., Baranchuk A. Common ECG lead placement errors. Part I: Limb lead reversals // Int J Med Students. 2014. Vol. 2, N 3. P. 92–98. doi: 10.5195/ijms.2014.95

2. Rosen A.V., Koppikar S., Shaw C., Baranchuk A. Common ECG lead placement errors. Part II: precordial misplacements // Int J Med Students. 2014. Vol. 2, N 3. P. 99–103. doi: 10.5195/ijms.2014.96

3. Jekova I., Krasteva V., Leberet R., et al. Inter-lead correlation analysis for automated detection of cable reversals in 12/16-lead ECG // Comput Methods Programs Biomed. 2016. N 134. P. 31–41. doi: 10.1016/j.cmpb.2016.06.003

4. Kania M., Rix H., Fereniec M., et al. The effect of precordial lead displacement on ECG morphology // Med Biological Engineering Computing. 2014. Vol. 52, N 2. P. 109–119. doi: 10.1007/s11517-013-1115-9

5. Wenger W., Kligfield P. Variability of precordial electrode placement during routine electrocardiography // J Electrocardiol. 1996. Vol. 29, N 3. P. 179–184. doi: 10.1016/s0022-0736(96)80080-x

6. García-Niebla J., Llontop-García P., Valle-Racero J.I., et al. Technical mistakes during the acquisition of the electrocardiogram // Ann Noninvasive Electrocardiol. 2009. Vol. 14, N 4. P. 389–403. doi: 10.1111/j.1542-474X.2009.00328.x

7. Peberdy M.A., Ornato J.P. Recognition of electrocardiographic lead misplacements // Am J Emergency Med. 1993. Vol. 11, N 4. P. 403–405. doi: 10.1016/0735-6757(93)90177-d

8. Kemp B., Olivan J. European data format 'plus' (EDF+), an EDF alike standard format for the exchange of physiological data // Clin Neurophysiol. 2003. Vol. 114, N 9. P. 1755–1761. doi: 10.1016/s1388-2457(03)00123-8

9. Дроздов Д.В., Шутов Д.В., Газашвили Т.М., и др. Согласование врачебных описаний ЭКГ с применением тезауруса (списка типовых фраз) заключений // Медицинский алфавит. 2022. № 10. С. 19–26. doi: 10.33667/2078-5631-2022-11-19-26

AUTHORS' INFO

*** Dmitry V. Shutov,** MD, Dr. Sci. (Med);
address: 24/1 Petrovka street, 127051 Moscow, Russia;
ORCID: 0000-0003-1836-3689;
eLibrary SPIN: 9381-2456;
e-mail: ShutovDV@zdrav.mos.ru

Dmitry V. Drozdov, MD, Cand. Sci. (Med);
ORCID: 0000-0001-7374-3604;
eLibrary SPIN: 2279-9657;
e-mail: cardioexp@gmail.com

Tamara M. Gazashvili;
ORCID: 0000-0002-5875-9699;
eLibrary SPIN: 4208-2303;
e-mail: Tamaradoc24@gmail.com

Andrey S. Shkoda, MD, Dr. Sci. (Med);
ORCID: 0000-0002-9783-1796;
eLibrary SPIN: 4520-2141;
e-mail: a.shkoda@67gkb.ru

ОБ АВТОРАХ

*** Шутов Дмитрий Валерьевич,** д-р мед. наук;
адрес: Россия, 127051, Москва, ул. Петровка, д. 24, стр. 1;
ORCID: 0000-0003-1836-3689;
eLibrary SPIN: 9381-2456;
e-mail: ShutovDV@zdrav.mos.ru

Дроздов Дмитрий Владимирович, канд. мед. наук;
ORCID: 0000-0001-7374-3604;
eLibrary SPIN: 2279-9657;
e-mail: cardioexp@gmail.com

Газашвили Тамара Михайловна;
ORCID: 0000-0002-5875-9699;
eLibrary SPIN: 4208-2303;
e-mail: Tamaradoc24@gmail.com

Шкода Андрей Сергеевич, д-р мед. наук;
ORCID: 0000-0002-9783-1796;
eLibrary SPIN: 4520-2141;
e-mail: a.shkoda@67gkb.ru

* Corresponding author / Автор, ответственный за переписку

DOI: https://doi.org/10.17816/DD375327

Проблемы облучения персонала в современных медицинских технологиях

С.А. Рыжкин[1, 7], Ю.В. Дружинина[1, 2], З.А. Лантух[2], И.В. Солдатов[2], В.Н. Лесняк[3], Д.П. Лебедев[3], Д.Н. Самочатов[4], М.П. Семенова[5], В.А. Сухов[6], С.Е. Охрименко[1]

[1] Российская медицинская академия непрерывного профессионального образования, Москва, Российская Федерация
[2] Научно-практический клинический центр диагностики и телемедицинских технологий, Москва, Российская Федерация
[3] Федеральный научно-клинический центр специализированных видов медицинской помощи и медицинских технологий, Москва, Российская Федерация
[4] Городская клиническая больница № 67 имени Л.А. Ворохобова, Москва, Российская Федерация
[5] Государственный научный центр Российской Федерации — Федеральный медицинский биофизический центр имени А.И. Бурназяна, Москва, Российская Федерация
[6] Первый Московский государственный медицинский университет имени И.М. Сеченова (Сеченовский Университет), Москва, Российская Федерация
[7] Казанский государственный медицинский университет, Казань, Российская Федерация

АННОТАЦИЯ

Обоснование. Широкое применение источников ионизирующего излучения в медицинской практике (кардиоэндоваскулярной хирургии, эндоскопии, травматологии, урологии, нейрохирургии, стоматологии, отделениях радиоизотопной диагностики) приводит к облучению хрусталика глаза и кожи рук рассеянным излучением низкой интенсивности. Введение МАГАТЭ новых рекомендаций по снижению предела годовой эквивалентной дозы на хрусталик (20 мЗв) привело к тому, что оценка дозы по хрусталику на основе эффективной дозы стала некорректной.

Цель — анализ подходов и оценка эквивалентных доз облучения хрусталика глаза и кожи рук медицинского персонала при проведении различных диагностических исследований под воздействием рентгеновского излучения и гамма-изучения радиофармпрепарата, а также сравнение полученных результатов с ранее опубликованными данными.

Материалы и методы. Применялся метод термолюминесцентной дозиметрии. Оценка доз проводилась у персонала кардиоэндоваскулярной хирургии, эндоскопии, изотопной диагностики, стоматологии, урологии.

Результаты. Расчётные годовые эквивалентные дозы на хрусталик глаза у врачей отделений кардиоэндоваскулярной хирургии находились в диапазоне от 35 до 90 мЗв, среднего медицинского персонала — от 6 до 19 мЗв (в отдельных случаях у врача — до 225 мЗв, у медицинской сестры — до 180 мЗв); персонала отделения радиоизотопной диагностики — от 4,5 до 9 мЗв. Годовые расчётные эквивалентные дозы на кожу рук у персонала кардиоэндоваскулярной хирургии составили от 17 до 100 мЗв, а при работе с радиофармпрепаратами — от 24 до 220 мЗв. Показано, что использование оценки усреднённой дозы за одну операцию у врачей кардиоэндоваскулярной хирургии, как правило, неизбежно приводит к превышению эквивалентной дозы на хрусталик глаза через определённое количество операций.

Заключение. При превышении определённого количества операций (от 100 до 200) у врачей кардиоэндоваскулярной хирургии могут формироваться эквивалентные дозы на хрусталик глаза более 20 мЗв в год. Установлено поражение хрусталика глаза при существующих уровнях облучения у врача кардиоэндоваскулярной хирургии. Полученные результаты свидетельствуют о необходимости дальнейших дозиметрических измерений и эпидемиологических исследований, на основании которых могут быть разработаны рекомендации по радиационной защите хрусталика глаза и кожи рук медицинского персонала, осуществляющего работу в поле рассеянного, гамма- и рентгеновского излучения низкой интенсивности.

Ключевые слова: источники ионизирующего излучения; персонал; кардиоэндоваскулярная хирургия; отделение радиоизотопной диагностики; хрусталик глаза; кожа рук; рассеянное излучение низкой интенсивности; годовая эквивалентная доза; термолюминесцентная дозиметрия; профессиональное поведение.

Как цитировать

Рыжкин С.А., Дружинина Ю.В., Лантух З.А., Солдатов И.В., Лесняк В.Н., Лебедев Д.П., Самочатов Д.Н., Семенова М.П., Сухов В.А., Охрименко С.Е. Проблемы облучения персонала в современных медицинских технологиях // *Digital Diagnostics*. 2023. Т. 4, № 2. С. 142–155. DOI: https://doi.org/10.17816/DD375327

Рукопись получена: 03.05.2023 **Рукопись одобрена:** 25.05.2023 **Опубликована:** 15.06.2023

DOI: https://doi.org/10.17816/DD375327

Problems of personnel irradiation in modern medical technologies

Sergey A. Ryzhkin[1, 7], Yuliya V. Druzhinina[1, 2], Zoya A. Lantuh[2], Ilya V. Soldatov[2], Viktor N. Lesnyak[3], Dmitriy P. Lebedev[3], Denis N. Samochatov[4], Maria P. Semenova[5], Vitaly A. Sukhov[6], Sergey E. Okhrimenko[1]

[1] Russian Medical Academy of Continuous Professional Education, Moscow, Russian Federation
[2] Research and Practical Clinical Center for Diagnostics and Telemedicine Technologies, Moscow, Russian Federation
[3] Federal Research and Clinical Center of Specialized Medical Care and Medical Technologies, Moscow, Russian Federation
[4] City Clinical Hospital No. 67 named after L.A. Vorokhobov, Moscow, Russian Federation
[5] State Research Center — Burnasyan Federal Medical Biophysical Center, Moscow, Russian Federation
[6] The First Sechenov Moscow State Medical University (Sechenov University), Moscow, Russian Federation
[7] Kazan State Medical University, Kazan, Russian federation

ABSTRACT

BACKGROUND: The widespread use of radiation sources in medical practice (cardio-endovascular surgery, endoscopy, traumatology, urology, neurosurgery, dentistry, and radioisotope diagnostics departments) leads to irradiation of the lens of the eye and the skin of the hands. The introduction of new recommendations by the IAEA to reduce the limit of the annual equivalent dose to the lens (20 mSv) has led to an inaccurate dose assessment based on the effective dose.

AIM: To analyze approaches and assess equivalent doses of irradiation of the lens of the eye and skin of the hands of medical personnel during various diagnostic studies under the influence of X-rays and radiopharmaceuticals studies and to compare the results obtained with previously published data.

MATERIALS AND METHODS: Thermo-luminescent dosimetry was used. Dose assessment was performed by cardio-endovascular surgery, endoscopy, isotope diagnostics, dentistry, and urology personnel.

RESULTS: The estimated annual equivalent doses to the lens of the eye for doctors of cardio-endovascular surgery departments, in most cases, ranging 35–90 mSv, 6–19 mSv for the average medical staff (in some cases, the doctor [⩽225 mSv] and the nurse [⩽180 mSv]) and 4.5–9 mSv for the staff of the department of radioisotope diagnostics. The annual calculated equivalent doses to the skin of the hands for cardio-endovascular surgery personnel were 17–100 and 24–220 mSv for the staff working with radiopharmaceuticals. It is shown that the use of an estimate of the average dose per operation by cardio-endovascular surgery doctors, as a rule, inevitably leads to an excess of the equivalent dose to the lens of the eye after a certain number of operations.

CONCLUSION: When a certain number of operations are exceeded (100–200), equivalent doses to the eye's lens in cardio-endovascular surgery doctors above 20 mSv per year can be formed. At current radiation levels, a lesion of the eye's lens was found in a cardio-endovascular surgery doctor. The results indicate the need for further dosimetric measurements and epidemiological studies, based on which recommendations for radiation protection of the eye's lens and the skin of the hands of medical personnel working in low-intensity, scattered, gamma X-ray radiation can be developed.

Keywords: annual equivalent dose; cardio-endovascular surgery; eye lens; hand skin; low-intensity scattered radiation; professional behavior; radiation sources; radioisotope diagnostics department; staff; thermo-luminescent dosimetry.

To cite this article

Ryzhkin SA, Druzhinina YuV, Lantuh ZA, Soldatov IV, Lesnyak VN, Lebedev DP, Samochatov DN, Semenova MP, Sukhov VA, Okhrimenko SE. Problems of personnel irradiation in modern medical technologies. *Digital Diagnostics.* 2023;4(2):142–155. DOI: https://doi.org/10.17816/DD375327

Received: 03.05.2023 **Accepted:** 25.05.2023 **Published:** 15.06.2023

DOI: https://doi.org/10.17816/DD375327

使用现代医疗技术时医务人员受到辐射的问题

Sergey A. Ryzhkin[1, 7], Yuliya V. Druzhinina[1, 2], Zoya A. Lantuh[2], Ilya V. Soldatov[2], Viktor N. Lesnyak[3], Dmitriy P. Lebedev[3], Denis N. Samochatov[4], Maria P. Semenova[5], Vitaly A. Sukhov[6], Sergey E. Okhrimenko[1]

[1] Russian Medical Academy of Continuous Professional Education, Moscow, Russian Federation
[2] Research and Practical Clinical Center for Diagnostics and Telemedicine Technologies, Moscow, Russian Federation
[3] Federal Research and Clinical Center of Specialized Medical Care and Medical Technologies, Moscow, Russian Federation
[4] City Clinical Hospital No. 67 named after L.A. Vorokhobov, Moscow, Russian Federation
[5] State Research Center — Burnasyan Federal Medical Biophysical Center, Moscow, Russian Federation
[6] The First Sechenov Moscow State Medical University (Sechenov University), Moscow, Russian Federation
[7] Kazan State Medical University, Kazan, Russian federation

简评

论证。电离辐射源在医疗实践（心血管内外科、内窥镜检查、创伤科、泌尿科、神经外科、牙科、放射性同位素诊断部门）中的广泛使用导致眼球晶状体和手部皮肤受到低强度散射辐射。国际原子能机构引入的关于减少晶状体的年度等效剂量限制（20毫西弗）的新建议导致基于有效剂量的晶状体剂量评估是不正确的。

该研究的目的是分析方法和评估医务人员在X射线辐射和放射性药物的伽马射线影响下进行各种诊断检查时眼球晶状体和手部皮肤的等效辐射剂量，并对所得结果与以前公布的数据进行比较。

材料和方法。采用了热释光剂量测定法。评估了心血管内外科、内窥镜、同位素诊断、牙科和泌尿科人员的剂量。

结果。心血管外科医生眼球晶状体的计算年度等效剂量为35至90毫西弗，护理人员的为6至19毫西弗（在某些情况下，医生的高达225毫西弗，护士的高达180毫西弗），放射性同位素诊断部门人员的为4.5至9毫西弗。心血管内外科人员手部皮肤的计算年度等效剂量为17至100毫西弗，而在使用放射性药物的工作中，则为24至220毫西弗。事实证明，使用心脑血管外科医生每次手术时的平均剂量估算，通常不可避免地会在一定数量的手术后导致晶状体的超标等效剂量。

结论。超过一定数量的手术（100至200），心血管内外科医生每年接受的眼球晶状体的等效剂量可能超过20毫西弗。在现有辐射水平下，心血管内外科医生眼球晶状体的病变已经是确定的。所得结果证明，有必要进行进一步的剂量测定和流行病学调查，在此基础上可以制定在散射、伽马和X射线的低强度辐射影响下工作的医务人员的眼球晶状体和手部皮肤的辐射防护建议。

关键词：电离辐射源；工作人员；心血管内外科；放射性同位素诊断部门；眼球晶状体；手部皮肤；低强度散射辐射；年度等效剂量；热释光剂量测定法；职业行为。

To cite this article
Ryzhkin SA, Druzhinina YuV, Lantuh ZA, Soldatov IV, Lesnyak VN, Lebedev DP, Samochatov DN, Semenova MP, Sukhov VA, Okhrimenko SE. 使用现代医疗技术时医务人员受到辐射的问题. *Digital Diagnostics.* 2023;4(2):142–155. DOI: https://doi.org/10.17816/DD375327

收到：03.05.2023 **接受：**25.05.2023 **发布日期：**15.06.2023

BACKGROUND

Sources of ionizing radiation are widely used in the current clinical practice. When they are used, sources of ionizing radiation can affect medical personnel of cardioendovascular surgery (CEVS), traumatology, urology, neurosurgery, dentistry, general surgery, and intensive care departments.

In the departments of nuclear diagnostics, the highest radiation exposure is on nurses who prepare and administer radiopharmaceuticals and radiology technicians who examine patients using gamma cameras and single-photon emission computed tomography (CT) or positron emission tomography combined with computed tomography (PET/CT). In these cases, medical personnel are exposed directly and permanently to low-intensity scattered gamma and X-ray radiation. Their eyes and skin are affected by radiation scattered by the patient's body and reflected from external objects. Based on the available data, the ratio of an equivalent lens dose to the effective dose can be calculated in the photon radiation energy range of 0.01–10 MeV. In the range of gamma radiation energies of 0.06–10 MeV, the equivalent lens dose numerically exceeds the effective dose by approximately 20%, whereas in the range of <0.05 MeV, this increase ranges from several times to several dozen times.

Therefore, the basic effective dose limit no longer ensures compliance with the dose limit when the eye lens is irradiated. While strong penetrating types of radiation make the main contribution to the effective dose, weak penetrating radiation (beta particles, photons with energies of <15 keV) provide the maximum doses in the sensitive layer of the skin and eye lens [1,2]. This issue attracted special attention after relevant publications of the International Commission on Radiological Protection and the International Atomic Energy Agency, which supported recommendations to reduce the equivalent dose limit for the lens from 150 to 20 mSv annually and optimize the radiation protection of personnel, considering the "as low as reasonably achievable" principle [3-9].

This study aimed to evaluate the equivalent radiation doses for the eye lens and hand skin of medical personnel in diagnostic examinations using X-ray radiation and gamma radiation of radiopharmaceuticals and compare these results with previously published data on radiation doses for the eye lens and hand skin of medical personnel.

MATERIALS AND METHODS

We have assessed equivalent radiation doses for the eye lens and hand skin of medical personnel exposed to X-ray and gamma radiation of radiopharmaceuticals. A thermoluminescent dosimetry (TLD) method was used to estimate doses. Personal dose equivalent Hp(3) dosimeters with TLD-1011T (Research and Technology Center "Praktika," Russia) and TLD-100 (USA) detectors were used. Measurement ranged from 30 μSv to 12 Sv for energies of 0.005–10 MeV. Dosimeters were exposed by attaching them to the central part of the frontal surface of the hair cover of the personnel. The calendar exposure time was 3–6 weeks; however, the total number of dosimetry operations was recorded for consideration when assessing and calculating radiation doses.

Detector data were processed using a HARSHAW TLD system 4000 thermoluminescent analyzer (Thermo Scientific Ltd., MA, USA) at the Department of Radiochemistry of the M. V. Lomonosov Moscow State University. After reading the thermoluminescence curve and detector annealing, detectors were individually calibrated in the air using a ^{137}Cs gamma radiation source (Eγ = 661 keV), type Ts2-5. The main measurement error with a confidence probability of 0.95 did not exceed 10%. To assess the contribution of the background radiation, some dosimeters were exposed as controls. In studies conducted in 2014–2021 in Moscow (four CEVS departments of three city hospitals, one department of urology, endoscopy, department of CEVS of the Federal Medical-Biological Agency, medical center, PET center and department of dentistry of a private medical center, and department of nuclear diagnostics of the clinic at Russian Medical Academy of Continuous Professional Education) and Kazan (four departments of CEVS in four healthcare organizations), 61 findings were obtained for the equivalent lens dose, including 46 findings in CEVS personnel (22 physicians, 24 nurses), 2 in endoscopy personnel, 4 in dentistry personnel, 1 in urology personnel, and 8 in nuclear diagnostics personnel (^{99м}Tc and ^{18}F).

Clinical examination of personnel included ophthalmological examination such as visometry (with and without correction), refractometry, biomicroscopy of the bulbar conjunctiva and vitreous body, Norn test, and B-scan of the eye.

The study assessed personal radiation doses not combined into a single statistical set because of the characteristics of the exposure conditions for each patient. Moreover, this allowed us to establish a range of radiation dose levels and factors potentially affecting the dose formation.

RESULTS

Several approaches are employed to investigate equivalent lenses in medical personnel. The first approach is to wear a thermoluminescent dosimeter (fixed in a certain site on the head of the medical personnel) for a predetermined time and measure the personal equivalent lens dose Hp(3) after the wearing period ends. This approach is described in MU 2.6.1.3747-22.[1] Such investigations for

[1] Guidelines MU 2.6.1.3747-22 "Control of personal equivalent doses of external radiation for the lens of the eye in personnel) (approved by the Federal Service for Surveillance on Consumer Rights Protection and Human Wellbeing on May 17, 2022). Available from: https://base.garant.ru/405781929/.

measuring equivalent lens doses in the personnel of Moscow healthcare institutions were conducted in 2014 for various medical professions in the radiation monitoring laboratory of the Department of Radiochemistry of M. V. Lomonosov Moscow State University. The exposure time of TLD Hp(3) was 1 month. The results are presented in Table 1.

The highest values were recorded in CEVS physicians. However, if full responsibility for the use of personal dosimeters is delegated to personnel, partial loss of information on some dosimetry operations may occur, and this is a weakness of such an approach. Another weakness is related to the unreliability of information about the actual number of operations with dosimeters. Therefore, the dose measurement for certain periods with subsequent annual dose recalculation is not suitable for radiation exposure assessment.

The second approach is to measure the accumulated lens radiation dose for a certain number of operations with individual dosimetry. This approach allowed estimating the average dose for one conditional interventional examination. Depending on the procedure type, interventional examinations are classified into "diagnostic" and "therapeutic." Diagnostic interventional examinations are typically 20–30 min long and have a total exposure time of approximately 3–7 min. Therapeutic interventional examinations are much longer (their duration depends on the complexity of the operation). In one case, the operation time was 2.5 h, and the high voltage time was 28 min.

Our results are presented in Tables 2–4.

Doses per operation (manipulation) differ significantly both in different technologies and within the same specialty. Special attention is needed to the extremely high dose of CEVS nurse exposure. Important factors appear to include the work methods of the individual specialist (number of images, ratio of image/scopy, etc.), particularly the distance from the main operating surgeon and their assistant or nurse to the direct beam zone. This factor can be defined as "professional behavior." The estimated annual doses in clinic A ranged from 35 to 90 mSv for CEVS physicians, up to 180 mSv for a nurse, and up to 8 mSv for a nurse in the nuclear diagnostics department.

The results of the lens dose assessment in clinic B are presented in Table 3. The estimated annual equivalent dose for the eye lens in clinic B was 60 mSv in physicians and 6–18 mSv in nurses. For the professional behavior parameter, due to the nature of work, the second nurse ("nurse 2") usually stays longer and closer to the doctor's workplace ("operator") than the first nurse ("nurse 1").

In clinic C, some features of lens dose formation were observed. The highest dose was recorded in a physician with the least number of operations. The estimated annual doses ranged from 53 to 225 mSv in physicians and approximately 19 mSv in nurses. The measurement results are presented in Table 4.

Some factors were assessed, which could potentially affect the dose formation: the number of "high-dose"

Table 1. Results of Hp(3) measurements and an approximate assessment of an annual equivalent dose for the eye lens (H) in various medical personnel [10,11]

Profession	Number of subjects, *n*	Hp(3), mSv	Annual H, mSv
CpeNurses (work with radiopharmaceuticals, ^{99m}Tc)	2	0,37–0,40	4,4–4,8
Angiographer	6	0,31–2,20	3,7–26,4
Nurses (angiography)	5	0,15–0,42	1,8–5,0
Urologist	1	0,72	8,6
Dentist	4	0,13–0,18	1,6–2,2

Table 2. Equivalent lens doses for physicians and nurses in cardioendovascular surgery, endoscopy, and nuclear diagnostics departments of clinic A [12,13]

Profession	Dose per exposure, mSv	Number of operations with dosimetry	Dose per operation, mSv	Acceptable number of operations annually	Approximate number of operations annually
CEVS nurse	12,6	31	0,4	50	450
CEVS physician 1	1,28	13	0,1	200	350
CEVS physician 2	1,69	20	0,085	235	450
CEVS physician 3	1,05	5	0,2	100	450
Endoscopic physician	2,82	58	0,05	400	380
Endoscopic nurse	2,79	58	0,05	400	380
Nurse ^{99m}Tc	0,7	134*	0,005	4000	1600

Note. * Patients.

Table 3. Equivalent lens doses for physicians and nurses in the cardioendovascular department of clinic B

Profession	Dose per exposure, mSv	Number of operations with dosimetry	Dose per operation, mSv	Acceptable number of operations annually	Approximate number of operations annually
Physician	5,7	64	0,1	200	600
Nurse 1	1,5	68	0,02	1000	300
Nurse 2	2,4	41	0,06	340	300

Table 4. Equivalent lens doses for physicians and nurses in the cardioendovascular department of clinic C

Profession	Dose per exposure, mSv	Number of operations with dosimetry	Dose per operation, mSv	Acceptable number of operations annually	Approximate number of operations annually
Physician 12	3,86	35	0,11	180	750
Physician 16	3,5	51	0,07	285	750
Physician 18	3,4	12	0,3	>70	750
Nurse	1,74	68	0,025	800	750

operations, ratio of operator-assistant functions, cumulative dose during operations, and height of the operator (Table 5). The table shows that none of the above factors has a direct effect on dosimetry results. Obviously, the most important exposure factors include not only the number of operations but also their specificity and "professional behavior," which determine the distance from the workplace of the "operator" to the tube. In this context, anthropometric characteristics (e.g., height) can be relevant because they affect the location of personnel relative to the direct beam zone.

Some attention should be also given to certain limitations of available collective protective equipment and the lack of personal eye protection in many organizations. Stationary protective equipment is clearly insufficient because of a narrow hanging screen and the absence or inappropriateness of hanging transparent screens. The use of such equipment could significantly reduce the requirements for the protective properties of personal protective equipment (e.g., 0.15 mm Pb for body protection and 0.1 mm Pb for eyes). Such an approach could generally improve the working conditions for medical personnel.

The equivalent lens doses for medical personnel in various nuclear diagnostics departments were compared with data on the personnel dose load in the diagnostic laboratory of the PET center. A study [14] evaluated the equivalent lens doses in medical personnel of the PET center working with ^{18}F-based products, including workload assessment for personnel working with ^{18}F (Table 6).

The equivalent effective dose for nuclear diagnostics personnel of the PET center ranged from 4.2 to 4.9 μSv/GBq (4.2–4.9 μSv/patient) during injection/packing operations and 6 μSv/GBq (2.3 μSv/patient) in a PET/CT technician,

Table 5. Factors potentially affecting radiation dose formation

Physician	Ratio of operation number and dose per patient >1 Gy/>2 Gy	Cumulative dose, Gy	Ratio operator/assistant	Height, cm
Physician 12	19/5	39	24/11	183
Physician 16	17/5	49	29/22	185
Physician 18	3/1	9,4	12/0	170

Table 6. Lens radiation doses (H_{lens}) and effective dose (E) in diagnostic laboratory personnel of the diagnostic laboratory of the PET center depending on the radiopharmaceutical activity and number of patients. [14]

Specialist	Operations	A, GBq	Number of patients	H_{lens}, mSv Hp(3)	E, mSv Hp(10)
A	Nurse, more administration than packing operations	109,2	283	0,63	0,53
B	Packer, more packing than administration operations	124,5	324	0,67	0,52
C	PET/CT technician, scan	135,2	354	0,8	0,81

Note. PET/CT, positron emission tomography/computed tomography.

according to the equivalent lens dose of 5.4–5.8 μSv/GBq (2.1–2.2 μSv/patient) and 5.9 μSv/GBq (2.3 μSv/patient), respectively. The exposure level was directly dependent on the total activity used (or the number of patients as an "equivalent" of activity). The evaluation of the dose–activity/dose–patient relationship makes it possible to calculate the minimum number of required staff. For packing/administration operations, the largest dose load is associated with the "administration" operation, which is the main dose-forming factor for this technology. Considering the workload, the highest lens radiation dose was reported in PET/CT technicians. This can be explained by his/her contact with all activities, whereas the nurse and packer "share" this activity. Values of Hp(10) and Hp(3) doses were nearly close when working with radiopharmaceuticals. Preliminary estimates of the annual equivalent lens doses for 11 months (excluding holidays) are presented in Table 7.

The highest dose is reported in a CT technician. However, he/she showed extremely cautious "working behavior" (keeping the maximum distance and minimizing contact). The staff workload was 26 patients per 14-h shift. With workload intensification (excluding a rather lengthy registration procedure), the dose load also increased proportionally. In the absence of activity distribution between personnel (a and b), the equivalent lens dose can be at least 15 mSv annually. Data obtained are consistent with previous data [15,16], in which the median and maximum values ranged from 4 to 14 and from 6 to 23 mSv, respectively. The ratio of the patient number and staff number is an important factor in determining the levels of exposure in nurses in nuclear diagnostic departments using specific technologies.

In addition to the lens dose assessment, hand skin exposure doses were assessed for the staff of the CEVS and nuclear diagnostics departments. Results are presented in Table 8. As shown in this table, equivalent doses in the above studies do not exceed the limit of the equivalent dose for the skin (500 mSv). These measurements characterize a separate local skin site (usually the back of the middle finger) and cannot fully characterize doses over the entire hand (both the back and palmar surface). Authors are aware of two cases of visible abnormal hand skin changes in CVES physicians, including permanent local foci of dry dermatitis in the palmar-outer edge of both hands and redness in backhand surfaces after surgery.

For this paper, the authors investigated skin radiation doses using hand phantoms for CVES surgeons. Obtained data indicate the possibility of hand skin exposure at the level of ⩾1 Gy annually [13]. The estimated annual equivalent skin doses for nuclear diagnostics personnel of the PET center for 11 working months are presented in Table 9 [15].

The largest contribution to the nurse skin dose load is the administration of a radiopharmaceutical to a patient. The distribution of the dose load between nurse 1 and the "packer" (or nurse 2) deserves special attention. If nurse 1 performs all (100%) injections, the equivalent hand skin dose can be approximately 450 mSv annually. The given data are

Table 7. Estimated annual equivalent lens doses in isotope laboratory personnel of the PET center. [12,14]

Personnel	Function	H, mSv annually
A	Administration ~60%, packing 40%	6,9
B	Packing ~60%, administration 40%	7,4
C	PET/CT technician	8,8

Note. PET/CT: positron emission tomography/computed tomography.

Table 8. Estimated annual equivalent hand skin doses in cardioendovascular surgery. [12,14]

Personnel	H_{skin**} per exposure, mSv	Number of operations	Number of operations annually	H_{skin} annual/estimated
CEVS nurse	1,2	31	450	17
CEVS physician 1	0,7	13	350	19
CEVS physician 2	4,5	20	450	100
CEVS physician 3	1,1	5	450	100

Note. CEVS, cardioendovascular surgery.

Table 9. Estimated annual equivalent skin doses (Hp, 0.07) for fingers (middle finger) in isotope laboratory personnel of the PET center

Personnel	Function	Hp (0.07), mSv annually
a	Administration ~60%, packing 40%	220
b	Packing ~60%, administration 40%	132
c	PET/CT technician	24

Note. PET/CT: positron emission tomography/computed tomography.

well comparable with work indicators [17] ranging from 3 to 512 mSv.

To clarify these data, equivalent skin doses were assessed using hand phantoms of CVES personnel. Equivalent doses for hand phantoms for one operation ranged from 0.5 to 2.5 mSv, with an average input dose of 500 mGy per patient body phantom. Considering the total number of operations per year for a particular surgeon (300–600 operations), equivalent doses for local hand skin sites may exceed the established dose limit of 500 mSv. In the study of DNA double-strand breaks in skin fibroblasts irradiated in parallel with dosimeters, the number of γH2AX and 53BP1 foci at 30 min and up to 24 h after irradiation statistically significantly (p <0.05) exceeded the control values by >2 times, and even after 72 h, indicators did not decrease to control values [13,18].

DISCUSSION

This problem has a long history of scientific discussion [19–24]. Equivalent lens and skin doses were assessed in interventional examinations per single operation. Lens doses ranged from 0.05 to 0.4 mSv. Hand skin doses ranged from 0.3 to 1.1 mSv. Data scatter is up to approximately eight times for the eye lens and up to four times for the hands. In a previous study [19], the skin dose was equal to the lens dose per operation. Equivalent lens doses per operation in interventional procedures have ranged significantly depending on the type of procedure and presence or absence of personal or collective protective equipment [2]. Owing to the significant uncertainty of available data, lens radiation doses still require further evaluation. In a previous study [25], an increased prevalence of cataracts was reported in medical personnel exposed to ionizing radiation, with a higher prevalence in CVES personnel.

In a 17-month study, three radiologists performed pediatric and adult interventions. For 1 year, 276–338 procedures were performed, and 20% of them were in pediatrics. The annual doses for the left eye exceeded 20 mSv and ranged from 21 to 61 mSv. Despite eye protection by special goggles, doses exceeded 6 mSv and ranged from 13 to 48 mSv for both eyes. No significant differences were found in lens doses per procedure between pediatric and adult interventions [26].

When studying the lens dose load in nine interventional radiologists, the equivalent doses for the eye lens and neck skin were evaluated for 6 months. The lens doses were 0.18 ± 0.11 mSv and 35.3 ± 6.6 mSv per working day and 200 working days, respectively. In 5 (56%) CVES physicians, the dose exceeded the annual limit (20 mSv). Studies have concluded that full-time CVES physicians may suffer from the deterministic effects of lens radiation, particularly on the left side. A study also reported the possibility of estimating lens radiation doses according to neck skin dosimetry data [$D_{lens} = 0.0179 + (0.5971 \times D_{neck})$] [27].

Results of the study with 44 CVES physicians and 22 controls are presented. Of the total number of examined participants, 26 CVES physicians and controls underwent a special eye examination. Lens doses were measured by thermoluminescent dosimetry. The average equivalent doses in surgeons were 0.83 ± 0.59 and 0.35 ± 0.38 mSv per month for the left and right eyes, respectively, and annual doses were approximately 0.7–11 mSv. No significant differences in the prevalence of nuclear or cortical lens opacities were noted between groups. Four CVES physicians had early-stage subcapsular sclerosis, although no statistical differences were noted between groups. Based on these data, a study concluded the possibility of significant lens doses in CVES physicians and recommended using eye protection [28].

A study [29] enrolled 69 interventional cardiologists and 78 controls who were not professionally exposed to ionizing radiation. Lens opacities were examined using a slit camera. Cumulative lens doses were assessed retrospectively using a questionnaire including occupational history and lens doses. The average cumulative lens doses for the left and right eyes were 224 S and 85 mSv, respectively. Nuclear opalescence and opacification of the lens nucleus in the left eye were found in 47% of CVES physicians and 42% of controls, cortical opacities were found in 25% and 29%, and posterior subcapsular opacities were found in 7% and 6%, respectively. A statistically significant increase was found in the risk of opacity in the CVES group compared with the control group after adjusting for age, sex, smoking status, and medical exposure. However, no significant increase in cataract incidence was found when compared with controls, including the lack of evidence on the increased risk of opacity with increasing doses. The authors cannot rule out the adverse effects of ionizing radiation because of the relatively small sample size.

In a study assessing doses to the personnel of St. Petersburg healthcare institutions, the following equivalent lens doses were found for 3 months of exposure: for radiologists, 0.29–2.9 mSv per month; CVES physicians and nurses, 0.44–1.49 mSv; radiologists, 0.1–8.54 mSv; surgeons, 0.89 mSv; surgical nurses, 0.11–4.6 mSv. Levels of lens radiation were assessed based on the estimated ratio of personal dose equivalents Hp(3) and Hp(10). Based on the annual Hp(3) and Hp(10) values with the approximation of the log-normal distribution, the probability rates of exceeding 1, 6, and 20 mSv were 13%, 10%, and <1%, respectively. Moreover, considering that interventional radiology teams are the most exposed group in medicine, the percentage of cases exceeding 20 mSv annually can be up to 10%, and lens damage can be stochastic (random) [30,31]. These results differ significantly from results obtained in the European project Optimization of Radiation Protection Medical Staff [32-34] assessing lens radiation doses in interventional specialists from >30 European medical centers. In nearly 50% of CVES physicians, the radiation lens dose exceeded 20 mSv annually.

However, the chronic exposure effect on cataract development was noted in a cohort of the Mayak Production

Association specialists, where 15,000 people exposed to gamma radiation at doses of <0.25 to >1 Gy, showed a statistically significant linear association between the incidence of senile cataracts and the total dose of external gamma radiation. More studies have also shown the increased risk of all types of cataracts, including posterior cortical, nuclear, and subcapsular cataracts in chronically exposed workers. Cataract risk was significantly higher in women [35]. As a result of a radiation accident in Southern Urals, population doses ranged up to 5 mSv in 793 people, 5–100 mSv in 517, and >100 mSv in 67. These data were obtained for a long period after exposure. Studies have shown a significant effect of radiation dose. Opacities in the lens nucleus and posterior capsule developed [36].

Personnel are also chronically exposed to healthcare technologies. According to Kazan data [37], equivalent lens doses in 11 CVES physicians and 15 CVES nurses ranged from <2 to 16.92 mSv for 3 months. In 7 of 21 physicians, equivalent lens doses exceeded or were close to 20 mSv annually. During a clinical examination, 5 of 7 physicians aged 30–70 years had hyperechoic lesions in the vitreous cavity without age-related vascular changes. Some changes were typical for the dry eye syndrome (complaints of eye discomfort, scanty mucous discharge from the conjunctival cavity, eye redness in the evening, eye floaters in the left eye, itching, foreign body sensation, a fold of the conjunctiva outside the limbus, and tear stream thinning) and a decrease in tear film rupture time during the Norn test. In 4 of 5 participants, a superficial injection of the bulbar conjunctiva was detected, and 1 physician had conjunctiva pigmentation. In 2 physicians (45 and 70 years old), an arcus senilis was detected, which is described in the literature as a corneal change typical for older people (according to the World Health Organization, older people are those aged ⩾60 years). A clinical examination showed the following abnormal eye changes in one CVES physician (34 years old, annual equivalent lens dose 18.7 mSv): conjunctival damage, dry eye syndrome, damage (destruction) of the vitreous body, and lens nucleus compaction. Changes observed may be associated with exposure to sources of ionizing radiation. The possibility of abnormal processes after low-dose exposure, caused by oxidative stress and the release of free radicals, was also reported [38,39].

Study Limitations

The study is limited by the study interval of one to several months, collection of data on radiation exposure of healthcare personnel, and limited number of participating organizations for data collection.

CONCLUSION

In all cases, considering the number of operations performed, the estimated annual equivalent doses for the eye lens in CVES physicians exceeded the level of 20 mSv and ranged from 35 to 90 mSv. Nurse doses ranged from 6 to 19 mSv. In two cases, the estimated lens dose was >150 mSv (nurse in clinic A: 185 mSv; “operator” of clinic C, 225 mSv).

The lens dose limit is achieved in CVES physicians when performing >200 operations and sometimes <70 operations and <50 operations in CVES nurses.

The distance from the workplace to the X-ray beam zone is the leading factor of radiation dose formation in CVES. This factor is partially associated with the professional behavior of the personnel. Based on the available data, we can assume the stochastic nature of eye damage in the studied dose range. Exposure may be manifested by abnormalities at a younger age than in non-exposed individuals, even in the absence of statistical differences with comparison groups. The hand skin doses of various personnel can come close to and even exceed the normalized annual limit (500 mSv) by ⩾2 times.

At present, in addition to monitoring the exposure levels for individual organs and tissues in personnel using state-of-art medical technologies, epidemiological studies are needed, and practical recommendations must be developed for personnel protection using personal and collective protective equipment, with consideration of factors that affect the radiation dose.

ADDITIONAL INFORMATION

Funding source. This article was prepared by a group of authors as a part of the research and development effort titled "Scientific advances in medical, technological and organizational aspects of radiation safety in health care" (USIS No.:№123031500006-9) in accordance with the Order No. 1196 dated December 21, 2022 "On approval of state assignments funded by means of allocations from the budget of the city of Moscow to the state budgetary (autonomous) institutions subordinate to the Moscow Health Care Department, for 2023 and the planned period of 2024 and 2025" issued by the Moscow Health Care Department.

Competing interests. The authors declare that they have no competing interests.

Authors' contribution. All authors made a substantial contribution to the conception of the work, acquisition, analysis, interpretation of data for the work, drafting and revising the work, final approval of the version to be published and agree to be accountable for all aspects of the work. S.A. Ryzhkin — idea of the article, experimental research, collection of material, preparation of the article; Y.V. Druzhinina, Z.A. Lantuh — search for relevant publications, article preparation and editing; I.V. Soldatov — article preparation and editing; V.N. Lesnyak, D.P. Lebedev, D.N. Samochatov — article preparation and editing; M.P. Semenova — preparation and editing, translation into English; V.A. Suhov — search for relevant publications, article preparation and editing; S.E. Okhrimenko — search for relevant publications, idea of the article, experimental research, collection of material, preparation of the article.

Acknowledgements. The authors express their sincere gratitude to RAS academician Leonid A. Ilyin for his recommendations in the field of eye lens monitoring and development of measures to protect the visual organ.

REFERENCES

1. Ivanov SI, Loginova SV, Akopova NA, et al. Problems of dosimetry of the eye lens. *Med Radiol Radiation Safety*. 2014;59(4):67–72. (In Russ).
2. International Commission on Radiological Protection [Internet]. ICRP, 1996. Conversion coefficients for use in radiological protection against external radiation. ICRP Publication 74. Ann. ICRP 26 (3-4). Available from: https://icrp.org/publication.asp?id=ICRP+Publication+74. Accessed: 15.04.2023.
3. International Atomic Energy Agency [Internet]. Radiation protection and safety of radiation sources: International basic safety standards. Interim edition. IAEA; 2011. 329 p.
4. International Atomic Energy Agency [Internet]. Radiation protection and safety of radiation sources: International basic safety standards. No. GSR Part 3. Vienna, IAEA; 2015. Available from: https://www.iaea.org/publications/8930/radiation-protection-and-safety-of-radiation-sources-international-basic-safety-standards. Accessed: 15.04.2023.
5. International Commission on Radiological Protection [Internet]. CRP, 2007. The 2007 recommendations of the international commission on radiological protection. ICRP Publication 103. Ann. ICRP 37 (2-4). Available from: https://icrp.org/publication.asp?id=ICRP%20Publication%20103. Accessed: 15.04.2023.
6. International Commission on Radiological Protection [Internet]. ICRP statement on tissue reactions. Ref. 4825-3093-1464, April 21, 2011. Available from: https://icrp.org/docs/2011%20Seoul.pdf. Accessed: 15.04.2023.
7. International Commission on Radiological Protection [Internet]. Implications for occupational radiation protection of the new dose limit for the lens of the eye. Interim guidance for use and comment. Draft 1. ICRP; 2013. Available from: https://www.iaea.org/publications/10628/implications-for-occupational-radiation-protection-of-the-new-dose-limit-for-the-lens-of-the-eye. Accessed: 15.04.2023.
8. International Commission on Radiological Protection [Internet]. ICRP, 2012 ICRP statement on tissue reactions / early and late effects of radiation in normal tissues and organs: threshold doses for tissue reactions in a radiation protection context. ICRP Publication 118. Ann. ICRP 41(1/2). Available from: https://icrp.org/publication.asp?id=ICRP%20Publication%20118. Accessed: 15.04.2023.
9. UNSCEAR 2010 Report [Internet]. Report of the United Nations Scientific Committee on the Effects of Atomic Radiation 2010. Summary of low-dose radiation effects on health. United Nations, New York; 2011. Available from: https://www.unscear.org/docs/reports/2010/UNSCEAR_2010_Report_M.pdf. Accessed: 15.04.2023.
10. Karpov NA, Okhrimenko SE, Ivanov SI, et al. Dose in the lens of the eye. In: All-Russian conference with international participation dedicated to the 85th anniversary of the birth V.A. Kuhtina: Collection of materials, 3–4 April. Cheboksary, 2014. P. 235–236. (In Russ).
11. Nuclear Energy Agency [Internet]. NEA Expert Group on the Dose Limit for the lens of the eye launches survey. nuclear energy agency [cite 2020 April 8]. Available from: https://oecd-nea.org/jcms/pl_40031/nea-expert-group-on-the-dose-limit-for-the-lens-of-the-eye-launches-survey. Accessed: 15.04.2023.
12. Okhrimenko SE, Korenkov IP, Shandala NK, et al. Dose assessment to the lens of the eye and skin of the personnel in advanced medical technologies. *Med Radiol Radiation Safety*. 2022;67(1):44–49. (In Russ).
13. Okhrimenko SE, Osipov AN, Korenkov IP, et al. Assessment of doses of irradiation of the skin of the hands in cardioendovascular surgery and the number of double-strand DNA breaks in the culture of skin fibroblasts on the phantom of the hands. In: Collection of abstracts of the All-Russian scientific and practical conference with international participation "Radiation hygiene and continuing professional education: New challenges and ways of development" dedicated to the 65th anniversary of the Department of Radiation Hygiene and Radiation Safety named after Academician F.G. Krotkov", October 27, 2022. Moscow; 2022. P. 64–68. (In Russ).
14. Okhrimenko SE, Korenkov IP, Prokhorov NI, et al. Radiation-hygienic assessment of modern medical technologies. *Hygiene Sanitation*. 2020;99(9):939–946. (In Russ). doi: 10.47470/0016-9900-2020-99-9-939-946
15. Shleenkova EN, Bazhin SY, Kaidanovsky GN, et al. The necessity of regular dose monitoring for the eye lens of the staff working with radiopharmaceuticals. *Radiation Hygiene*. 2021;14(3):101–111. (In Russ). doi: 10.21514/1998-426X-2021-14-3-101-111
16. Wrzesień M. 18F-FDG production procedures as a source of eye lens exposure to radiation. *J Radiol*. 2018;(38):382–393. doi: 10.1088/1361-6498/aaa287
17. Wrzesień M. The effect of work system on the hand exposure of workers in 18F-FDG production centers. *Australasian Physical Engineering Sciences Med*. 2018;41(2):541–548. doi: 10.1007/s13246-018-0644-9
18. Okhrimenko SE, Korenkov IP, Yashkina EI, et al. Irradiation of the skin of the hands in interventional cardiac surgery (report). In: III National Congress with international participation "Sysin readings", November 16–18, 2022. Moscow; 2022. (In Russ).
19. McParland BJ, Nosil J, Barry B. A survey of radiation exposure received by the staff at two cardiac catherization laboratories. *Br J Radiol*. 1990;63(755):885–888. doi: 10.1259/0007-1285-63-755-885
20. Steffanino G, Rossetti V, Rubichini F, et al. Short communication: Staff dose reduction during coronary angiography using low framing speed. *Br J Radiol*. 1996;69(825):860–864. doi: 10.1259/0007-1285-69-825-860
21. Li IB, Kai M, Takano K, et al. Occupational exposure in pediatric cardiac cauterization. *Health Phis*. 1995;69(2):261–264. doi: 10.1097/00004032-199508000-00011
22. Medeiros RD, Mennucci TA. [Evolution of X-ray exposure dosage during coronary cineangiolography. (In Portuguese)] *Arg Bras Cardiol*. 1990;55(1):31–33.
23. Karppinen J, Parviainen T, Servomaa A, Komppa T. Radiation risk and exposure of radiologists and patients during coronary angiography and percutaneous transluminal coronary angioplasty (PTCA). *Radiation Protection Dosimetry*. 1995;57(1-4):481–484.
24. David EF, Andrew K, Christopher O, Sanjog P. The risk of radiation exposure to the eyes of the interventional pain. *Physician Radiol Res Practice*. 2011;2011:609537. doi: 10.1155/2011/609537
25. Vecchia ED, Modenese A, Loney T. Risk of cataract in health care workers exposed to ionizing radiation: A systematic review. *Med Lav*. 2020;111(4):269–284. doi: 10.23749/mdl.v111i4.9045
26. Morcillo AB, Alejo L, Huerga C, et al. Occupational doses to the eye lens in pediatric and adult noncardiac interventional radiology procedures. *Med Physics*. 2021;48(4):1956–1966. doi: 10.1002/mp.14753
27. Merrachi NA, Bouchard-Bellavance R, Perreault P. Eye lens dosimetry in interventional radiology: Assessment with dedicated Hp(3) dosimeters. *Can Assoc Radiol J*. 2021;72(2):317–323. doi: 10.1177/0846537120911755
28. Thrapsanioti Z, Askounis P, Datseris I, et al. Eye lens radiation exposure in Greek interventional cardiology article. Radiation Protection Dosimetry. 2017;175(3):344–356. doi: 10.1093/rpd/ncw356

29. Domienik-Andrzejewska J, Kałużny P, Piernik G. Occupational exposure to ionizing radiation and lens opacity in interventional cardiologists. *Int J Occupational Med Environmental Health*. 2019;32(5):663–675. doi: 10.13075/ijomeh.1896.01456
30. Kaydanovsky GN, Shleenkova EN. On problems of the lens ofthe eye radiation dose monitoring. *Radiation Hygiene*. 2016;9(3):75–80. (In Russ). doi: 10.21514/1998-426X-2016-9-3-75-80
31. Shleenkova EN, Golikov VY, Kaidanovsky GN, et al. Results of eye lens doses control of medical personnel in St. Petersburg. *Radiation Hygiene*. 2019;12(4):29–36. (In Russ). doi: 10.21514/1998-426X-2019-12-4-29-36
32. UPCommons. Global access to UPC knowledge [Internet]. Ginjaume M, Carnicer A. Oramed: Optimization of radiation protection of medical staff. 2012. EURADOS Report 2012-02. Available from: https://upcommons.upc.edu/handle/2117/17229. Accessed: 15.04.2023.
33. Vanhavere F, Carinou E, Domienik JL, et al. Measurements of eye lens doses in interventional radiology and cardiology: Final results of the ORAMED project. *Radiation Measurements*. 2011;46(11):1243–1244. doi: 10.1016/j.radmeas.2011.08.013
34. EUR-Lex [Internet]. Council Directive 2013/59/Euratom of 5 December 2013 laying down basic safety standards for protection against the dangers arising from exposure to ionising radiation, and repealing Directives 89/618/Euratom, 90/641/Euratom, 96/29/Euratom, 97/43/Euratom and 2003/122/Euratom. Available from: https://eur-lex.europa.eu/eli/dir/2013/59/oj. Accessed: 15.04.2023.
35. Azizova TV, Hamada N, Grigorieva ES, Bragin EV. Risk of various types of cataracts in the cohort of workers exposed to occupational chronic radiation. *Med Radiology Radiation Safety*. 2020;65(4):48–57. (In Russ). doi: 10.12737/1024-6177-2020-65-4-48-57
36. Mikryukova LD, Krestinina LY, Epiphanova SB. A study of layered lens change in the process of cataract formation in persons exposed to radiation as a result of radiation accidents in the Southern Urals. *Radiation Hygiene*. 2018;11(4):51–63. (In Russ). doi: 10.21514/1998-426X-2018-11-4-51-63
37. Ryzhkin SA, Slesareva AN, Galeeva GZ, Ivanov SI. Clinical examination of the eyes functional status and assessment of equivalent dose to eye lens in medical staff performing endovascular interventions under X-ray guidance. *Radiation Risks*. 2017;26(3):90–99. (In Russ). doi: 10.21870/0131-3878-2017-26-3-90-99
38. Galeeva GZ, Ryzhkin SA, Sergeeva SU. The effect of ionizing radiation on a person and the organ of vision. *Practical Med*. 2016; 99(7): 37–41. (In Russ).
39. Ryzhkin SA, Galeeva GZ, Sergeeva SU. Radiation cataract in the light of modern research achievements in ophthalmology (review). *Bulletin Medical Institute REAVIZ: Rehabilitation Doctor Health*. 2016;24(4):37–42. (In Russ).

СПИСОК ЛИТЕРАТУРЫ

1. Иванов С.И., Логинова С.В., Акопова Н.А., и др. Проблемы дозиметрии хрусталика глаза // Радиобиология и радиационная безопасность. 2014. Т. 59, № 4. С. 67–72.
2. International Commission on Radiological Protection [интернет]. ICRP, 1996. Conversion coefficients for use in radiological protection against external radiation. ICRP Publication 74. Ann. ICRP 26 (3-4). Режим доступа: https://icrp.org/publication.asp?id=ICRP+Publication+74. Дата обращения: 15.04.2023.
3. International Atomic Energy Agency [интернет]. Radiation protection and safety of radiation sources: International basic safety standards. Interim edition. IAEA, 2011. 329 p.
4. International Atomic Energy Agency [интернет]. Radiation protection and safety of radiation sources: International basic safety standards. No. GSR Part 3. Vienna, IAEA, 2015. 436 p. Режим доступа: https://www.iaea.org/publications/8930/radiation-protection-and-safety-of-radiation-sources-international-basic-safety-standards. Дата обращения: 15.04.2023.
5. International Commission on Radiological Protection [интернет]. CRP, 2007. The 2007 recommendations of the international commission on radiological protection. ICRP Publication 103. Ann. ICRP 37 (2-4). Режим доступа: https://icrp.org/publication.asp?id=ICRP%20Publication%20103. Дата обращения: 15.04.2023.
6. International Commission on Radiological Protection [интернет]. ICRP statement on tissue reactions. Ref. 4825-3093-1464, April 21, 2011. Режим доступа: https://icrp.org/docs/2011%20Seoul.pdf. Дата обращения: 15.04.2023.
7. International Commission on Radiological Protection [интернет]. Implications for occupational radiation protection of the new dose limit for the lens of the eye. Interim guidance for use and comment. Draft 1. ICRP, 2013. 110 p. Режим доступа: https://www.iaea.org/publications/10628/implications-for-occupational-radiation-protection-of-the-new-dose-limit-for-the-lens-of-the-eye. Дата обращения: 15.04.2023.
8. International Commission on Radiological Protection [интернет]. ICRP, 2012 ICRP statement on tissue reactions / early and late effects of radiation in normal tissues and organs: threshold doses for tissue reactions in a radiation protection context. ICRP Publication 118. Ann. ICRP 41(1/2). Режим доступа: https://icrp.org/publication.asp?id=ICRP%20Publication%20118. Дата обращения: 15.04.2023.
9. UNSCEAR 2010 Report [интернет]. Report of the United Nations Scientific Committee on the Effects of Atomic Radiation 2010. Summary of low-dose radiation effects on health. United Nations, New York, 20111. P. 51–64. Режим доступа: https://www.unscear.org/docs/reports/2010/UNSCEAR_2010_Report_M.pdf. Дата обращения: 15.04.2023.
10. Карпов Н.А., Охрименко С.Е., Иванов С.И., и др. Доза в хрусталике глаза: ближайшие перспективы // Всероссийская конференция с международным участием, посвященная 85-летию со дня рождения В.А. Кухтина: сборник материалов. Чебоксары, 3–4 апреля. Чебоксары, 2014. С. 235–236.
11. Nuclear Energy Agency [интернет]. NEA Expert Group on the Dose Limit for the lens of the eye launches survey. nuclear energy agency [cite 2020 April 8]. Режим доступа: https://oecd-nea.org/jcms/pl_40031/nea-expert-group-on-the-dose-limit-for-the-lens-of-the-eye-launches-survey. Дата обращения: 15.04.2023.
12. Коренков И.П., Охрименко С.Е., Шандала Н.К., и др. Оценка доз облучения хрусталика глаза и кожи персонала в современных медицинских технологиях // Медицинская радиология и радиационная безопасность. 2022. Т. 67, № 1. С. 44–49. doi: 10.12737/1024-6177-2022-67-1-44-49
13. Охрименко С.Е., Осипов А.Н., Коренков И.П., и др. Оценка доз облучения кожи рук в кардиоэндоваскулярной хирургии и количества двунитевых разрывов ДНК в культуре фибробластов кожи на фантоме кистей рук // Всероссийская научно-практическая конференция с международным участием «Радиационная гигиена и непрерывное профессиональное

образование: новые вызовы и пути развития», посвященная 65-летию кафедры радиационной гигиены и радиационной безопасности имени академика Ф.Г. Кроткова»: сборник тезисов, 27 октября 2022 года. Москва, 2022. С. 64–68.

14. Охрименко С.Е., Коренков И.П., Прохоров Н.И., и др. Радиационно-гигиеническая оценка современных медицинских технологий // Гигиена и санитария. 2020. Т. 99, № 9. С. 939–946. doi: 10.47470/0016-9900-2020-99-9-939-946

15. Шлеенкова Е.Н., Бажин С.Ю., Кайдановский Г.Н., и др. О необходимости проведения регулярного контроля доз облучения хрусталиков глаз у персонала, занятого на работах с использованием радиофармацевтических препаратов // Радиационная гигиена. 2021. Т. 14, № 3. doi: 10.21514/1998-426X-2021-14-3-101-111

16. Wrzesień M. 18F-FDG production procedures as a source of eye lens exposure to radiation // J Radiol. 2018. Vol. 38, N 1. P. 382–393. doi: 10.1088/1361-6498/aaa287

17. Wrzesień M. The effect of work system on the hand exposure of workers in 18F-FDG production centers // Australasian Physical Engineering Sci Med. 2018. Vol. 41. P. 541–548. doi: 10.1007/s13246-018-0644-9

18. Охрименко С.Е., Коренков И.П., Яшкина Е.И., и др. Облучение кожи кистей рук в интервенционной кардиохирургии (доклад) // III Национальный конгресс с международным участием «Сысинские чтения», 16–18 ноября 2022 г. Москва, 2022.

19. McParland B.J., Nosil J., Barry B. A survey of radiation exposure received by the staff at two cardiac catherization laboratories // Br J Radiol. 1990. Vol. 63, N 755. P. 885–888. doi: 10.1259/0007-1285-63-755-885

20. Steffanino G., Rossetti V., Rubichini F., et al. Short communication: Staff dose reduction during coronaty angiography using low framing speed // Br J Radiol. 1996. Vol. 69, N 825. P. 860–864. doi: 10.1259/0007-1285-69-825-860

21. Li I.B., Kai M., Takano K., et al. Occupational exposure in pediatric cardiac cauterization // Health Phis. 1995. Vol. 69, N 2. P. 261–264. doi: 10.1097/00004032-199508000-00011

22. Medeiros R.D., Mennucci T.A. [Evolution of X-ray exposure dosage during coronary cineangiolography. (In Portuguese)] // Arg Bras Cardiol. 1990. Vol. 55, N 1. P. 31–33.

23. Karppinen J., Parviainen T., Servomaa A., Komppa T. Radiation risk and exposure of radiologists and patients during coronary angiography and percutaneous transluminal coronary angioplasty (PTCA) // Radiation Protection Dosimetry. 1995. Vol. 57, N 1–4. P. 481–485.

24. David E.F., Andrew K., Christopher O., et al. The risk of radiation exposure to the eyes of the interventional pain // Physician Radiology Research and Practice. 2011. Vol. 2011. P. 609537. doi: 10.1155/2011/609537

25. Vecchia E.D., Modenese A., Loney T. Risk of cataract in health care workers exposed to ionizing radiation: A systematic review // Med Lav. 2020. Vol. 111, N 4. P. 269–284. doi: 10.23749/mdl.v111i4.9045

26. Morcillo A.B., Alejo L., Huerga C., et al. Occupational doses to the eye lens in pediatric and adult noncardiac interventional radiology procedures // Medical Physics. 2021. Vol. 48, N 4. P. 1956–1966. doi: 10.1002/mp.14753

27. Merrachi N.A., Bouchard-Bellavance R., Perreault P. Eye lens dosimetry in interventional radiology: Assessment with dedicated Hp(3) dosimeters // Can Assoc Radiol J. 2021. Vol. 72, N 2. P. 317–323. doi: 10.1177/0846537120911755

28. Thrapsanioti Z., Askounis P., Datseris I. Eye lens radiation exposure in Greek interventional cardiology article // Radiat Prot Dosimetry. 2017. Vol. 175, N 3. P. 344–356. doi: 10.1093/rpd/ncw356

29. Domienik-Andrzejewska J., Kałużny P., Piernik G. Occupational exposure to ionizing radiation and lens opacity in interventional cardiologists // International Journal of Occupational Medicine and Environmental Health. 2019. Vol. 32, N 5. P. 663–675. doi: 10.13075/ijomeh.1896.01456

30. Кайдановский Г.Н., Шлеенкова Е.Н. On problems of the lens ofthe eye radiation dose monitoring // Радиационная гигиена. 2016. Т. 9, № 3. С. 75–80. doi: 10.21514/1998-426X-2016-9-3-75-80

31. Шлеенкова Е.Н., Голиков В.Ю., Кайдановский Г.Н., и др. Результаты контроля доз облучения хрусталиков глаз у медицинского персонала г. Санкт-Петербурга // Радиационная гигиена. 2019. Т. 12, № 4. С. 29–36. doi: 10.21514/1998-426X-2019-12-4-29-36

32. UPCommons. Global access to UPC knowledge [интернет]. Ginjaume M., Carnicer A. Oramed: Optimization of radiation protection of medical staff. 2012. EURADOS Report 2012-02. Режим доступа: https://upcommons.upc.edu/handle/2117/17229. Дата обращения: 15.04.2023.

33. Vanhavere F., Carinou E., Domienik J., et al. Measurements of eye lens doses in interventional radiology and cardiology: Final results of the ORAMED project // Radiation Measurements. 2011. Vol. 46, N 11. P. 1243–1247. doi: 10.1016/j.radmeas.2011.08.013

34. EUR-Lex [интернет]. Council Directive 2013/59/Euratom of 5 December 2013 laying down basic safety standards for protection against the dangers arising from exposure to ionising radiation, and repealing Directives 89/618/Euratom, 90/641/Euratom, 96/29/Euratom, 97/43/Euratom and 2003/122/Euratom. Режим доступа: https://eur-lex.europa.eu/eli/dir/2013/59/oj. Дата обращения: 15.04.2023.

35. Азизова Т.В., Хамада Н., Григорьева Е.С., и др. Риск катаракты различных типов в когорте работников, подвергшихся профессиональному хроническому облучению // Медицинская радиология и радиационная безопасность. 2020. Т. 65, № 4. С. 48–57. doi: 10.12737/1024-6177-2020-65-4-48-57

36. Микрюкова Л.Д., Крестинина Л.Ю., Епифанова С.Б. Изучение послойных изменений хрусталика в процессе формирования катаракты у лиц, подвергшихся облучению в результате радиационных инцидентов на Южном Урале // Радиационная гигиена. 2018. Т. 11, № 4. С. 51–63. doi: 10.21514/1998-426X-2018-11-4-51-63

37. Рыжкин С.А., Слесарева А.Н., Галеева Г.З., и др. Клиническое изучение органа зрения и дозиметрия хрусталика глаза персонала, выполняющего хирургические вмешательства под контролем рентгеновского излучения // Радиация и риск. 2017. Т. 26, № 3. С. 90–99. doi: 10.21870/0131-3878-2017-26-3-90-99

38. Галеева Г.З., Рыжкин С.А., Сергеева С.Ю. Воздействие ионизирующего излучения на человека и орган зрения // Практическая медицина. 2016. Т. 99, № 7. С. 37–41.

39. Рыжкин С.А. Галеева Г.З., Сергеева С.Ю. Лучевая катаракта в свете современных научно-исследовательских достижений в офтальмологии (обзор) // Вестник медицинского института «РЕАВИЗ»: реабилитация, врач и здоровье. 2016. Т. 24, № 4. С. 37–42.

AUTHORS' INFO

*** Yuliya V. Druzhinina;**
address: 24/1 Petrovka street, 127051 Moscow, Russia;
ORCID: 0000-0002-3230-3722;
eLibrary SPIN: 1973-2848;
e-mail: druzhininaYV2@zdrav.mos.ru

Sergey A. Ryzhkin;
ORCID: 0000-0003-2595-353X;
eLibrary SPIN: 5955-5712;
e-mail: rsa777@inbox.ru

Zoya A. Lantukh;
ORCID: 0000-0001-6623-9610;
eLibrary SPIN: 5486-6496;
e-mail: LantukhZA@zdrav.mos.ru

Ilya V. Soldatov;
ORCID: 0000-0002-4867-0746;
eLibrary SPIN: 4065-6048;
e-mail: SoldatovIV2@zdrav.mos.ru

Viktor N. Lesnyak;
ORCID: 0000-0002-2739-0649;
eLibrary SPIN: 5483-3113;
e-mail: lesnyak_kb83@mail.ru

Dmitriy P. Lebedev;
ORCID: 0000-0003-1551-3127;
eLibrary SPIN: 4770-5722;
e-mail: lebedevdp@gmail.com

Denis N. Samochatov;
ORCID: 0000-0002-5230-2006;
eLibrary SPIN: 3340-2715;
e-mail: dnsamochatov@gmail.com

Maria P. Semenova;
ORCID: 0000-0003-0904-0415;
eLibrary SPIN: 7205-0062;
e-mail: mps-fmbc@yandex.ru

Vitaly A. Sukhov;
ORCID: 0000-0003-2993-0108;
e-mail: cyxowv@gmail.com>

Sergey E. Okhrimenko;
ORCID: 0000-0002-8282-1798;
eLibrary SPIN: 6595-4011;
e-mail: ooniii@mail.ru

ОБ АВТОРАХ

*** Дружинина Юлия Владимировна;**
адрес: Россия, 127051, Москва, ул. Петровка, д. 24, стр. 1;
ORCID: 0000-0002-3230-3722;
eLibrary SPIN: 1973-2848;
e-mail: druzhininaYV2@zdrav.mos.ru

Рыжкин Сергей Александрович;
ORCID: 0000-0003-2595-353X;
eLibrary SPIN: 5955-5712;
e-mail: rsa777@inbox.ru

Лантух Зоя Александровна;
ORCID: 0000-0001-6623-9610;
eLibrary SPIN: 5486-6496;
e-mail: LantukhZA@zdrav.mos.ru

Солдатов Илья Владимирович;
ORCID: 0000-0002-4867-0746;
eLibrary SPIN: 4065-6048;
e-mail: SoldatovIV2@zdrav.mos.ru

Лесняк Виктор Николаевич;
ORCID: 0000-0002-2739-0649;
eLibrary SPIN: 5483-3113;
e-mail: lesnyak_kb83@mail.ru

Лебедев Дмитрий Петрович;
ORCID: 0000-0003-1551-3127;
eLibrary SPIN: 4770-5722;
e-mail: lebedevdp@gmail.com

Самочатов Денис Николаевич;
ORCID: 0000-0002-5230-2006;
eLibrary SPIN: 3340-2715;
e-mail: dnsamochatov@gmail.com

Семенова Мария Петровна;
ORCID: 0000-0003-0904-0415;
eLibrary SPIN: 7205-0062;
e-mail: mps-fmbc@yandex.ru

Сухов Виталий Александрович;
ORCID: 0000-0003-2993-0108;
e-mail: cyxowv@gmail.com>

Охрименко Сергей Евгеньевич;
ORCID: 0000-0002-8282-1798;
eLibrary SPIN: 6595-4011;
e-mail: ooniii@mail.ru

* Corresponding author / Автор, ответственный за переписку

DOI: https://doi.org/10.17816/DD284706

Поражение сердца при COVID-19: вопросы патогенеза и диагностики

Д.А. Филатова[1], Е.А. Мершина[1, 2], В.Е. Синицын[1, 2]

[1] Московский государственный университет имени М.В. Ломоносова, факультет фундаментальной медицины, Москва, Российская Федерация
[2] Медицинский научно-образовательный центр Московского государственного университета имени М.В. Ломоносова, Москва, Российская Федерация

АННОТАЦИЯ

Тема коронавирусной инфекции до настоящего времени не теряет своей актуальности в медицинской среде. Среди гетерогенных клинических проявлений этого заболевания выделяют поражение структур сердца, главным образом воспалительного характера. Помимо миокардита, при коронавирусной инфекции возможен целый спектр острых или отсроченных поражений сердца, в частности острый коронарный синдром, тромбоэмболические события, сердечная недостаточность, нарушения ритма сердца. Известно, что прогноз для пациентов с поражением сердца значимо ухудшается. Своевременные постановка диагноза и начало лечения играют принципиально важную роль для предотвращения тяжёлых осложнений.

В обзоре приводятся современные литературные данные о патогенезе поражения сердца при COVID-19, обсуждаются вопросы рациональной диагностики данной патологии с помощью современных методик (лабораторных, функциональных, визуализирующих), в том числе инвазивных. Главную роль среди визуализирующих методов играет магнитно-резонансная томография сердца с контрастированием. В настоящее время признано, что диагностика миокардита, ассоциированного с коронавирусной инфекцией, имеет ряд принципиальных отличий от диагностики миокардита другой природы. Кроме того, отражены основные аспекты воспалительного поражения сердца, ассоциированного с вакцинацией против COVID-19, поскольку такое осложнение возникает чаще, чем принято считать. Нередко оно является поводом для отказа от вакцинации, что может повлечь за собой тяжёлые последствия как для отдельного человека, так и популяции в целом.

Ключевые слова: COVID-19; миокардит; острый коронарный синдром; нарушения ритма сердца; магнитно-резонансная томография; вакцинация.

Как цитировать

Филатова Д.А., Мершина Е.А., Синицын В.Е. Поражение сердца при COVID-19: вопросы патогенеза и диагностики // *Digital Diagnostics*. 2023. Т. 4, № 2. С. 156–169. DOI: https://doi.org/10.17816/DD284706

Рукопись получена: 25.02.2023 **Рукопись одобрена:** 31.03.2023 **Опубликована:** 14.04.2023

DOI: https://doi.org/10.17816/DD284706

COVID-19-related cardiac lesion: The questions of pathogenesis and diagnostics

Daria A. Filatova[1], Elena A. Mershina[1, 2], Valentin E. Sinitsyn[1, 2]

[1] Faculty of Fundamental Medicine of Lomonosov Moscow State University, Moscow, Russian Federation
[2] Medical Research and Education Center of Lomonosov Moscow State University, Moscow, Russian Federation

ABSTRACT

Coronavirus infection is still a topic of interest in the medical community today. Among the heterogeneous clinical manifestations of this disease, lesions of cardiac structures often occur. They are mainly inflammatory in nature and can be acute or delayed. Aside from myocarditis, coronavirus infection can induce cardiac injuries, including acute coronary syndrome, thromboembolic events, heart failure, and heart rhythm disturbances. It is well known that the prognosis for patients with cardiac lesions significantly worsens; timely diagnosis and treatment initiation play an important role in preventing severe complications.

This review presents the most recent literature data on the pathogenesis of cardiac lesions in COVID-19 patients and discusses the rational diagnosis of this pathology using modern techniques, such as laboratory, functional imaging (cardiac magnetic resonance is the most important of these), and invasive ones. It is now established that diagnosing myocarditis caused by coronavirus infection differs fundamentally from diagnosing other types of myocarditis. Furthermore, the main aspects of inflammatory heart lesions associated with COVID-19 vaccination are discussed, as this complication occurs more frequently than is commonly believed. It is often used as a rationale for refusing vaccination; however, this decision may severely affect the individual and the population.

Keywords: acute coronary syndrome; COVID-19; heart rhythm disturbances; magnetic resonance imaging; myocarditis; vaccination.

To cite this article

Filatova DA, Mershina EA, Sinitsyn VE. COVID-19-related cardiac lesion: The questions of pathogenesis and diagnostics. *Digital Diagnostics.* 2023;4(2):156–169. DOI: https://doi.org/10.17816/DD284706

Received: 25.02.2023 **Accepted:** 31.03.2023 **Published:** 14.04.2023

DOI: https://doi.org/10.17816/DD284706

COVID-19的心脏受损：发病机制和诊断的问题

Daria A. Filatova[1], Elena A. Mershina[1, 2], Valentin E. Sinitsyn[1, 2]

[1] Faculty of Fundamental Medicine of Lomonosov Moscow State University, Moscow, Russian Federation
[2] Medical Research and Education Center of Lomonosov Moscow State University, Moscow, Russian Federation

简评

冠状病毒感染仍然是医学界的一个热门话题。心脏结构受损从该病的异质性临床表现中脱颖而出，主要是炎性的。除心肌炎外，冠状病毒感染还可导致一系列急性或迟发性的心脏受损，如急性冠状动脉综合征、血栓栓塞性事件、心力衰竭和心律紊乱。众所周知，有心脏受损的病人的预后大幅度恶化。及时诊断和启动治疗对于严重并发症的预防至关重要。

本综述介绍了与COVID-19心脏受损发病机制有关的现代文献资料，讨论了利用现代技术（实验室、功能、影像学），包括侵入性技术，对这种病理进行合理诊断的问题。在影像技术中起主要作用的是心脏超影磁共振成像。现在专家认为，与冠状病毒感染有关的心肌炎诊断，与其他心肌炎诊断相比，有一些根本区别。此外，还反映了与COVID-19疫苗接种相关的炎症性心脏受损的主要方面，因为这种并发症的发生率比通常认为的高。它往往是不打疫苗的一个理由，这对个人和整个人群都会产生严重的后果。

关键词： COVID-19；心肌炎；急性冠状动脉综合征；心律紊乱；磁共振成像；疫苗接种。

To cite this article
Filatova DA, Mershina EA, Sinitsyn VE. COVID-19的心脏受损：发病机制和诊断的问题. *Digital Diagnostics.* 2023;4(2):156–169.
DOI: https://doi.org/10.17816/DD284706

收到： 25.02.2023 **接受：** 31.03.2023 **发布日期：** 14.04.2023

INTRODUCTION

The coronavirus disease 2019 (COVID-19) caused by the SARS-CoV-2 was first detected in December 2019 and quickly spread worldwide. Its clinical manifestations include all influenza symptoms, such as cough, fever, fatigue, dyspnea, anosmia, ageusia, and pharyngodynia, which can progress to acute respiratory distress syndrome and multiple organ failure. Furthermore, acute injury to heart structures, primarily the myocardium, is also possible. Many studies have found that high troponin levels are associated with higher mortality in patients with COVID-19. The timely and accurate diagnosis of this condition is critical for patient survival; however, it remains a challenge.

This review aimed to critically summarize available data on COVID-19-associated myocarditis and investigate the main aspects of its pathogenesis and differential diagnosis.

The PubMed database was searched for relevant publications. The search terms were "COVID-19/SARS-CoV-2 and myocardit*" in the titles of publications (as indicated by adding [ti]). Only full-text articles were selected, such as meta-analyses, systematic reviews, and reviews; these conditions were determined via the appropriate filters. The literature on post-vaccine myocarditis was selected by adding "and vaccin*" to the above search terms, and other search parameters were the same as described above.

Following data collection, the initial sample for the literature review included 126 publications, of which 67 discussed vaccinations against COVID-19.

COVID-19-RELATED CARDIAC LESION

COVID-19 is caused by the SARS-CoV-2, which was discovered in late 2019 in the Chinese city of Wuhan and quickly spread worldwide, causing a pandemic.

Possible symptoms of COVID-19 include fever, cough, dyspnea, anosmia, ageusia, and pharyngodynia. The most severe complications include acute respiratory distress syndrome and multiple organ failure. Clinical manifestations also include acute injury to the structures of the heart, primarily the myocardium. Approximately 20% of hospitalized patients have high specific troponins [1], which do not always correlate with other signs of myocardial damage. A study of troponin I levels in patients with COVID-19 on the first day of hospitalization found elevations in 36% of cases. Even minor myocardial damage is associated with a significant increase in mortality [2]. However, many aspects of myocardial damage in COVID-19 remain unclear.

Pathogenesis and clinical manifestations

A thorough understanding of the pathogenesis of cardiac lesion is critical because it allows early initiation of treatment and prevention of severe consequences, including death.

To date, little evidence shows that SARS-CoV-2 enters cardiomyocytes and causes direct harm to them. Associated lymphocytic myocarditis is common in patients with COVID-19, although its etiology is linked to a generalized cytokine-mediated inflammatory response. In several studies [3–5], myocardial biopsy revealed lymphocytic infiltration, interstitial edema, and isolated foci of necrosis; however, no intracellular viral material was found. Lindner et al. [3] discovered the COVID-19 pathogen in the myocardium while studying autopsy materials from patients with COVID-19 who did not have a clinical picture of fulminant myocarditis. However, it was found primarily in interstitial cells and macrophages that penetrated into the myocardium rather than in cardiomyocytes. The presence of the virus was not associated with increased mononuclear infiltration of the myocardium, and no histological signs of myocarditis were detected, i.e., no massive cellular infiltrates or necrosis areas were reported [6]. Other authors have reported timilar findings [7, 8]. According to Fox et al. [9], 10 autopsies of African Americans who died from COVID-19 revealed single-cell necrosis (without large areas of cardiomyocyte necrosis) in the myocardium without overt lymphocytic myocarditis. This suggested that viral particles were present in cardiac macrophages caused by a viremic phase or migration of infiltrated alveolar macrophages into extrapulmonary tissues. Moreover, the possible cardiotoxicity of drug therapy cannot be overlooked in the genesis of inflammatory myocardial damage identified at autopsy in patients with COVID-19 [10].

Another potential mechanism for cardiac lesion is direct virus entrance into the endothelial cells of the heart. The endothelium is a para-, auto-, or endocrine tissue, and its damage causes microvascular dysfunction and a shift in vascular homeostasis toward vasoconstriction, resulting in organ and tissue ischemia, inflammation, edema, and thrombosis. SARS-CoV-2 enters endothelial cells through angiotensin-converting enzyme 2 (ACE2) receptors, causing active inflammation. Some authors describe SARS-CoV-2-induced diffuse vasculitis: presumably, endothelitis can cause multiple organ damage typical of COVID-19 caused by microvascular dysfunction [11]; however, these data are currently limited and require additional confirmation.

Another theory is that cardiac lesion is triggered by an overactive immune system that releases various inflammatory mediators, and this condition is commonly described as "cytokine storm." The activation of platelets, neutrophils, and other components of the inflammatory response results in micro- and macrovascular thrombosis, which leads to vascular occlusion and cell death. Both arterial and venous thrombosis is common in COVID-19 [12]. In an observational study, patients with COVID-19 and ST segment elevation myocardial infarction had higher troponin levels and higher incidence of thrombosis than patients with COVID-19 but without infarction [13]. Acute coronary syndrome without signs of coronary occlusion is also quite common. According to Bangalore et al. [14], only 44% of 18 patients with COVID-19 and ST segment elevation on the ECG were diagnosed with acute coronary thrombosis resulting in myocardial infarction,

and non-coronary myocardial damage was observed in 56% of cases. Diagnostic quandaries are fairly common in these circumstances, particularly considering the nonspecific symptoms of myocarditis, which include fatigue, dyspnea, tachycardia, and chest tightness.

Inflammatory myocardial injuries seen in COVID-19 include fulminant myocarditis, which causes a rapid decrease in the left ventricular contractility, most often secondary to bilateral lung damage, and pericardial effusion leading to cardiac tamponade. Cardiogenic shock affects roughly one-third of patients, and the mortality rate is approximately 26%. Isolated cases of fulminant myocarditis following vaccination against COVID-19 have been reported; however, the disease has a less severe course. A study reported that the risk of fulminant myocarditis is influenced not by COVID-19 or vaccination but by a predisposition [15].

Rhythm disturbance is one of the most serious clinical manifestations of cardiac lesion. Although the true prevalence of this condition is unknown, evidence shows that arrhythmia results in a transfer to the intensive care unit in 44.4% of cases [16]. Moreover, determining how many COVID-19 arrhythmias are caused by electrolyte imbalance or pre-existing rhythm disturbance is difficult; moreover, arrhythmia can develop in myocarditis [17]. In a study by Peretto et al. [18], 78.7% of patients with confirmed myocarditis had some forms of ventricular arrhythmia. Thus, the pathophysiology of rhythm disturbance is affected by the stage of myocardial damage, and the characteristics of arrhythmia in acute and healed myocarditis vary.

Possible mechanisms of rhythm disturbance in COVID-19 are direct damage to cardiomyocytes with impaired plasma membrane integrity and electrical conductivity, pericardial infection and massive edema, ischemia due to microvascular pathology caused by pericyte infection, arrhythmias caused by myocardial fibrosis, and action of pro-inflammatory cytokines [19, 20]. The latter mechanism is based on inflammatory cytokines, including interleukin-6 (IL-6), displacing the desmosome protein plakoglobin from the membrane of cardiomyocytes [21]. This can result in arrhythmias because insufficient cell adhesion is hypothesized to harm the membrane, resulting in cell death and eventual fibrosis. One of the primary mechanisms of arrhythmogenic cardiomyopathies is a decrease in the surface expression of desmosome proteins is [22]. Evidence shows that patients with COVID-19 have higher serum concentrations of IL-6 [23], and the level of IL-6 correlated with the severity of the patient's condition. Thus, COVID-19 is most likely to blame for rhythm disturbances, particularly if a patient has a genetic susceptibility. Notably, the first three scenarios can occur in active myocarditis, whereas the last two can occur in chronic or healed myocarditis.

COVID-19 predisposes a cohort of professional athletes to myocarditis. In turn, myocarditis, contributes significantly to the pathogenesis of sudden cardiac death in athletes. Physical activity can trigger life-threatening cardiac arrhythmias and affect immune function: moderate-intensity exercise can boost the immune system, whereas high-intensity exercise sharply lowers the immune response [24]. The condition of the muscle layer of the heart causes sudden death in acute myocarditis: the affected myocardium is predisposes a patient to ventricular arrhythmias; in chronic myocarditis, myocardial fibrosis contributes to ventricular arrhythmias by the formation of re-entry sites in adjacent areas. As a result, current guidelines recommend limiting physical activity for 3–6 months after a diagnosis of myocarditis [25].

Studies have reported myocardial infarction after COVID-19. Several possible mechanisms for this complication have been proposed, including viral envelope glycoprotein binding to porphyrin and the hemoglobin beta chain, which produces hypoxia and, as a result, type 2 myocardial infarction caused by an imbalance between myocardial oxygen demand and supply. In addition, we hypothesized that the prothrombotic condition associated with COVID-19 plays a role in the pathogenesis of myocardial infarction, which may contribute to the development of type 1 myocardial infarction associated with atherosclerotic plaque instability [26]. However, evidence shows that patients with COVID-19 have higher levels of thrombophilia than hospitalized patients with severe pneumonia of another etiology, indicating the likely role of other mechanisms [27].

COVID-19-related cardiac lesions often result in heart failure. Possible causes include direct viral damage to the myocardium, inflammatory damage, imbalance between oxygen demand and supply, and increased atherothrombosis caused by plaque instability. Prior cardiac disease is a predictor of more severe clinical manifestations and increased mortality in these patients [28].

Takotsubo syndrome, characterized by high troponin and brain natriuretic hormone (NT-proBNP) levels, T wave inversion, and ST segment elevation on the electrocardiogram, as well as signs of ballooning of the middle and apical segments of the myocardium according to imaging, is a less common cardiac manifestation of COVID-19. Psycho-emotional stress is the most prevalent cause of takotsubo cardiomyopathy, which results in the release of catecholamines, which is not uncommon in a pandemic [17].

The main mechanisms of structural heart damage and the clinical manifestations they cause are summarized in Fig. 1.

Diagnosis of myocarditis, including COVID-19-associated myocarditis

In clinical practice, diagnosing myocarditis can be difficult. In 2013, the European Society of Cardiology Working Group on Myocardial and Pericardial Diseases established presumptive and definite criteria for myocarditis diagnosis. Myocarditis is suspected based on the clinical presentation (chest pain), electrocardiogram findings (ST segment elevation), laboratory findings (e.g., high troponin), and imaging findings such as echocardiography and magnetic resonance imaging (MRI) [29]. The effectiveness of the

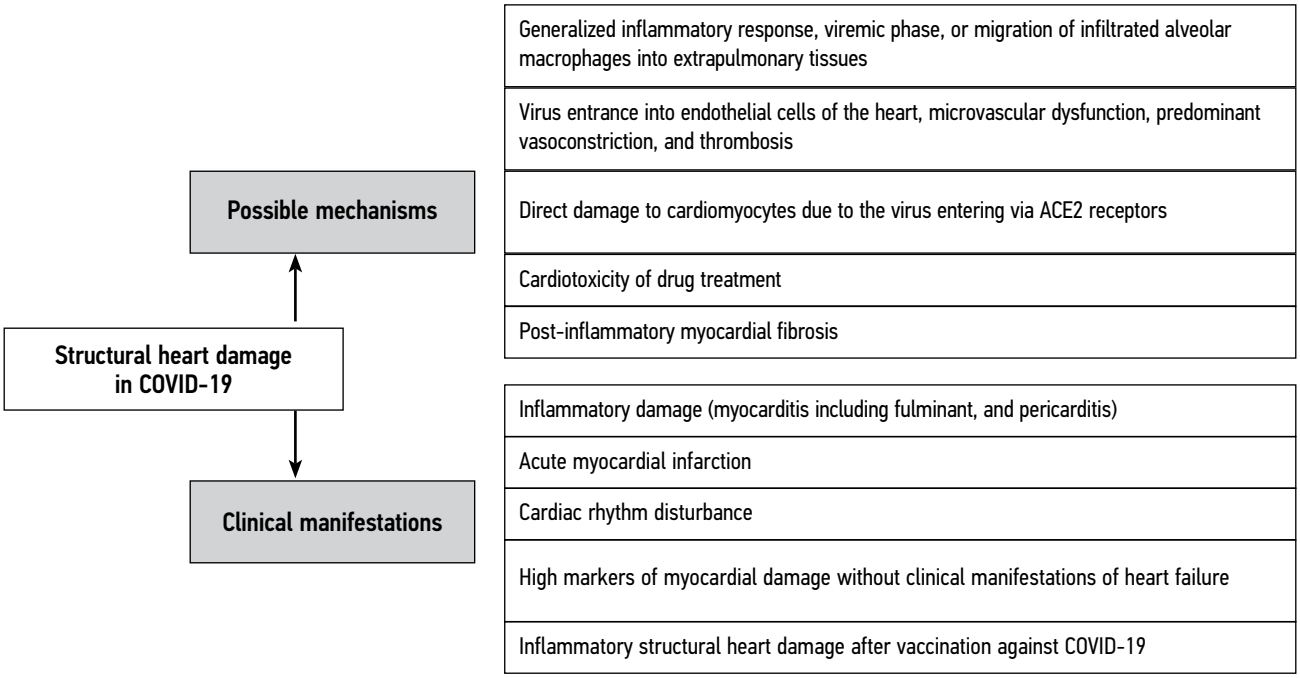

Fig. 1. Main mechanisms of structural damage in the heart of patients with COVID-19 and the clinical manifestations they cause.

latter technique is also emphasized in Russian guidelines for myocarditis diagnosis [30].

MRI is a valuable tool for diagnosing myocarditis according to the Lake Louise Criteria, originally published in 2009, which at that time included the evaluation of signs such as signal hyperintensity on T2-weighted imaging (T2WI), short T1 inversion recovery, and delayed non-coronary contrast uptake [31]. The use of the original Lake Louise Criteria was limited because of the subjectivity of the qualitative assessment of the above signs. Therefore, in 2018, the criteria were revised and supplemented with parametric mapping, allowing us to measure the regional and global T1 and T2 relaxation times of the myocardium and the extracellular volume (ECV). The 2018 Lake Louise Criteria have higher sensitivity and specificity (88% and 96%, respectively) [32]. On MRI, inflammatory structural heart damage can be confirmed if at least one criterion is present in each of the two categories: T2WI signs of myocardial edema (myocardial hyperintensity or elevated T2) [33] and T1WI signs of myocardial damage (non-ischemic pattern of delayed contrast uptake or elevated T1 and/or ECV) [34]. If only one marker is present, inflammatory myocardial damage is still considered in the presence of relevant clinical and/or laboratory signs; however, the specificity of MRI is lower in this scenario. Systolic dysfunction (hypo- or akinesia areas) and pericarditis (contrasted pericardial layers) are additional (but not mandatory) signs. These criteria should only be used if there's a clinical suspicion of inflammatory cardiac lesion, not as a screening strategy in asymptomatic cases. Furthermore, MRI helps in identifying important factors associated with myocarditis, such as signs of cardiomyopathies, which can all worsen a patient's prognosis [35].

A crucial component of diagnosis is the need to rule out coronary artery lesions, particularly when the clinical picture does not rule out coronary heart disease [36]. However, even ruling out coronary artery disease does not allow us to be certain that the clinical symptoms are caused by myocarditis; in addition, various types of non-coronary myocardial damage exist. Endomyocardial biopsy is frequently required, which also helps in discovering the causative factor of the damage. Despite this, biopsy is rarely performed in patients who do not have heart failure and/or imminent cardiac arrhythmias because of its invasiveness and complications. According to current guidelines of the American Heart Association, a biopsy is required in patients with new-onset heart failure and hemodynamic instability to rule out giant cell or eosinophilic infiltration, for which there is a specific therapy; if untreated, the prognosis is usually poor [37].

Histological findings of biopsy and autopsy of the heart for myocarditis were summarized in the Dallas criteria (Dallas, 1985) and defined as histological evidence of inflammatory infiltrates in the myocardium associated with non-ischemic degeneration or necrosis of cardiomyocytes [38]. Myocarditis is classified as borderline when there is lymphocytic infiltration but no necrosis. However, in viral myocarditis, the Dallas criteria are not always effective: on average, the criteria for myocarditis are lacking in 50% of such cases with verified presence of a pathogen [39]. The Dallas criteria have recently been updated to include immunohistochemistry findings that allow for the presence of an aberrant inflammatory infiltration [36]. In addition, signs of non-ischemic degeneration and necrosis of myocytes must be observed.

The presence of an inflammatory infiltrate in the absence of cardiomyocyte necrosis is also possible in the normal myocardium [40]. Myocarditis is primarily determined by the nature of the inflammatory infiltrate (accumulation of inflammatory cells around myocytes with a predominance of lymphocytes over macrophages) and presence of myocardial necrosis. Referring to the most recent literature data, classifying myocarditis as infectious (the presence of a laboratory-confirmed pathogen) or non-infectious (the absence of such) is necessary. Because of the existence of non-infectious myocarditis, whether myocardial biopsy should be used to diagnose myocarditis has been controversial. Currently, this method is not used to diagnose myocarditis, particularly COVID-19-associated myocarditis; instead, diagnosis is based on circumstantial evidence, such as echocardiography or MRI abnormalities [41].

In general, the criteria for diagnosing myocarditis in COVID-19 remain the same; however, the path to this diagnosis may differ from that in other etiologies of myocarditis, which is mostly due to the need to protect healthcare professionals from infection.

Some laboratory parameters are suggestive of COVID-19-associated myocarditis, lymphocytopenia is common (up to 83% of patients), and as the disease progresses, the role of inflammatory markers (D-dimer, ferritin, and C-reactive protein) becomes more important [42]. High troponin levels are suggestive of possible myocardial damage and may indicate acute myocarditis. High troponin levels, combined with high levels of inflammatory markers, indicate a hyperinflammatory state and multiple organ failure [43]. Furthermore, high NT-proBNP levels may indicate hemodynamic overload [44].

Electrocardiographic markers of myocardial injury are not pathognomonic for myocarditis: numerous patterns, ranging from sinus tachycardia to ST elevation and T wave inversion, were reported [44].

Echocardiography is the first-line imaging modality in both stable and unstable cases with suspected myocarditis. However, this method has limitations in detecting myocarditis: for example, ventricular dysfunction can be caused by various other ischemic and non-ischemic disorders and is not a pathognomonic sign of myocarditis, and a normal left ventricular ejection fraction does not rule out myocarditis [45].

In general, cardiac lesion is determined by an increase in cardiac troponin levels, which occurs in 18%–28% of patients with COVID-19 [28]. As previously stated, detecting myocarditis in patients with COVID-19 is uncommon: for example, only approximately 7.8% of such cases were identified in a major review of 277 reports (22 studies) on the autopsy of the myocardium of patients who died from COVID-19. However, other histopathologies are associated with this disease: an inflammatory infiltration without signs of myocarditis was detected in 12.6% of cases, ischemia damage to individual cardiomyocytes in 13.7%, and acute myocardial infarction in 4.7% [46]. The reported 60% incidence of myocarditis on MRI in COVID-19 survivors contrasts strongly with the relatively low incidence of myocarditis at autopsy. For example, in a study of 15 patients with characteristic symptoms who recovered from COVID-19, signs of myocardial damage (edema, fibrosis, and ventricular dysfunction) were observed on MRI in 58% of cases [47]. Another study with a similar design showed that 78% of convalescents had MR signs of myocardial damage, whereas troponin levels were high in 75% of cases [48]. Even after recovery, the risk of cardiac lesion and subsequent ventricular dysfunction remains.

Scientists are actively working to develop fundamentally new methods for diagnosing myocarditis in cases where cardiac MRI does not always detect myocarditis due to method limitations, and myocardial biopsy is not recommended because of the inability to detect the virus in cardiomyocytes. These include detecting microRNA produced by T-helper type 17, which are active participants in acute myocardial damage and development of myocarditis and dilated cardiomyopathy in its aftermath. Researchers have already identified a new microRNA as a marker of myocarditis in murine models (with experimental autoimmune and viral myocarditis) and its human homolog. This marker allows differentiating myocarditis from myocardial infarction. Nonetheless, more questions require answers: for example, the greater variability in the level of this microRNA and whether this reflects the severity of the patient's condition; and whether it will differentiate between conditions such as myocarditis and dilated cardiomyopathy [49]. Further research in this area will help in developing a method for non-invasive diagnosis of myocarditis.

During earlier coronavirus epidemics, cases of myocarditis were either not found (as with SARS) or were isolated (as with MERS) [50, 51]. The tropism of the COVID-19 pathogen to cardiomyocytes was generally because of the limited expression of ACE2 receptors on the surface of these cells. These and other findings suggest that endothelial cell activation, cytokine storm, electrolyte imbalance, and other potential immune mechanisms may directly cause myocardial damage in COVID-19 [46]. Furthermore, in the context of electrocardiographic abnormalities and positive troponin tests in normal coronary arteries, takotsubo syndrome should not be overlooked as a potential cause of myocardial damage [52]. In addition, myocarditis should be differentiated from other disorders such as sepsis-associated cardiomyopathy and acute coronary syndrome (particularly in fulminant myocarditis).

Myocarditis due to COVID-19 vaccination

Currently, no etiotropic therapy is available for COVID-19, and vaccination is the primary method of combating the pandemic; effective vaccines lower mortality rates dramatically. To date, the following vaccines are the most well-known worldwide: AstraZeneca/Oxford, Johnson and Johnson, Moderna, Pfizer/BioNTech, Sinopharm, Sinovac, and Sputnik V. Several vaccine principles have been

proposed, including RNA- and DNA-based preparations (i.e., an approach that uses genetically modified RNA or DNA to create a protein that triggers an immune response, and vector-based preparations (i.e., using a harmless virus that cannot cause disease but serves as a platform for the production of coronavirus proteins that trigger an immune response), inactivated vaccines (a weakened virus to trigger an immune response), and protein-based vaccines (safe proteins or protein fragments that mimic the COVID-19 pathogen to trigger an immune response). AstraZeneca/Oxford, Johnson and Johnson, and Sputnik V vaccines are based on DNA delivered via a non-replicating recombinant adenovirus vector system. Moderna and Pfizer/BioNTech vaccines are based on mRNA technology and lipid nanoparticle delivery system [53–56]. Vector-based vaccines, such as mRNA-based vaccines, boost SARS-CoV-2 S protein production, which is the principal target for neutralizing antibodies produced by natural infection or vaccination.

During the vaccination program, data on the side effects of vaccines are published over time. In some cases, these reactions are thought to cause increased platelet aggregation, thrombosis, and inflammation. A possible mechanism is the synthesis of freely circulating spike proteins that can interact with ACE2 receptors by cells in the body that are targeted by vaccines [57].

Myocarditis and pericarditis have been reported [58, 59] following COVID-19 vaccination (usually within 6 h to 4 days), predominantly in patients who received mRNA-based vaccines (Pfizer and Moderna). In Israel, two large retrospective studies have been conducted in patients who received the Pfizer vaccine. One of these studies, with >5.1 million participants (21 days after the first dose and 30 days after the second dose), discovered 136 cases of myocarditis; 95% had mild symptoms, and one case was fatal [60]. Such symptoms were observed to be common in young men. Another study in Israel examined the medical records of more than 2.5 million Pfizer vaccinated patients and discovered that myocarditis occurs in 2.3 per 100,000 people. However, in young people aged 16–29 years, the incidence was 10 per 100,000 people [61]. In addition, those infected with the COVID-19 pathogen have an 18.28 times higher risk of myocarditis than those who are not infected, i.e., a significantly higher risk of myocarditis than after vaccination (on average 3.24 times higher than in unvaccinated patients) [62]. Although the symptoms of myocarditis were observed close to the vaccination time and researchers ruled out other probable causes (i.e., vaccination was identified as the cause of myocarditis), the pathophysiology of COVID-19 remains unknown. Existing hypotheses that this is caused by a nonspecific inflammatory reaction or antibody cross-reactivity due to molecular mimicry are consistent with the fact that the condition improves on anti-inflammatory therapy [58].

CONCLUSION

COVID-19 has a high mortality rate, including in the presence of concomitant cardiac lesion; however, its mechanisms are still unclear. Although COVID-19-associated myocarditis is thought to be the primary cause, inflammatory myocardial damage is rarely detected in histological examinations in patients with confirmed COVID-19. The virus is rarely discovered in the heart tissues and is found in immune cells rather than cardiomyocytes. It is primarily identified in nonspecific inflammatory infiltrate of the myocardium. Given these findings, endomyocardial biopsy should not be routinely employed to detect myocarditis in COVID-19.

Inflammatory myocardial damage is also possible occurs following vaccination, particularly with mRNA-based vaccines. This complication is more common in young patients, with moderate symptoms in the majority of cases. A high incidence of myocarditis following vaccination is not a sensible reason to avoid it, particularly among young people.

ADDITIONAL INFORMATION

Funding source. This article was not supported by any external sources of funding.

Competing interests. The authors declare that they have no competing interests.

Authors' contribution. All authors made a substantial contribution to the conception of the work, acquisition, analysis, interpretation of data for the work, drafting and revising the work, final approval of the version to be published and agree to be accountable for all aspects of the work. D.A. Filatova — collection and processing of materials, writing the text of the manuscript; E.A. Mershina — concept and design of the work; V.E. Sinitsyn — concept and design of the work, approval of the final text of the manuscript.

REFERENCES

1. Shi S, Qin M, Shen B, et al. Association of cardiac injury with mortality in hospitalized patients with COVID-19 in Wuhan, China. *JAMA Cardiol*. 2020;5(7):802–810. doi: 10.1001/jamacardio.2020.0950

2. Lala A, Johnson KW, Januzzi JL, et al. Prevalence and impact of myocardial injury in patients hospitalized with COVID-19 infection. *J Am Coll Cardiol*. 2020;76(5):533–546. doi: 10.1016/j.jacc.2020.06.007

3. Lindner D, Fitzek A, Bräuninger H, et al. Association of cardiac infection with SARS-CoV-2 in confirmed COVID-19 autopsy cases. *JAMA Cardiol*. 2020;5(11):1–5. doi: 10.1001/jamacardio.2020.3551

4. Sala S, Peretto G, Gramegna M, et al. Acute myocarditis presenting as a reverse Tako-Tsubo syndrome in a patient with SARS-CoV-2 respiratory infection. *Eur Heart J*. 2020;41(19):1861–1862. doi: 10.1093/eurheartj/ehaa286

5. Escher F, Pietsch H, Aleshcheva G, et al. Detection of viral SARS-CoV-2 genomes and histopathological changes in endomyocardial biopsies. *ESC Heart Fail*. 2020;7(5):2440–2447. doi: 10.1002/ehf2.12805
6. Tavazzi G, Pellegrini C, Maurelli M, et al. Myocardial localization of coronavirus in COVID-19 cardiogenic shock. *Eur J Heart Fail*. 2020;22(5):911–915. doi: 10.1002/ejhf.1828
7. Wichmann D. Autopsy findings and venous thromboembolism in patients with COVID-19. *Ann Intern Med*. 2020;173(12):1030. doi: 10.7326/L20-1206
8. Buja LM, Wolf DA, Zhao B, et al. The emerging spectrum of cardiopulmonary pathology of the coronavirus disease 2019 (COVID-19): Report of 3 autopsies from Houston, Texas, and review of autopsy findings from other United States cities. *Cardiovasc Pathol*. 2020;(48):107233. doi: 10.1016/j.carpath.2020.107233
9. Fox SE, Akmatbekov A, Harbert JL, et al. Pulmonary and cardiac pathology in African American patients with COVID-19: An autopsy series from New Orleans. *Lancet Respir Med*. 2020;10(7):681–686. doi: 10.1016/S2213-2600(20)30243-5
10. Alijotas-Reig J, Esteve-Valverde E, Belizna C, et al. Immunomodulatory therapy for the management of severe COVID-19. Beyond the anti-viral therapy: A comprehensive review. *Autoimmun Rev*. 2020;19(7):102569. doi: 10.1016/j.autrev.2020.102569
11. Varga Z, Flammer AJ, Steiger P, et al. Endothelial cell infection and endotheliitis in COVID-19. *Lancet Lond Engl*. 2020;395(10234):1417–1418. doi: 10.1016/S0140-6736(20)30937-5
12. Bikdeli B, Madhavan MV, Jimenez D, et al. COVID-19 and thrombotic or thromboembolic disease: Implications for prevention, antithrombotic therapy, and follow-up: JACC state-of-the-art review. *J Am Coll Cardiol*. 2020;75(23):2950–2973. doi: 10.1016/j.jacc.2020.04.031
13. Choudry FA, Hamshere SM, Rathod KS, et al. High thrombus burden in patients with Covid-19 presenting with ST-segment elevation myocardial infarction. *J Am Coll Cardiol*. 2020;76(10):1168–1176. doi: 10.1016/j.jacc.2020.07.022
14. Bangalore S, Hamshere SM, Rathod KS, et al. ST-Segment elevation in patients with Covid-19: A case series. *N Engl J Med*. 2020;382(25):2478–2480. doi: 10.1056/NEJMc2009020
15. Guglin ME, Etuk A, Shah C, et al. Fulminant myocarditis and cardiogenic shock following COVID-19 infection versus COVID-19 vaccination: A systematic literature review. *J Clin Med*. 2023;12(5):1849. doi: 10.3390/jcm12051849
16. Wang D, Hu B, Hu C, et al. Clinical characteristics of 138 hospitalized patients with 2019 novel coronavirus-infected pneumonia in Wuhan, China. *JAMA*. 2020;323(11):1061–1069. doi: 10.1001/jama.2020.1585
17. Siripanthong B, Nazarian S, Muser D, et al. Recognizing COVID-19-related myocarditis: The possible pathophysiology and proposed guideline for diagnosis and management. *Heart Rhythm*. 2020;17(9):1463–1471. doi: 10.1016/j.hrthm.2020.05.001
18. Peretto G, Sala S, Rizzo S, et al. Ventricular arrhythmias in myocarditis: Characterization and relationships with myocardial inflammation. *J Am Coll Cardiol*. 2020;75(9):1046–1057. doi: 10.1016/j.jacc.2020.01.036
19. Peretto G, Sala S, Rizzo S, et al. Arrhythmias in myocarditis: State of the art. *Heart Rhythm*. 2019;16(5):793–801. doi: 10.1016/j.hrthm.2018.11.024
20. Chen L, Li X, Chen M, et al. The ACE2 expression in human heart indicates new potential mechanism of heart injury among patients infected with SARS-CoV-2. *Cardiovasc Res*. 2020;116(6):1097–1100. doi: 10.1093/cvr/cvaa078
21. Asimaki A, Tandri H, Duffy ER, et al. Altered desmosomal proteins in granulomatous myocarditis and potential pathogenic links to arrhythmogenic right ventricular cardiomyopathy. *Circ Arrhythm Electrophysiol*. 2011;4(5):743–752. doi: 10.1161/CIRCEP.111.964890
22. Gemayel C, Pelliccia A, Thompson PD. Arrhythmogenic right ventricular cardiomyopathy. *J Am Coll Cardiol*. 2001;38(7):1773–1781. doi: 10.1016/s0735-1097(01)01654-0
23. Coomes EA, Haghbayan H. Interleukin-6 in Covid-19: A systematic review and meta-analysis. *Rev Med Virol*. 2020;30(6):1–9. doi: 10.1002/rmv.2141
24. Modica G, Bianco M, Sollazzo F, et al. Myocarditis in athletes recovering from COVID-19: A systematic review and meta-analysis. *Int J Environ Res Public Health*. 2022;19(7):4279. doi: 10.3390/ijerph19074279
25. Eichhorn C, Biere L, Schnell F, et al. Myocarditis in athletes is a challenge: Diagnosis, risk stratification, and uncertainties. *JACC Cardiovasc Imaging*. 2020;13(2):494–507. doi: 10.1016/j.jcmg.2019.01.039
26. Azevedo RB, Botelho BG, de Hollanda G, et al. Covid-19 and the cardiovascular system: A comprehensive review. *J Hum Hypertens*. 2021;35(1):4–11. doi: 10.1038/s41371-020-0387-4
27. Klok FA, Kruip MJ, van der Meer HJ, et al. Incidence of thrombotic complications in critically ill ICU patients with COVID-19. *Thromb Res*. 2020;(191):145–147. doi: 10.1016/j.thromres.2020.04.013
28. Guo T, Fan Y, Chen M, et al. Cardiovascular implications of fatal outcomes of patients with coronavirus disease 2019 (COVID-19). *JAMA Cardiol*. 2020;5(7):811–818. doi: 10.1001/jamacardio.2020.1017
29. Larina OM. Cardiac magnetic resonance imaging in the diagnosis of acute myocarditis: A clinical case and review of the literature. *Bulletin Radiol Radiol*. 2014;(5):54–59. (In Russ).
30. Arutyunov GB, Paleev FN, Moiseeva OM. Myocarditis in adults. Clinical recommendations 2020. *Russ Cardiol J*. 2021;26(11):4790. (In Russ). doi: 10.15829/1560-4071-2021-4790
31. Friedrich MG, Sechtem U, Schulz-Menger J, et al. Cardiovascular magnetic resonance in myocarditis: A JACC white paper. *J Am Coll Cardiol.* 2009;53(17):1475–1487. doi: 10.1016/j.jacc.2009.02.007
32. Tijmes SF, Thavendiranathan P, Udell JA, et al. Cardiac MRI assessment of nonischemic myocardial inflammation: State of the art review and update on myocarditis associated with COVID-19 *Vaccination Radiol Cardiothorac Imaging*. 2021;3(6):e210252. doi: 10.1148/ryct.210252
33. Srichai MB, Lim RP, Lath N, et al. Diagnostic performance of dark-blood T2-weighted CMR for evaluation of acute myocardial injury. *Invest Radiol*. 2013;48(1):24–31. doi: 10.1097/RLI.0b013e3182718672
34. Galán-Arriola C, Lim RP, Lath N, et al. Serial magnetic resonance imaging to identify early stages of anthracycline-induced cardiotoxicity. *J Am Coll Cardiol*. 2019;73(7):779–791. doi: 10.1016/j.jacc.2018.11.046
35. Blagova OV, Pavlenko EV, Varionchik NV, et al. Myocarditis as a natural phenomenon in patients with primary non-compact myocardium: Diagnosis, treatment and impact on outcomes // *Russ J Cardiol*. 2018;(2):44–52. (In Russ). doi: 10.15829/1560-4071-2018-2-44-52
36. Caforio AL, Pankuweit S, Arbustini E, et al. Current state of knowledge on aetiology, diagnosis, management, and therapy of myocarditis: A position statement of the European Society of Cardiology Working Group on Myocardial and Pericardial Diseases. *Eur Heart J*. 2013;34(33)2636–2648, 2648a–2648d. doi: 10.1093/eurheartj/eht210

37. Cooper LT, Baughman KL, Feldman AM, et al. The role of endomyocardial biopsy in the management of cardiovascular disease: A scientific statement from the American Heart Association, the American College of Cardiology, and the European Society of Cardiology. *Circulation.* 2007;116(19):2216–2233. doi: 10.1161/CIRCULATIONAHA.107.186093
38. Aretz HT. Myocarditis: The Dallas criteria. *Hum Pathol*. 1987;18(6):619–624. doi: 10.1016/s0046-8177(87)80363-5
39. Dennert R, Crijns HJ, Heymans S. Acute viral myocarditis. *Eur Heart J*. 2008;29(17):2073–2082. doi: 10.1093/eurheartj/ehn296
40. Zhang M, Tavora F, Zhang Y, et al. The role of focal myocardial inflammation in sudden unexpected cardiac and noncardiac deaths: A clinicopathological study. *Int J Legal Med.* 2013;127(1):131–138. doi: 10.1007/s00414-011-0634-x
41. Titov VA, Ignatyeva VS, Mitrofanova LB. Comparative study of informativeness of noninvasive methods for diagnosis of myocardial inflammatory diseases. *Russ J Cardiol*. 2018;23(2):53–59. (In Russ).
42. Zhou F, Yu T, Du R, et al. Clinical course and risk factors for mortality of adult inpatients with COVID-19 in Wuhan, China: A retrospective cohort study. *Lancet Lond Engl*. 2020;395(10229):1054–1062. doi: 10.1016/S0140-6736(20)30566-3
43. Mehta P, McAuley DF, Brown M, et al. COVID-19: Consider cytokine storm syndromes and immunosuppression. *Lancet Lond Engl*. 2020;395(10229):1033–1034. doi: 10.1016/S0140-6736(20)30628-0
44. Castiello T, Georgiopoulos G, Finocchiaro G, et al. COVID-19 and myocarditis: A systematic review and overview of current challenges. *Heart Fail Rev*. 2022;27(1):251–261. doi: 10.1007/s10741-021-10087-9
45. Mele D, Flamigni F, Rapezzi C, et al. Myocarditis in COVID-19 patients: Current problems. *Intern Emerg Med*. 2021;16(5):1123–1129. doi: 10.1007/s11739-021-02635-w
46. Halushka MK, Vander Heide RS. Myocarditis is rare in COVID-19 autopsies: Cardiovascular findings across 277 postmortem examinations. *Cardiovasc Pathol*. 2021;(50):107300. doi: 10.1016/j.carpath.2020.107300
47. Huang L, Zhao P, Tang D, et al. Cardiac involvement in patients recovered from COVID-2019 identified using magnetic resonance imaging. *JACC Cardiovasc Imaging*. 2020;13(11):2330–2339. doi: 10.1016/j.jcmg.2020.05.004
48. Puntmann VO, Carerj ML, Wieters I, et al. Outcomes of cardiovascular magnetic resonance imaging in patients recently recovered from coronavirus disease 2019 (COVID-19). *JAMA Cardiol*. 2020;5(11):1265–1273. doi: 10.1001/jamacardio.2020.3557
49. Blanco-Domínguez R, Sánchez-Díaz R, de la Fuente H, et al. A novel circulating MicroRNA for the detection of acute myocarditis. *N Engl J Med*. 2021;384(21):2014–2027. doi: 10.1056/NEJMoa2003608
50. Tan L, Wang Q, Zhang D, et al. Lymphopenia predicts disease severity of COVID-19: A descriptive and predictive study. *Signal Transduct Target Ther*. 2020;5(1):33. doi: 10.1038/s41392-020-0148-4
51. Xu Z, Shi L, Wang Y, et al. Pathological findings of COVID-19 associated with acute respiratory distress syndrome. *Lancet Respir Med*. 2020;8(4):420–422. doi: 10.1016/S2213-2600(20)30076-X
52. Kawakami R, Sakamoto A, Kawai K, et al. Pathological evidence for SARS-CoV-2 as a cause of myocarditis. *J Am Coll Cardiol*. 2021;77(3):314–325. doi: 10.1016/j.jacc.2020.11.031
53. Baden LR, El Sahly HM, Essink B, et al. Efficacy and safety of the mRNA-1273 SARS-CoV-2 vaccine. *N Engl J Med*. 2021;384(5):403–416. doi: 10.1056/NEJMoa2035389
54. Logunov DY, Dolzhikova IV, Shcheblyakov DV, et al. Safety and efficacy of an rAd26 and rAd5 vector-based heterologous prime-boost COVID-19 vaccine: An interim analysis of a randomised controlled phase 3 trial in Russia. *Lancet*. 2021;397(10275):671–681. doi: 10.1016/S0140-6736(21)00234-8
55. Polack FP, Thomas SJ, Kitchin N, et al. Safety and efficacy of the BNT162b2 mRNA Covid-19 vaccine. *N Engl J Med*. 2020;383(27):2603–2615. doi: 10.1056/NEJMoa2034577
56. Voysey M, Clemens SA, Madhi SA, et al. Safety and efficacy of the ChAdOx1 nCoV-19 vaccine (AZD1222) against SARS-CoV-2: An interim analysis of four randomised controlled trials in Brazil, South Africa, and the UK. *Lancet*. 2021;397(10269):99–111. doi: 10.1016/S0140-6736(20)32661-1
57. Shiravi AA, Ardekani A, Sheikhbahaei E, et al. Cardiovascular complications of SARS-CoV-2 vaccines: An overview. *Cardiol Ther*. 2021;11(1):13–21. doi: 10.1007/s40119-021-00248-0
58. Watad A, De Marco G, Mahajna H, et al. Immune-Mediated disease flares or new-onset disease in 27 subjects following mRNA/DNA SARS-CoV-2 Vaccination: 5. *Vaccines*. 2021;9(5):435. doi: 10.3390/vaccines9050435
59. Albert E, Aurigemma G, Saucedo J, et al. Myocarditis following COVID-19 vaccination. *Radiol Case Rep*. 2021;16(8):2142–2145. doi: 10.1016/j.radcr.2021.05.033
60. Mevorach D, Anis E, Cedar N, et al. Myocarditis after BNT162b2 mRNA vaccine against Covid-19 in Israel. *N Engl J Med*. 2021;385(23):2140–2149. doi: 10.1056/NEJMoa2109730
61. Witberg G, Barda N, Hoss S, et al. Myocarditis after Covid-19 vaccination in a large health care organization. *N Engl J Med*. 2021;385(23):2132–2139. doi: 10.1056/NEJMoa2110737
62. Barda N, Dagan N, Ben-Shlomo Y, et al. Safety of the BNT162b2 mRNA Covid-19 vaccine in a nationwide setting. *N Engl J Med*. 2021;385(12):1078–1090. doi: 10.1056/NEJMoa2110475

СПИСОК ЛИТЕРАТУРЫ

1. Shi S., Qin M., Shen B., et al. Association of cardiac injury with mortality in hospitalized patients with COVID-19 in Wuhan, China // JAMA Cardiol. 2020. Vol. 5, N 7. P. 802–810. doi: 10.1001/jamacardio.2020.0950
2. Lala A., Johnson K.W., Januzzi J.L., et al. Prevalence and impact of myocardial injury in patients hospitalized with COVID-19 infection // J Am Coll Cardiol. 2020. Vol. 76, N 5. P. 533–546. doi: 10.1016/j.jacc.2020.06.007
3. Lindner D., Fitzek A., Bräuninger H., et al. Association of cardiac infection with SARS-CoV-2 in confirmed COVID-19 autopsy cases // JAMA Cardiol. 2020. Vol. 5, N 11. P. 1–5. doi: 10.1001/jamacardio.2020.3551
4. Sala S., Peretto G., Gramegna M., et al. Acute myocarditis presenting as a reverse Tako-Tsubo syndrome in a patient with SARS-CoV-2 respiratory infection // Eur Heart J. 2020. Vol. 41, N 19. P. 1861–1862. doi: 10.1093/eurheartj/ehaa286
5. Escher F., Pietsch G., Aleshcheva G., et al. Detection of viral SARS-CoV-2 genomes and histopathological changes in endomyocardial biopsies // ESC Heart Fail. 2020. Vol. 7, N 5. P. 2440–2447. doi: 10.1002/ehf2.12805
6. Tavazzi G., Pellegrini C., Maurelli M., et al. Myocardial localization of coronavirus in COVID-19 cardiogenic shock // Eur J Heart Fail. 2020. Vol. 22, N 5. P. 911–915. doi: 10.1002/ejhf.1828

7. Wichmann D. Autopsy findings and venous thromboembolism in patients with COVID-19 // Ann Intern Med. 2020. Vol. 173, N 12. P. 1030. doi: 10.7326/L20-1206
8. Buja L.M., Wolf D.A., Zhao B., et al. The emerging spectrum of cardiopulmonary pathology of the coronavirus disease 2019 (COVID-19): Report of 3 autopsies from Houston, Texas, and review of autopsy findings from other United States cities // Cardiovasc Pathol. 2020. N 48. P. 107233. doi: 10.1016/j.carpath.2020.107233
9. Fox S.E., Akmatbekov A., Harbert J.L., et al. Pulmonary and cardiac pathology in African American patients with COVID-19: An autopsy series from New Orleans // Lancet Respir Med. 2020. Vol. 8, N 7. P. 681–686. doi: 10.1016/S2213-2600(20)30243-5
10. Alijotas-Reig J., Esteve-Valverde E., Belizna C., et al. Immunomodulatory therapy for the management of severe COVID-19. Beyond the anti-viral therapy: A comprehensive review // Autoimmun Rev. 2020. Vol. 19, N 7. P. 102569. doi: 10.1016/j.autrev.2020.102569
11. Varga Z., Flammer A.J., Steiger P., et al. Endothelial cell infection and endotheliitis in COVID-19 // Lancet Lond Engl. 2020. Vol. 395, N 10234. P. 1417–1418. doi: 10.1016/S0140-6736(20)30937-5
12. Bikdeli B., Madhavan M.V., Jimenez D., et al. COVID-19 and thrombotic or thromboembolic disease: Implications for prevention, antithrombotic therapy, and follow-up: JACC state-of-the-art review // J Am Coll Cardiol. 2020. Vol. 75, N 23. P. 2950–2973. doi: 10.1016/j.jacc.2020.04.031
13. Choudry F.A., Hamshere S.M., Rathod K.S., et al. High thrombus burden in patients with COVID-19 presenting with ST-segment elevation myocardial infarction // J Am Coll Cardiol. 2020. Vol. 76, N 10. P. 1168–1176. doi: 10.1016/j.jacc.2020.07.022
14. Bangalore S., Sharma D., Slotwiner A., et al. ST-Segment elevation in patients with Covid-19: A case series // N Engl J Med. 2020. Vol. 382, N 25. P. 2478–2480. doi: 10.1056/NEJMc2009020
15. Guglin M.E., Etuk A., Shah C., et al. Fulminant myocarditis and cardiogenic shock following COVID-19 infection versus COVID-19 vaccination: A systematic literature review // J Clin Med. 2023. Vol. 12, N 5. P. 1849. doi: 10.3390/jcm12051849
16. Wang D., Hu B., Hu C., et al. Clinical characteristics of 138 hospitalized patients with 2019 novel coronavirus-infected pneumonia in Wuhan, China // JAMA. 2020. Vol. 323, N 11. P. 1061–1069. doi: 10.1001/jama.2020.1585
17. Siripanthong B., Nazarian S., Muser D., et al. Recognizing COVID-19-related myocarditis: The possible pathophysiology and proposed guideline for diagnosis and management // Heart Rhythm. 2020. Vol. 17, N 9. P. 1463–1471. doi: 10.1016/j.hrthm.2020.05.001
18. Peretto G., Sala S., Rizzo S., et al. Ventricular arrhythmias in myocarditis: Characterization and relationships with myocardial inflammation // J Am Coll Cardiol. 2020. Vol. 75, N 9. P. 1046–1057. doi: 10.1016/j.jacc.2020.01.036
19. Peretto G., Sala S., Rizzo S., et al. Arrhythmias in myocarditis: State of the art // Heart Rhythm. 2019. Vol. 16, N 5. P. 793–801. doi: 10.1016/j.hrthm.2018.11.024
20. Chen L., Li X., Chen M., et al. The ACE2 expression in human heart indicates new potential mechanism of heart injury among patients infected with SARS-CoV-2 // Cardiovasc Res. 2020. Vol. 116, N 6. P. 1097–1100P. doi: 10.1093/cvr/cvaa078
21. Asimaki A., Tandri H., Duffi E.R., et al. Altered desmosomal proteins in granulomatous myocarditis and potential pathogenic links to arrhythmogenic right ventricular cardiomyopathy // Circ Arrhythm Electrophysiol. 2011. Vol. 4, N 5. P. 743–752. doi: 10.1161/CIRCEP.111.964890
22. Gemayel C., Pelliccia A., Thompson P.D. Arrhythmogenic right ventricular cardiomyopathy // J Am Coll Cardiol. 2001. Vol. 38, N 7. P. 1773–1781. doi: 10.1016/s0735-1097(01)01654-0
23. Coomes E.A., Haghbayan H. Interleukin-6 in Covid-19: A systematic review and meta-analysis // Rev Med Virol. 2020. Vol. 30, N 6. P. 1–9. doi: 10.1002/rmv.2141
24. Modica G., Bianco M., Sollazzo F., et al. Myocarditis in athletes recovering from COVID-19: A systematic review and meta-analysis // Int J Environ Res Public Health. 2022. Vol. 19, N 7. P. 4279. doi: 10.3390/ijerph19074279
25. Eichhorn C., Biere L., Schnell F., et al. Myocarditis in athletes is a challenge: Diagnosis, risk stratification, and uncertainties // JACC Cardiovasc Imaging. 2020. Vol. 13, N 2, Pt. 1. P. 494–507. doi: 10.1016/j.jcmg.2019.01.039
26. Azevedo R.B., Botelho B.G., de Hollanda G., et al. Covid-19 and the cardiovascular system: A comprehensive review: 1 // J Hum Hypertens. 2021. Vol. 35, N 1. P. 4–11. doi: 10.1038/s41371-020-0387-4
27. Klok F.A., Kruip M.J., van der Meer H.J., et al. Incidence of thrombotic complications in critically ill ICU patients with COVID-19 // Thromb Res. 2020. N 191. P. 145–147. doi: 10.1016/j.thromres.2020.04.013
28. Guo T., Fan Y., Chen M., et al. Cardiovascular Implications of fatal outcomes of patients with coronavirus disease 2019 (COVID-19) // JAMA Cardiol. 2020. Vol. 5, N 7. P. 811–818. doi: 10.1001/jamacardio.2020.1017
29. Ларина О.М. Магнитно-резонансная томография сердца в диагностике острого миокардита: клинический случай и обзор литературы // Вестник рентгенологии и радиологии. 2014. № 5. С. 54–59.
30. Арутюнов Г.Б., Палеев Ф.Н., Моисеева О.М. Миокардиты у взрослых. Клинические рекомендации 2020 // Российский кардиологический журнал. 2021. Т. 26, № 11. С. 47–90. doi: 10.15829/1560-4071-2021-4790
31. Friedrich M.G., Sechtem U., Schulz-Menger J., et al. Cardiovascular magnetic resonance in myocarditis: A JACC white paper // J Am Coll Cardiol. 2009. Vol. 53, N 17. P. 1475–1487. doi: 10.1016/j.jacc.2009.02.007
32. Tijmes S.F., Thavendiranathan P., Udell J.A., et al. Cardiac MRI assessment of nonischemic myocardial inflammation: State of the art review and update on myocarditis associated with COVID-19 vaccination // Radiol Cardiothorac Imaging. 2021. Vol. 3, N 6. P. e210252. doi: 10.1148/ryct.210252
33. Srichai M.B., Lim R.P., Lath N., et al. Diagnostic performance of dark-blood T2-weighted CMR for evaluation of acute myocardial injury // Invest Radiol. 2013. Vol. 48, N 1. P. 24–31. doi: 10.1097/RLI.0b013e3182718672
34. Galán-Arriola C., Lobo M., Vílchez-Tschischke J.P., et al. Serial magnetic resonance imaging to identify early stages of anthracycline-induced cardiotoxicity // J Am Coll Cardiol. 2019. Vol. 73, N 7. P. 779–791. doi: 10.1016/j.jacc.2018.11.046
35. Благова О.В., Павленко Е.В., Вариончик Н.В., и др. Миокардит как закономерный феномен у больных с первичным некомпактным миокардом: диагностика, лечение и влияние на исходы // Российский кардиологический журнал. 2018. N 2. С. 44–52. doi: 10.15829/1560-4071-2018-2-44-52
36. Caforio A.L., Pankuweit S., Arbustini E., et al. Current state of knowledge on aetiology, diagnosis, management, and therapy of myocarditis: A position statement of the European Society of Cardiology Working Group on Myocardial and Pericardial Diseases // Eur

Heart J. 2013. Vol. 34, N 33. P. 2636–2648, 2648a–2648d. doi: 10.1093/eurheartj/eht210
37. Cooper L.T., Baughman K.L., Feldman A.M., et al. The role of endomyocardial biopsy in the management of cardiovascular disease: A scientific statement from the American Heart Association, the American College of Cardiology, and the European Society of Cardiology // Circulation. 2007. Vol. 116, N 19. P. 2216–2233. doi: 10.1161/CIRCULATIONAHA.107.186093
38. Aretz H.T. Myocarditis: The Dallas criteria // Hum Pathol. 1987. Vol. 18, N 6. P. 619–624. doi: 10.1016/s0046-8177(87)80363-5
39. Dennert R., Crijns H.J., Heymans S. Acute viral myocarditis // Eur Heart J. 2008. Vol. 29, N 17. P. 2073–2082. doi: 10.1093/eurheartj/ehn296
40. Zhang M., Tavora F., Zhang Y., et al. The role of focal myocardial inflammation in sudden unexpected cardiac and noncardiac deaths: A clinicopathological study // Int J Legal Med. 2013. Vol. 127, N 1. P. 131–138. doi: 10.1007/s00414-011-0634-x
41. Титов В.А., Игнатьева В.С., Митрофанова Л.Б. Сравнительное исследование информативности неинвазивных методов диагностики воспалительных заболеваний миокарда // Российский кардиологический журнал. 2018. Т. 23, N 2. С. 53–59.
42. Zhou F., Yu T., Fan R., et al. Clinical course and risk factors for mortality of adult inpatients with COVID-19 in Wuhan, China: A retrospective cohort study // Lancet Lond Engl. 2020. Vol. 395, N 10229. P. 10541062. doi: 10.1016/S0140-6736(20)30566-3
43. Mehta P., McAuley D.F., Brown M., et al. COVID-19: Consider cytokine storm syndromes and immunosuppression // Lancet Lond Engl. 2020. Vol. 395, N 10229. P. 1033–1034. doi: 10.1016/S0140-6736(20)30628-0
44. Castiello T., Georgiopoulos G., Finocchiaro G., et al. COVID-19 and myocarditis: A systematic review and overview of current challenges // Heart Fail Rev. 2022. Vol. 27, N 1. P. 251–261. doi: 10.1007/s10741-021-10087-9
45. Mele D., Flamigni F., Rapezzi C., et al. Myocarditis in COVID-19 patients: Current problems // Intern Emerg Med. 2021. Vol. 16, N 5. P. 1123–1129. doi: 10.1007/s11739-021-02635-w
46. Halushka M.K., Vander Heide R.S. Myocarditis is rare in COVID-19 autopsies: Cardiovascular findings across 277 postmortem examinations // Cardiovasc Pathol. 2021. N 50. P. 107300. doi: 10.1016/j.carpath.2020.107300
47. Huang L., Zhao P., Tang D., et al. Cardiac involvement in patients recovered from COVID-2019 identified using magnetic resonance imaging // JACC Cardiovasc Imaging. 2020. Vol. 13, N 11. P. 2330–2339. doi: 10.1016/j.jcmg.2020.05.004
48. Puntmann V.O., Carerj M.L., Wieters I., et al. Outcomes of cardiovascular magnetic resonance imaging in patients recently recovered from coronavirus disease 2019 (COVID-19) // JAMA Cardiol. 2020. Vol. 5, N 11. P. 1265–1273. doi: 10.1001/jamacardio.2020.3557
49. Blanco-Domínguez R., Sánchez-Díaz R., de la Fuente H., et al. A novel circulating MicroRNA for the detection of acute myocarditis // N Engl J Med. 2021. Vol. 384, N 21. P. 2014–2027. doi: 10.1056/NEJMoa2003608
50. Tan L., Wang Q., Zhang D., et al. Lymphopenia predicts disease severity of COVID-19: A descriptive and predictive study // Signal Transduct Target Ther. 2020. Vol. 5, N 1. P. 33. doi: 10.1038/s41392-020-0148-4
51. Xu Z., Shi L., Zhang J., et al. Pathological findings of COVID-19 associated with acute respiratory distress syndrome // Lancet Respir Med. 2020. Vol. 8, N 4. P. 420–422. doi: 10.1016/S2213-2600(20)30076-X
52. Kawakami R., Sakamoto A., Kawai K., et al. Pathological evidence for SARS-CoV-2 as a cause of myocarditis // J Am Coll Cardiol. 2021. Vol. 77, N 3. P. 314–325. doi: 10.1016/j.jacc.2020.11.031
53. Baden L.R., Sahly H.M., Essink B., et al. Efficacy and Safety of the mRNA-1273 SARS-CoV-2 Vaccine // N Engl J Med. 2021. Vol. 384, N 5. P. 403–416. doi: 10.1056/NEJMoa2035389
54. Logunov D.Y., Dolzhikova I.V., Shcheblyakov D.V., et al. Safety and efficacy of an rAd26 and rAd5 vector-based heterologous prime-boost COVID-19 vaccine: An interim analysis of a randomised controlled phase 3 trial in Russia // Lancet. 2021. Vol. 397, N 10275. P. 671–681. doi: 10.1016/S0140-6736(21)00234-8
55. Polack F.P., Thomas S.J., Kitchin N., et al. Safety and efficacy of the BNT162b2 mRNA Covid-19 vaccine // N Engl J Med. 2020. Vol. 383, N 27. P. 2603–2615. doi: 10.1056/NEJMoa2034577
56. Voysey M., Costa Clemens S.A., Madhi S.A., et al. Safety and efficacy of the ChAdOx1 nCoV-19 vaccine (AZD1222) against SARS-CoV-2: An interim analysis of four randomised controlled trials in Brazil, South Africa, and the UK // Lancet. 2021. Vol. 397, N 10269. P. 99–111. doi: 10.1016/S0140-6736(20)32661-1
57. Shiravi A.A., Ardekani A., Sheikhbahaei E., et al. Cardiovascular complications of SARS-CoV-2 vaccines: An overview // Cardiol Ther. 2021. Vol. 11, N 1. P. 13–21 doi: 10.1007/s40119-021-00248-0
58. Watad A., De Marco G., Mahajna H., et al. Immune-Mediated disease flares or new-onset disease in 27 subjects following mRNA/DNA SARS-CoV-2 Vaccination: 5 // Vaccines. 2021. Vol. 9, N 5. P. 435. doi: 10.3390/vaccines9050435
59. Albert E., Aurigemma G., Saucedo J., et al. Myocarditis following COVID-19 vaccination // Radiol Case Rep. 2021. Vol. 16, N 8. P. 2142–2145. doi: 10.1016/j.radcr.2021.05.033
60. Mevorach D., Anis E., Cedar N., et al. Myocarditis after BNT162b2 mRNA Vaccine against Covid-19 in Israel // N Engl J Med. 2021. Vol. 385, N 23. P. 2140–2149. doi: 10.1056/NEJMoa2109730
61. Witberg G., Barda N., Hoss S., et al. Myocarditis after Covid-19 vaccination in a large health care organization // N Engl J Med. 2021. Vol. 385, N 23. P. 2132–2139. doi: 10.1056/NEJMoa2110737
62. Barda N., Dagan N., Ben-Shlomo Y., et al. Safety of the BNT162b2 mRNA Covid-19 vaccine in a nationwide setting // N Engl J Med. 2021. Vol. 385, N 12. P. 1078–1090. doi: 10.1056/NEJMoa2110475

AUTHORS' INFO

*** Daria A. Filatova;**
address: 27/10 Lomonosovsky prospekt, 119991 Moscow, Russia;
ORCID: 0000-0002-0894-1994;
eLibrary SPIN: 2665-5973;
e-mail: dariafilatova.msu@mail.ru

ОБ АВТОРАХ

*** Филатова Дарья Андреевна;**
адрес: Россия, 119991, Москва, Ломоносовский пр-т, д. 27/10;
ORCID: 0000-0002-0894-1994;
eLibrary SPIN: 2665-5973;
e-mail: dariafilatova.msu@mail.ru

* Corresponding author / Автор, ответственный за переписку

Elena A. Mershina, MD, Cand. Sci. (Med), Associate Professor;
ORCID: 0000-0002-1266-4926;
eLibrary SPIN: 6897-9641;
e-mail: elena_mershina@mail.ru

Valentin E. Sinitsyn, MD, Dr. Sci. (Med), Professor;
ORCID: 0000-0002-5649-2193;
eLibrary SPIN: 8449-6590;
e-mail: vsini@mail.ru

Мершина Елена Александровна, канд. мед. наук, доцент;
ORCID: 0000-0002-1266-4926;
eLibrary SPIN: 6897-9641;
e-mail: elena_mershina@mail.ru

Синицын Валентин Евгеньевич, д-р мед. наук, профессор;
ORCID: 0000-0002-5649-2193;
eLibrary SPIN: 8449-6590;
e-mail: vsini@mail.ru

DOI: https://doi.org/10.17816/DD472150

Оценка поглощённых доз в плоде у беременных при компьютерной томографии: систематический обзор

А.В. Водоватов[1], О.А. Гольченко[2], И.А. Мащенко[3], Д.В. Алексеева[3], Л.А. Чипига[1, 3], И.В. Хуторной[4], П.В. Козлова[3], Г.Е. Труфанов[3], П.С. Дружинина[1], С.А. Рыжов[5], И.В. Солдатов[5]

[1] Санкт-Петербургский научно-исследовательский институт радиационной гигиены имени профессора П.В. Рамзаева, Санкт-Петербург, Российская Федерация
[2] Городская поликлиника № 19, Санкт-Петербург, Российская Федерация
[3] Национальный медицинский исследовательский центр имени В.А. Алмазова, Санкт-Петербург, Российская Федерация
[4] Московский государственный университет имени М.В. Ломоносова, Москва, Российская Федерация
[5] Научно-практический клинический центр диагностики и телемедицинских технологий, Москва, Российская Федерация

АННОТАЦИЯ

Обоснование. Отсутствие в отечественной практике утверждённых методик расчёта и систематизированных данных в отношении доз облучения плода при рентгенорадиологических исследованиях у беременных затрудняет их практическое применение. Данная проблема особенно актуальна для компьютерной томографии как широко распространённого высокоинформативного метода лучевой диагностики, ассоциированного со значительными уровнями облучения пациентов.

Цель — систематизировать существующие данные о поглощённых дозах в плоде при проведении компьютерной томографии.

Материалы и методы. Проведены поиск и анализ публикаций на русском и английском языках. Поиск осуществлялся в системах PubMed/Medline, Google Scholar и eLibrary. В окончательный анализ включено 12 публикаций, в том числе 8 исследований с использованием антропоморфных фантомов, 3 ретроспективных и 1 проспективное клиническое исследование.

Результаты. Наиболее высокие значения поглощённых доз в плоде получены при проведении компьютерных сканирований брюшной полости и малого таза, а также сканировании всего тела. Во включённых в обзор публикациях не зафиксировано превышения предельно допустимой дозы облучения плода.

Заключение. При проведении однократных однофазных компьютерных сканирований у беременных превышение допустимого порога поглощённой дозы 100 мГр в плоде маловероятно независимо от зоны сканирования, что позволяет назначать исследование при наличии клинических показаний. Однако этот порог может быть превышен при многократных или многофазных исследованиях методом компьютерной томографии брюшной полости и малого таза, а также всего тела при травме. В таких случаях мультидисциплинарной командой специалистов по радиационной безопасности (врачи-рентгенологи и клинические специалисты) должна быть проведена дополнительная оценка рисков.

Ключевые слова: беременность; радиационный риск; доза облучения органов; диагностическая визуализация; риск для плода во время беременности; облучение; компьютерная томография; поглощённые дозы в плоде.

Как цитировать

Водоватов А.В., Гольченко О.А, Мащенко И.А., Алексеева Д.В., Чипига Л.А., Хуторной И.В., Козлова П.В., Труфанов Г.Е., Дружинина П.С., Рыжов С.А., Солдатов И.В. Оценка поглощённых доз в плоде у беременных при компьютерной томографии: систематический обзор // *Digital Diagnostics*. 2023. Т. 4, № 2. С. 170–184. DOI: https://doi.org/10.17816/DD472150

Рукопись получена: 05.06.2023 **Рукопись одобрена:** 19.06.2023 **Опубликована:** 27.06.2023

DOI: https://doi.org/10.17816/DD472150

Evaluation of fetal absorbed doses from computed tomography examinations of pregnant patients: A systematic review

Alexander V. Vodovatov[1], Olga A. Golchenko[2], Irina A. Mashchenko[3], Daria V. Alekseeva[3], Larisa A. Chipiga[1, 3], Ivan V. Khutornoy[4], Polina V. Kozlova[3], Gennady E. Trufanov[3], Polina S. Druzhinina[1], Sergey A. Ryzhov[5], Ilya V. Soldatov[5]

[1] Saint-Petersburg Research Institute of Radiation Hygiene after Professor P.V. Ramzaev, Saint Petersburg, Russian Federation
[2] City polyclinic № 19, Saint Petersburg, Russian Federation
[3] Almazov National Medical Research Centre, Saint Petersburg, Russian Federation
[4] Lomonosov Moscow State University, Moscow, Russian Federation
[5] Research and Practice Center of Diagnostics and Telemedicine Technologies, Moscow, Russian Federation

ABSTRACT

BACKGROUND: Currently, no systematic data are available on fetal radiation exposure as a result of radiographic studies during pregnancy. Consequently, there are no approved methods of its calculation that can be used in clinical practice. It is especially relevant for computed tomography scans as it is a widely used and highly informative method of diagnostic imaging associated with high exposure levels.

AIM: to systematize currently available data on radiation dose absorbed by the fetus from computed tomography scans in pregnant women.

MATERIALS AND METHODS: The search for publications in Russian and English was conducted in PubMed/Medline, Google Scholar and eLibrary. The final analysis included 12 papers including 8 studies using human body phantoms, 3 retrospective studies and one prospective clinical study.

RESULTS: Abdominal and pelvic computed tomography scans as well as whole-body scans were found to be associated with the highest fetal radiation exposure. However, in none of the publications the fetal exposure limit was exceeded.

CONCLUSION: Clinically indicated non-contrast-enhanced computed tomography scans in pregnant women are not likely to be associated with the fetal absorbed doses that exceed the limit of 100 mGy regardless of the scanned area. However, this limit might be exceeded in case of performing multiple studies or if multiphase abdominal or pelvic computed tomography scans, or whole-body computed tomography scans are performed in patients with multiple trauma. In these cases, a decision regarding the need for these investigations should be made by a multi-disciplinary team (including radiation safety specialists, diagnostic radiologists and clinicians) based on the results of additional risk assessment.

Keywords: computed tomography scans; pregnancy; radiation risk; organ dose; diagnostic imaging; fetal absorbed dose; fetal risks pregnancy radiation.

To cite this article

Vodovatov AV, Golchenko OA, Mashchenko IA, Alekseeva DV, Chipiga LA, Khutornoy IV, Kozlova PV, Trufanov GE, Druzhinina PS, Ryzhov SA, Soldatov IV. Evaluation of fetal absorbed doses from computed tomography examinations of pregnant patients: a systematic review. *Digital Diagnostics*. 2023;4(2):170–184. DOI: https://doi.org/10.17816/DD472150

Received: 05.06.2023 **Accepted:** 19.06.2023 **Published:** 27.06.2023

DOI: https://doi.org/10.17816/DD472150

当对孕妇进行电子计算机断层扫描时胎儿吸收剂量的评估：系统综述

Alexander V. Vodovatov[1], Olga A. Golchenko[2], Irina A. Mashchenko[3], Daria V. Alekseeva[3], Larisa A. Chipiga[1, 3], Ivan V. Khutornoy[4], Polina V. Kozlova[3], Gennady E. Trufanov[3], Polina S. Druzhinina[1], Sergey A. Ryzhov[5], Ilya V. Soldatov[5]

[1] Saint-Petersburg Research Institute of Radiation Hygiene after Professor P.V. Ramzaev, Saint Petersburg, Russian Federation
[2] City polyclinic № 19, Saint Petersburg, Russian Federation
[3] Almazov National Medical Research Centre, Saint Petersburg, Russian Federation
[4] Lomonosov Moscow State University, Moscow, Russian Federation
[5] Research and Practice Center of Diagnostics and Telemedicine Technologies, Moscow, Russian Federation

简评

论证。由于在国内实践中缺乏经批准的计算方法和关于当对孕妇进行X线放射检查时胎儿辐射剂量的系统化数据，因此在实践中很难应用这些检查方法。该问题对于电子计算机断层扫描来说尤其重要，因为虽然该这个问题对于电子计算机断层扫描是一种被广泛使用的、信息量大的放射诊断技术，但是与较高病人辐射剂量有关的。

该研究的目的是使现有的关于进行电子计算机断层扫描时胎儿吸收剂量的数据系统化。

材料和方法。对俄文和英文出版物进行了搜索和分析。在PubMed/Medline、Google Scholar和eLibrary系统中进行了搜索。最后的分析包括12份出版物，其中有8项使用拟人模型的研究、3项回顾性研究和1个前瞻性临床研究。

结果。当进行腹部、盆腔和全身电子计算机断层扫描时胎儿吸收的剂量最高。在审查所包括的出版物中，没有关于超过胎儿剂量限制的报告。

结论。无论扫描区域如何，对孕妇进行一次性单相电子计算机断层扫描的时候，超过胎儿吸收剂量限制（100 mGy）是不太可能的，因此，有需要的话，可以对孕妇进行这样的检查。然而，在进行腹部、盆腔或受伤全身的多次或多相电子计算机断层扫描的情况下，会超过这个阈值。在这种情况下，多科目辐射安全小组（放射科医生和临床专家）应该进行额外的风险评估。

关键词：怀孕；辐射风险；器官剂量；诊断成像；怀孕期间的胎儿风险；辐射剂量；电子计算机断层扫描；胎儿吸收的剂量。

To cite this article

Vodovatov AV, Golchenko OA, Mashchenko IA, Alekseeva DV, Chipiga LA, Khutornoy IV, Kozlova PV, Trufanov GE, Druzhinina PS, Ryzhov SA, Soldatov IV. 当对孕妇进行电子计算机断层扫描时胎儿吸收剂量的评估：系统综述. *Digital Diagnostics.* 2023;4(2):170–184. DOI: https://doi.org/10.17816/DD472150

收到：05.06.2023 **接受：**19.06.2023 **发布日期：**27.06.2023

BACKGROUND

During pregnancy, the safety of diagnostic radiology is a priority for radiologists and other specialists. Until the middle of the 20th century, medical imaging methods using ionizing radiation sources were widely used in obstetrics for diagnostic and therapeutic purposes. However, later experimental and epidemiological data on the effects of ionizing radiation on fetal development were obtained. The International Commission on Radiation Protection established limitations for the use of ionizing radiation during pregnancy [1].

The negative effects of ionizing radiation are usually classified into deterministic and stochastic effects. Deterministic effects are associated with direct cell damage or death resulting from radiation exposure above the threshold level. The probability of these effects depends on the radiation dose and gestational age of the fetus. The main fetal risks include congenital malformations of the internal organs and central nervous system (such as neurological disorders and developmental delays). The severity of the deterministic effects is proportional to the dose and frequency of examinations.

Fetal sensitivity to radiation depends on the gestational age of the fetus. Organogenesis (pregnancy weeks 5–17 or post-conception weeks 3–15) is the most dangerous period for radiation exposure. In the second and third trimesters, fetal resistance to radiation increases; however, in this period, exposure to >500 mGy can still lead to adverse effects, including growth retardation and malformations [2].

Currently, the no-effect threshold value of the fetal absorbed dose is 100 mGy [3,4]. International professional societies (International Commission on Radiation Protection, U.S. National Council on Radiation Protection, American College of Radiology, and American College of Obstetricians and Gynecologists) consider the risk of spontaneous abortion and serious malformations to be negligible in fetuses exposed to radiation doses <50 mGy [3-6].

Stochastic effects are radiation-induced changes in cells that can lead to malignant neoplasms. Stochastic effects do not have a threshold, and data on the corresponding risk are inconsistent [7]. According to the clinical practical guidelines of the American College of Radiology, an absorbed fetal dose of 20 mGy corresponds to a cancer risk of 1/125 in addition to background incidence [6]. According to the International Commission on Radiation Protection, the fetal cancer risk is lower and is 1/500 at the fetal absorbed dose of 30 mGy. In Russian research practice, the risk of radiation-induced cancers and genetic fetal effects following medical radiation exposure have not been examined [8].

Improvements in medical imaging techniques have led to their widespread application and use in the differential diagnosis of some life-threatening conditions, which requires an assessment of their safety in pregnancy. A quantitative evaluation of fetal radiation exposure level is the most reliable assessment of the safety profile of medical imaging techniques in pregnancy. Moreover, pathological conditions that most often require various imaging studies in pregnant patients must be assessed, such as pulmonary embolism (PE), aortic dissection, polytrauma, urolithiasis, acute appendicitis, and lung damage in COVID-19 [9–12].

Fetal safety is the main parameter for imaging technique selection in pregnant women [6]. To reduce potential risks of negative effects, pregnant patients should be protected from radiation using recommended means. Unfortunately, in Russian practice, no such recommendations have been established, and no Russian data on fetal exposure doses when using certain medical imaging techniques are available [8]. Thus, the authors conducted this systematic review to summarize and analyze current data on fetal radiation exposure levels when using computed tomography (CT), the highest-dose imaging technique.

MATERIALS AND METHODS

Study design

The systematic review was based on PRISMA guidelines (2009).

Literature search

Study materials included scientific publications searched from PubMed/Medline, Google Scholar, and eLibrary databases. Existing foreign and national guidelines for imaging studies in pregnancy were also reviewed. The following keywords were used: CT, pregnancy, radiation risk, organ dose, diagnostic imaging, fetal risks pregnancy radiation, computed tomography, and fetal absorbed doses.

Following the database search query, duplicate results were excluded. The content of the selected studies, including parameters such as the year of publication, study design, purpose, methodology, and results were analyzed, and publications on non-ionizing techniques of diagnostic radiology were excluded. The systematic review excluded studies that did not measure fetal and uterus absorbed doses and studies measuring dose loads during radiation therapy and fluoroscopy. Finally, the systematic review included 12 studies. The study design is presented in Fig. 1.

Estimated parameters

The systematic review evaluated selected publications using the following parameters: doses absorbed by the fetus/embryo, gestational age, pathological condition, anatomical area of interest, method of absorbed dose estimation, and number of studied cases using CT in pregnant women. The systematic review included clinical and experimental studies using anthropomorphic phantoms.

RESULTS

In total, 837 studies were found in PubMed/Medline, Google Scholar, and eLibrary databases for the following search queries: “CT radiation risk in pregnancy,” “fetal

absorbed doses from diagnostic imaging," "CT fetal dosimetry," and "assessment of fetal doses in CT" from 2007 to 2022. After a preliminary analysis and removal of duplicate results, 12 studies in English and Russian were included in the review, including 8 studies using anthropomorphic phantoms, 3 retrospective studies, and 1 prospective clinical study. Each study was evaluated by the study type and design, measurement method, and calculation method of absorbed doses. Information on studies is summarized in Tables 1–7.

Measurement and calculation of absorbed doses

Absorbed doses were measured using a thermoluminescent dosimeter (TLD) or metal oxide semiconductor field-effect transistor (MOSFET). In 2 of 8 studies, a virtual phantom technology was used, which involves mathematical modeling of the absorbed doses.

Absorbed doses were estimated based on measurement results or using special software for assessing absorbed doses in radiosensitive organs and tissues (ImPACT MC, CT EXPO, NCICT 3.0, and virtual dose CT).

In 2 of 4 clinical studies, absorbed doses were calculated using the special calculation program ImPACT. Two other studies did not provide information on calculation methods.

The gestational age modeled in anthropomorphic phantoms ranged from 5 to 40 weeks. In 5 of 8 studies, the scan length was 32 cm, which corresponds to the length of a standard phantom. In four studies, programs with decreased

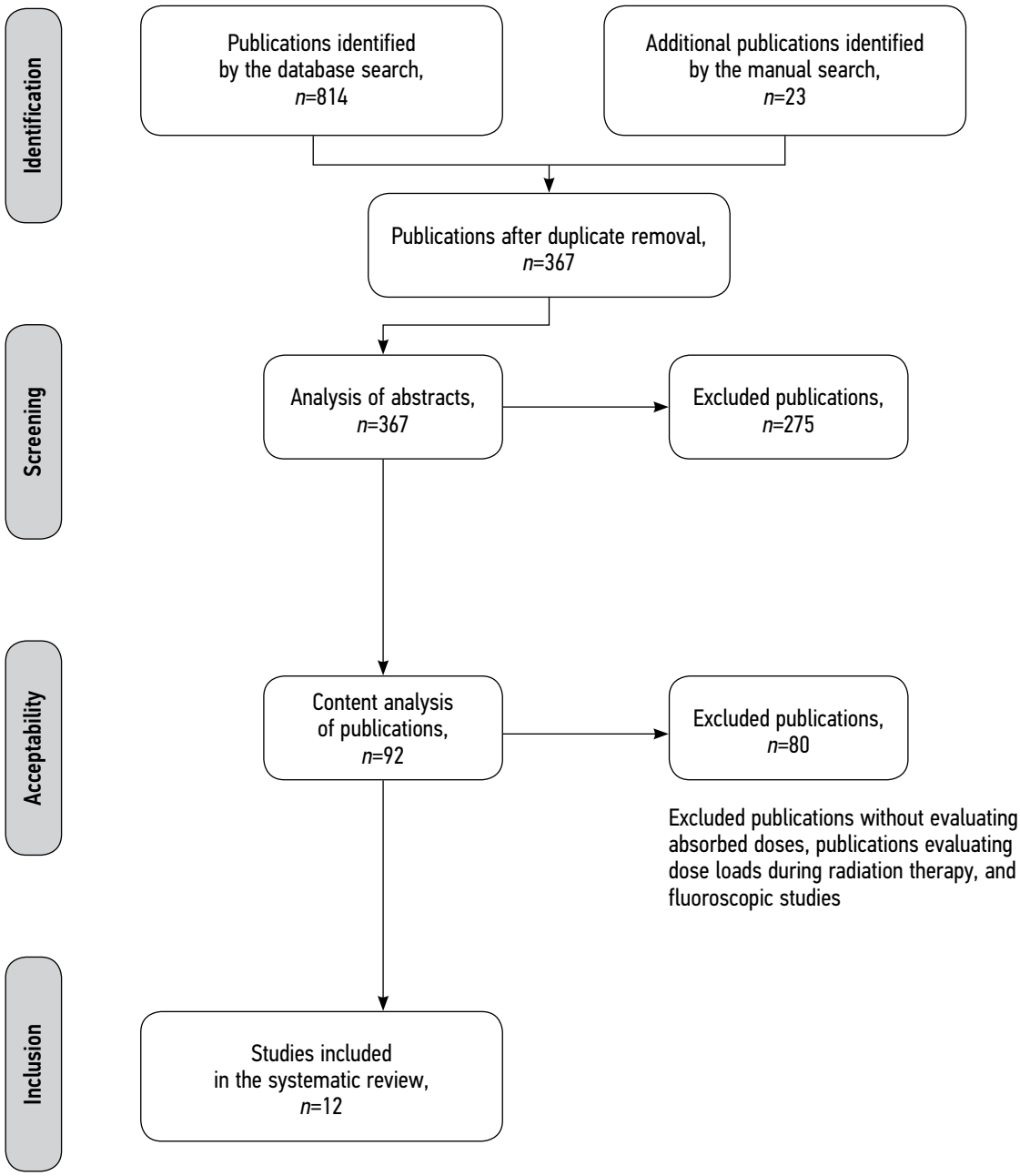

Fig. 1. Study design in the PRISMA scheme.

scan length were also used, and three studies used programs with increased scan length.

Comparative analysis

The fetal absorbed doses were compared in several groups by anatomical scan regions including chest, abdomen, pelvis, and whole body in trauma (Tables 5–7).

Considering the presented data of phantom studies, two pairs of studies were combined (Vodovatova et al. [8] and Gu et al. [13], and Kelaranta et al. [14] and Angel et al. [15]) to determine general patterns in absorbed dose change depending on the gestational age and scan region. In these studies, the gestational age and scan regions were comparable (chest in studies by Vodovatova and Gu, and abdomen or pelvis in studies by Kelaranta and Angel), and similar technical scan parameters (exposure, pitch factor, and voltage) were reported. The comparable nature of the above data made it possible to compare pooled data. The results of the comparative analysis are presented in Fig. 2. Chest scan showed a significantly lower fetal absorbed dose than the abdominal scan. In addition, in chest CT, the fetal absorbed dose tends to decrease slightly with increases in gestational age. To confirm these findings, more powerful studies are needed.

Finally, evidence suggests that the fetal absorbed dose threshold of 100 mGy [3,5] indicated in regulatory and methodological documents significantly exceeds the observed levels of fetal exposure during phantom studies. Moreover, exposure levels of 20 and 30 mGy [5,6], potentially leading to stochastic effects, are not achieved in single-phase CT on a once-only basis.

In all clinical studies included in the systematic review (except for the study by Goldberg-Stein et al. [16]), the fetal absorbed doses also did not exceed the above range of 20–100 mGy. In the study by Goldberg-Stein et al. [16], scan parameters were overestimated (up to 140 kV and 815 mAs), which led to a high fetal absorbed dose. Moreover, multiphase CT and multiple examinations were considered (highlighted in the text of the publication).

This comparison allows radiologists to conduct one single-phase CT in eligible pregnant women without undue concerns. If repeated scans are necessary, additional risk assessment shall be performed.

DISCUSSION

The main approaches to radiation safety in pregnant women are similar to those in other populations. In general, if ultrasound and magnetic resonance imaging are impossible to use as diagnostic techniques, ionizing radiation techniques should be used only in life-threatening situations with minimized radiation doses [17]. Life-threatening complications requiring diagnosis of pathological conditions should exceed the potential negative effect of diagnostic techniques. The choice of imaging techniques should be regulated in clinical standards of care with recommendations for their use in established or suspected diseases.

For the safe use of ionizing diagnostic techniques, the level of fetal absorbed doses must be monitored during the examination, and duplicate studies should not be conducted whenever appropriate [18].

Table 1. Characteristics of studies using anthropomorphic phantoms

Source	Method for measuring doses	Estimated absorbed doses
Angel et al. 2008 [15]	Not reported	ImPACT; MC; CT Expo
Begano et al. 2020 [33]	TLD	VirtualDose CT
Doshi et al. 2008 [36]	TLD	According to TLD measurements
Kelaranta et al. 2017 [14]	MOSFET	ImPACT MC
Vodovatov et al. 2021 [8]	Not reported	NCICT3.0
Gilet et al. 2011 [37]	TLD	According to TLD measurements
Gu et al. 2009 [13]	MOSFET	MCNPX According to MOSFET measurements
Jaffe et al. 2008 [26]	MOSFET	According to MOSFET measurements

Note. MOSFET, metal oxide semiconductor field-effect transistor; TLD, thermoluminescent dosimeter.

Table 2. Characteristics of clinical studies

Paper	Type of study	Estimated absorbed doses
Lazarus et al. 2009 [29]	Retrospective clinical study	Not reported
Goldberg-Stein et al. 2011 [16]	Retrospective clinical study	ImPACT
Litmanovich et al. 2009 [32]	Prospective clinical study	ImPACT
Lazarus et al. 2007 [30]	Retrospective clinical study	Not reported

Table 3. Protocols of CT for anthropomorphic phantoms

Source	CT machine model	Voltage, kV	Exposure, mAs	Pitch factor	Gestational age, weeks	Scan length, cm
Angel et al. 2008 [15]	LightSpeed 16, GE	120	100–300	1,375	5–36	46,2
Begano et al. 2020 [33]	Definition Flash CT (Siemens Healthineers,Germany)	120	85	1,5	28–38	32 cm, standard program; 22 cm, short program
Doshi et al. 2008 [36]	Siemens Sensation 16 Siemens Somatom Emotion / Marconi MX8000	100–130	125–250	1,25	35–40	32 cm, standard program; 27 cm, short program
Gilet et al. 2011 [37]	LightSpeed 4 LightSpeed 16 LightSpeed 64 VCT, GE Healthcare	120	100–500	1,375–1,5	5, 10, 18, 32	32
Gu et al. 2013 [13]	LightSpeed 16 GE-MDCT	80–140	100	1,375	15,20,31	22 cm, ches; 36 cm, abdomen
Kelaranta et al. 2017 [14]	LightSpeed 64-MDCT GE	100–120	100–300	1,375	12, 20, 28, 38	27 cm, chest; 32 cm, abdomen; 94 cm, trauma
Vodovatov et al. 2021 [8]	Ingenuity 128, Philips Somatom Definition AS, Siemens Somatom Scope, Siemens Emotion 16, Siemens	100–130	60–142	1,048–1,5	8, 10, 12, 15, 20, 25, 30, 35, 38	33
Jaffe et al. 2008 [26]	GE LightSpeed 16-MDCT	140	300–380	0,9–1,75	5	32

Table 4. Protocols of CT for pregnant women

Source	CT machine model	Voltage, kV	Exposure, mAs	Pitch factor	Gestational age, weeks	Scan region (anatomical landmarks)
Lazarus et al. 2007 [30]	Either single-detector row scanner (CTI GE Healthcare, Waukesha, WI), 4 MDCT Lightspeed; GE Healthcare) 16-MDCT Somatom; Siemens, Malvern	140	-	-	5–40	Abdomen
Lazarus et al. 2009 [29]	-	-	-	-	-	Head Chest Abdomen and pelvis
Litmanovich et al. 2009 [32]	64-MDCT LightSpeed VCT	100	200	0,984	5–36	Chest Aortic arch to the diaphragmatic cupula 19.846 ± 2.98 cm
Goldberg-Stein et al. 2011 [16]	LightSpeed Plus, LightSpeed 16 Pro, LightSpeed Qx/I, High-Speed RP,HighSpeed CT/GE Healthcare)	120–140	180–716	0,9–1,5	5–36	Abdomen and pelvis

Table 5. Systematized data on the assessment of fetal absorbed doses in chest CT

Source	Volume CT dose index (CTDI vol), mGy	DLP, mGy×cm	Gestational age, weeks	Fetal absorbed dose, mean, mGy	Uterus absorbed dose, mean, mGy
In phantom studies					
Kelaranta et al. 2017 [14]	1,34–1,97	476,63–582,22	12 20 28 38	0,03 0,08 0,14 0,22	0,04 0,09 0,29 1,13
Doshi et al. 2008 [36]	-	-	35–40	0,23	-
Begano et al. 2020 [33]	1,5–4,0	44–137	28–38	0,02–0,12	-
Gilet et al. 2011 [37]	-	-	5–32	0,33–0,77	-
Gu et al. 2013 [13]	8,1–14,7	-	15 20 31	0,13 0,21 0,26	0,17 0,33 0,37
Vodovatov et al. 2021 [8]	5,6–9,3	185–306	8 10 15 20 25 30 35 38	0,09 0,10 0,08 0,13 0,12 0,16 0,39 0,52	0,09 0,10 0,07 0,09 0,11 0,15 0,33 0,64
In clinical studies					
Litmanovich et al. 2009 [32]	5,21	105,65	5–38	0,02	-
Lazarus et al. 2009 [29]	-	-	1st, 2nd, and 3rd trimesters	0,22	-

Note. CTDI, computed tomography dose index; DLP, dose–length product.

Table 6. Systematized data on the assessment of fetal absorbed doses in abdominal and pelvic CT

Source	Volume CT dose index (CTDI vol), mGy	DLP, mGy×cm	Gestational age, weeks	Fetal absorbed dose, mean, mGy	Uterus absorbed dose, mean, mGy
In phantom studies					
Kelaranta et al. 2017 [14]	2,63–3,91	102,34–151,86	12 20 28 38	4,7 5,5 4,8 4,8	5,1 5,8 4,9 5,1
Angel et al. 2008 [15]	-	-	5 12 15 20 25 30 35	- 14,2 11,2 8,5 12,3 9,7 10,4	11,8
Gu et al. 2013 [13]	-	-	15	6,9	-
Gilet et al. 2011 [37]	-	-	5, 10, 18, 32	15–20,5	-
In clinical studies					
Lazarus et al. 2009 [29]	-	-	1st, 2nd, and 3rd trimesters	17,1	-
Lazarus et al. 2007 [30]	-	-	5–40	16	-
Goldberg-Stein et al. 2011 [16]	-	-	5–36	24,8	-

Note. CTDI, computed tomography dose index; DLP, dose–length product.

Table 7. Systematized data on the assessment of fetal absorbed doses in CT for trauma in phantom studies

Source	CTDI, mGy	DLP, mGy×cm	Gestational age, weeks	Fetal absorbed dose, mean, mGy	Uterus absorbed dose, mean, mGy
Kelaranta et al. 2017 [14]	4,74–5,79	45,18–66,52	12	10,6	11,3
			20	11,2	12,6
			28	10,1	10,3
			38	9,9	10,7
Jaffe et al. 2008 [26]	6,55–26,02	-	5	18,0	-

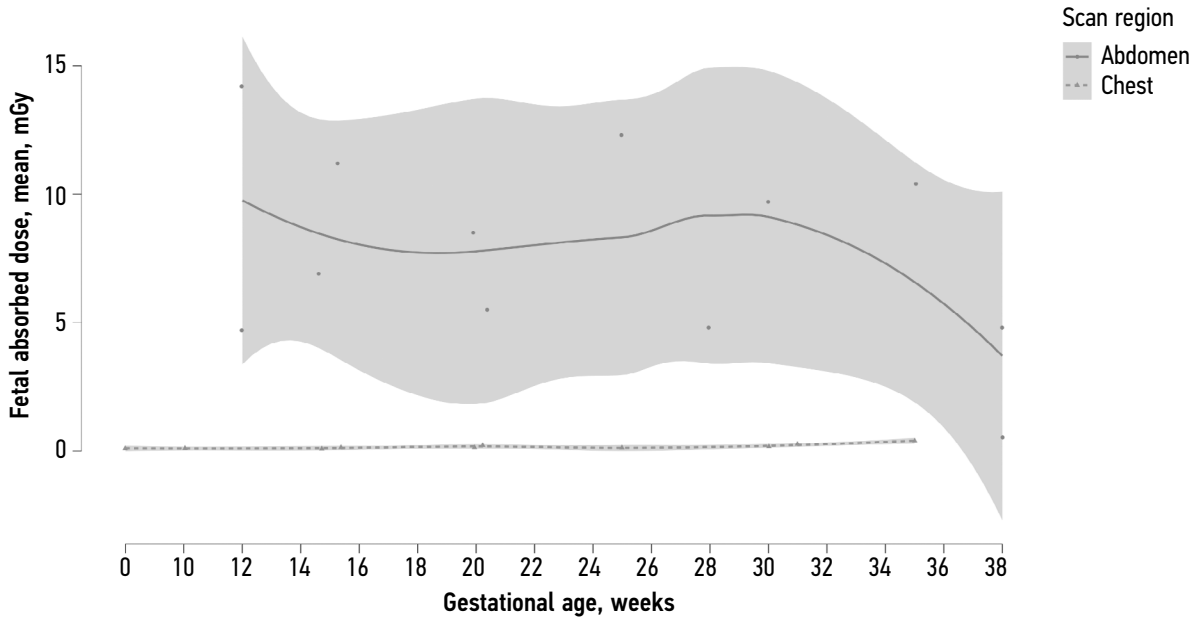

Fig. 2. Summary results of fetal dosimetry in chest CT (led by Vodovatov [8] and Gu [13]) and abdominal CT (led by Kelaranta [14] and Angel [15]) with LOESS regression line modeling and 95% confidence interval.

CT is the most conclusive ionizing technique of diagnostic radiology. CT has an undeniable advantage such as short examination time combined with high informative value, making CT an optimal method for diagnosing life-threatening conditions that require immediate treatment [19,20]. Depending on the indication and diagnostic goals, CT may be performed either as a native or a contrast-enhanced examination. Native examinations can be used in pregnant women to diagnose inflammatory lung diseases, urolithiasis, various traumatic injuries, etc. [21,22]. Contrast-enhanced examination is necessary for differential diagnosis of neoplasms, inflammatory changes, and CT angiography for diagnosing thrombosis and vascular wall damage and assessing blood supply to certain structures [19,23]. In pregnant patients, only one of these options must be selected. If contrast-enhanced CT is necessary, a native examination must be excluded to reduce the procedure time and radiation dose.

In diagnostic imaging of pregnant patients, the fetal absorbed dose must be assessed [24]. Owing to the limited capabilities of cohort studies on this issue, physical (anthropomorphic) or digital phantoms are currently widely used [25]. However, phantom studies using human body simulators have some limitations. They are mainly related to differences in phantom sizes and real patients. If real body parameters exceed the parameters of the phantom used, the absorbed dose will be overestimated, and vice versa, the dose may be underestimated if the patient's dimensions are smaller than the dimensions of the phantom [25]. However, phantom studies are reasonable for use as experimental guidance because they provide more information on absorbed doses to be calculated for each week of pregnancy, in contrast to cohort studies, which provide calculation results as averaged doses. In addition, fetal absorbed doses in cohort and phantom studies were not significantly different (Tables 5–7).

Radiation doses directly depend on the scan region. When the fetus is outside the radiation field (CT region), it is exposed to scattered radiation. Therefore, the farther the scan region is located from the fetus, the lower the absorbed dose and the likelihood of negative effects [14].

The literature review showed that fetal absorbed doses directly correlated with the anatomical scan region. As shown in Tables 5–7, the maximum fetal absorbed doses are observed during CT of the whole body, abdomen, and pelvis. The lowest fetal absorbed doses are observed in chest CT.

The estimated absorbed doses for phantoms are comparable with those obtained in cohort studies.

None of the foreign studies included in the review reported a fetal absorbed dose threshold exceeding 100 mGy. In Russia, no studies were conducted to evaluate indications for CT and the number of absorbed doses in pregnant women and fetuses during abdominal and pelvic CT.

In early gestation, the fetal absorbed dose assessment is difficult because of the small size of the embryo. Some studies [8,26,27] have shown insignificant differences in doses absorbed by the uterus and fetus. Therefore, the uterus absorbed dose can be used as an equivalent of the fetal absorbed dose [28]. Experimental studies have shown a relationship between the absorbed dose and gestational age.

Since the reviewed cohort studies presented data as average fetal absorbed doses for different gestational ages, determining the correlation between the gestational age and the level of absorbed dose is impossible for these studies [29–31].

In addition to the gestational age and anatomical scan regions, the absorbed dose depends on technical parameters such as the length of the scan region, algorithm for automatic modulation of the current strength, if any, pitch factor, and voltage.

The radiation dose can be decreased by changing the parameters of the scanning protocol and reducing the length of the scan region. In the study by Litmanovich et al. [32], 26 pregnant women with suspected PE underwent CT angiography of the pulmonary artery with decreased voltage and current and decreased scan length compared with the standard protocol. The effective dose was significantly lower than that in the control group (1.8 and 9.8 mSv, respectively) without a decrease in the diagnostic quality of the examination.

The decreased length of the scan region has also shown its effectiveness in phantom studies [33]. The authors reported a significant decrease in the mean fetal absorbed dose compared with doses for the standard scan length (0.03 and 0.1 mSv, respectively). However, some risks are associated with excluding part of anatomical structures from the scan region, and this should be considered when reducing the scan length.

Some studies have also considered the need to use screens (personal protective equipment) when conducting radiological examinations during pregnancy [33,34]. The reviewed publications did not use additional protective measures when examining organs located at some distance from the uterus, since the fetus is mainly exposed to scattered radiation rather than direct radiation. In this case, shielding does not reduce fetal exposure to scattered radiation but provides psychological protection. When compared with shielding, the decreased scan length is the most effective means of reducing fetal absorbed doses [34–36]. In addition, when the shielding material is introduced into the scan region, the image optimization system of the CT scanner is forced to dramatically increase the radiation power of the tube, which ultimately increased the exposure dose to pregnant women and their fetuses [37].

CONCLUSION

Diagnostic radiology in pregnancy should be performed in accordance with radiological safety principles because of the likelihood of negative effects, and completely avoiding diagnostic techniques using ionizing radiation is a mistake.

Examinations using ionizing radiation may be necessary for various life-threatening conditions, and they are also preferred in the diagnosis of some diseases. Note that the risk of complications, arising from delayed diagnosis, many times exceeds the risk of negative effects from exposure to ionizing radiation.

These studies confirm that doses absorbed by the fetus during CT do not reach the threshold values. In chest CT, the doses absorbed by the fetus are insignificant and cannot lead to deterministic effects. More significant fetal radiation exposure occurs during abdominal and pelvic CT and whole-body scans; however, even in these studies, exceeding the permissible exposure threshold is unlikely if a single-phase examination is performed only once. Moreover, multiple abdominal or whole-body CT or multiphase CT with an intravenous contrast enhancement may lead to exceeding the permissible threshold for the absorbed dose of ionizing radiation. This information should be considered when referring a pregnant woman to CT in these areas. Other undesirable effects on fetal development when using contrast enhancement must be also considered.

ADDITIONAL INFORMATION

Funding source. This study was not supported by any external sources of funding.

Competing interests. The authors declare that they have no competing interests.

Authors' contribution. All authors made a substantial contribution to the conception of the work, acquisition, analysis, interpretation of data for the work, drafting and revising the work, final approval of the version to be published and agree to be accountable for all aspects of the work. A.V. Vodovatov — development of the study concept, systematization of data, peer review, and final editing of the systematic review; O.A. Golchenko — search for publications on the topic, analysis of literature data, design of tables, writing the text; I.A. Mashchenko — development of the research concept, peer review and final editing of the systematic review; D.V. Alekseeva — development of the study concept, analysis of the obtained data, final editing of the systematic review; L.A. Chipiga — data systematization, peer review, and final editing of the systematic review; I.V. Khutornoy — study design, statistical processing of the results, preparation of illustrations; P.V. Kozlova — search for publications on the topic, analysis of literature data, text editing; G.E. Trufanov — development of the research concept, expert evaluation, approval of

the final version of the article; P.S. Druzhinina — adaptation of the text of the article, processing of the research results; S.A. Ryzhov, setting research objectives, participating in the description of the discussion of the results obtained; I.V. Soldatov — participation in the discussion of the obtained results, expert evaluation, approval of the final version of the article.

REFERENCES

1. Shtentsel RE, Semenova ES, Mashchenko IA, et al. The history of the formation and development of methods of radiation diagnostics in perinatology. *Translational Med*. 2021;8(3):29–36. (In Russ). doi: 10.18705/2311-4495-2021-8-3-29-36

2. Sadro C, Bernstein MP, Kanal KM. Imaging of trauma. Part 2, Abdominal trauma and pregnancy: A radiologist's guide to doing what is best for the mother and baby. *Am J Roentgenol*. 2012;199(6):1207–1219. doi: 10.2214/AJR.12.9091

3. Wang PI, Chong ST, Kielar AZ, et al. Imaging of pregnant and lactating patients: Part 1, evidence-based review and recommendations. *Am J Roentgenol*. 2012;198(4):778–784. doi: 10.2214/AJR.11.7405

4. Committee Opinion No. 723: Guidelines for diagnostic imaging during pregnancy and lactation. *Obstet Gynecol*. 2017;130(4):210–216. doi: 10.1097/AOG.0000000000002355

5. ICRP. Recommendations International Commission on Radiation Protection 2007. Publication ICRP No. 103. Transl. from English. Ed. by M.F. Kiselev and N.K. Shandala. Moscow: Alana; 2009. 312 p.

6. ACR-SPR practice parameter for imaging pregnant or potentially pregnant adolescents and women with ionizing radiation. 2018. 23 p. Available from: https://www.acr.org/-/media/acr/files/practice-parameters/pregnant-pts.pdf. Accessed: 17.05.2023.

7. Frush D. The cumulative radiation dose paradigm in pediatric imaging. *Br J Radiol*. 2021;94(1126):20210478. doi: 10.1259/bjr.20210478

8. Vodovatov AV, Chipiga LA, Piven PA, et al. Assessment of the absorbed doses in the fetus from the computed tomography of the chest for the pregnant women. *Radiatsionnaya Gygiena*. 2021;14(3):126–135. (In Russ). doi: 10.21514/1998-426X-2021-14-3-126-135

9. Liu H, Liu F, Li J, et al. Clinical and CT imaging features of the COVID-19 pneumonia: Focus on pregnant women and children. *J Infect*. 2020;80(5):7–13. doi: 10.1016/j.jinf.2020.03.007

10. Dehan L, Lin L, Xin W, et al. Pregnancy and perinatal outcomes of women with coronavirus disease (COVID-19) pneumonia: A preliminary analysis. *Am J Roentgenol*. 2020;215(1):127–132. doi: 10.2214/AJR.20.23072

11. Garcia EM, Camacho MA, Karolyi DR, et al.; Expert Panel on Gastrointestinal Imaging. ACR appropriateness criteria right lower quadrant pain-suspected appendicitis. *Am J Roentgenol*. 2018;15(11):373–387. doi: 10.1016/j.jacr.2018.09.033

12. Sazhin AV, Kirienko AI, Kurtser MA, et al. Acute appendicitis during pregnancy (in Russian only). *Pirogov Russian Journal of Surgery*. 2019;(1):70–77. (In Russ).

13. 13.Gu J, Bednarz B, Caracappa PF, Xu XG. The development, validation and application of a multi-detector CT (MDCT) scanner model for assessing organ doses to the pregnant patient and the fetus using Monte Carlo simulations. *Phys Med Biol*. 2009;54(9):2699–2717. doi: 10.1088/0031-9155/54/9/007

14. Kelaranta A, Mäkelä T, Kaasalainen T, Kortesniemi M. Fetal radiation dose in three common CT examinations during pregnancy: Monte Carlo study. *Phys Med*. 2017;(43):199–206. doi: 10.1016/j.ejmp.2017.09.120

15. Angel E, Wellnitz CV, Goodsitt MM, et al. Radiation dose to the fetus for pregnant patients undergoing multidetector CT imaging: Monte Carlo simulations estimating fetal dose for a range of gestational age and patient size. *Radiology*. 2008;249(1):220–227. doi: 10.1148/radiol.2491071665

16. Goldberg-Stein S, Liu B, Hahn PF, Lee SI. Body CT during pregnancy: Utilization trends, examination indications, and fetal radiation doses. *Am J Roentgenol*. 2011;196(1):146–151. doi: 10.2214/AJR.10.4271

17. Vandecaveye V, Amant F, Lecouvet F, et al. Imaging modalities in pregnant cancer patients. *Int J Gynecol Cancer*. 2021;31(3):423–431. doi: 10.1136/ijgc-2020-001779

18. Kwan ML, Miglioretti DL, Marlow EC, et al.; Radiation-Induced Cancers Study Team. Trends in medical imaging during pregnancy in the United States and Ontario, Canada, 1996 to 2016. *JAMA Network Open*. 2019(7):197–249. doi: 10.1001/jamanetworkopen.2019.7249

19. Prokop M, Galanski M. Spiral and multilayered computed tomography. Moscow; 2011. 440 p. (In Russ).

20. Arablinskiy AV, Magdebura YA. CT in the diagnosis of nontraumatic acute abdomen. *REJR*. 2018;8(2):58–71. (In Russ). doi: 10.21569/2222-7415-2018-8-2-58-71

21. Kirsch J, Brown RK, Henry TS, et al.; Expert Panels on Cardiac and Thoracic Imaging. ACR appropriateness criteria acute chest pain-suspected pulmonary embolism. *J Am Coll Radiol*. 2017;14(5):2–12. doi: 10.1016/j.jacr.2017.02.027

22. Shyu JY, Khurana B, Soto JA, et al. Expert Panel on Major Trauma Imaging. ACR appropriateness criteria major blunt trauma. *J Am Coll Radiol*. 2020;17(5):160–174. doi: 10.1016/j.jacr.2020.01.024

23. Panchenko EP, Balahonova TV, Danilov NM, et al. Diagnosis and management of pulmonary embolism Eurasian Association of Cardiology (EAC) clinical practice guidelines (2021). *Eurasian Heart J*. 2021;(1):44–77. (In Russ). doi: 10.381092225-1685-2021-1-44-77

24. Ria F, D'Ercole L, Origgi D, et al.; Association of Medical Physics Task Group. Statement of the Italian Association of Medical Physics (AIFM) task group on radiation dose monitoring systems. *Insights Imaging*. 2022;13(1):23. doi: 10.1186/s13244-022-01155-1

25. Sensakovic WF, Royall I, Hough M, et al. Fetal dosimetry at CT: A primer. *Radiographics*. 2020;40(4):1061–1070. doi: 10.1148/rg.2020190166

26. Jaffe TA, Yoshizumi TT, Toncheva GI, et al. Early first-trimester fetal radiation dose estimation in 16-MDCT without and with automated tube current modulation. *Am J Roentgenol*. 2008;190(4):860–864. doi: 10.2214/AJR.07.2925

27. Huda W, Randazzo W, Tipnis S, et al. Embryo dose estimates in body CT. *Am J Roentgenol*. 2010;194(4):874–880. doi: 10.2214/AJR.09.4032

28. Damilakis J, Perisinakis K, Tzedakis A, et al. Radiation dose to the conceptus from multidetector CT during early gestation: A method that allows for variations in maternal body size and conceptus position. *Radiology*. 2010;257(2):483–489. doi: 10.1148/radiol.10092397

29. Lazarus E, Debenedectis C, North D, et al. Utilization of imaging in pregnant patients: 10-year review of 5270 examinations in 3285 patients 1997–2006. *Radiology*. 2009;251(2):517–524. doi: 10.1148/radiol.2512080736
30. Lazarus E, Mayo-Smith WW, Mainiero MB, Spencer PK. CT in the evaluation of nontraumatic abdominal pain in pregnant women. *Radiology*. 2007;244(3):784–790. doi: 10.1148/radiol.2443061634
31. Goldberg-Stein SA, Liu B, Hahn PF, Lee SI. Radiation dose management: Part 2, estimating fetal radiation risk from CT during pregnancy. *Am J Roentgenol*. 2012;198(4):352–356. doi: 10.2214/AJR.11.7458
32. Litmanovich D, Boiselle PM, Bankier AA, et al. Dose reduction in computed tomographic angiography of pregnant patients with suspected acute pulmonary embolism. *J Comput Assist Tomogr*. 2009;33(6):961–966. doi: 10.1097/RCT.0b013e318198cd18
33. Begano D, Söderberg M, Bolejko A. To use or not use patient shielding on pregnant women undergoing CT pulmonary angiography: A phantom study. *Radiation Protection Dosimetry*. 2020;189(4):458–465.
34. Ryckx N, Sans-Merce M, Schmidt S, et al. The use of out-of-plane high Z patient shielding for fetal dose reduction in computed tomography: Literature review and comparison with Monte-Carlo calculations of an alternative optimisation technique. *Phys Med*. 2018;(48):156–161. doi: 10.1016/j.ejmp.2018.03.017
35. Tack D, Kalra MK, Gevenois PA. Radiation dose from multidetector CT (2nd ed.). Springer; 2012. doi: 10.1007/978-3-642-24535-0
36. Doshi SK, Negus IS, Oduko JM. Fetal radiation dose from CT pulmonary angiography in late pregnancy: A phantom study. *Br J Radiol*. 2008;81(968):653–658. doi: 10.1259/bjr/22775594
37. Gilet AG, Dunkin JM, Fernandez TJ, et al. Fetal radiation dose during gestation estimated on an anthropomorphic phantom for three generations of CT scanners. *Am J Roentgenol*. 2011;196(5):1133–1137. doi: 10.2214/AJR.10.4497

СПИСОК ЛИТЕРАТУРЫ

1. Штенцель Р.Э., Семенова Е.С., Мащенко И.А., и др. Исторические аспекты становления и развития методов лучевой диагностики в перинатологии // Трансляционная медицина. 2021. Т. 8, № 3. С. 29–36. doi: 10.18705/2311-4495-2021-8-3-29-36
2. Sadro C., Bernstein M.P., Kanal K.M. Imaging of trauma. Part 2, Abdominal trauma and pregnancy: A radiologist's guide to doing what is best for the mother and baby // Am J Roentgenol. 2012. Vol. 199, N 6. P. 1207–1219. doi: 10.2214/AJR.12.9091
3. Wang P.I., Chong S.T., Kielar A.Z., et al. Imaging of pregnant and lactating patients: Part 1, evidence-based review and recommendations // Am J Roentgenol. 2012. Vol. 198, N 4. P. 778–784. doi: 10.2214/AJR.11.7405
4. Committee Opinion No. 723: Guidelines for diagnostic imaging during pregnancy and lactation // Obstet Gynecol. 2017. Vol. 130, N 4. P. 210–216. doi: 10.1097/AOG.0000000000002355
5. ICRP. Recommendations International Commission on Radiation Protection 2007. Publication ICRP No. 103. Transl. from English. Ed. by M.F. Kiselev, N.K. Shandala. Moscow: Alana; 2009. 312 p.
6. ACR-SPR practice parameter for imaging pregnant or potentially pregnant adolescents and women with ionizing radiation. 2018. 23 p. Режим доступа: https://www.acr.org/-/media/acr/files/practice-parameters/pregnant-pts.pdf. Дата обращения: 17.05.2023.
7. Frush D. The cumulative radiation dose paradigm in pediatric imaging // Br J Radiol. 2021. Vol. 94, N 1126. P. 20210478. doi: 10.1259/bjr.20210478
8. Водоватов А.В., Чипига Л.А., Пивень П.А., и др. Оценка поглощённых доз в плоде при проведении компьютерной томографии органов грудной клетки беременной женщины // Радиационная гигиена. 2021. Т. 14, № 3. С. 126–135. doi: 10.21514/1998-426X-2021-14-3-126-135
9. Liu H., Liu F., Li J., et al. Clinical and CT imaging features of the COVID-19 pneumonia: Focus on pregnant women and children // J Infect. 2020. Vol. 80, N 5. P. 7–13. doi: 10.1016/j.jinf.2020.03.007
10. Dehan L., Lin L., Xin W., et al. Pregnancy and perinatal outcomes of women with coronavirus disease (COVID-19) pneumonia: A preliminary analysis // Am J Roentgenol. 2020. Vol. 215, N 1. P. 127–132. doi: 10.2214/AJR.20.23072
11. Garcia E.M., Camacho M.A., Karolyi D.R., et al.; Expert Panel on Gastrointestinal Imaging. ACR appropriateness criteria right lower quadrant pain-suspected appendicitis // Am J Roentgenol. 2018. Vol. 15, N 11. P. 373–387. doi: 10.1016/j.jacr.2018.09.033
12. Сажин А.В., Кириенко А.И., Курцер М.А., и др. Острый аппендицит у беременных // Хирургия. Журнал им. Н.И. Пирогова. 2019. № 1. С. 70–77.
13. Gu J., Bednarz B., Caracappa P.F., Xu X.G. The development, validation and application of a multi-detector CT (MDCT) scanner model for assessing organ doses to the pregnant patient and the fetus using Monte Carlo simulations // Phys Med Biol. 2009. Vol. 54, N 9. P. 2699–2717. doi: 10.1088/0031-9155/54/9/007
14. Kelaranta A., Mäkelä T., Kaasalainen T., Kortesniemi M. Fetal radiation dose in three common CT examinations during pregnancy: Monte Carlo study // Phys Med. 2017. N 43. P. 199–206. doi: 10.1016/j.ejmp.2017.09.120
15. Angel E., Wellnitz C.V., Goodsitt M.M., et al. Radiation dose to the fetus for pregnant patients undergoing multidetector CT imaging: Monte Carlo simulations estimating fetal dose for a range of gestational age and patient size // Radiology. 2008. Vol. 249, N 1. P. 220–227. doi: 10.1148/radiol.2491071665
16. Goldberg-Stein S., Liu B., Hahn P.F., Lee S.I. Body CT during pregnancy: Utilization trends, examination indications, and fetal radiation doses // Am J Roentgenol. 2011. Vol. 196, N 1. P. 146–151. doi: 10.2214/AJR.10.4271
17. Vandecaveye V., Amant F., Lecouvet F., et al. Imaging modalities in pregnant cancer patients // Int J Gynecol Cancer. 2021. Vol. 31, N 3. P. 423–431. doi: 10.1136/ijgc-2020-001779
18. Kwan M.L., Miglioretti D.L., Marlow E.C., et al.; Radiation-Induced Cancers Study Team. Trends in medical imaging during pregnancy in the United States and Ontario, Canada, 1996 to 2016 // JAMA Network Open. 2019. N 7. P. 197–249. doi: 10.1001/jamanetworkopen.2019.7249

19. Прокоп М., Галански М. Спиральная и многослойная компьютерная томография. Москва, 2011. 440 с.
20. Араблинский А.В., Магдебура Ю.А. КТ в диагностике абдоминальной патологии нетравматического генеза // REJR. 2018. Т. 8, № 2. С. 58–71. doi: 10.21569/2222-7415-2018-8-2-58-71
21. Kirsch J., Brown R.K., Henry T.S., et al.; Expert Panels on Cardiac and Thoracic Imaging. ACR appropriateness criteria acute chest pain-suspected pulmonary embolism // J Am Coll Radiol. 2017. Vol. 14, N 5. P. 2–12. doi: 10.1016/j.jacr.2017.02.027
22. Shyu J.Y., Khurana B., Soto J.A., et al.; Expert Panel on Major Trauma Imaging. ACR appropriateness criteria major blunt trauma // J Am Coll Radiol. 2020. Vol. 17, N 5. P. 160–174. doi: 10.1016/j.jacr.2020.01.024
23. Панченко Е.П., Балахонова Т.В., Данилов Н.М., и др. Диагностика и лечение тромбоэмболии лёгочной артерии: клинические рекомендации Евразийской ассоциации кардиологов для практических врачей (2021) // Евразийский кардиологический журнал. 2021. № 1. С. 44–77. doi: 10.38109/2225-1685-2021-1-44-77
24. Ria F., D'Ercole L., Origgi D., et al.; Association of Medical Physics Task Group. Statement of the Italian Association of Medical Physics (AIFM) task group on radiation dose monitoring systems // Insights Imaging. 2022. Vol. 13, N 1. P. 23. doi: 10.1186/s13244-022-01155-1
25. Sensakovic W.F., Royall I., Hough M., et al. Fetal dosimetry at CT: A primer // Radiographics. 2020. Vol. 40, N 4. P. 1061–1070. doi: 10.1148/rg.2020190166
26. Jaffe T.A., Yoshizumi T.T., Toncheva G.I., et al. Early first-trimester fetal radiation dose estimation in 16-MDCT without and with automated tube current modulation // Am J Roentgenol. 2008. Vol. 190, N 4. P. 860–864. doi: 10.2214/AJR.07.2925
27. Huda W., Randazzo W., Tipnis S., et al. Embryo dose estimates in body CT // Am J Roentgenol. 2010. Vol. 194, N 4. P. 874–880. doi: 10.2214/AJR.09.4032
28. Damilakis J., Perisinakis K., Tzedakis A., et al. Radiation dose to the conceptus from multidetector CT during early gestation: A method that allows for variations in maternal body size and conceptus position // Radiology. 2010. Vol. 257, N 2. P. 483–489. doi: 10.1148/radiol.10092397
29. Lazarus E., Debenedectis C., North D., et al. Utilization of imaging in pregnant patients: 10-year review of 5270 examinations in 3285 patients 1997–2006 // Radiology. 2009. Vol. 251, N 2. P. 517–524. doi: 10.1148/radiol.2512080736
30. Lazarus E., Mayo-Smith W.W., Mainiero M.B., Spencer P.K. CT in the evaluation of nontraumatic abdominal pain in pregnant women // Radiology. 2007. Vol. 244, N 3. P. 784–790. doi: 10.1148/radiol.2443061634
31. Goldberg-Stein S.A., Liu B., Hahn P.F., Lee S.I. Radiation dose management: Part 2, estimating fetal radiation risk from CT during pregnancy // Am J Roentgenol. 2012. Vol. 198, N 4. P. 352–356. doi: 10.2214/AJR.11.7458
32. Litmanovich D., Boiselle P.M., Bankier A.A., et al. Dose reduction in computed tomographic angiography of pregnant patients with suspected acute pulmonary embolism // J Comput Assist Tomogr. 2009. Vol. 33, N 6. P. 961–966. doi: 10.1097/RCT.0b013e318198cd18
33. Begano D., Söderberg M., Bolejko A. To use or not use patient shielding on pregnant women undergoing CT pulmonary angiography: A phantom study // Radiation Protection Dosimetry. 2020. Vol. 189, N 4. P. 458–465.
34. Ryckx N., Sans-Merce M., Schmidt S., et al. The use of out-of-plane high Z patient shielding for fetal dose reduction in computed tomography: Literature review and comparison with Monte-Carlo calculations of an alternative optimisation technique // Phys Med. 2018. N 48. P. 156–161. doi: 10.1016/j.ejmp.2018.03.017
35. Tack D., Kalra M.K., Gevenois P.A. Radiation dose from multidetector CT (2nd ed.). Springer, 2012. doi: 10.1007/978-3-642-24535-0
36. Doshi S.K., Negus I.S., Oduko J.M. Fetal radiation dose from CT pulmonary angiography in late pregnancy: A phantom study // Br J Radiol. 2008. Vol. 81, N 968. P. 653–658. doi: 10.1259/bjr/22775594
37. Gilet A.G., Dunkin J.M., Fernandez T.J., et al. Fetal radiation dose during gestation estimated on an anthropomorphic phantom for three generations of CT scanners // Am J Roentgenol. 2011. Vol. 196, N 5. P. 1133–1137. doi: 10.2214/AJR.10.4497

AUTHORS' INFO

*** Aleksandr V. Vodovatov,** Cand. Sci. (Biol.);
address: 8 Mira street, 197101 Saint Petersburg, Russia;
ORCID: 0000-0002-5191-7535;
eLibrary SPIN: 4560-8978;
e-mail: vodovatoff@gmail.com

Olga A. Golchenko;
ORCID: 0000-0003-4614-9241;
e-mail: breakerxolyga@yandex.ru

Irina A. Mashchenko, MD, Cand. Sci. (Med.), Leading Researcher, Assistant Professor;
ORCID: 0000-0002-4949-8829;
eLibrary SPIN: 5154-7080;
e-mail: mashchenko_ia@almazovcentre.ru

ОБ АВТОРАХ

*** Водоватов Александр Валерьевич,** канд. биол. наук;
адрес: Россия, 197101, Санкт-Петербург, ул. Мира, д. 8;
ORCID: 0000-0002-5191-7535;
eLibrary SPIN: 4560-8978;
e-mail: vodovatoff@gmail.com

Гольченко Ольга Андреевна;
ORCID: 0000-0003-4614-9241;
e-mail: breakerxolyga@yandex.ru

Мащенко Ирина Александровна, канд. мед. наук, вед. науч. сотр., доцент;
ORCID: 0000-0002-4949-8829;
eLibrary SPIN: 5154-7080;
e-mail: mashchenko_ia@almazovcentre.ru

* Corresponding author / Автор, ответственный за переписку

Darya V. Alekseeva, Assistant Lecturer;
ORCID: 0000-0001-9528-9377;
eLibrary SPIN: 6484-4327;
e-mail: darja-karpova@yandex.ru

Larisa A. Chipiga, Cand. Sci. (Engin.), Research Associate, Assistant Professor;
ORCID: 0000-0001-9153-3061;
eLibrary SPIN: 3920-7798;
e-mail: larisa.chipiga@gmail.com

Ivan V. Khutornoy, Graduate Student;
ORCID: 0000-0002-5405-603X;
eLibrary SPIN: 8020-0222;
e-mail: mcdm.avk@gmail.com

Polina V. Kozlova, Assistant Lecturer;
ORCID: 0000-0002-3240-7038;
eLibrary SPIN: 3555-0410;
e-mail: apollinaria@bk.ru

Gennady E. Trufanov, MD, Dr. Sci. (Med.);
ORCID: 0000-0002-1611-5000;
eLibrary SPIN: 3139-3581;
e-mail: trufanovge@mail.ru

Polina S. Druzhinina, Junior Research Associate;
ORCID: 0000-0003-2921-067X;
eLibrary SPIN: 9003-3234;
e-mail: druzhininapauline@gmail.com

Sergey A. Ryzhov, Research Associate;
ORCID: 0000-0002-0640-7368;
eLibrary SPIN: 6595-4011;
e-mail: mosrg@mail.ru

Ilya V. Soldatov;
ORCID: 0000-0002-4867-0746;
eLibrary SPIN: 4065-6048;
e-mail: npcmr@mail.ru

Алексеева Дарья Владимировна, ассистент;
ORCID: 0000-0001-9528-9377;
eLibrary SPIN: 6484-4327;
e-mail: darja-karpova@yandex.ru

Чипига Лариса Александровна, канд. тех. наук, науч. сотр., доцент;
ORCID: 0000-0001-9153-3061;
eLibrary SPIN: 3920-7798;
e-mail: larisa.chipiga@gmail.com

Хуторной Иван Валерьевич, аспирант;
ORCID: 0000-0002-5405-603X;
eLibrary SPIN: 8020-0222;
e-mail: mcdm.avk@gmail.com

Козлова Полина Викторовна, ассистент;
ORCID: 0000-0002-3240-7038;
eLibrary SPIN: 3555-0410;
e-mail: apollinaria@bk.ru

Труфанов Геннадий Евгеньевич, докт. мед. наук;
ORCID: 0000-0002-1611-5000;
eLibrary SPIN: 3139-3581;
e-mail: trufanovge@mail.ru

Дружинина Полина Сергеевна, мл. науч. сотр.;
ORCID: 0000-0003-2921-067X;
eLibrary SPIN: 9003-3234;
e-mail: druzhininapauline@gmail.com

Рыжов Сергей Анатольевич, науч. сотр.;
ORCID: 0000-0002-0640-7368;
eLibrary SPIN: 6595-4011;
e-mail: mosrg@mail.ru

Солдатов Илья Владимирович;
ORCID: 0000-0002-4867-0746;
eLibrary SPIN: 4065-6048;
e-mail: npcmr@mail.ru

DOI: https://doi.org/10.17816/DD321420

Технология распознавания речи в лучевой диагностике

Н.Д. Кудрявцев[1], К.А. Бардасова[2], А.Н. Хоружая[1]

[1] Научно-практический клинический центр диагностики и телемедицинских технологий, Москва, Российская Федерация
[2] Уральский государственный медицинский университет, Екатеринбург, Российская Федерация

АННОТАЦИЯ

Устройства, способные распознавать речь, являются перспективным инструментом для системы здравоохранения. Технология распознавания речи имеет довольно длинную историю применения в западных системах здравоохранения (с 1970-х годов), однако широкое распространение она получила лишь в начале XXI века, заменив медицинских транскрипционистов. Для отечественного здравоохранения данная технология относительно новая. Её активная разработка началась лишь в начале 2010-х годов, а повсеместное внедрение в здравоохранение — в конце 2010-х годов. Такая задержка связана с особенностями русского языка и ограничением вычислительных мощностей, присутствующих в начале XXI века.

В настоящее время комплексы устройств и программного обеспечения для распознавания речи используются в голосовом заполнении медицинской документации и позволяют сократить время подготовки протоколов рентгенологических исследований при сравнении с традиционным (клавиатурным) вводом текста.

В литературном обзоре отражена краткая история развития и применения технологии распознавания речи в лучевой диагностике. Отражены ключевые научные исследования, подтверждающие эффективность её использования в западных системах здравоохранения. Продемонстрирован отечественный опыт применения технологии распознавания речи и оценена её эффективность. Описаны перспективы дальнейшего развития данной технологии в российском здравоохранении.

Ключевые слова: научный обзор; технология распознавания речи; голосовой ввод; лучевая диагностика; рентгенология; заполнение медицинской документации.

Как цитировать

Кудрявцев Н.Д., Бардасова К.А., Хоружая А.Н. Технология распознавания речи в лучевой диагностике // *Digital Diagnostics*. 2023. Т. 4, № 2. С. 185–196. DOI: https://doi.org/10.17816/DD321420

Рукопись получена: 17.03.2023 **Рукопись одобрена:** 19.04.2023 **Опубликована:** 25.05.2023

DOI: https://doi.org/10.17816/DD321420

Speech recognition technology in radiology

Nikita D. Kudryavtsev[1], Kristina A. Bardasova[2], Anna N. Khoruzhaya[1]

[1] Moscow Center for Diagnostics and Telemedicine, Moscow, Russian Federation
[2] Ural State Medical University, Ekaterinburg, Russian Federation

ABSTRACT

Speech recognition devices are promising tools for the healthcare system. Speech recognition technology has had a relatively long history of use in Western healthcare systems since the 1970s. However, it became widely used at the beginning of the 21st century, replacing medical transcriptionists. This technology is relatively new in home healthcare. Its active development began only in the early 2010s, and its implementation in healthcare started in late 2010. This delay is due to the idiosyncrasies of the Russian language and the limited computational power present at the beginning of the 21st century.

Currently, complexes of devices and software for speech recognition are used in the voice filling of medical records and can reduce the time for preparing reports for radiological examinations compared with traditional (keyboard) text input.

The literature review provides a brief history of speech recognition technology development and application in radiography. Key scientific studies showing its efficacy in Western healthcare systems are reflected. Voice recognition technology in the home is demonstrated, and its effectiveness is evaluated. The prospects for further development of this technology in Russian healthcare are described.

Keywords: medical records; radiation diagnostics; radiology; speech recognition software; voice input.

To cite this article

Kudryavtsev ND, Bardasova KA, Khoruzhaya AN. Speech recognition technology in radiology. *Digital Diagnostics.* 2023;4(2):185–196.
DOI: https://doi.org/10.17816/DD321420

Received: 17.03.2023 **Accepted:** 19.04.2023 **Published:** 25.05.2023

DOI: https://doi.org/10.17816/DD321420

语音识别技术在放射诊断中的应用

Nikita D. Kudryavtsev[1], Kristina A. Bardasova[2], Anna N. Khoruzhaya[1]

[1] Moscow Center for Diagnostics and Telemedicine, Moscow, Russian Federation
[2] Ural State Medical University, Ekaterinburg, Russian Federation

简评

能够进行语音识别的设备是保健系统的一个有前途的工具。语音识别技术在西方医疗系统中有相当长的使用历史（自20世纪70年代以来），但它在21世纪初才得到了广泛推广，取代了医疗抄写员。对于国内的医疗保健来说，该技术是相对较新的。它的积极开发是在2010年代初才开始，并2010年代末才在保健事业广泛采用的。这种延迟是由于俄语的特点和21世纪初计算能力的限制而导致的。

语音识别的设备和软件包现在被用于通过语言输入填写病历，此外，与传统（用键盘）文本输入相比，减少了准备X射线学协议所需的时间。

本文献综述简要介绍了语音识别技术在放射诊断中的发展和应用的历史。介绍了证实其在西方医疗系统中使用的有效性的主要科学研究。展示了国内使用语音识别技术的经验，并对其有效性进行了评估。描述了该技术在俄罗斯保健事业进一步发展的前景。

关键词：科学综述；语音识别技术；语音输入；放射诊断；X射线学；填写病历。

To cite this article
Kudryavtsev ND, Bardasova KA, Khoruzhaya AN. 语音识别技术在放射诊断中的应用. *Digital Diagnostics.* 2023;4(2):185–196.
DOI: https://doi.org/10.17816/DD321420

收到： 17.03.2023 **接受：** 19.04.2023 **发布日期：** 25.05.2023

INTRODUCTION

At present, voice control has become a standard feature for many home smart devices. This was made possible by the development of speech recognition technology (SRT), which can be used in systems analyzing and transforming the user's speech into digital data. Furthermore, to controlling smart devices, SRT has become very popular in telephone communications. Currently, when calling many government and commercial organizations, the user is met by an automatic responding machine that recognizes the caller's voice request and refers them to a selected specialist. In 2019, in Moscow, a project was launched to notify citizens of an appointment with a doctor and remind them of regular check-up using a voice assistant. During a call, the citizen could make an appointment with a medical specialist, cancel, or reschedule the visit, and the system also asked the patient about complaints.[1]

In healthcare, SRT systems are actively used in the voice filling of medical records. This is because healthcare professionals spend most of their working time preparing medical documentation [1–4]. This factor negatively affects the quality of medical care, particularly considering the limited duration of appointments for each patient. Opportunities for using this technology, for example, in diagnostic radiology, are associated with decreased time spent filling out protocols for diagnostic examinations and increased time analyzing diagnostic images and medical records and communicating with patients. Thus, voice input systems have become the most popular tool in imaging departments because their workflows are the most convenient for the implementation of such technology. Current systematic reviews [5–7] have shown that SRT systems are effective in these conditions, and good implementability is explained by large volumes of textual information that radiologists are required to record in protocols.

EVOLUTION OF SPEECH RECOGNITION TECHNOLOGY IN RADIOLOGY

Early years

Medical use of SRTs was first attempted in the 1970s and 1980s. In 1975, a prototype SRT system was described. It could analyze an extremely limited amount of medical vocabulary and terminology [8]. The technology was first tested in diagnostic radiology in 1981 [9]. Beth Israel Hospital started to use it for preparing protocols for X-ray examinations. Initially, local specialists used the coded language information processing (CLIP) system, which is a hierarchical standardized language of medical terms developed by M. Simon and BW Leeming [10]**.** This language contained specially encoded medical terms. For example, value A was used for the anatomical region, A6 for the lower limb, and A61 for the thigh. Values B, B6, B61, B611, and B612 encoded bones, bones of the lower limbs, femur, lesser trochanter, and grosser trochanter, respectively. By keyboarding various code combinations, a radiologist can prepare a protocol of any complexity and volume [11].

A main disadvantage of those SRT systems is a limited vocabulary (approximately 200 unique medical terms) because of the small random-access memory (RAM). This factor did not allow making a full description of diagnostic examinations. The combined use of STLs with the CLIP system was one of the solutions for the limited RAM.

In 1981, keyboard and voice inputs were compared [9]. The speed and quality of protocol preparation were evaluated for 60 imaging examinations. Consequently, the length of the protocol did not depend on the filling method, which indirectly confirmed the similar complexity of the examinations described. The period of filling out the protocol using voice input was four times longer than the period of the keyboard input. Voice-filled protocols contained an average of 12 recognition errors; whereas protocols prepared using the keyboard had none. This study also described some other limitations of the technology. The first systems could not completely suppress external noise; thus, the quality of medical speech recognition was low, which contributed to errors. The increased period of filling out a medical document was related to the system's ability to recognize only separately spoken words. A specialist had to pause between words and between codes if the CLIP system was used. This voice-filling method was uncomfortable and unnatural for human communication. Moreover, the voice input system required 3–6 h of preconfiguration and adaptation to the specific speech of the user (specialist).

All these limitations prevented those SRT systems from wider use in healthcare. Thus, medical transcriptionists were highly sought at that time. Nevertheless, all these attempts formed a basis for considering "weak points" of the technology at subsequent stages of development.

The increasing availability of imaging examinations, emergence of computed and magnetic resonance tomographs, and transition from analog to digital media have increased the workload of radiologists and duration of protocol preparation. In the mid-80s, in Western countries, audio transcription centers were opened to solve this problem and optimize human resources. A radiologist taped descriptions of findings identified during the interpretation of diagnostic images using audio recorders. Audio recordings were transferred to the audio transcription center, where medical transcriptionists transcribed the audio recordings and prepared the research protocols in text. The prepared protocols were checked and endorsed by the radiologist.

[1] Official website of the Moscow Mayor [Web]. The voice assistant will collect patient complaints by phone before a clinic appointment. Available from: https://www.mos.ru/news/item/89302073/.

In some cases, they were returned to the transcriptionists for error correction [12]. Dictaphone centers were widely used in foreign healthcare institutions until the 2010s [5, 13].

Some authors compared the efficiency of preparing imaging protocols using medical transcriptionists and SRT. They concluded that the main advantage of a medical transcriptionist is the ability to notice grammatical errors and consider contextual information about the patient. These advantages allow them to correctly understand and adjust audio recordings, even if the quality is poor [14]. However, given the scarcity of medical transcriptionists, printed protocols were often returned to the radiologist only 16 h after dictation [15]. Depending on the capacities of audio transcription centers, transcription of audio recordings took 6–24 h.

Later, medical transcriptionists were no longer needed because of further developments in SRT systems [14]. Despite the lower recognition accuracy of SRTs than medical transcriptionists, SRTs can reduce the monthly economic costs of the radiology department by 81% and significantly reduce the time for preparing examination protocols [5, 13, 16].

In the Russian healthcare system, attempts have also been made to introduce voice recorder centers,[2]; however, no open-access studies have evaluated their effectiveness. Owing to the lack of such centers in the modern Russian healthcare system, their use was considered inappropriate.

1990s: A new round of innovation

At the end of the 20th century, the amount of memory and vocabulary in SRT systems had increased (up to 19,000 radiology terms). The pre-setting time was reduced to several minutes, and the recognition accuracy was increased. In 1995, the first natural language transcription programs were introduced in the USA, allowing the detection of continuous English speech. Currently, radiologists could dictate at a comfortable conversational pace, without pausing between words. At this stage, these programs were less accurate than systems with separate input [17]. Further technological advances and increased speech recognition accuracy allowed the creation of continuous voice input systems instead of separate input systems.

21ST Century

In Western countries, automated SRTs started to be widely introduced and used in radiology departments in the early 2000s. Foreign studies have compared the speed of voice and keyboard filling of English-language medical records, volume of a medical document prepared, and satisfaction level of specialists. Data showed that technology leads to an increase in document filling speed by 26% and an increase in the volume of protocols. Voice input also allowed optimizing the workflow by reducing the time preparing medical records and improving the quality of protocol content. Specialists showed increased satisfaction from working with such documents [16, 18]. The frequency of errors also decreased, and most errors were related to punctuation [7]. The above factors led to a decrease in the total time for protocol preparation from 16 to 5 h [15]. Studies evaluating the time spent on protocol preparation have revealed that the average number of characters per minute and number and frequency of errors reflect the positive evolution of SRTs and their wider implementation in radiology departments. The percentage of protocols completed within 1 h increased from 26% to 58%. Protocol content became more structured [19].

Costs have also decreased over time. Thus, 5 of 7 cost-evaluating systematic reviews [5] have reported a decrease in costs, and two have reported an increase in costs. Similar results have been obtained in endocrinology and psychiatry, where SRT systems have improved the productivity and efficiency of HCPs [20]. The use of these systems in surgery helped reduce the time for protocol preparation from 4 to 3 days. The number of protocols prepared within 1 day increased from 22% to 37% [21]. From 2019 to the 2020s, foreign studies have concluded that SRTs save HCP time, increases HCP efficiency, and allows them to document more important details when filling out medical papers [22–24]. However, the main barrier to voice input system implementation can be considered a human factor, which is related to HCP resistance to change and fear of new technologies [25].

In 2016, a Microsoft research study showed that SRT systems have an accuracy of 94% and corresponded to the human level [26]. At present, this technology is widely used in medical practice in English-speaking countries, and the implementation level of voice input in radiology departments has reached 85%.[3] Currently, the market share of such programs in healthcare is approximately 25% globally.[4] Nuance Communications, IBM, and Philips are leaders in speech recognition software development.[5]

In approximately 45 years, speech recognition has become widespread in healthcare in English-speaking countries.

[2] Official site of State Budgetary Healthcare Institution "Infectious Clinical Hospital No. 1 of Moscow Health Department" [Internet]. History of the Hospital, Available from: https://ikb1.ru/about/.

[3] Reaction Data [Web]. Speech Rec in Radiology-State of the Market. 2019 [cited 2019 Dec 23]. Available from: https://www.reactiondata.com/report/speech-recognition-in-radiology-state-of-the-market/.

[4] Grand View Research [Web]. Voice And Speech Recognition Market Size Report, 2030. Available from: https://www.grandviewresearch.com/industry-analysis/voice-recognition-market.

[5] Nuance Communications. Healthcare Clinical Documentation AI Solutions & Services for the NHS (https://www.nuance.com/en-gb/healthcare.html); Philips. Healthcare--Philips (https://www.dictation.philips.com/gb/industries/industry/healthcare-professionals/); IBM. Watson Speech to Text (https://www.ibm.com/cloud/watson-speech-to-text).

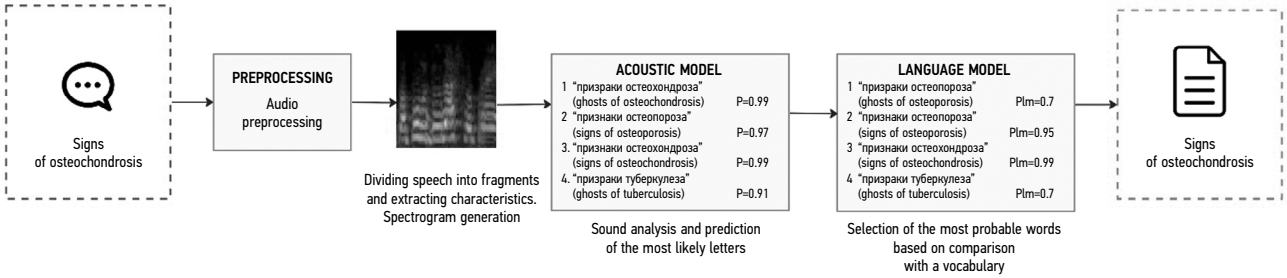

Fig. 1. A simplified scheme of the operation of a classical speech recognition system. An algorithm for recognizing the "signs of osteochondrosis" phrase is presented.

It covered all healthcare levels, from primary care and emergency care to tertiary care clinics. State-of-art medical SRT systems for English-speaking users have an accuracy of up to 99%, can be adapted to different accents, and do not require machine training with the specialist's voice profile.[6]

HOW DOES A STATE-OF-THE-ART SPEECH RECOGNITION SYSTEM WORK?

As mentioned earlier, SRT involves translating human speech into text using a computer. Modern voice input systems use artificial intelligence (AI) algorithms that can significantly improve the quality and speed of user speech recognition [27]. The recognition process consists of several stages, with their characteristics (Fig. 1):

1. *Receiving an audio signal.* Sound recording is the first stage of speech recognition. It can be performed using the built-in microphone in any audio recording device, such as a smartphone. Then, the sound wave is converted into a digital format so that it can be processed by a computer.
2. *Audio preprocessing.* The received audio data are preprocessed to eliminate external background noise and make the user's speech clearer. This improves the quality of speech recognition.
3. *Splitting into fragments.* The audio file is then split into small fragments of 10–25 ms. This is necessary to optimize audio data analysis. Each fragment is analyzed by the SRT system separately.
4. *Extraction of speech characteristics.* At this stage, speech parameters are calculated, including frequency, duration, and amplitude of sounds. They are used to identify phonemes that make up spoken words.
5. *Comparison with recognition models.* Phonemes are matched using acoustic models that are trained on many speech samples. These models can use various techniques including Hidden Markov models, neural networks, and other machine-learning algorithms [28–30].
6. *Composition of words and text.* The language model combines phonemes into words and phrases and then into full text. This text may require additional processing to correct spelling errors and other inaccuracies.
7. *Inserting the generated text.* This is the final stage. The generated text is inserted into the medical document. Considering that speech recognition systems have not yet reached 100% accuracy, in some cases, the radiologist should manually adjust the recognized text.

To enable the system to recognize sounds regardless of sex, age, and intonation of the dictator and convert them into letters with greater accuracy, acoustic and language models use AI modules. Developers train neural networks on a dataset. The dataset includes various audio recordings and text examples. After receiving a voice signal, the neural network searches for a match in the database. The neural network continues its learning during the use and creates new combinations of "sound–letter" pairs, which makes it more likely to reproduce the intended text without spelling errors. During the learning process, the computer recognizes the most important features of the pronunciation of phonemes and records the received data as a user profile [31].[7]

Recently, the so-called end-to-end approaches to building SRT systems have become widespread. End-to-end approaches in SRT are methods of automatic processing of all speech signals, without performing separate processing steps such as feature extraction and speech recognition model generation [32]. Deep learning is one of the most popular end-to-end approaches. In this case, the neural network is trained directly on raw audio data without preprocessing [32]. Recurrent neural networks or convolutional neural networks are other examples of end-to-end approaches for speech recognition. In this case, the neural network is trained on the input signal and output text using the supervised learning technique [32].

[6] Nuance Communications [Internet]. Dragon Medical One--#1 Clinical Documentation Companion. Available from: https://www.nuance.com/healthcare/provider-solutions/speech-recognition/dragon-medical-one.html.

[7] Cloud.mts.ru [Internet]. Speech recognition technology and its role for business. Available from: https://cloud.mts.ru/cloud-thinking/blog/tekhnologiya-raspoznavaniya-rechi/.

End-to-end approaches can provide higher recognition accuracy because the neural network is trained using all speech information. However, these approaches can be more difficult to implement and require more training data [33].

RUSSIAN EXPERIENCE IN THE USE OF SPEECH RECOGNITION TECHNOLOGY IN RADIOLOGY

The first speech recognition systems for the Russian language appeared in the mid-2000s [34, 35]; however, the use of a general colloquial vocabulary did not allow the use of such systems in medical practice. The development of voice input systems that allows transcribing Russian speech with medical terms took several years [36]. The active development of SRTs was started only in the later 2010s. Such a delay was associated with difficulties in recognizing Russian speech.

The Russian language has a more complex structure of word formation than English because it is a synthetic language with many word forms. To recognize words, a larger vocabulary must be used; however, this slows down system performance [37]. For example, modern SRT systems for English-speaking users use a dictionary containing up to 300,000 words and terms, and for the Russian language, the vocabulary can contain more than 5 million words, word forms, and phrases [33, 38, 39]. In addition, most forms of the same word differ only in endings, which are often vaguely pronounced by users. This leads to an error in recognizing the entire phrase and the need to correct the final document. The Russian language has more options for sentence arrangement, whereas the English language uses strict grammatical constructions. This makes it difficult to create language models of the SRT system and reduces work accuracy.

In Russia, the Speech Technology Center Group (STC) is the leading developer of voice input systems for healthcare.[8] The first study of the effectiveness of SRTs in radiology departments was conducted in 2020 in seven city clinics of the Moscow Department of Health using the early version of Voice2Med voice input system (STC Group) with a recognition accuracy of 93%. The study compared the speed of completing medical records using keyboard input and an SRT system. Radiologists filled out protocols of computed and magnetic resonance imaging examinations. The time study showed that the average period of describing one examination using keyboard input was 10 min 15 s, and for an SRT system, it was 8 min 2 s. At the current stage of development, the accuracy of recognition of medical terms in Russian has reached 98%. This became possible thanks to preparing a vocabulary of medical terms, based on 2.5 million imaging protocols, and analyzing feedback from radiologists[9] (Fig. 2).

Fig. 2. Workplace of a radiologist at the Moscow Reference Center for Radiation Diagnostics, equipped with a speech recognition system. The process of filling medical records.

In 2022, a survey of radiologists showed that 62.8% of the respondents noted an increase in their efficiency when using an SRT system. Most specialists who use voice input routinely rate the quality of recognition of radiological terms as good or excellent. Respondents note that when extraneous speech was recognized, the endings of words were recognized incorrectly. Moreover, the quality of recognition can be negatively affected by external background noise (working diagnostic equipment and communication of medical personnel with a patient or with colleagues) and low-quality sound recording devices. Important factors in new technology loyalty were the age of HCPs and their interest in innovation. Young professionals are more open to technology, and professionals aged 30–40 years are also more likely to use voice input systems in their work. Surveys showed a positive trend in the attitude of radiologists to SRTs within 2 years from the launch [40].

OPPORTUNITIES FOR THE DEVELOPMENT OF SPEECH RECOGNITION TECHNOLOGY

Improvements in recognition accuracy will further reduce the preparation time of electronic medical records. One of the main tasks facing SRT system developers is to ensure high accuracy of speech analysis in difficult acoustic conditions, when the recording contains numerous noise or voices. As already mentioned, owing to some special characteristics of the Russian language, recognizing word endings become one of the most difficult tasks. Therefore, for Russian SRT

[8] Speech Technology Center Group [Internet]. Speech synthesis and recognition, recording and analysis, face and voice identification. Available from: http://www.speechpro.ru/.

[9] Speech Technology Center Group [Internet]. Voice2Med: Program for voice filling of medical records. Available from: https://www.speechpro.ru/product/programmy-dlya-raspoznavaniya-rechi-v-tekst/voice2med.

systems, a language model that can predict and match words in sentences with high accuracy is needed.

The integration of voice input programs with medical information systems will allow remote filling of structured electronic medical records. As the system is developing, it cannot only recognize HCP phrases but also understand in which section of the medical record the recognized text should be placed. These functions will allow ultrasound diagnostic specialists, pathologists, endoscopists, and surgeons to fill out medical records directly during the medical intervention, not later, and this will significantly affect the quality of documents and the speed of their preparation.

SRT also has great potential in standardizing and unifying the vocabulary used in preparing medical records, including radiological protocols. Currently, no single list of terms has described the same pathological condition in radiology [41]. Even two radiologists working in the same department may use different synonyms to describe the same finding when preparing protocols. Some papers noted that the use of structured and standardized protocols with unified terms simplifies the perception of the necessary information by both other radiologists and other specialists [42–44].

To date, some researchers have attempted to develop a thesaurus to standardize the description of abnormal changes detected in computed tomography. A thesaurus contains 120 Russian radiological terms and examples of their description [45]. However, the development of a thesaurus is a complex task requiring consistent terminology agreed by numerous specialists and the radiology community.

CONCLUSION

The literature review provides a brief historical background on the development of SRTs in radiology departments, describes their evolution in detail, and evaluates the advantages and disadvantages of SRT based on literature data. Special attention is paid to the use of SRTs in Russian radiology departments. Some studies have demonstrated a significant improvement in the accuracy of recognition of Russian medical terms. In the future, the use of such technologies can reduce the preparation period of medical records to allow spending more time communicating with patients and analyzing their medical histories. This opens new opportunities for personalized healthcare development. However, errors remain in ending recognition and word agreement in a sentence, and specialists must spend more time correcting them. In the future, new AI algorithms can solve these problems.

Some studies have demonstrated the positive attitude of radiologists to SRT systems, which is manifested in their more frequent use in their work. This technology should be further developed in the Russian healthcare sector because pilot national and well-established foreign projects indicate positive changes. Further improving the accuracy of medical term recognition will attract even more SRT supporters among HCPs.

ADDITIONAL INFORMATION

Funding source. This article was prepared by a group of authors as a part of the research and development effort titled "Theoretical and methodological framework for digital transformation in radiology" (USIS No. 123031400118-0) in accordance with the Order No. 1196 dated December 21, 2022 "On approval of state assignments funded by means of allocations from the budget of the city of Moscow to the state budgetary (autonomous) institutions subordinate to the Moscow Health Care Department, for 2023 and the planned period of 2024 and 2025" issued by the Moscow Health Care Department.

Competing interests. The authors declare that they have no competing interests.

Authors' contribution. All authors made a substantial contribution to the conception of the work, acquisition, analysis, interpretation of data for the work, drafting and revising the work, final approval of the version to be published and agree to be accountable for all aspects of the work. N. Kudryavtsev — concept and design of the paper, text writing, approval of the final version of the paper; K. Bardasova — data collection and analysis; A. Khoruzhaya — data interpretation, text editing.

REFERENCES

1. Vechorko VI. Distribution of working time at an outpatient appointment of a district therapist with a nurse in a polyclinic in Moscow (photochronometric observation). *Social Aspects Public Health*. 2016;(6):4. (In Russ).

2. Kaplieva OV, Marega LA, Vorobyeva LP. Timekeeping of working hours of doctors of the children's consultative and diagnostic department. *Far Eastern Med J*. 2018;(4):72–76. (In Russ).

3. Ryabchikov IV, Zagafarov RR, Mukhina VV, et al. Distribution of the traumatologist-orthopaedician's working time with outpatients. *Moscow Sur J*. 2018;(6):38–43. (In Russ). doi: 10.17238/issn2072-3180.2018.6.38-43

4. Kudryavtsev ND, Sergunova KA, Ivanova GV, et al. Evaluation of the effectiveness of the implementation of speech recognition technology for the preparation of radiological protocols. *VIT*. 2020;6(S1):58–64. (In Russ). doi: 10.37690/1811-0193-2020-S1-58-64

5. Blackley SV, Huynh J, Wang L, et al. Speech recognition for clinical documentation from 1990 to 2018: A systematic review. *J Am Med Inf Association*. 2019;26(4):324–338. doi: 10.1093/jamia/ocy179

6. Motyer RE, Liddy S, Torreggiani WC, Buckley O. Frequency and analysis of non-clinical errors made in radiology reports using the National Integrated Medical Imaging System voice recognition dictation software. *Ir J Med Sci*. 2016;185(4):921–927. doi: 10.1007/s11845-016-1507-6

7. Hodgson T, Coiera E. Risks and benefits of speech recognition for clinical documentation: A systematic review. *J Am Med Inf Association*. 2016;23(e1):e169–e179. doi: 10.1093/jamia/ocv152

8. Itakura F. Minimum prediction residual principle applied to speech recognition. *IEEE Trans Acoust Speech Signal Process*. 1975;23(1):67–72. doi: 10.1109/TASSP.1975.1162641
9. Leeming W, Porter D, Jackson JD, et al. Computerized radiologic reporting with voice data-entry. *Radiology*. 1981;138(3):585–588. doi: 10.1148/radiology.138.3.7465833
10. Simon M, Leeming BW, Bleich HL, et al. Computerized radiology reporting using coded language. *Radiology*. 1974;113(2):343–349. doi: 10.1148/113.2.343
11. Vogel M, Kaisers W, Wassmuth R, Mayatepek E. Analysis of documentation speed using web-based medical speech recognition technology: Randomized controlled trial. *J Med Internet Res*. 2015;17(11):e247. doi: 10.2196/jmir.5072
12. Ramaswamy MR, Chaljub G, Esch O, et al. Continuous speech recognition in MR imaging reporting. *Am J Roentgenol*. 2000;174(3):617–622. doi: 10.2214/ajr.174.3.1740617
13. Poder TG, Fisette JF, Déry V. Speech recognition for medical dictation: Overview in quebec and systematic review. *J Med Systems*. 2018;42(5):89. doi: 10.1007/s10916-018-0947-0
14. Sankaranarayanan B, David G, Vishwanath KR, et al. Would technology obliterate medical transcription? In: Proceedings of the 2017 ACM SIGMIS Conference on Computers and People Research. New York, NY, USA: ACM; 2017. P. 97–104. doi: 10.1145/3084381.3084414
15. Houston JD, Rupp FW. Experience with implementation of a radiology speech recognition system. *J Digital Imaging*. 2000;13(3):124–128. doi: 10.1007/BF03168385
16. Saxena K, Diamond R, Conant RF, et al. Provider adoption of speech recognition and its impact on satisfaction, documentation quality, efficiency, and cost in an inpatient EHR. *AMIA Jt Summits Transl Sci Proc*. 2018;2017:186–195.
17. Schwartz LH, Kijewski P, Hertogen H, et al. Voice recognition in radiology reporting. *Am J Roentgenol*. 1997;169(1):27–29. doi: 10.2214/ajr.169.1.9207496
18. Vogel M, Kaisers W, Wassmuth R, Mayatepek E. Analysis of documentation speed using web-based medical speech recognition technology: Randomized controlled trial. *J Med Int Research*. 2015;17(11):e247. doi: 10.2196/jmir.5072
19. Hammana I, Lepanto L, Poder T, et al. Speech recognition in the radiology department: A systematic review. *Health Inf Manag*. 2015;44(2):4–10. doi: 10.1177/183335831504400201
20. Mohr DN, Turner DW, Pond GR, et al. speech recognition as a transcription aid: A randomized comparison with standard transcription. *J Am Med Inf Association*. 2003;10(1):85–93. doi: 10.1197/jamia.m1130
21. Singh M, Pal TR. Voice recognition technology implementation in surgical pathology: Advantages and limitations. *Arch Pathol Laboratory Med*. 2011;135(11):1476–1481. doi: 10.5858/arpa.2010-0714-OA
22. Goss FR, Blackley SV, Ortega CA, et al. A clinician survey of using speech recognition for clinical documentation in the electronic health record. *Int J Med Inf*. 2019;(130):103938. doi: 10.1016/j.ijmedinf.2019.07.017
23. Blackley SV, Schubert VD, Goss FR, et al. Physician use of speech recognition versus typing in clinical documentation: A controlled observational study. *Int J Med Inform*. 2020;(141):104178. doi: 10.1016/j.ijmedinf.2020.104178
24. Yang L, Ene IC, Belaghi RA, et al. Stakeholders' perspectives on the future of artificial intelligence in radiology: A scoping review. *Eur Radiol*. 2022;32(3):1477–1495. doi: 10.1007/s00330-021-08214-z
25. European Society of Radiology (ESR). Impact of artificial intelligence on radiology: A EuroAIM survey among members of the European Society of Radiology. *Insights Imaging*. 2019;10(1):105. doi: 10.1186/s13244-019-0798-3
26. Szymański P, Żelasko P, Morzyet M, et al. WER we are and WER we think we are. *arXiv*. arXiv:2010.03432.2020. doi: 10.48550/arXiv.2010.03432
27. Li J. Recent advances in end-to-end automatic speech recognition. *arXiv*. arXiv:2111.01690.2022. doi: 10.48550/arXiv.2111.01690
28. Juang BH, Rabiner LR. Hidden markov models for speech recognition. *Technometrics*. 1991;33(3):251–272.
29. Graves A, Mohamed A, Hinton G. Speech recognition with deep recurrent neural networks In: 2013 IEEE International Conference on Acoustics, Speech and Signal Processing. Vancouver, BC, Canada: IEEE; 2013. P. 6645–6649. doi: 10.48550/arXiv.1303.5778
30. Deng L, Li X. Machine learning paradigms for speech recognition: An overview. *IEEE Trans Audio Speech Lang Process*. 2013;21(5):1060–1089.
31. Kazachkin AE. Speech recognition methods, modern speech technologies. *Young Scientist*. 2019;(39):6–8. (In Russ).
32. Kamath U, Liu J, Whitaker J. Deep learning for NLP and speech recognition. Cham: Springer International Publishing; 2019. 621 p.
33. Wang D, Wang X, Lv S. An overview of end-to-end automatic speech recognition. *Symmetry*. 2019;11(8):1018. doi: 10.3390/sym11081018
34. Zhozhikashvili VA, Farkhadov MP, Petukhova NV, Zhozhikashvili AV. The first voice recognition applications in Russian language for use in The Interactive Information Systems. In: Speech and Computer. Saint-Petersburg, SPECOM; 2004. P. 304–307. (In Russ).
35. Karpov AA, Ronzhin AA, Li IV. SIRIUS system of dictoron-independent recognition of the merged Russian speech. *Izvestia Southern Federal University. Technical Sci*. 2005;54(10):44–54. (In Russ).
36. Irzaev MG. The use of voice input of information in medical institutions to fill in electronic charts and patient medical histories. *New technologies and techniques in medicine, biology and ecology*: Collection of scientific papers. 2013;(3):149–154. (In Russ).
37. Vazhenina D, Markov K, Karpov A, et al. State-of-the-art speech recognition technologies for Russian language. In: Proceedings of the 2012 Joint International Conference on Human-Centered Computer Environments. Aizu-Wakamatsu Japan: ACM; 2012. P. 59–63. doi: 10.1145/2160749.2160763
38. Kamvar M, Chelba C. Optimal size, freshness and time-frame for voice search vocabulary. *arXiv*. arXiv:1210.8436.2012.
39. Kipyatkova IS, Karpov AA. An analytical survey of large vocabulary Russian speech recognition systems. *SPIIRAS Proceedings*. 2014;1(12):7. (In Russ). doi: 10.15622/sp.12.1
40. Kudryavtsev ND, Semenov DS, Kozhikhina DD, Vladzymyrskyy AV. Speech recognition technology: Results of a survey of radiologists at the Moscow reference center for diagnostic radiology. *Healthcare Management*. 2022;8(3):95–104. (In Russ). doi: 10.33029/2411-8621-2022-8-3-95-104
41. Sinitsyn VE, Komarova MA, Mershina EA. Protocol of radiological description: Past, present, future. *Bulletin Radiology Radiology*. 2014;(3):35–40. (In Russ).
42. Sobez LM, Kim SH, Angstwurm M, et al. Creating high-quality radiology reports in foreign languages through multilingual structured reporting. *Eur Radiol*. 2019;29(11):6038–6048. doi: 10.1007/s00330-019-06206-8
43. Ganeshan D, Duong PA, Probyn L, et al. Structured reporting in radiology. *Academic Radiology*. 2018;25(1):66–73. doi: 10.1016/j.acra.2017.08.005
44. Dos Santos PD, Hempel JM, Mildenberger P, et al. Structured reporting in clinical routine. *Rofo*. 2019. Vol. 191, N 01. P. 33–39. doi: 10.1055/a-0636-3851
45. Andrianova MG, Kudryavtsev ND, Petryaykin AV. Development of a thesaurus of radiological terms for voice filling of diagnostic research protocols. *Digital Diagnostics*. 2022;3(S1):21–22. (In Russ). doi: 10.17816/DD105703

СПИСОК ЛИТЕРАТУРЫ

1. Вечорко В.И. Распределение рабочего времени на амбулаторном приеме врача-терапевта участкового с медицинской сестрой в поликлинике города Москвы (фотохронометражное наблюдение) // Социальные аспекты здоровья населения. 2016. № 6. С. 4.

2. Каплиева О.В., Марега Л.А., Воробьева Л.П. Хронометраж рабочего времени врачей детского консультативно-диагностического отделения // Дальневосточный медицинский журнал. 2018. № 4. С. 72–76.

3. Ryabchikov I.V., Zagafarov R.R., Mukhina V.V., et al. Distribution of the traumatologist-orthopaedician's working time with outpatients // Moscow Sur J. 2018. N 6. P. 38–43. doi: 10.17238/issn2072-3180.2018.6.38-43

4. Kudryavtsev N.D., Sergunova K.A., Ivanova G.V., et al. Evaluation of the effectiveness of the implementation of speech recognition technology for the preparation of radiological protocols // VIT. 2020. Vol. 6, N S1. P. 58–64. doi: 10.37690/1811-0193-2020-S1-58-64

5. Blackley S.V., Huynh J., Wang L., et al. Speech recognition for clinical documentation from 1990 to 2018: A systematic review // J Am Med Inf Association. 2019. Vol. 26, N 4. P. 324–338. doi: 10.1093/jamia/ocy179

6. Motyer R.E., Liddy S., Torreggiani W.C., Buckley O. Frequency and analysis of non-clinical errors made in radiology reports using the National Integrated Medical Imaging System voice recognition dictation software // Ir J Med Sci. 2016. Vol. 185, N 4. P. 921–927. doi: 10.1007/s11845-016-1507-6

7. Hodgson T., Coiera E. Risks and benefits of speech recognition for clinical documentation: A systematic review // J Am Med Inf Association. 2016. Vol. 23, N e1. P. e169–e179. doi: 10.1093/jamia/ocv152

8. Itakura F. Minimum prediction residual principle applied to speech recognition // IEEE Trans Acoust Speech Signal Process. 1975. Vol. 23, N 1. P. 67–72. doi: 10.1109/TASSP.1975.1162641

9. Leeming W., Porter D., Jackson J.D., et al. Computerized radiologic reporting with voice data-entry // Radiology. 1981. Vol. 138, N 3. P. 585–588. doi: 10.1148/radiology.138.3.7465833

10. Simon M., Leeming B.W., Bleich H.L., et al. Computerized radiology reporting using coded language // Radiology. 1974. Vol. 113, N 2. P. 343–349. doi: 10.1148/113.2.343

11. Vogel M., Kaisers W., Wassmuth R., Mayatepek E. Analysis of documentation speed using web-based medical speech recognition technology: Randomized controlled trial // J Med Internet Res. 2015. Vol. 17, N 11. P. e247. doi: 10.2196/jmir.5072

12. Ramaswamy M.R., Chaljub G., Esch O., et al. Continuous speech recognition in MR imaging reporting // Am J Roentgenol. 2000. Vol. 174, N 3. P. 617–622. doi: 10.2214/ajr.174.3.1740617

13. Poder T.G., Fisette J.F., Déry V. Speech recognition for medical dictation: Overview in quebec and systematic review // J Med Systems. 2018. Vol. 42, N 5. P. 89. doi: 10.1007/s10916-018-0947-0

14. Sankaranarayanan B., David G., Vishwanath K.R., et al. Would technology obliterate medical transcription? // Proceedings of the 2017 ACM SIGMIS Conference on Computers and People Research. New York, NY, USA: ACM, 2017. P. 97–104. doi: 10.1145/3084381.3084414

15. Houston J.D., Rupp F.W. Experience with implementation of a radiology speech recognition system // J Digital Imaging. 2000. Vol. 13, N 3. P. 124–128. doi: 10.1007/BF03168385

16. Saxena K., Diamond R., Conant R.F., et al. Provider adoption of speech recognition and its impact on satisfaction, documentation quality, efficiency, and cost in an inpatient EHR // AMIA Jt Summits Transl Sci Proc. 2018. Vol. 2017. P. 186–195.

17. Schwartz L.H., Kijewski P., Hertogen H., et al. Voice recognition in radiology reporting // Am J Roentgenol. 1997. Vol. 169, N 1. P. 27–29. doi: 10.2214/ajr.169.1.9207496

18. Vogel M., Kaisers W., Wassmuth R., Mayatepek E. Analysis of documentation speed using web-based medical speech recognition technology: Randomized controlled trial // J Med Int Research. 2015. Vol. 17, N 11. P. e247. doi: 10.2196/jmir.5072

19. Hammana I., Lepanto L., Poder T., et al. Speech recognition in the radiology department: A systematic review // Health Inf Manag. 2015. Vol. 44, N 2. P. 4–10. doi: 10.1177/183335831504400201

20. Mohr D.N., Turner D.W., Pond G.R., et al. Speech recognition as a transcription aid: A randomized comparison with standard transcription // J Am Med Inf Association. 2003. Vol. 10, N 1. P. 85–93. doi: 10.1197/jamia.m1130

21. Singh M., Pal T.R. Voice recognition technology implementation in surgical pathology: Advantages and limitations // Arch Pathol Laboratory Med. 2011. Vol. 135, N 11. P. 1476–1481. doi: 10.5858/arpa.2010-0714-OA

22. Goss F.R., Blackley S.V., Ortega C.A., et al. A clinician survey of using speech recognition for clinical documentation in the electronic health record // Int J Med Inf. 2019. N 130. P. 103938. doi: 10.1016/j.ijmedinf.2019.07.017

23. Blackley S.V., Schubert V.D., Goss F.R., et al. Physician use of speech recognition versus typing in clinical documentation: A controlled observational study // Int J Med Inform. 2020. N 141. P. 104178. doi: 10.1016/j.ijmedinf.2020.104178

24. Yang L., Ene I.C., Belaghi R.A., et al. Stakeholders' perspectives on the future of artificial intelligence in radiology: A scoping review // Eur Radiol. 2022. Vol. 32, N 3. P. 1477–1495. doi: 10.1007/s00330-021-08214-z

25. European Society of Radiology (ESR). Impact of artificial intelligence on radiology: A EuroAIM survey among members of the European Society of Radiology // Insights Imaging. 2019. Vol. 10, N 1. P. 105. doi: 10.1186/s13244-019-0798-3

26. Szymański P., Żelasko P., Morzyet M., et al. WER we are and WER we think we are // arXiv. arXiv:2010.03432.2020. doi: 10.48550/arXiv.2010.03432

27. Li J. Recent advances in end-to-end automatic speech recognition // arXiv. arXiv:2111.01690. 2022. doi: 10.48550/arXiv.2111.01690

28. Juang B.H., Rabiner L.R. Hidden markov models for speech recognition // Technometrics. 1991. Vol. 33, N 3. P. 251–272.

29. Graves A., Mohamed A., Hinton G. Speech recognition with deep recurrent neural networks // 2013 IEEE International Conference on Acoustics, Speech and Signal Processing. Vancouver, BC, Canada: IEEE, 2013. P. 6645–6649. doi: 10.48550/arXiv.1303.5778

30. Deng L., Li X. Machine learning paradigms for speech recognition: An overview // IEEE Trans Audio Speech Lang Process. 2013. Vol. 21, N 5. P. 1060–1089.

31. Казачкин А.Е. Методы распознавания речи, современные речевые технологии // Молодой ученый. 2019. № 39. С. 6–8.

32. Kamath U., Liu J., Whitaker J. Deep learning for NLP and speech recognition. Cham: Springer International Publishing, 2019. 621 p.

33. Wang D., Wang X., Lv S. An overview of end-to-end automatic speech recognition // Symmetry. 2019. Vol. 11, N 8. P. 1018. doi: 10.3390/sym11081018

34. Zhozhikashvili V.A., Farkhadov M.P., Petukhova N.V., Zhozhikashvili A.V. The first voice recognition applications in Russian language for use in The Interactive Information Systems // Speech and Computer. Saint-Petersburg, SPECOM, 2004. P. 304–307.

35. Карпов А.А., Ронжин А.А., Ли И.В. SIRIUS система дикторнезависимого распознавания слитной русской речи // Известия Южного федерального университета. Технические науки. 2005. Т. 54, № 10. С. 44–54.

36. Ирзаев М.Г. Использование голосового ввода информации в медицинских учреждениях для заполнения электронных карт и историй болезней пациентов // Новые технологии и техника в медицине, биологии и экологии: сборник научных трудов. 2013. № 3. С. 149–154.

37. Vazhenina D., Markov K., Karpov A., et al. State-of-the-art speech recognition technologies for Russian language // Proceedings of the 2012 Joint International Conference on Human-Centered Computer Environments. Aizu-Wakamatsu Japan: ACM, 2012. P. 59–63. doi: 10.1145/2160749.2160763

38. Kamvar M., Chelba C. Optimal size, freshness and time-frame for voice search vocabulary // arXiv. arXiv:1210.8436.2012.

39. Kipyatkova I.S., Karpov A.A. An analytical survey of large vocabulary Russian speech recognition systems // SPIIRAS Proceedings. 2014. Vol. 1, N 12. P. 7. doi: 10.15622/sp.12.1

40. Kudryavtsev N.D., Semenov D.S., Kozhikhina D.D., Vladzymyrskyy A.V. Speech recognition technology: Results of a survey of radiologists at the Moscow reference center for diagnostic radiology // Healthcare Management. 2022. Vol. 8, N 3. P. 95–104. doi: 10.33029/2411-8621-2022-8-3-95-104

41. Синицын В.Е., Комарова М.А., Мершина Е.А. Протокол рентгенологического описания: прошлое, настоящее, будущее // Вестник рентгенологии и радиологии. 2014. № 3. С. 35–40.

42. Sobez L.M., Kim S.H., Angstwurm M., et al. Creating high-quality radiology reports in foreign languages through multilingual structured reporting // Eur Radiol. 2019. Vol. 29, N 11. P. 6038–6048. doi: 10.1007/s00330-019-06206-8

43. Ganeshan D., Duong P.A., Probyn L., et al. Structured reporting in radiology // Academic Radiology. 2018. Vol. 25, N 1. P. 66–73. doi: 10.1016/j.acra.2017.08.005

44. Dos Santos P.D., Hempel J.M., Mildenberger P., et al. Structured reporting in clinical routine // Rofo. 2019. Vol. 191, N 01. P. 33–39. doi: 10.1055/a-0636-3851

45. Андрианова М.Г., Кудрявцев Н.Д., Петряйкин А.В. Разработка тезауруса рентгенологических терминов для голосового заполнения протоколов диагностических исследований // Digital Diagnostics. 2022. Т. 3, № S1. С. 21–22. doi: 10.17816/DD105703

AUTHORS' INFO

*** Nikita D. Kudryavtsev;**
address: 24/1 Petrovka street, 127051 Moscow, Russia;
ORCID: 0000-0003-4203-0630;
eLibrary SPIN: 1125-8637;
e-mail: KudryavtsevND@zdrav.mos.ru

Kristina A. Bardasova;
ORCID: 0009-0002-4310-1357;
eLibrary SPIN: 1156-7627;
e-mail: bardasovakris@mail.ru

Anna N. Khoruzhaya;
ORCID: 0000-0003-4857-5404;
eLibrary SPIN: 7948-6427;
e-mail: KhoruzhayaAN@zdrav.mos.ru

ОБ АВТОРАХ

*** Кудрявцев Никита Дмитриевич;**
адрес: Россия, 127051, Москва, ул. Петровка, д. 24, стр. 1;
ORCID: 0000-0003-4203-0630;
eLibrary SPIN: 1125-8637;
e-mail: KudryavtsevND@zdrav.mos.ru

Бардасова Кристина Алексеевна;
ORCID: 0009-0002-4310-1357;
eLibrary SPIN: 1156-7627;
e-mail: bardasovakris@mail.ru

Хоружая Анна Николаевна;
ORCID: 0000-0003-4857-5404;
eLibrary SPIN: 7948-6427;
e-mail: KhoruzhayaAN@zdrav.mos.ru

* Corresponding author / Автор, ответственный за переписку

DOI: https://doi.org/10.17816/DD322758

Роль двухэнергетической компьютерной томографии в диагностике подагры и других кристаллических артропатий: обзор литературы

М.В. Онойко, Е.А. Мершина, О.А. Георгинова, М.Л. Плотникова, А.В. Панюкова, В.Е. Синицын

Московский государственный университет имени М.В. Ломоносова, Москва, Российская Федерация

АННОТАЦИЯ

В статье обсуждается принцип работы двухэнергетической компьютерной томографии, её диагностическая точность, наиболее часто встречаемые виды артефактов. Рассматривается возможная зависимость наличия депозитов моноурата натрия при выполнении двухэнергетической компьютерной томографии от других клинических данных, значение двухэнергетической компьютерной томографии в диагностике подагры, её роль в дифференциальной диагностике кристаллических артропатий.

Метод двухэнергетической компьютерной томографии имеет ряд преимуществ по сравнению с диагностическим артроцентезом, являющимся золотым стандартом в диагностике подагры: неинвазивность, скорость выполнения, многократное снижение риска ятрогенных осложнений. Выявление подагры, контроль эффективности лечения, возможность проведения дифференциальной диагностики — все эти задачи могут реализоваться с помощью двухэнергетической компьютерной томографии.

Ключевые слова: двухэнергетическая компьютерная томография; ДЭКТ; подагра; пирофосфат кальция; кристаллические артропатии; диагностическая визуализация.

Как цитировать

Онойко М.В., Мершина Е.А., Георгинова О.А., Плотникова М.Л., Панюкова А.В., Синицын В.Е. Роль двухэнергетической компьютерной томографии в диагностике подагры и других кристаллических артропатий: обзор литературы // *Digital Diagnostics.* 2023. Т. 4, № 2. С. 197–213. DOI: https://doi.org/10.17816/DD322758

Рукопись получена: 08.04.2023 **Рукопись одобрена:** 11.05.2023 **Опубликована:** 27.05.2023

DOI: https://doi.org/10.17816/DD322758

The role of dual-energy computed tomography in the diagnosis of gout and other crystalline arthropathies: A review

Maria V. Onoyko, Elena A. Mershina, Olga A. Georginova, Maria L. Plotnikova, Aleksandra V. Panyukova, Valentin E. Sinitsyn

Lomonosov Moscow State University, Moscow, Russian Federation

ABSTRACT

The importance of dual-energy computed tomography in the diagnosis of gout, the principles of dual-energy computed tomography, the accuracy of the methodology, and the types of artifacts are discussed in this study. The possible dependence of the presence of deposits of sodium monourate on other clinical data and the role of dual-energy computed tomography in the differential diagnosis of other crystalline arthropathies are considered.

The dual-energy computed tomography has several advantages, including noninvasiveness, speed of execution, and a significant reduction in the risk of iatrogenic consequences compared with diagnostic arthrocentesis, which is the gold standard in diagnosing gout. Dual-energy computed tomography can accomplish gout detection, treatment, and differential diagnosis.

Keywords: calcium pyrophosphate, crystal arthropathies, diagnostic imaging, dual-energy computed tomography, gout

To cite this article

Onoyko MV, Mershina EA, Georginova OA, Plotnikova ML, Panyukova AV, Sinitsyn VE. The role of dual-energy computed tomography in the diagnosis of gout and other crystalline arthropathies: A review. *Digital Diagnostics.* 2023;4(2):197–213. DOI: https://doi.org/10.17816/DD322758

Received: 08.04.2023 **Accepted:** 11.05.2023 **Published:** 27.05.2023

DOI: https://doi.org/10.17816/DD322758

双能量计算机断层扫描在诊断痛风和其他结晶性关节病中的作用：文献综述

Maria V. Onoyko, Elena A. Mershina, Olga A. Georginova, Maria L. Plotnikova, Aleksandra V. Panyukova, Valentin E. Sinitsyn

Lomonosov Moscow State University, Moscow, Russian Federation

简评

本文讨论了双能量计算机断层扫描的操作原理、其诊断准确性以及最常见的伪影类型。考虑了在双能量计算机断层扫描过程中，单钠尿酸盐沉积的存在对其他临床数据的可能依赖性，双能量计算机断层扫描在诊断痛风中的意义以及其在结晶性关节病的鉴别诊断中的作用。

与作为诊断痛风金标准的诊断性关节穿刺术相比，双能量计算机断层扫描有几个优点：无创性、执行速度、医源性并发症风险的多次减少。痛风的检测、治疗效果的监测、鉴别诊断的可能性，都是可以通过双能量计算机断层扫描来实现的。

关键词：双能量计算机断层扫描；DECT；痛风；焦磷酸钙盐；结晶性关节病；诊断成像。

To cite this article

Onoyko MV, Mershina EA, Georginova OA, Plotnikova ML, Panyukova AV, Sinitsyn VE. 双能量计算机断层扫描在诊断痛风和其他结晶性关节病中的作用：文献综述. *Digital Diagnostics*. 2023;4(2):197–213. DOI: https://doi.org/10.17816/DD322758

收到： 08.04.2023 **接受：** 11.05.2023 **发布日期：** 27.05.2023

INTRODUCTION

Gout is a systemic rheumatological disease in which monosodium urate crystals accumulate in the articular, bone, cartilage, or soft tissues following an elevation in uric acid levels in the blood serum (hyperuricemia). Gouty arthritis and gouty nephropathy or urate nephrolithiasis might develop, depending on the lesion type.

GOUT: A SYSTEMIC TOPHACEOUS DISEASE

Over the last decade, accumulated data have made hyperuricemia more than just a marker of gout and urolithiasis. Hyperuricemia plays a role in the onset and progression of various metabolic and hemodynamic diseases, including metabolic syndrome, chronic heart failure, hypertension, atherosclerosis, early infarction and stroke, and diabetes mellitus.

The American College of Rheumatology (ACR) and European Alliance of Associations for Rheumatology (EULAR) (2015) classification criteria include clinical, laboratory, and instrumental data to diagnose gout [1]. The sensitivity and specificity of these criteria are 92% and 89%, respectively [1].

These criteria can be used if the patient has an "input sign": at least one episode of pain and edema in a peripheral joint or joint capsule. The presence of monosodium urate crystals in the synovial fluid or tophaceous tissue (macroscopic conglomerates of monosodium urate surrounded by granulomatous inflammation) by polarized light microscopy is a sufficient criterion for diagnosing gout, making this method the gold standard. In the absence of a sufficient criterion, clinical (typical clinical symptoms of gout, tophi detection, and temporal pattern of an attack), laboratory (serum uric acid level and synovial fluid analysis), and instrumental (ultrasonography of the affected joint and dual-energy computed tomography [CT]) diagnosis methods must be used. Each criterion is assigned a certain number of points, based on its degree of specificity. The ACR/EULAR-2015 classification criteria evaluate the visual determination of signs of urate deposits during dual-energy CT (DECT) as 4 points, and 8 of 23 points are sufficient to confirm gout. Thus, DECT plays a substantial role in confirming the diagnosis.

Joint puncture with synovial fluid aspiration is an invasive and painful method associated with various limitations and complications, necessitating the search for alternative diagnostic methods to make an accurate diagnosis [2, 3]. DECT, a non-invasive procedure for distinguishing urate deposits from surrounding tissues with excellent sensitivity and specificity, is one of the alternative diagnostic methods [4].

Hyperuricemia and monosodium urate crystals

Gout is a systemic tophaceous disease defined by monosodium urate crystal deposition in various tissues, which causes inflammation in patients with hyperuricemia caused by environmental and/or hereditary factors [5].

Regardless of hereditary predisposition, gout must be viewed as a staged disease [6], with hyperuricemia as the starting point. In hyperuricemia, the uric acid levels in the blood serum increase to >420 μmol/L or 6 mg/dL, resulting in the formation of monosodium urate crystals [7].

According to clinical, laboratory, and instrumental findings, gout has four distinct stages that do not necessarily transition from one to the next: (a) hyperuricemia with no symptoms or history of gout and no urate crystal deposits, (b) asymptomatic hyperuricemia with signs of urate crystal deposits, (c) hyperuricemia with a current or previous episode of gouty arthritis, and (d) hyperuricemia with tophi, chronic arthritis, or erosive arthritis [5].

The disease progresses in the absence of effective urate-lowering therapy. Initially, conglomerates of monosodium urate crystals form, which are detected in specific tissues and are dependent on environmental factors. Monosodium urate is soluble at 7 mg/dL (416 μmol/L) in normal saline at 37°C. As the monosodium urate concentration in synovial fluid increases, it subsequently deposits on the cartilage surface, with further destruction and penetration of monosodium urate crystals into the subchondral bone [8], which eventually leads to active bone remodeling. Long-term monosodium urate crystal saturation of synovial fluid results in the formation of macroscopic monosodium urate deposits surrounded by granulomatous inflammation (tophi) [9]. They are most commonly present in proteoglycan-rich tissues (joint capsule, tubular bones, tendons, and skin); however, they can be (infrequently) also found in parenchymal organ tissues. The tissue reaction to monosodium urate deposition is chronic inflammation, involving both innate and adaptive immunity [10].

In chronic gout, the frequency, duration, and severity of attacks increase, tophi form, severe deforming arthropathy develops, and concomitant diseases progress.

According to recent epidemiological studies, the prevalence of hyperuricemia in adults is gradually increasing. High uric acid levels are found in 0.68–3.9% of cases in Europe and the United States, which range from 6.4% to 21.04% in some parts of China [11]. In Russia, this value is 16.8% [7]; however, hyperuricemia might remain asymptomatic for a long time in 5%–8% of the population. Hyperuricemia increases the risk of chronic kidney disease, obesity, type 2 diabetes, cardiovascular risk, and death [12, 13].

Gout diagnosis methods

Gout is diagnosed by at least one episode of joint arthritis (one metatarsophalangeal joint, ankle joint, or midfoot) or joint capsule inflammation. The second sufficient criterion for diagnosing is the determination of uric acid levels in the blood serum, synovial fluid analysis of the affected joint, or tofus aspiration for the detection of monosodium urate crystals by polarized light microscopy [14]. Joint puncture for diagnostic

purposes can be performed in both the acute and attack-free periods. However, processing and long-term storage of the synovial fluid and urate-lowering therapy in some cases can affect the reliability and sensitivity of detecting monosodium urate [15]. Serum uric acid levels fluctuate in all patients with gout. However, in 30% of patients with hyperuricemia, serum uric acid elevation is not detected even during an acute gout attack [16]; thus, the diagnosis of gout should not be based solely on serum uric acid levels. In patients with an atypical clinical course of inflammatory arthropathy, various imaging methods must be used for diagnosing gout, including radiography, ultrasound diagnosis, and DECT. This is critical for differential diagnosis, including when synovial fluid analysis by polarized light microscopy is impossible.

Typical radiographic signs of gout are punched-out bone erosions with sclerotic contours and overhanging borders, also known as "rat bite" or "gull wing" erosions (Fig. 1).

Articular tophi, which resemble inhomogeneous soft tissue indurations, can be seen in chronic gout. X-ray changes are seen several years after gout onset and may be useful in confirming the diagnosis later in the disease progression [16, 17].

DUAL-ENERGY COMPUTED TOMOGRAPHY: AN ALTERNATIVE METHOD OF INSTRUMENTAL DIAGNOSIS OF GOUT

Ultrasound examination of the joints and DECT, which detects urate deposits, tophi, and bone degradation, are alternative instrumental methods of gout diagnosis.

On ultrasound examination of the joints, urate deposits can be detected on the surface of the articular cartilage as a hyperechoic intermittent band, independent of the viewing angle (double contour effect), or in synovial fluid as floating hyperechoic heterogeneous foci that look like a "snowstorm," and hyperechoic aggregates visualized in the joint space or along the tendons [18].

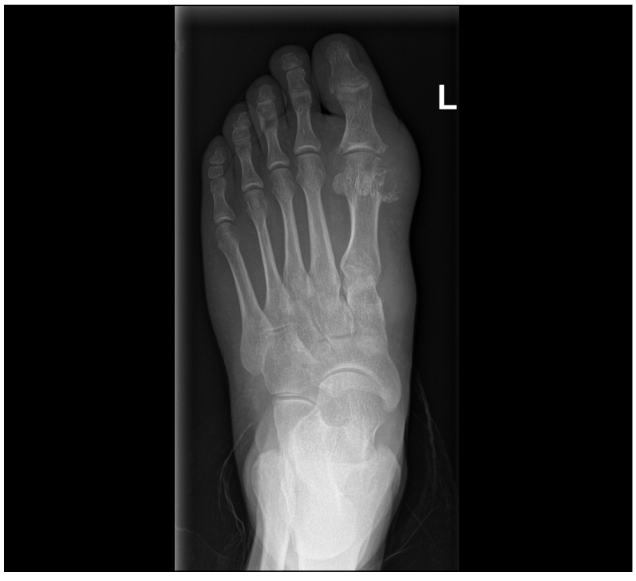

Fig. 1. Bone erosions in a patient with gout (radiography findings of the Medical Research and Education Center of the Lomonosov Moscow State University).

DECT is also useful in differentiating between gout and septic arthritis or between monosodium urate accumulation and calcium pyrophosphate deposition (pseudogout and chondrocalcinosis) [19, 20]. DECT allows investigating the numerous anatomical locations in great detail, finding deposits of monosodium urate crystals noninvasively [21–23].

How dual-energy computed tomography works?

DECT, a modern and promising research method, involves the spectral differentiation of materials by scanning a specific body part with two different types of X-rays with varying energies. Signal absorption coefficients identify substances under these conditions, allowing them to be distinguished by their chemical composition. At low X-ray tube voltages (20–50 kV), X-ray energy is totally absorbed by the substance (with prevailing photoelectric effect), whereas at high voltages (50–150 kV), Compton scattering prevails, resulting in signal attenuation [24, 25]. The role of the photoelectric and Compton effects for each compound is determined by the substance's electron density and atomic number [24, 26]: the higher the atomic number and lower the electron density (e.g., iodine, calcium, barium, and xenon), the greater the effect of photoelectric absorption, whereas elements with a low atomic number and higher electron density (carbon, nitrogen, hydrogen, and oxygen) depend more on the Compton effect [24]. For example, in iodine, calcium, and barium, the K-edge phenomenon is observed, characterized by photon absorption and photoelectron ejection from the K-shell. DECT is based on this phenomenon. Because some elements have well-defined K-edges, the difference between the absorption coefficients of the tested substances at different energies increases, allowing them to be distinguished.

DECT has several configurations: with two perpendicular sources and detectors, with a single source-detector system with quick voltage switching, or with a single X-ray source and a multilayer sandwich detector [26]. Data are processed using three- or two-material decomposition analysis. Two-material decomposition analysis in the diagnosis of gout is performed by uric acid and calcium. Soft tissues are the "reference point" for the algorithm to make judgment concerning the presence of calcium or monosodium urate in the area under study. Thus, a material density (MD) map can be created, on which each component is color coded. In the Siemens DECT systems, cortical bones, cancellous bones, and monosodium urate crystals are coded blue, pink, and green, respectively. Color scales used by other manufacturers' processing algorithms may differ.

In addition to the qualitative assessment, a quantitative assessment of the chemical of interest is possible. The dual-energy gout software automatically determines the total

volume of monosodium urate deposits in the field of view (FOV) [23]. Artifacts are included in the total volume; therefore, understanding their types and potential location is critical. Green areas corresponding to artifacts can be removed using the cropping tool. After this, the total volume of monosodium urate deposits will be automatically recalculated.

Three-dimensional reconstruction (volume-rendering technique image) with color coding is possible, as are other reconstruction algorithms employed in research (Fig. 2).

The key advantage of DECT over other diagnosis methods is its ability to determine the chemical composition by scanning at two energy levels and quantifying the chemical of interest. The non-invasiveness, speed of study, and absence of iatrogenic complications in DECT are all evident benefits.

An incorrect belief is that the radiation exposure during dual-energy scanning is double that received during single-energy scanning. However, numerous studies have found that the radiation exposure and image quality in DECT and single-energy CT are comparable [27–29]. This is accomplished not only through the device's technical features but also through the use of methods that reduce radiation dose, such as the ability to independently set the current strength, iterative reconstruction and other modern algorithms, use of virtual non-contrast images, FOV size limitation to the area of interest [30, 31].

DECT allows for the reconstruction of virtual monochromatic images, which are the result of theoretical scanning with monochromatic radiation. This application aids in increasing contrast and decreasing the number of artifacts from metal structures [32].

The disadvantages include a small FOV for dual-energy images, which is a circle with a diameter of only 33–35 cm for different generations of tomographs, possibility of false-positive and false-negative results, and cross-scattering (when photons emitted by one source hit a detector designed for photons emitted by another source) [33, 34]. These technical flaws can result in data loss (Fig. 3*a*).

Diagnostic accuracy of dual-energy computed tomography

According to Baer et al. [35], DECT has 100% sensitivity in the tophi form of gout and 64% in the absence of tophi. According to the meta-analysis by Ogdie et al. [20], DECT has sensitivity and specificity of 87% and 84%, respectively, which exceed the same parameters for ultrasonography. Bongartz et al. [36] found reported sensitivity and specificity rates of 90% and 83%, respectively. According to Huppertz et al. [37], DECT is less sensitive than ultrasound (100% vs. 84.6%) because of lower resolution.

These data suggest that DECT has good diagnostic accuracy. Varying scan areas, which may be crucial in determining the accuracy of the method, and varying disease durations in some studies are likely to explain the discrepancy in findings between study groups [38].

However, the presence of false-positive and false-negative results is unavoidable in every study method. Objects mimicking monosodium urate crystals can be seen in the nail bed and skin calluses (Fig. 3*b*). This false-positive result is caused by the similarity of the dual-energy index of keratin to that of monosodium urate, which results in similar color coding [39]. Interestingly, these artifacts are more commonly found in the feet than in the hands [39, 40]. Generally, the skin above the knee and elbow joints does not produce such artifacts.

Metal structures and dense areas of cortical bone produce artifacts of increased radiation hardness, which might be misinterpreted as monosodium urate deposits [40]. When using polychromatic radiation, radiation hardness (beam hardening) increases, causing faster absorption of low-energy photons and slower absorption of high-energy photons, resulting in an increase in the total energy of X-ray

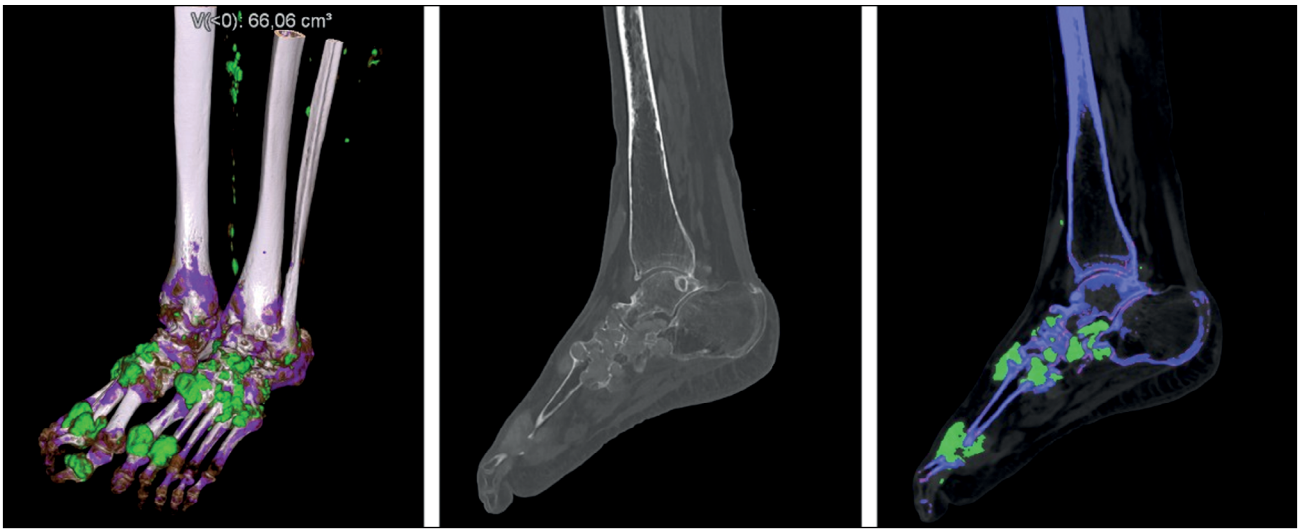

Fig. 2. Three-dimensional reconstruction, blended and color-coded image (right ankle joint and small foot joints): blue, pink, and green represent cortical bone, cancellous bone, and monosodium urate crystals, respectively (dual-energy computed tomography findings of the Medical Research and Education Center of the Lomonosov Moscow State University).

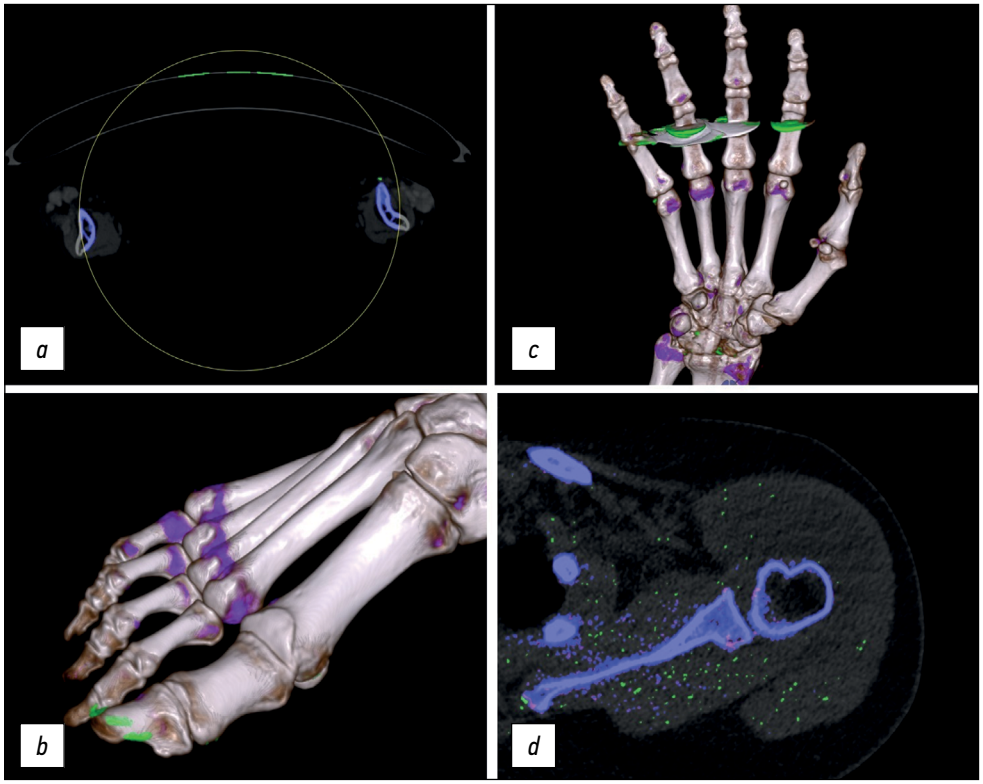

Fig. 3. Artifacts in dual-energy computed tomography: *a*) data loss owing to incorrect positioning of the patient, *b*) nail bed artifact, *c*) increased radiation hardness artifact from a wedding ring, and *d*) multiple small dotted artifacts (dual-energy computed tomography findings of the Medical Research and Education Center of the Lomonosov Moscow State University).

radiation. Because of beam hardening, the attenuation of the radiation decreases and the intensity at the detectors increases, resulting in a deviation from the optimum absorption profile. Thus, the artifact appears in the image as depressions and dark bands between dense objects (Fig. 3*c*).

At low signal-to-noise ratios, small dotted green inclusions appear, mimicking monosodium urate crystals (Fig. 3*d*). However, if small dotted green inclusions are observed along any anatomical structure, such as the Achilles tendon, a case of true monosodium urate deposition must be considered [39].

A false-negative result is obtained when the monosodium urate microcrystals are <2 mm in diameter, when visualizing tophi with a monosodium urate concentration that is too low, and when the technical parameters are incorrectly set. However, in most cases, artifacts are quite typical and easily identified by an experienced radiologist. Artifacts can be removed using various image reconstruction algorithms, such as a kernel, and correctly setting image parameters on the workstation, such as "air distance," "resolution," "minimum [HU]," and "ratio" (for Syngo.via VB20A_HF06 class Dual-Energy Gout).

A kernel (reconstruction filter) is a mathematical algorithm that is used to reconstruct CT images [41].

The "air distance" parameter (the distance in voxels between monosodium urate crystals and the air and bone) allows the reduction of artifacts in the nailbed and skin. This operation removes all green elements within the specified distance from the skin surface, except for those that are simultaneously near bone structures at a distance not exceeding the specified value.

The "ratio" parameter is the dual-energy ratio, which is the ratio of low-energy MD to high-energy MD in Hounsfield units (HU). When using the two-material decomposition method, this value is critical for separating calcium from urate. An increase in the "ratio" parameter increases the sensitivity of DECT to monosodium urate crystals because of a decrease in specificity [39].

The "minimum [HU]" parameter determines the HU threshold in mixed images, which are virtually equal to images obtained at 120 kV [42]. Objects with densities less than the specified value will not have their dual-energy index calculated; however, they will be assigned "0" HU on MD maps and hence will not be color-coded [39].

The "resolution" parameter specifies the minimum amount of green pixels that the application will identify as monosodium urate deposition. If the number of such pixels in the given area is less than the specified value, they will not be displayed.

An extra tin filter can be used to shut off low-energy photons, lowering radiation exposure and enhancing image quality.

Comparison of clinical data and dual-energy computed tomography findings

Lee et al. [43] focused on parameters that are more likely to predict the presence of monosodium urate deposits

on DECT. These parameters include uric acid levels in the blood serum, renal failure, and disease duration. Thus, the diagnostic value of DECT is limited in patients with new-onset gouty arthritis, and the likelihood of a positive DECT result is increased in patients who have chronic gout. Jia et al. [44] found that the sensitivity of DECT increases as the disease progresses. DECT had a sensitivity of 35.7% at the first visit for gout, 61.5% in patients with gout <2 years, and 92.9% in patients with gout >3 years. Other data suggest that monosodium urate deposits are found on DECT in 15%–24% of patients with asymptomatic hyperuricemia and 32.8% of patients with the first episode of gouty arthritis. This can be explained by the lack of monosodium urate volume and concentration for visualization in patients on their first attack of gouty arthritis [45]. Thus, DECT may be more effective for case follow-up than for primary diagnosis, whereas ultrasound examination may be useful for the first gout attack.

Chronic kidney disease and gout are comorbid conditions. A decrease in renal excretory function contributes to urate retention in the body, which increases the risk of monosodium urate crystal deposition in the joints and other tissues. On the contrary, Shang et al. [46] did not find a significant link between the presence of renal failure and the volume of monosodium urate deposits on DECT.

That a high serum uric acid concentration correlates with positive DECT findings is not always true. Hypouricemic therapy reduces uric acid levels in the blood serum, which leads to the breakdown of monosodium urate deposits. During a specific period, monosodium urate crystals have not yet dissolved at a specific time, at a sufficiently low uric acid level. Thus, using DECT to monitor urate deposit absorption allows the evaluation of treatment efficacy, and visible changes contribute to better compliance. Furthermore, not all patients with the same high level of uric acid in the blood have detectable monosodium urate deposits; thus, additional factors, such as genetic predisposition and age, influence the positive result of DECT [47].

Bayat et al. [23] developed a semiquantitative system for assessing monosodium urate crystal deposition (DECT urate scoring system) for the most affected area (feet). The analyzed area is divided into four parts, namely, first metatarsophalangeal joint, other joints of the foot, ankles, and tendons in the feet and ankles, which are assigned points and then summed up, depending on the number and nature of deposits. The results can be used to confirm the presence of gout and monitor the success of hypouricemic therapy. When compared with the automatic calculation of the volume of monosodium urate deposits, this technique saves time and makes it easier to work in difficult-to-measure locations. However, this scoring system only applies to foot lesions.

The semiquantitative method (DECT urate scoring system) was used by Shang et al. [46], and no correlation was found between the score and concentration of uric acid in the blood serum. However, the relationship between the amount of monosodium urate in tissues and a long disease period, presence of erosions, and presence of tophi was confirmed. The study timing could be a factor in the disparity between DECT findings and uric acid levels. Specifically, uric acid excretion in the urine increases during a gout attack [48].

However, studies have shown a link between uric acid levels in the blood serum and the presence of monosodium urate deposits on DECT. For example, Dalbeth et al. [49] report that urate deposits were discovered in 90.0% of patients with blood uric acid levels ⩾360 mM and palpable tophi; however, monosodium urate deposits were only seen in 46.9% of patients with non-palpable tophi and lower laboratory findings. All study participants received allopurinol at a dose of ⩾300 mg. In addition, patients with blood uric acid levels ⩾360 mM and palpable tophi had a higher volume of monosodium urate crystals and a higher number of erosions than patients in the other group.

Dual-energy computed tomography in the differential diagnosis of microcrystalline arthropathies associated with calcium salt deposition

In addition to gouty arthritis, microcrystalline arthropathies include arthritis caused by the deposition of calcium pyrophosphate and calcium hydroxyapatite crystals.

Calcium pyrophosphate crystal deposition disease is characterized by the accumulation of crystals, primarily calcium pyrophosphate, in the fibrous and hyaline cartilage. Risk factors include age, joint injury, hereditary predisposition, and diseases such as hemochromatosis, primary hyperparathyroidism, hypophosphatasia, and hypomagnesemia [50].

Calcium pyrophosphate crystal deposition disease frequently mimics other conditions, making diagnosis challenging for specialists. It can also be combined with other forms of inflammatory arthritis. For example, patients with gout or rheumatoid arthritis are more likely to develop calcium pyrophosphate crystal deposition disease [51]. Given the foregoing, the search for an appropriate differential diagnosis method becomes necessary.

Clinically, acute crystalline arthritis associated with calcium pyrophosphate deposition is similar to acute gouty arthritis, with the sole difference being the disease duration. Acute arthritis associated with calcium pyrophosphate deposition can persist for weeks or even months [52, 53].

Chronic crystalline arthritis associated with calcium pyrophosphate deposition frequently progresses as degenerative osteoarthritis with mechanical joint pain and intermittent clinical outbreaks of acute arthritis associated with calcium pyrophosphate deposition [52]. The interphalangeal, second and third metacarpophalangeal, and knee joints are the most commonly affected [52–54].

Calcium pyrophosphate crystals may deposit along the cruciform ligament of the atlas, which is manifested

as the crowned dens syndrome. The clinical presentation is nonspecific, consisting of severe neck pain, fever, neck muscle stiffness, and occipital headache [55]. In this case, the differential diagnosis includes meningitis, giant cell arteritis, rheumatoid arthritis, and others.

Calcium pyrophosphate deposition-associated crystalline arthritis can occasionally manifest as polyarthritis and thus mimic rheumatoid arthritis. Clinically, the distinction is that joint damage caused by calcium pyrophosphate crystals proceeds sequentially and less symmetrically than in rheumatoid arthritis [53]. Nonetheless, relying on this clinical parameter is problematic. Calcium pyrophosphate deposition-associated crystalline arthritis might mimic not just rheumatological diseases but also neurological diseases, cancers, and other conditions. The development of novel instrumental methods is critical for accurate and timely differential diagnosis.

The informative value of blood parameters is minimal for the diagnosis of arthritis associated with calcium pyrophosphate deposits. Polarized light microscopy of the synovial fluid and instrumental methods such as X-ray imaging, ultrasonography, and CT make a larger contribution.

To date, X-ray imaging is the most commonly used method in routine practice for diagnosing calcium pyrophosphate crystal deposition disease, whereas polarized light microscopy of the synovial fluid is the gold standard, according to the European League Against Rheumatism (EULAR) recommendations. As previously stated, this method has limitations and disadvantages that often cannot be corrected.

In X-ray imaging, the presence of chondrocalcinosis, which most commonly affects menisci, triangular cartilage in the triangular fibrocartilage complex, and pubic symphysis, is the primary symptom of calcium pyrophosphate crystal deposition disease. Chondrocalcinosis is visualized as linear zones of compaction parallel to the cortical bone surface, spicular inclusions along the cartilaginous structure, or cloud-like overlays along the contour of the synovial membrane [56]. This method has undeniable advantages, including noninvasiveness, absence of iatrogenic complications, rapidity with which it can be implemented, and low cost. Moreover, radiography is neither a very sensitive nor a completely specific method for diagnosing calcium pyrophosphate crystal deposition disease because a similar presentation can be seen with calcium hydroxyapatite deposition in the cartilage [50]. According to Lee et al. [57], the specificity and sensitivity of this method were 96.9% and 44.2%, respectively.

Distinguishing osteoarthritis associated with calcium pyrophosphate deposition from degenerative osteoarthritis using X-ray examination is difficult because the signs of differential diagnosis used are not absolute. These include the presence of more pronounced osteophytes and subchondral cysts, bone tissue degradation, lesion localization, and inflammation [50, 53, 54, 58]. Thus, the involvement of the shoulder, hand, and metacarpophalangeal joints is less common in degenerative osteoarthritis than in calcium pyrophosphate deposition-associated osteoarthritis [53]. Larger subchondral cysts and severe bone destruction are more common in calcium pyrophosphate deposition-associated osteoarthritis [54]. It is also worth paying attention to the calcified tendon of the quadriceps muscle and the Achilles tendon in the presence of chondrocalcinosis, which most likely implies calcium pyrophosphate crystal deposition disease.

Ultrasonography is becoming more popular because of its low cost, portability of equipment, and ease of usage. Frediani et al. [59] described three types of ultrasound findings in patients with calcium pyrophosphate crystal deposition disease. One of them is the presence of hyperechoic linear bands parallel to the cartilage surface, and this is more common with calcium pyrophosphate deposition in the hyaline cartilage. Another sign is more typical for calcium pyrophosphate deposition in the fibrocartilage. It is the formation of dotted hyperechoic inclusions along the cartilage tissue. In the joint cavity, the hyperechoic suspension containing mobile aggregates of round and/or oval calcium pyrophosphate crystals was seen the least. According to Lee et al. [57], the specificity and sensitivity of ultrasonography were 77.1% and 74.4%, respectively. Crucially, distinguishing between the ultrasound signs of gout and calcium pyrophosphate crystal deposition disease may be difficult when using this method, particularly for physicians who are not ultrasound specialists. One of the method's drawbacks is the operator-dependent results. Furthermore, with pronounced osteophytes in the advanced stages of osteoarthritis, difficulties may be caused by an acoustic shadow from the bone tissue [60].

CT is primarily used in cases of axial skeleton localization in the crowned dens syndrome, injury to the intervertebral discs, etc. [61]. Calcifications of the transverse, alar, apical, and cruciate ligaments are clearly visualized in the atlantoaxial joint, and calcification of the yellow ligament as nodular foci was also reported [62].

The role of DECT in the diagnosis of calcium pyrophosphate crystal deposition disease is unclear. Calcium-containing deposits will be colored blue on color-coded images obtained with DECT in the dual-energy gout class, allowing them to be distinguished from monosodium urate-containing deposits. The cortical bone is color-coded similarly to calcium pyrophosphate and hydroxyapatite deposits because of its high calcium concentration (Fig. 4).

According to Kravchenko et al. [63], the sensitivity and specificity of DECT for the detection of calcium pyrophosphate crystals were 55% and 92%, respectively (with a mean disease duration of 1 month, using established imaging techniques for gout) [63]. Tanikawa et al. [60] reported that DECT had a sensitivity and specificity of 77.8% and 93.8%, respectively, for the detection of calcium pyrophosphate crystals in the menisci ex vivo.

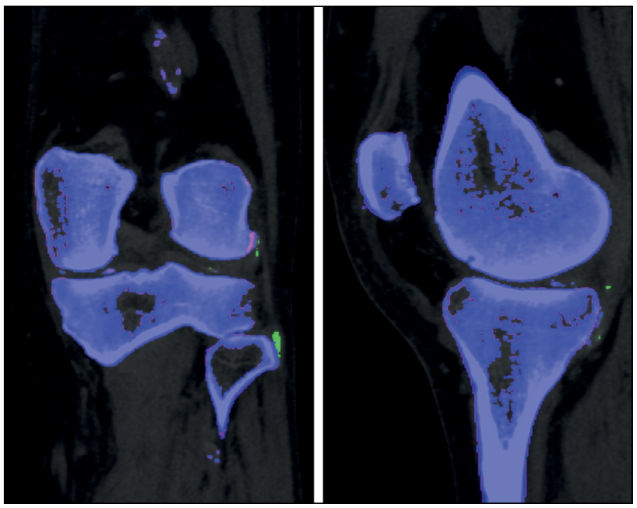

Fig. 4. Color-coded dual-energy coronal and sagittal images (left knee joint). Calcification of the medial meniscus (dual-energy computed tomography findings of the Medical Research and Education Center of the Lomonosov Moscow State University).

Currently, no specific protocol has been made for calcium pyrophosphate crystal deposition disease, making it impossible to calculate the volume of calcium pyrophosphate deposits and, in some cases, distinguish them from bone tissue. Tedeschi et al. [64] modified the image reconstruction parameters for gout by increasing the "iodine ratio" parameter, resulting in an increase in the method's sensitivity for calcium pyrophosphate crystals up to 90%–100%. Moreover, the possibility of distinguishing monosodium urate crystals from calcium pyrophosphate crystals disappeared.

An advantage of DECT is its ability to distinguish deposits of calcium hydroxyapatite from calcium pyrophosphate. Although calcium hydroxyapatite deposits are commonly found along the tendons, this characteristic is not absolute for the differential diagnosis. Calcium salts are radiographically defined as chondrocalcinosis, which also makes determining the chemical composition of the deposits difficult. Density values in multislice CT cannot be used as an unambiguous recommendation.

With DECT, a spectral analysis of calcium hydroxyapatite and calcium pyrophosphate deposits can be performed using the values of the dual-energy index and effective atomic number (Zeff), which are the result of the mathematical processing of DECT findings. These parameters help in distinguishing the two types of crystals [65]. Although the dual-energy index and Zeff for the differential diagnosis of calcium salt deposits is not currently the standard practice, this avenue is promising and worth further investigation.

CONCLUSION

DECT is a promising method for diagnosing crystalline arthropathy and has several advantages over other research methods such as polarized light microscopy, ultrasonography, X-ray, and CT. The advantages of DECT include its speed, absence of iatrogenic complications, qualitative and quantitative examination of materials, and dynamic monitoring. This radiation diagnostic technology solves numerous problems, including monitoring the efficacy of gout therapy and the potential of differential diagnosis of crystalline arthropathies.

Despite the drawbacks of this technique, there are methods that can aid in the correct interpretation of DECT results. DECT may simplify the confirmation of arthritis associated with the deposition of different types of crystals with atypical symptoms. However, questions remain regarding the early diagnosis of gout, possibility of accurate differentiation of calcium pyrophosphate from calcium hydroxyapatite crystals, and determining their volume, which necessitates additional research.

ADDITIONAL INFORMATION

Funding source. The work was conducted within the framework of the state assignment of the Lomonosov Moscow State University.

Competing interests. The authors declare that they have no competing interests.

Authors' contribution. All authors made a substantial contribution to the conception of the work, acquisition, analysis, interpretation of data for the work, drafting and revising the work, final approval of the version to be published and agree to be accountable for all aspects of the work. M.V. Onoyko — search for publications on the article topic, writing the text of the manuscript; E.A. Mershina — expert evaluation of information, editing of the text of the manuscript, final version approval; O.A. Georginova — expert evaluation of information, editing of the text of the manuscript, final version approval; M.L. Plotnikova — editing of the text of the manuscript; A.V. Panyukova — editing of the text of the manuscript; V.E. Sinitsin — expert evaluation of information, final version approval.

REFERENCES

1. Neogi T, Jansen TL, Dalbeth N, et al. 2015 Gout classification criteria: An American college of rheumatology / European league against rheumatism collaborative initiative. *Arthritis Rheumatol*. 2015;67(10):2557–2568. doi: 10.1002/art.39254

2. Taylor WJ, Fransen J, Dalbeth N, et al. Diagnostic arthrocentesis for suspicion of gout is safe and well tolerated. *J Rheumatol*. 2016;43(1):150–153. doi: 10.3899/jrheum.150684

3. Sikilinda V, Alabut A. Protocols of technique of punctions of joints and treatment blocades in trauma and orthopedic diseases of support-moving apparatus. *Chief Physician South Russia*. 2018;2 (60):14–20. (In Russ).

4. Stauder SK, Peloso PM. Dual-Energy computed tomography has additional prognostic value over clinical measures in gout including tophi: A systematic

literature review. *J Rheumatol*. 2022;49(11):1256–1268. doi: 10.3899/jrheum.211246

5. Federal Clinical Guidelines. Gout. All-Russian Public Organization Association of Rheumatologists of Russia; 2014. (In Russ).

6. Dalbeth N, Phipps-Green A, Frampton C, et al. Relationship between serum urate concentration and clinically evident incident gout: An individual participant data analysis. *Ann Rheum Dis*. 2018;77(7):1048–1052. doi: 10.1136/annrheumdis-2017-212288

7. Pereverzev AP, Ostroumova OD. Drug-induced hyperuricemia/gout. Part I: Prevalence, pathophysiology, risk factors, clinical pattern. *Therapy*. 2021;7(6):136–145. (In Russ). doi: 10.18565/therapy.2021.7.159-169

8. Chhana A, Lee G, Dalbeth N. Factors influencing the crystallization of monosodium urate: A systematic literature review. *BMC Musculoskelet Disord*. 2015;16(1):1–11. doi: 10.1186/s12891-015-0762-4

9. Fiddis RW, Vlachos N, Calvert PD. Studies of urate crystallisation in relation to gout. *Ann Rheum Dis*. 1983;42(Suppl 1):12. doi: 10.1136/ard.42.suppl_1.12

10. Dalbeth N, Pool B, Gamble GD, et al. Cellular characterization of the gouty tophus: A quantitative analysis. *Arthritis Rheum*. 2010;62(5):1549–1556. doi: 10.1002/art.27356

11. Butler F, Alghubayshi A, Roman Y. The epidemiology and genetics of hyperuricemia and gout across major racial groups: A literature review and population genetics secondary database analysis. *J Personalized Med*. 2021;11(3):231. doi: 10.3390/jpm11030231

12. Meneses-Leon J, Denova-Gutiérrez E, Castañón-Robles S, et al. Sweetened beverage consumption and the risk of hyperuricemia in Mexican adults: A cross-sectional study. *BMC Public Health*. 2014;14(1):1–11. doi: 10.1186/1471-2458-14-445

13. Bae J, Chun BY, Park PS, et al. Higher consumption of sugar-sweetened soft drinks increases the risk of hyperuricemia in Korean population: The Korean multi-rural communities cohort study. *Semin Arthritis Rheum*. 2014;43(5):654–661. doi: 10.1016/j.semarthrit.2013.10.008

14. Zhang W, Doherty M, Pascual E, et al. EULAR evidence based recommendations for gout. Part I: Diagnosis. Report of a task force of the standing committee for international clinical studies including therapeutics (ESCISIT). *Ann Rheum Dis*. 2006;65(10):1301–1311. doi: 10.1136/ard.2006.055251

15. Kienhorst LB, Janssens HJ, Eijgelaar RS, et al. The detection of monosodium urate crystals in synovial fluid after long-term and varying storage conditions. *Joint Bone Spine*. 2015;82(6):470–471. doi: 10.1016/j.jbspin.2014.10.020

16. Secrets of rheumatology. Ed. by S.D. West. Trans. from English ed. by O.M. Lesnyak. Moscow: GEOTAR-Media; 2021. 756 p. (In Russ).

17. Malik A, Schumacher HR, Dinnella JE, Clayburne GM. Clinical diagnostic criteria for gout: Comparsion with the gold standard of synovial fluid crystal analysis. *J Clin Rheumatol*. 2009;15(1):22–24. doi: 10.1097/RHU.0b013e3181945b79

18. Pascal Z, Valcov R, Fabreguet I, et al. A prospective evaluation of ultrasound as a diagnostic tool in acute microcrystalline arthritis. *Arthritis Res Ther*. 2015;17(1):1–8. doi: 10.1186/s13075-015-0701-7

19. Omoumi P, Becce F, Racine D, et al. Basic principles, technical approaches, and applications in musculoskeletal imaging (Part I). *Semin Musculoskelet Radiol*. 2015;19(5):431–437. doi: 10.1055/s-0035-1569253

20. Ogdie A, Taylor WJ, Weatherall M, et al. Imaging modalities for the classification of gout: systematic literature review and meta-analysis. *Ann Rheum Dis*. 2015;74(10):1868–1874. doi: 10.1136/annrheumdis-2014-205431

21. Sapsford M, Gamble GD, Aati O, et al. Relationship of bone erosion with the urate and soft tissue components of the tophus in gout: A dual energy computed tomography study. *Rheumatology (Oxford)*. 2017;56(1):129–133. doi: 10.1093/rheumatology/kew383

22. Towiwat P, Doyle AJ, Gamble GD, et al. Urate crystal deposition and bone erosion in gout: "Inside-out" or "outside-in"? A dual-energy computed tomography study. *Arthritis Res Ther*. 2016;18(1):208. doi: 10.1186/s13075-016-1105-z

23. Bayat S, Aati O, Rech J, et al. Development of a dual-energy computed tomography scoring system for measurement of urate deposition in gout. *Arthritis Care Res (Hoboken)*. 2016;68(6):769–775. doi: 10.1002/acr.22754

24. Rajiah P, Sundaram M, Subhas N. Dual-energy CT in musculoskeletal imaging: What is the role beyond gout? *AJR Am J Roentgenol*. 2019;213(3):493–505. doi: 10.2214/AJR.19.21095

25. Klimkova MM, Sinitsyn VE, Mazurenko DA, et al. Perspectives of dual-energy computed tomography in diagnostic of urinary stone disease for the determination of urinary calculi composition (review). *Med Visualization*. 2016;(6):84–92. (In Russ).

26. McCollough CH, Leng S, Yu L, Fletcher JG. Dual- and multi-energy CT: Principles, technical approaches, and clinical applications. *Radiology*. 2015;276(3):637–653. doi: 10.1148/radiol.2015142631

27. Sodickson AD, Keraliya A, Czakowski B, et al. Dual energy CT in clinical routine: How it works and how it adds value. *Emerg Radiol*. 2021;28(1):103–117. doi: 10.1007/s10140-020-01785-2

28. Megibow AJ, Kambadakone A, Ananthakrishnan L. Dual-energy computed tomography: Image acquisition, processing, and workflow. *Radiol Clin North Am*. 2018;56(4):507–520. doi: 10.1016/j.rcl.2018.03.001

29. Forghani R, De Man B, Gupta R. Dual-energy computed tomography: Physical principles, approaches to scanning, usage, and implementation: Part 2. *Neuroimaging Clin N Am*. 2017;27(3):385–400. doi: 10.1016/j.nic.2017.03.002

30. Henzler T, Fink C, Schoenberg SO, et al. Radiation dose aspects. *AJR Am J Roentgenol*. 2012;199(5 Suppl):S16–S25. doi: 10.2214/AJR.12.9210

31. Borges AP, Antunes C, Curvo-Semedo L. Pros and cons of dual-energy CT systems: "One does not fit all". *Tomography*. 2023;9(1):195–216. doi: 10.3390/tomography9010017

32. Parakh A, Lennartz S, An C, et al. Dual-energy CT images: Pearls and pitfalls. *Radiographics*. 2021;41(1):98–119. doi: 10.1148/rg.2021200102

33. Gosangi B, Mandell MC, Weaver MJ, et al. Bone marrow edema at dual-energy CT: A game changer in the emergency department. *Radiographics*. 2020;40(3):859–874. doi: 10.1148/rg.2020190173

34. Goo HW, Goo JM. Dual-energy CT. New horizon in medical imaging. *Korean J Radiol*. 2017;18(4):555–569. doi: 10.3348/kjr.2017.18.4.555

35. Baer AN, Kurano T, Thakur UJ, et al. Dual-energy computed tomography has limited sensitivity for non-tophaceous gout:

A comparison study with tophaceous gout. *BMC Musculoskelet Disord*. 2016;17(1):1–9. doi: 10.1186/s12891-016-0943-9

36. Bongartz T, Glazebrook KN, Kavros SJ, et al. Dual-energy CT for the diagnosis of gout: an accuracy and diagnostic yield study. *Ann Rheum Dis*. 2015;74(6):1072–1077. doi: 10.1136/annrheumdis-2013-205095

37. Huppertz A, Hermann A, Diekhoff T, et al. Systemic staging for urate crystal deposits with dual-energy CT and ultrasound in patients with suspected gout. *Rheumatol Int*. 2014;(3):763–771. doi: 10.1007/s00296-014-2979-1

38. Strobl S, Halpern EJ, Abd Ellah M, et al. Acute gouty knee arthritis: Ultrasound findings compared with dual-energy CT findings. *AJR Am J Roentgenol*. 2018;210(6):1323–1329. doi: 10.2214/AJR.17.19199

39. Mallinson PI, Coupal T, Reisinger C, et al. Artifacts in dual-energy CT gout protocol: A review of 50 suspected cases with an artifact identification guide. *AJR Am J Roentgenol*. 2014;203(1):103–109. doi: 10.2214/AJR.13.11396

40. Omoumi P, Zufferey P, Malghem J, So A. Imaging in gout and other crystal-related arthropathies. *Rheum Dis Clin North Am*. 2016;42(4):624–644. doi: 10.1016/j.rdc.2016.07.005

41. Lee SM, Lee JG, Lee G, et al. CT Image conversion among different reconstruction kernels without a sinogram by using a convolutional neural network. *Korean J Radiol*. 2019;20(2):295–303. doi: 10.3348/kjr.2018.0249

42. Alavandar E, Arunachalam VK, Narappulan N, et al. Principles and available hardware in DECT. *J Gastrointestinal Abdominal Radiology*. 2022;5(6). doi: 10.1055/s-0042-1742772

43. Lee JS, Seo WJ. What is the diagnostic value of dual-energy computed tomography in patients with clinical diagnosis of gout? *Adv Rheumatol*. 2021;61(1):1–7. doi: 10.1186/s42358-021-00198-0

44. Jia E, Zhu J, Huang W, et al. Dual-energy computed tomography has limited diagnostic sensitivity for short-term gout. *Clin Rheumatol*. 2018;37(3):773–777. doi: 10.1007/s10067-017-3753-z

45. Ramon A, Ornetti P. Dual energy computed tomography: A breakthrough for gout? *Joint Bone Spine*. 2020;87(4):289–291. doi: 10.1016/j.jbspin.2019.12.002

46. Shang J, Li XH, Lu SQ, et al. Gout of feet and ankles in different disease durations: Diagnostic value of single-source DECT and evaluation of urate deposition with a novel semi-quantitative DECT scoring system. *Adv Rheumatol*. 2021;61(1):1–14. doi: 10.1186/s42358-021-00194-4

47. Wang P, Smith SE, Garg R, et al. Identification of monosodium urate crystal deposits in patients with asymptomatic hyperuricemia using dual-energy CT. *RMD Open*. 2018;4(1):593–597. doi: 10.1136/rmdopen-2017-000593

48. Urano W, Yamanaka H, Tsutani H, et al. The inflammatory process in the mechanism of decreased serum uric acid concentrations during acute gouty arthritis. *J Rheumatol*. 2002;29(9):1950–1953.

49. Dalbeth N, Nicolaou S, Baumgartner S, et al. Presence of monosodium urate crystal deposition by dual-energy CT in patients with gout treated with allopurinol. *Ann Rheum Dis*. 2018;77(3):364–370. doi: 10.1136/annrheumdis-2017-212046

50. Zhang W, Doherty M, Bardin T, et al. European league against rheumatism recommendations for calcium pyrophosphate deposition. Part I: Terminology and diagnosis. *Ann Rheum Dis*. 2011;70(4):563–570. doi: 10.1136/ard.2010.139105

51. Sabchyshyn V, Konon I, Ryan LM, Rosenthal AK. Concurrence of rheumatoid arthritis and calcium pyrophosphate deposition disease: A case collection and review of the literature. *Semin Arthritis Rheum*. 2018;48(1):9–11. doi: 10.1016/j.semarthrit.2017.11.009

52. Williams CJ, Rosenthal AK. Pathogenesis of calcium pyrophosphate deposition disease. *Best Pract Res Clin Rheumatol*. 2021;35(4):101718. doi: 10.1016/j.berh.2021.101718

53. Abhishek A. Calcium pyrophosphate deposition. *Br J Hosp Med (Lond)*. 2014;75(4):61–64. doi: 10.12968/hmed.2014.75.sup4.c61

54. Miksanek J, Rosenthal AK. Imaging of calcium pyrophosphate deposition disease. *Curr Rheumatol Rep*. 2015;17(3):20. doi: 10.1007/s11926-015-0496-1

55. Godfrin-Valnet M, Godfrin G, Godard J, et al. Eighteen cases of crowned dens syndrome: Presentation and diagnosis. *Neurochirurgie*. 2013;59(3):115–120. doi: 10.1016/j.neuchi.2013.03.003

56. Cipolletta E, Filippou G, Scirè CA, et al. The diagnostic value of conventional radiography and musculoskeletal ultrasonography in calcium pyrophosphate deposition disease: a systematic literature review and meta-analysis. *Osteoarthr Cartil*. 2021;29(5):619–632. doi: 10.1016/j.joca.2021.01.007

57. Lee KA, Lee SH, Kim HR. Diagnostic value of ultrasound in calcium pyrophosphate deposition disease of the knee joint. *Osteoarthr Cartil*. 2019;27(5):781–787. doi: 10.1016/j.joca.2018.11.013

58. Neame RL, Carr AJ, Muir K, Doherty M. UK community prevalence of knee chondrocalcinosis: Evidence that correlation with osteoarthritis is through a shared association with osteophyte. *Ann Rheum Dis*. 2003;62(6):513–518. doi: 10.1136/ard.62.6.513

59. Frediani B, Filippou G, Falsetti P, et al. Diagnosis of calcium pyrophosphate dihydrate crystal deposition disease: Ultrasonographic criteria proposed. *Ann Rheum Dis*. 2005;64(4):638–640. doi: 10.1136/ard.2004.024109

60. Tanikawa H, Ogawa R, Okuma K, et al. Detection of calcium pyrophosphate dihydrate crystals in knee meniscus by dual-energy computed tomography. *J Orthop Surg Res*. 2018;13(1):73. doi: 10.1186/s13018-018-0787-0

61. Rosales-Alexander JL, Aznar JB, Magro-Checa C. Calcium pyrophosphate crystal deposition disease: Diagnosis and treatment. *Open Access Rheumatol*. 2014;(6):39–47. doi: 10.2147/OARRR.S39039

62. Sekijima Y, Yoshida T, Ikeda SI. CPPD crystal deposition disease of the cervical spine: A common cause of acute neck pain encountered in the neurology department. *J Neurol Sci*. 2010;296(1–2):79–82. doi: 10.1016/j.jns.2010.05.028

63. Kravchenko D, Karakostas P, Kuetting D, et al. The role of dual energy computed tomography in the differentiation of acute gout flares and acute calcium pyrophosphate crystal arthritis. *Clin Rheumatol*. 2022;41(1):223–233. doi: 10.1007/s10067-021-05949-4

64. Tedeschi SK, Solomon DH, Yoshida K, et al. A prospective study of dual-energy CT scanning, US and X-ray in acute calcium pyrophosphate crystal arthritis. *Rheumatology (Oxford)*. 2020;59(4):900–903. doi: 10.1093/rheumatology/kez431

65. Pascart T, Norberciak L, Legrand J, et al. Dual-energy computed tomography in calcium pyrophosphate deposition: Initial clinical experience. *Osteoarthr Cartil*. 2019;27(9):1309–1314. doi: 10.1016/j.joca.2019.05.007

СПИСОК ЛИТЕРАТУРЫ

1. Neogi T., Jansen T.L., Dalbeth N., et al. 2015 Gout classification criteria: An American college of rheumatology / European league against rheumatism collaborative initiative // Arthritis Rheumatol. 2015. Vol. 67, N 10. P. 2557–2568. doi: 10.1002/art.39254

2. Taylor W.J., Fransen J., Dalbeth N., et al. Diagnostic arthrocentesis for suspicion of gout is safe and well tolerated // J Rheumatol. 2016. Vol. 43, N 1. P. 150–153. doi: 10.3899/jrheum.150684

3. Сикилинда Д.В., Алабут А.В. Протоколы техники пункций суставов и лечебных блокад при травмах и ортопедических заболеваниях опорно-двигательного аппарата // Главный врач Юга России. 2018. Т. 2, № 60. С. 14–20.

4. Stauder S.K., Peloso P.M. Dual-Energy computed tomography has additional prognostic value over clinical measures in gout including tophi: A systematic literature review // J Rheumatol. 2022. Vol. 49, N 11. P. 1256–1268. doi: 10.3899/jrheum.211246

5. Федеральные клинические рекомендации. Подагра. Общероссийская общественная организация Ассоциация ревматологов России, 2014.

6. Dalbeth N., Phipps-Green A., Frampton C., et al. Relationship between serum urate concentration and clinically evident incident gout: An individual participant data analysis // Ann Rheum Dis. 2018. Vol. 77, N 7. P. 1048–1052. doi: 10.1136/annrheumdis-2017-212288

7. Переверзев А.П., Остроумова О.Д. Лекарственно-индуцированные гиперурикемия/подагра. Часть 2: отдельные лекарственные средства, прием которых ассоциирован с повышенным риском развития этих заболеваний // Терапия. 2021. Т. 7, № 6. С. 136–145. doi: 10.18565/therapy.2021.7.159-169

8. Chhana A., Lee G., Dalbeth N. Factors influencing the crystallization of monosodium urate: a systematic literature review // BMC Musculoskelet Disord. 2015. Vol. 16, N 1. P. 1–11. doi: 10.1186/s12891-015-0762-4

9. Fiddis R.W., Vlachos N., Calvert P.D. Studies of urate crystallisation in relation to gout // Ann Rheum Dis. 1983. Vol. 42, Suppl. 1. P. 12. doi: 10.1136/ard.42.suppl_1.12

10. Dalbeth N., Pool B., Gamble G.D., et al. Cellular characterization of the gouty tophus: A quantitative analysis // Arthritis Rheum. 2010. Vol. 62, N 5. P. 1549–1556. doi: 10.1002/art.27356

11. Butler F., Alghubayshi A., Roman Y. The epidemiology and genetics of hyperuricemia and gout across major racial groups: A literature review and population genetics secondary database analysis // J Personalized Med. 2021. Vol. 11, N 3. P. 231. doi: 10.3390/jpm11030231

12. Meneses-Leon J., Denova-Gutiérrez E., Castañón-Robles S., et al. Sweetened beverage consumption and the risk of hyperuricemia in Mexican adults: A cross-sectional study // BMC Public Health. 2014. Vol. 14, N 1. P. 1–11. doi: 10.1186/1471-2458-14-445

13. Bae J., Chun B.Y., Park P.S., et al. Higher consumption of sugar-sweetened soft drinks increases the risk of hyperuricemia in Korean population: The Korean multi-rural communities cohort study // Semin Arthritis Rheum. 2014. Vol. 43, N 5. P. 654–661. doi: 10.1016/j.semarthrit.2013.10.008

14. Zhang W., Doherty M., Pascual E., et al. EULAR evidence based recommendations for gout. Part I: Diagnosis. Report of a task force of the standing committee for international clinical studies including therapeutics (ESCISIT) // Ann Rheum Dis. 2006. Vol. 65, N 10. P. 1301–1311. doi: 10.1136/ard.2006.055251

15. Kienhorst L.B., Janssens H.J., Eijgelaar R.S., et al. The detection of monosodium urate crystals in synovial fluid after long-term and varying storage conditions // Joint Bone Spine. 2015. Vol. 82, N 6. P. 470–471. doi: 10.1016/j.jbspin.2014.10.020

16. Секреты ревматологии / под ред. С.Д. Уэст. Пер. с англ. под ред. О.М. Лесняк. Москва: ГЭОТАР-Медиа, 2021. 756 с.

17. Malik A., Schumacher H.R., Dinnella J.E., Clayburne G.M. Clinical diagnostic criteria for gout: Comparsion with the gold standard of synovial fluid crystal analysis // J Clin Rheumatol. 2009. Vol. 15, N 1. P. 22–24. doi: 10.1097/RHU.0b013e3181945b79

18. Pascal Z., Valcov R., Fabreguet I., et al. A prospective evaluation of ultrasound as a diagnostic tool in acute microcrystalline arthritis // Arthritis Res Ther. 2015. Vol. 17, N 1. P. 1–8. doi: 10.1186/s13075-015-0701-7

19. Omoumi P., Becce F., Racine D., et al. Dual-Energy CT: Basic principles, technical approaches, and applications in musculoskeletal imaging (Part 1) // Semin Musculoskelet Radiol. 2015. Vol. 19, N 5. P. 431–437. doi: 10.1055/s-0035-1569253

20. Ogdie A., Taylor W.J., Weatherall M., et al. Imaging modalities for the classification of gout: Systematic literature review and meta-analysis // Ann Rheum Dis. 2015. Vol. 74, N 10. P. 1868–1874. doi: 10.1136/annrheumdis-2014-205431

21. Sapsford M., Gamble G.D., Aati O., et al. Relationship of bone erosion with the urate and soft tissue components of the tophus in gout: A dual energy computed tomography study // Rheumatology (Oxford). 2017. Vol. 56, N 1. P. 129–133. doi: 10.1093/rheumatology/kew383

22. Towiwat P., Doyle A.J., Gamble G.D., et al. Urate crystal deposition and bone erosion in gout: "Inside-out" or "outside-in"? A dual-energy computed tomography study // Arthritis Res Ther. 2016. Vol. 18, N 1. P. 208. doi: 10.1186/s13075-016-1105-z

23. Bayat S., Aati O., Rech J., et al. Development of a dual-energy computed tomography scoring system for measurement of urate deposition in gout // Arthritis Care Res (Hoboken). 2016. Vol. 68, N 6. P. 769–775. doi: 10.1002/acr.22754

24. Rajiah P., Sundaram M., Subhas N. Dual-energy CT in musculoskeletal imaging: What is the role beyond gout? // AJR Am J Roentgenol. 2019. Vol. 213, N 3. P. 493–505. doi: 10.2214/AJR.19.21095

25. Климкова М.М., Синицын В.Е., Мазуренко Д.А., и др. Перспективы применения двухэнергетической компьютерной томографии в диагностике мочекаменной болезни и определении химического состава мочевых камней (обзор литературы) // Медицинская визуализация. 2016. № 6. С. 84–92.

26. McCollough C.H., Leng S., Yu L., et al. Principles, technical approaches, and clinical applications // Radiology. 2015. Vol. 276, N 3. P. 637–653. doi: 10.1148/radiol.2015142631

27. Sodickson A.D., Keraliya A., Czakowski B., et al. Dual energy CT in clinical routine: How it works and how it adds value // Emerg Radiol. 2021. Vol. 28, N 1. P. 103–117. doi: 10.1007/s10140-020-01785-2

28. Megibow A.J., Kambadakone A., Ananthakrishnan L. Dual-energy computed tomography: Image acquisition, processing, and workflow // Radiol Clin North Am. 2018. Vol. 56, N 4. P. 507–520. doi: 10.1016/j.rcl.2018.03.001

29. Forghani R., De Man B., Gupta R. Dual-energy computed tomography: Physical principles, approaches to scanning, usage, and

implementation: Part 2 // Neuroimaging Clin N Am. 2017. Vol. 27, N 3. P. 385–400. doi: 10.1016/j.nic.2017.03.002
30. Henzler T., Fink C., Schoenberg S.O., et al. Radiation dose aspects // AJR Am J Roentgenol. 2012. Vol. 199, N 5. P. S16–S25. doi: 10.2214/AJR.12.9210
31. Borges A.P., Antunes C., Curvo-Semedo L. Pros and cons of dual-energy CT systems: "One does not fit all" // Tomography. 2023. Vol. 9, N 1. P. 195–216. doi: 10.3390/tomography9010017
32. Parakh A., Lennartz S., An C., et al. Dual-energy CT images: Pearls and pitfalls // Radiographics. 2021. Vol. 41, N 1. P. 98–119. doi: 10.1148/rg.2021200102
33. Gosangi B., Mandell M.C., Weaver M.J., et al. Bone marrow edema at dual-energy CT: A game changer in the emergency department // Radiographics. 2020. Vol. 40, N 3. P. 859–874. doi: 10.1148/rg.2020190173
34. Goo H.W., Goo J.M. Dual-energy CT: New horizon in medical imaging // Korean J Radiol. 2017. Vol. 18, N 4. P. 555–569. doi: 10.3348/kjr.2017.18.4.555
35. Baer A.N., Kurano T., Thakur U.J., et al. Dual-energy computed tomography has limited sensitivity for non-tophaceous gout: A comparison study with tophaceous gout // BMC Musculoskelet Disord. 2016. Vol. 17, N 1. P. 1–9. doi: 10.1186/s12891-016-0943-9
36. Bongartz T., Glazebrook K.N., Kavros S.J., et al. Dual-energy CT for the diagnosis of gout: An accuracy and diagnostic yield study // Ann Rheum Dis. 2015. Vol. 74, N 6. P. 1072–1077. doi: 10.1136/annrheumdis-2013-205095
37. Huppertz A., Hermann A., Diekhoff T., et al. Systemic staging for urate crystal deposits with dual-energy CT and ultrasound in patients with suspected gout // Rheumatol Int. 2014. Vol. 3. P. 763–771. doi: 10.1007/s00296-014-2979-19
38. Strobl S., Halpern E.J., Abd Ellah M., et al. Acute gouty knee arthritis: Ultrasound findings compared with dual-energy CT findings // AJR Am J Roentgenol. 2018. Vol. 210, N 6. P. 1323–1329. doi: 10.2214/AJR.17.19199
39. Mallinson P.I., Coupal T., Reisinger C., et al. Artifacts in dual-energy CT gout protocol: A review of 50 suspected cases with an artifact identification guide // AJR Am J Roentgenol. 2014. Vol. 203, N 1. P. 103–109. doi: 10.2214/AJR.13.11396
40. Omoumi P., Zufferey P., Malghem J., So A. Imaging in gout and other crystal-related arthropathies // Rheum Dis Clin North Am. 2016. Vol. 42, N 4. P. 624–644. doi: 10.1016/j.rdc.2016.07.005
41. Lee S.M., Lee J.G., Lee G., et al. CT image conversion among different reconstruction kernels without a sinogram by using a convolutional neural network // Korean J Radiol. 2019. Vol. 20, N 2. P. 295–303. doi: 10.3348/kjr.2018.0249
42. Alavandar E., Arunachalam V.K., Narappulan N., et al. Principles and available hardware in dect // J Gastrointestinal Abdominal Radiol. 2022. Vol. 5, N 6. doi: 10.1055/s-0042-1742772
43. Lee J.S., Seo W.J. What is the diagnostic value of dual-energy computed tomography in patients with clinical diagnosis of gout? // Adv Rheumatol. 2021. Vol. 61, N 1. P. 1–7. doi: 10.1186/s42358-021-00198-0
44. Jia E., Zhu J., Huang W., et al. Dual-energy computed tomography has limited diagnostic sensitivity for short-term gout // Clin Rheumatol. Vol. 37, N 3. P. 773–777. doi: 10.1007/s10067-017-3753-z
45. Ramon A., Ornetti P. Dual energy computed tomography: A breakthrough for gout? // Joint Bone Spine. 2020. Vol. 87, N 4. P. 289–291. doi: 10.1016/j.jbspin.2019.12.002
46. Shang J., Li X.H., Lu S.Q., et al. Gout of feet and ankles in different disease durations: Diagnostic value of single-source DECT and evaluation of urate deposition with a novel semi-quantitative DECT scoring system // Adv Rheumatol. 2021. Vol. 61, N 1. P. 1–14. doi: 10.1186/s42358-021-00194-4
47. Wang P., Smith S.E., Garg R., et al. Identification of monosodium urate crystal deposits in patients with asymptomatic hyperuricemia using dual-energy CT // RMD Open. 2018. Vol. 4, N 1. P. 593–597. doi: 10.1136/rmdopen-2017-000593
48. Urano W., Yamanaka H., Tsutani H., et al. The inflammatory process in the mechanism of decreased serum uric acid concentrations during acute gouty arthritis // J Rheumatol. 2002. Vol. 29, N 9. P. 1950–1953.
49. Dalbeth N., Nicolaou S., Baumgartner S., et al. Presence of monosodium urate crystal deposition by dual-energy CT in patients with gout treated with allopurinol // Ann Rheum Dis. 2018. Vol. 77, N 3. P. 364–370. doi: 10.1136/annrheumdis-2017-212046
50. Zhang W., Doherty M., Bardin T., et al. European league against rheumatism recommendations for calcium pyrophosphate deposition. Part I: Terminology and diagnosis // Ann Rheum Dis. 2011. Vol. 70, N 4. P. 563–570. doi: 10.1136/ard.2010.139105
51. Sabchyshyn V., Konon I., Ryan L.M., Rosenthal A.K. Concurrence of rheumatoid arthritis and calcium pyrophosphate deposition disease: A case collection and review of the literature // Semin Arthritis Rheum. 2018. Vol. 48, N 1. P. 9–11. doi: 10.1016/j.semarthrit.2017.11.009
52. Williams C.J., Rosenthal A.K. Pathogenesis of calcium pyrophosphate deposition disease // Best Pract Res Clin Rheumatol. 2021. Vol. 35, N 4. P. 101718. doi: 10.1016/j.berh.2021.101718
53. Abhishek A. Calcium pyrophosphate deposition // Br J Hosp Med (Lond). 2014. Vol. 75, N 4. P. 61–64. doi: 10.12968/hmed.2014.75.sup4.c61
54. Miksanek J., Rosenthal A.K. Imaging of calcium pyrophosphate deposition disease // Curr Rheumatol Rep. 2015. Vol. 17, N 3. P. 20. doi: 10.1007/s11926-015-0496-1
55. Godfrin-Valnet M., Godfrin G., Godard J., et al. Eighteen cases of crowned dens syndrome: Presentation and diagnosis // Neurochirurgie. 2013. Vol. 59, N 3. P. 115–120. doi: 10.1016/j.neuchi.2013.03.003
56. Cipolletta E., Filippou G., Scirè C.A., et al. The diagnostic value of conventional radiography and musculoskeletal ultrasonography in calcium pyrophosphate deposition disease: A systematic literature review and meta-analysis // Osteoarthritis Cartilage. 2021. Vol. 29, N 5. P. 619–632. doi: 10.1016/j.joca.2021.01.007
57. Lee K.A., Lee S.H., Kim H.R. Diagnostic value of ultrasound in calcium pyrophosphate deposition disease of the knee joint // Osteoarthritis Cartilage. 2019. Vol. 27, N 5. P. 781–787. doi: 10.1016/j.joca.2018.11.013
58. Neame R.L., Carr A.J., Muir K., Doherty M. UK community prevalence of knee chondrocalcinosis: Evidence that correlation with osteoarthritis is through a shared association with osteophyte // Ann Rheum Dis. 2003. Vol. 62, N 6. P. 513–518. doi: 10.1136/ard.62.6.513
59. Frediani B., Filippou G., Falsetti P., et al. Diagnosis of calcium pyrophosphate dihydrate crystal deposition disease: Ultrasonographic criteria proposed // Ann Rheum Dis. 2005. Vol. 64, N 4. P. 638–640. doi: 10.1136/ard.2004.024109
60. Tanikawa H., Ogawa R., Okuma K., et al. Detection of calcium pyrophosphate dihydrate crystals in knee meniscus by dual-energy computed tomography // J Orthop Surg Res. 2018. Vol. 13, N 1. P. 73. doi: 10.1186/s13018-018-0787-0

61. Rosales-Alexander J.L., Aznar J.B., Magro-Checa C. Calcium pyrophosphate crystal deposition disease: Diagnosis and treatment // Open Access Rheumatol. 2014. Vol. 6. P. 39–47. doi: 10.2147/OARRR.S39039
62. Sekijima Y., Yoshida T., Ikeda S.I. CPPD crystal deposition disease of the cervical spine: A common cause of acute neck pain encountered in the neurology department // J Neurol Sci. 2010. Vol. 296, N 1-2. P. 79–82. doi: 10.1016/j.jns.2010.05.028
63. Kravchenko D., Karakostas P., Kuetting D., et al. The role of dual energy computed tomography in the differentiation of acute gout flares and acute calcium pyrophosphate crystal arthritis // Clin Rheumatol. 2022. Vol. 41, N 1. P. 223–233. doi: 10.1007/s10067-021-05949-4
64. Tedeschi S.K., Solomon D.H., Yoshida K., et al. A prospective study of dual-energy CT scanning, US and X-ray in acute calcium pyrophosphate crystal arthritis // Rheumatology (Oxford). 2020. Vol. 59, N 4. P. 900–903. doi: 10.1093/rheumatology/kez431
65. Pascart T., Norberciak L., Legrand J., et al. Dual-energy computed tomography in calcium pyrophosphate deposition: Initial clinical experience // Osteoarthritis Cartilage. 2019. Vol. 27, N 9. P. 1309–1314. doi: 10.1016/j.joca.2019.05.007

AUTHORS' INFO

*** Maria V. Onoyko;**
address: 27 Lomonosovsky prospekt, 119234 Moscow, Russia;
ORCID: 0000-0002-7727-3360;
e-mail: onoykomary@gmail.com

Elena A. Mershina, MD, Cand. Sci. (Med), Associate Professor;
ORCID: 0000-0002-1266-4926;
eLibrary SPIN: 6897-9641;
e-mail: elena_mershina@mail.ru

Olga A. Georginova, MD, Cand. Sci. (Med), Assistant Professor;
ORCID: 0000-0002-7542-8189;
eLibrary SPIN: 8331-3656;
e-mail: olga.georginova@gmail.com

Maria L. Plotnikova;
ORCID: 0000-0001-7533-9867;
e-mail: maria_plotnikova@inbox.ru

Alexandra V. Panyukova;
ORCID: 0000-0002-5367-280X;
e-mail: panyukovaalexandra@gmail.com

Valentin E. Sinitsyn, MD, Dr. Sci. (Med), Professor;
ORCID: 0000-0002-5649-2193;
eLibrary SPIN: 8449-6590;
e-mail: vsini@mail.ru

ОБ АВТОРАХ

*** Онойко Мария Викторовна;**
адрес: Россия, 119234, Москва, Ломоносовский пр-т, д. 27;
ORCID: 0000-0002-7727-3360;
e-mail: onoykomary@gmail.com

Мершина Елена Александровна, канд. мед. наук, доцент;
ORCID: 0000-0002-1266-4926;
eLibrary SPIN: 6897-9641;
e-mail: elena_mershina@mail.ru

Георгинова Ольга Анатольевна, канд. мед. наук, доцент;
ORCID: 0000-0002-7542-8189;
eLibrary SPIN: 8331-3656;
e-mail: olga.georginova@gmail.com

Плотникова Мария Леонидовна;
ORCID: 0000-0001-7533-9867;
e-mail: maria_plotnikova@inbox.ru

Панюкова Александра Вадимовна;
ORCID: 0000-0002-5367-280X;
e-mail: panyukovaalexandra@gmail.com

Синицын Валентин Евгеньевич, д-р мед. наук, профессор;
ORCID: 0000-0002-5649-2193;
eLibrary SPIN: 8449-6590;
e-mail: vsini@mail.ru

* Corresponding author / Автор, ответственный за переписку

DOI: https://doi.org/10.17816/DD322846

Лучевые методы в диагностике первичной и рецидивной злокачественной струмы яичников: клинический случай

Н.В. Нуднов, С.В. Ивашина, С.П. Аксенова

Российский научный центр рентгенорадиологии, Москва, Российская Федерация

АННОТАЦИЯ

Представлено редкое клинико-диагностическое наблюдение первичной и рецидивной злокачественной струмы яичников.

Злокачественная струма правого яичника выявлена через 2 года после хирургического лечения первичной доброкачественной струмы левого яичника. Спустя полгода у пациентки выявлен рецидив заболевания, визуализируемый исключительно по данным радиоизотопных методов исследования. Визуализация рецидивных очагов по брюшине на ультразвуковом исследовании была отмечена на четвёртом году противоопухолевого лечения. По данным ультразвукового исследования, по брюшине малого таза на всём протяжении визуализировались множественные солидные опухолевые очаги изо-гипоэхогенной структуры с наличием локусов низко- и умеренно скоростного кровотока даже в мелких очагах: скорость кровотока (peak systolic velocity, PS) была в диапазоне от 2 до 9 см/сек, максимальный индекс сосудистого сопротивления (resistivity index, RI max) — 0,53. На протяжении 4 лет пациентке проводилась радиойодтерапия ^{131}I активностью 6,0 ГБк. Состояние пациентки на фоне проводимого лечения удовлетворительное.

Ключевые слова: ультразвуковое исследование; трёхмерная ангиография; ультразвуковая томография; энергетическое допплеровское картирование; МРТ; рецидив; злокачественная струма яичника; перитонеальный струмоз.

Как цитировать

Нуднов Н.В., Ивашина С.В., Аксенова С.П. Лучевые методы в диагностике первичной и рецидивной злокачественной струмы яичников: клинический случай // *Digital Diagnostics.* 2023. Т. 4, № 2. С. 214–225. DOI: https://doi.org/10.17816/DD322846

Рукопись получена: 12.04.2023 **Рукопись одобрена:** 16.05.2023 **Опубликована:** 30.05.2023

DOI: https://doi.org/10.17816/DD322846

Radiation methods in the diagnosis of primary and recurrent malignant ovarian struma: A case report

Nikolai V. Nudnov, Svetlana V. Ivashina, Svetlana P. Aksenova

Russian Scientific Center of Roentgenoradiology, Moscow, Russian Federation

ABSTRACT

We provide a rare clinical and diagnostic observation of primary and recurring malignant ovarian struma.

Malignant struma of the right ovary was detected 2 years after surgical treatment of primary benign struma of the left ovary. Six months later, the patient was diagnosed with a disease relapse, visualized exclusively according to radioisotope research methods. In the fourth year of anticancer treatment, ultrasonography revealed recurring foci along the peritoneum. According to the ultrasound data on the pelvic peritoneum and the projection of the removed right ovary, multiple solid nodes with high blood flow were visualized. Peak systolic velocity ranged from 2 to 9 cm/s in minor lesions from 4 to 12 mm, with an RI max of 0.53. For 4 years, the patient underwent radioiodine therapy with ^{131}I with an activity of 6.0 GBq; the patient's condition during the treatment was satisfactory.

Keywords: 3D angiography; magnetic resonance imaging; malignant struma ovarii; peritoneal strumosis; power Doppler mapping; relapse; ultrasound; ultrasound tomography.

To cite this article

Nudnov NV, Ivashina SV, Aksenova SP. Radiation methods in the diagnosis of primary and recurrent malignant ovarian struma: A case report. *Digital Diagnostics.* 2023;4(2):214–225. DOI: https://doi.org/10.17816/DD322846

Received: 12.04.2023 **Accepted:** 16.05.2023 **Published:** 30.05.2023

DOI: https://doi.org/10.17816/DD322846

放射治疗方法在原发性和复发性恶性卵巢甲状腺肿诊断中的应用：临床病例

Nikolai V. Nudnov, Svetlana V. Ivashina, Svetlana P. Aksenova

Russian Scientific Center of Roentgenoradiology, Moscow, Russian Federation

简评

本文介绍了一个罕见的原发性和复发性恶性卵巢甲状腺肿的临床诊断观察。

右侧卵巢的恶性甲状腺肿是在左侧卵巢的原发性良性甲状腺肿手术治疗2年后发现的。6个月后，患者出现了只有放射性同位素技术数据才能观察到的疾病复发。在抗肿瘤治疗的第四年，超声检查发现了复发的腹膜病灶。根据超声检查，在全体盆腔腹膜上可以看到多个等渗及低回声结构的实体肿瘤病灶，存在低到中等速度的血流病灶，即使是小病灶：血流速度（peak systolic velocity，PS）在2到9cm/s之间，最大血管阻力指数（resistivity index，RI max）为0.53。患者曾接受放射性碘治疗^{131}I，活性为6.0GBq，治疗了4年。在治疗的背景下，患者的情况是令人满意的。

关键词：超声检查；三维血管造影；超声层析成像；能量多普勒成像；MRI；复发；恶性卵巢甲状腺肿；腹膜甲状腺肿。

To cite this article

Nudnov NV, Ivashina SV, Aksenova SP. 放射治疗方法在原发性和复发性恶性卵巢甲状腺肿诊断中的应用：临床病例. *Digital Diagnostics*. 2023;4(2):214–225. DOI: https://doi.org/10.17816/DD322846

收到：12.04.2023 **接受：**16.05.2023 **发布日期：**30.05.2023

INTRODUCTION

Malignant struma ovarii is a rare disease referred as monodermal teratomas and somatic-type tumors (WHO Classification of Tumours, 2020) [1].

Major contributions to the knowledge about this condition were made in the late 19th century. Richard Böttlin was the first to describe thyroid tissue in the ovary in 1889, whereas struma ovarii was first characterized by Clemens von Kalden in 1895. The term "struma ovarii colloides" came into common use thanks to Julius Robert von Meyer. At about the same time, Ludwig Pick supposed that thyroid elements in "ovarian goiter" may be transformed. Over time, the whole range of thyroid disorders was characterized for struma ovarii, including nodular goiter, toxic goiter, auto-immune thyroiditis, adenoma, and carcinoma [2, 3].

Moreover, 90%–95% of struma ovarii cases are benign, and carcinoma is very rare in its setting. Available clinical and diagnostic data on struma ovarii is primarily descriptive [3–11].

The timely diagnosis of struma ovarii plays a key role in patients of reproductive age who plan to preserve fertility because the extent of surgical treatment varies based on the histological subtype of this condition. Although laparoscopic oophorectomy or ovarian resection may be considered for benign struma ovarii, malignant struma ovarii may require the removal of the uterus and its appendages and resection of the greater omentum [8]. A study showed that the average time from the initial diagnosis of struma ovarii (both benign and malignant) to advanced malignancy ranged from 2 to 9 years [2].

Considering that ovarian goiter is a neoplasm rather than hypertrophy of the ovarian stroma, as it is the case in the thyroid gland, its dissemination and metastatic potential to other organs support the point made in the latest 2020 World Health Organization Classification of Female Genital Tumors: "Peritoneal implants well-differentiated thyroid tissue in a patient with a histologically benign struma ovarii, known as "peritoneal strumosis," is currently considered to be a metastasis of a well-differentiated follicular carcinoma originating in the struma ovarii" [1, 12]. The 5-year survival rate of patients treated with radioactive iodine (iodine-131, ^{131}I) was higher than that of untreated patients (94.9 vs. 64.8%) [4, 10].

Medical database (PubMed and Medline) search identified studies of ultrasound (US) or magnetic resonance imaging (MRI) patterns of malignant struma ovarii and recurrent peritoneal strumosis; however, descriptions of the disease and its perfusion features are still unclear, which was the reason for publishing this study.

CASE REPORT

Patient

This study presents the features of a case of T3cN0M0 primary recurrent malignant struma ovarii in patient R. aged 25 years.

One month after childbirth, the patient underwent a left oophorectomy for a benign struma of the left ovary and right ovarian resection for a dermoid cyst of the right ovary. She was event-free for 2 years. In 2015, diagnostic laparoscopy and biopsy of peritoneal lesions were performed for ascites and ovarian enlargement in another medical institution. The Federal State Budgetary Institution "Russian Research Center for Radiology" of the Ministry of Health of Russia (RRCR) reviewed the tissue specimen slides and revealed poorly differentiated malignant struma ovarii. In blood tests performed in 2015, thyroglobulin level was 35.156 (normal, 0–50) ng/mL; anti-thyroglobulin antibodies, 0.52 U/mL; thyroid-stimulating hormone, 0.76 ng/mL (normal, <0.2); thyroxine, 0.69 pmol/L; CA-125, 1,339.5 U/mL; human chorionic gonadotropin, 1.2 mIU/mL; and alpha fetoprotein, 2.25 IU/mL.

Investigations

After diagnostic laparoscopy and biopsy of lesions in the pelvic peritoneum performed in another medical institution, complex ultrasonography was performed at the RRCR. An inhomogeneous isohypoechoic mass with areas of an anechoic structure of irregular and rounded shape was found in the projection of the right appendages. Pronounced pathological blood flow in the solid component of the mass, ascites, and carcinomatosis of the peritoneum of the small pelvis were also found. Figure 1 shows a 3D angiogram of the primary malignant struma ovarii on the right ovary.

eSaote Pro machine US was used; the transvaginal transducer and volume transvaginal transducer were used. Ultrasonography was performed in a standard 2D mode, and high-tech US methods were then used: power Doppler mapping, US computed tomography (CT), and 3D angiography.

Figure 2 shows uneven thickening of the pelvic peritoneum covering the anterior wall of the uterus. The structure of the blastomatously altered peritoneum of the small pelvis is isohypoechoic, with ill-defined edges on the interface with the body of the uterus.

The intensity of the blood flow in the tumor lesion in the retrouterine pouch is remarkable, as well as its smoothness in the thickened (up to 5–7 mm) peritoneum of the small pelvis (Fig. 3).

In addition to US, a multiparametric MRI of the pelvic organs was performed using a high-field tomograph with a magnetic field strength of 1.5 Tesla. The MRI examination was in line with the guidelines of the European Society of Urogenital Radiology (ESUR Guidelines, 2019) and included several modes: T2-weighted imaging (T2-WI), T1-weighted imaging (T1-WI), diffusion-weighted imaging (DWI; b = 800, b = 1,400), and T1 with dynamic contrast enhancement [13].

The MRI of the malignant struma ovarii demonstrated a space-occupying predominantly solid mass of the right ovary with uneven poorly defined bumpy edges, areas of multiple cystic inclusions ranging in size from 0.7 to 3 cm with a heterogeneously increased MR signal in T1-WI,

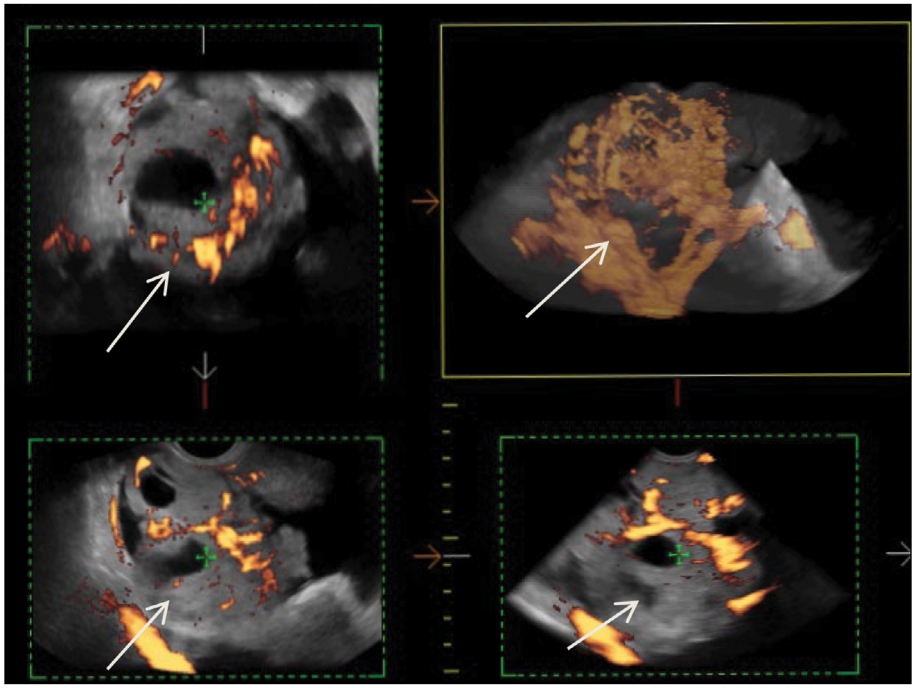

Fig. 1. 3D angiography of a poorly differentiated malignant struma ovarii on the right (arrows).

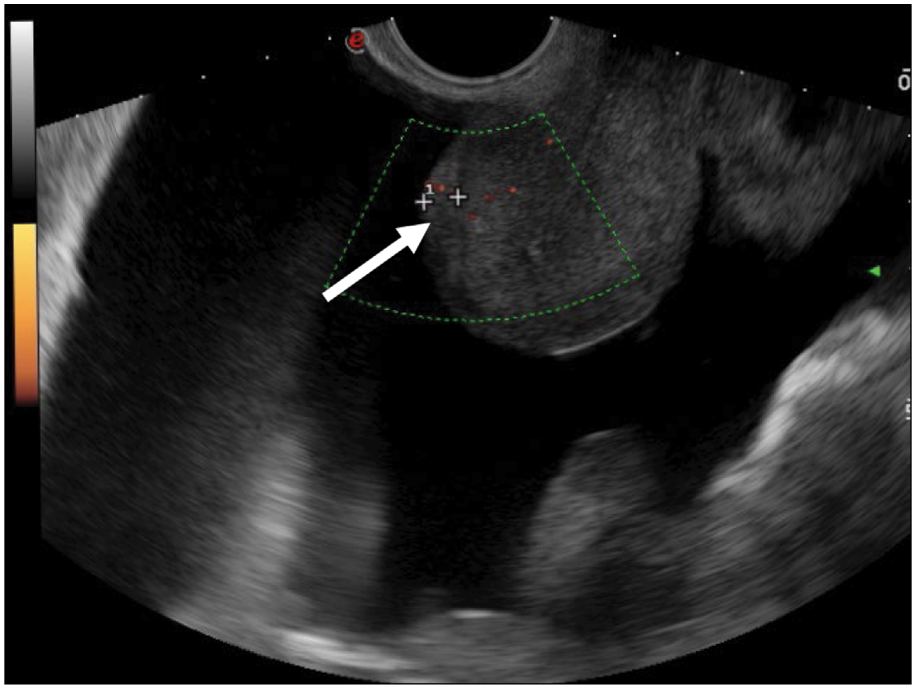

Fig. 2. Dopplerography in the energy mode. Malignant struma ovarii. Carcinomatosis of the pelvic peritoneum anterior to the uterus (arrow). The visualized tumor lesion is 6 mm thick.

heterogeneous (from hyper- to hypo-) MR signal in T2-WI, which was consistent with colloid nodules with high-protein contents of different viscosities. Solid areas of the tumor were characterized by different rates of diffusion restriction, from 0.7 to 1.4 $mm^2/s \times 10^{-3}$. Multiple nodular masses along the peritoneum of the small pelvis and diffuse thickening of the peritoneum were also detected. The paramagnetic accumulation in the tumor node along the peritoneum and nodes of the peritoneum was sharply increased in T1-WI, with suppression of the signal from the adipose tissue (Fig. 4). Meanwhile, sagittal post-contrast images clearly show the absence of paramagnetic accumulation in the colloid nodules of the malignant struma of the right ovary (Fig. 4*f*).

Three months after the extirpation of the uterus with the right appendages, omentectomy, and thyroidectomy, the US showed 5–10 mL of free fluid in the small pelvis. Based on the comprehensive US findings, the free fluid persisted for 4 years despite ongoing radioiodine therapy (^{131}I; 6.0 GBq; a total of 11 cycles); however, no lesions were detected. The

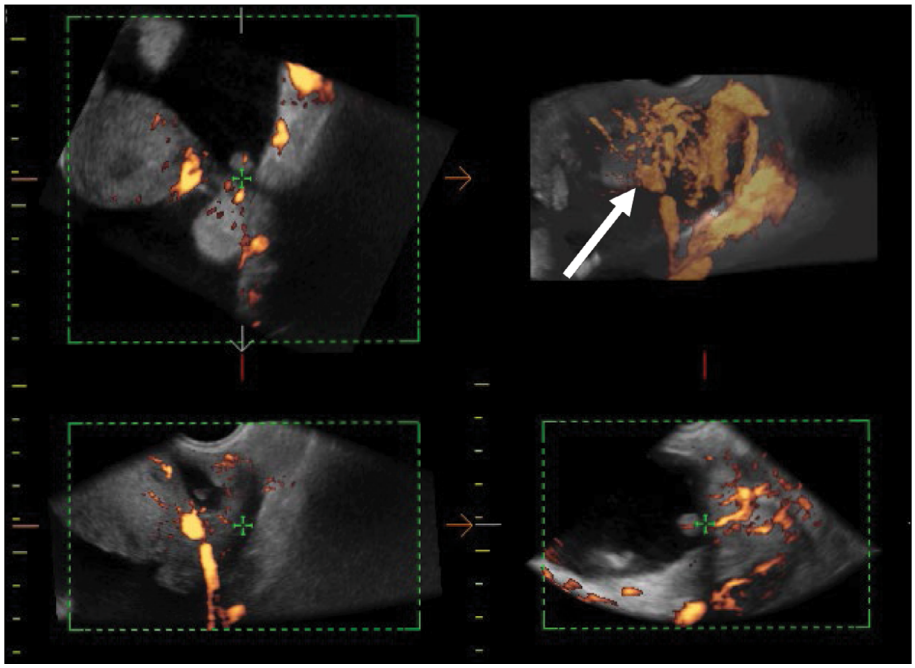

Fig. 3. 3D angiography of the malignant struma lesion along the peritoneum in the retrouterine space (arrow).

first recurrent lesion of the primary tumor along the pelvic peritoneum, visualized by US, appeared 4 years after the start of the combination therapy.

US demonstrated that the recurrent lesion of malignant struma ovarii along the pelvic peritoneum, identified in the presence of ascites, had an iso-hypoechoic structure with

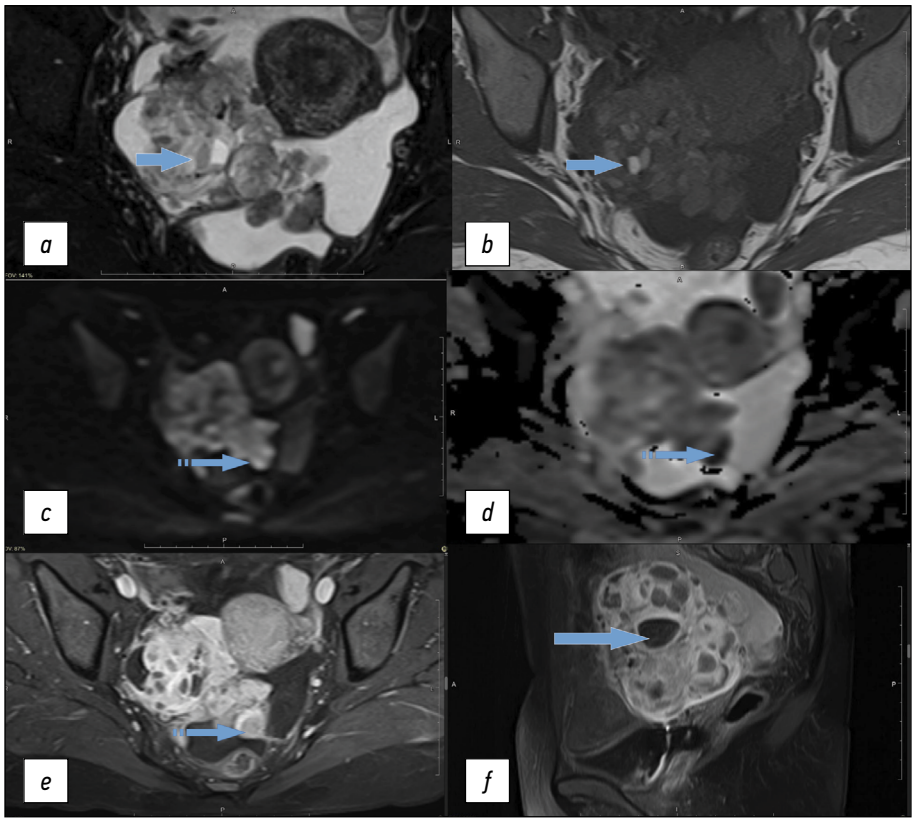

Fig. 4. Pelvic magnetic resonance images of patient R. with malignant struma of the right ovary: (*a*) T2-FS-WI in the axial plane; (*b*) T1-WI in the axial plane; (c) diffusion-weighted imaging (b = 1,000); (*d*) apparent diffusion coefficient map; (*e*) T1-FS-WI + contrast in the axial plane; (*f*) T1-FS-WI + contrast in the sagittal plane. The solid arrow indicates colloid nodules in the malignant struma of the right ovary. The dotted arrow shows lesions along the pelvic peritoneum with increased paramagnetic accumulation and restricted diffusion similar to the solid component of the primary tumor.

fuzzy contours and small size (4–12 mm). The peritoneum of the small pelvis outside the lesion was <4 mm thick; however, 3D angiography and US-CT revealed that even small blastomatous lesions were well vascularized. Blood flow was also present in the 4–5 mm thick structure of the pelvic peritoneum (Figs. 5–7).

To identify specific US signs of malignant struma ovarii, recurrent tumor lesions along the peritoneum of the malignant struma in one patient were compared with recurrent lesions of serous ovarian adenocarcinoma in 12 patients. When comparing the tumor lesions in the retrouterine space, a more pronounced neoangiogenesis was noted in the tumor lesion of the malignant struma ovarii, where the peak systolic velocity (PS) was recorded in small lesions (4–12 mm) and ranged from 2 to 9 cm/s. The maximum vascular resistivity index (RI max) was 0.53. No blood flow was noted in recurrent lesions along the pelvic peritoneum of the serous adenocarcinoma up to 9 mm, and in lesions up to 15–20 mm, PS varied from 2 to 4 cm/s or was <2 cm/s (Figs. 5 and 8).

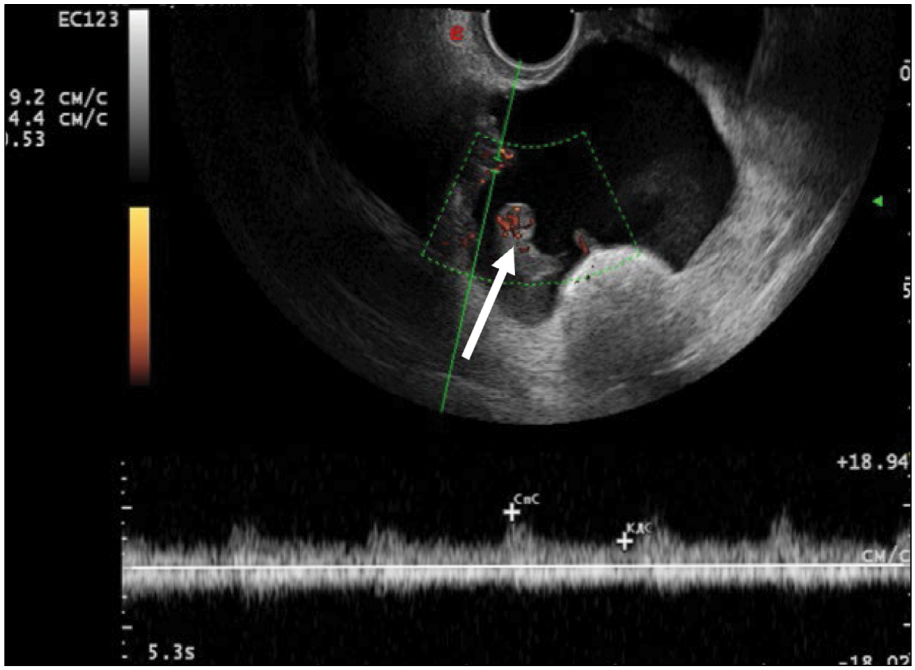

Fig. 5. Dopplerography in the energy mode. The arrows show recurrent lesions of the malignant struma ovarii.

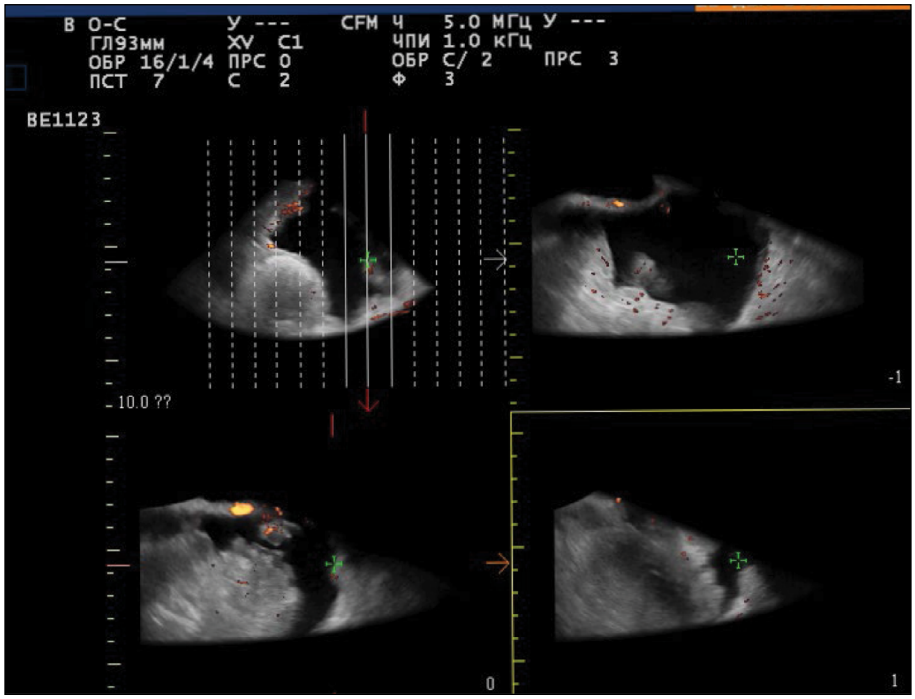

Fig. 6. US-CT of the recurrent lesions of the malignant struma ovarii.

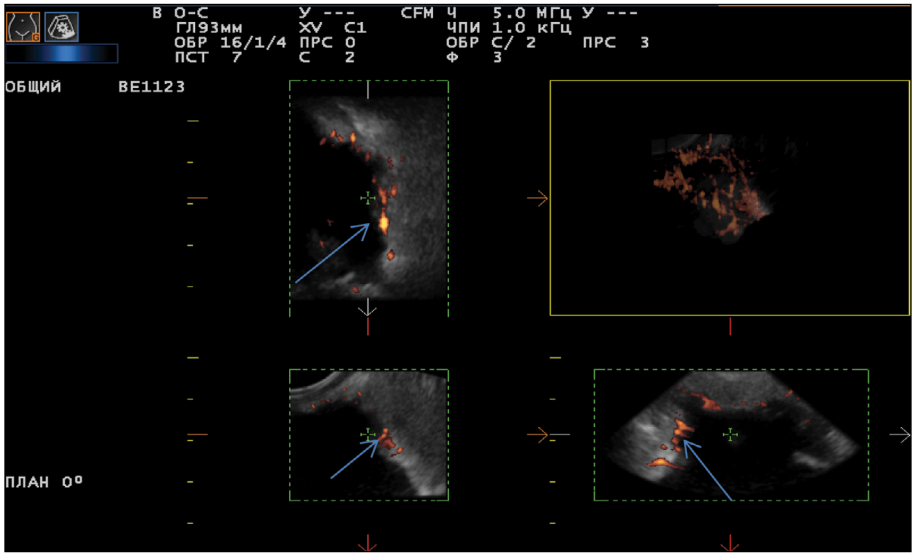

Fig. 7. 3D angiography of the recurrent lesions of the malignant struma ovarii in the pelvic peritoneum in the presence of ascites.

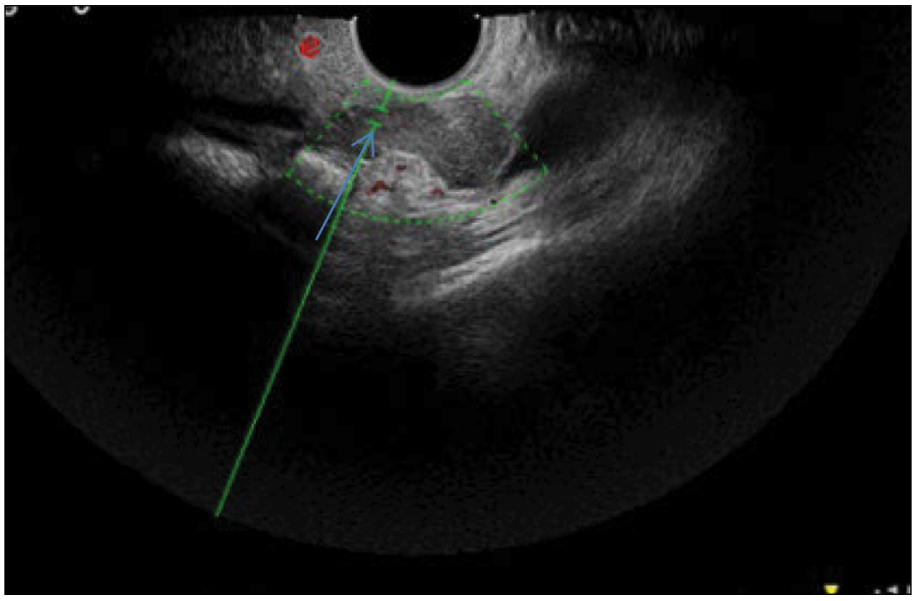

Fig. 8. Dopplerography (energy mode) of the tumor lesion along the peritoneum in the retrouterine space in a patient with stage IIIC serous ovarian cancer.

Thus, this case demonstrated that the combined MRI findings of the thyroid tissue (colloid nodules), restricted diffusion areas, and increased paramagnetic accumulation in its solid component may indicate a malignant struma ovarii. Recurrent lesions of malignant struma, even small ones (up to 4–5 mm), are well vascularized. Malignant struma of the right ovary was detected 2 years after surgical treatment of primary benign struma of the left ovary.

The somatic condition of the patient was not aggravated by ascites and persistent recurrent tumor lesions in the small pelvis.

DISCUSSION

In this study, we analyzed US and MRI signs of primary recurrent malignant struma ovarii. Our data are generally consistent with those of individual case reports of this neoplasm in the literature. US visualizes a malignant struma ovarii as a multicystic tumor with irregular septa and heterogeneous echogenic solid components. Complex US (power Doppler mapping, US-CT, and 3D angiography) show pronounced neoangiogenesis in both primary malignant struma ovarii and its small recurrent lesions. Its characteristic feature is the so-called struma pearls, i.e., well-defined rounded solid areas, which are consistent with the colloid-rich thyroid tissue [8, 14–17].

In the presented case, the tumor did not show typical MRI signs for a malignant struma ovarii; however, the MRI pattern allows suspicion of the inclusions of colloid nodules in the thyroid tissue of the solid component of the ovarian tumor. Varying degrees of restricted diffusion were observed in the solid tumor component and lesions along

the pelvic peritoneum. Extremely pronounced paramagnetic accumulation in the solid component of the tumor visualized in the post-contrast series and the absence of accumulation in the colloid nodules were pathognomonic. In the study by Gil et al. [14], MR images revealed struma ovarii as multicystic tumors with solid components, often with high T1-WI signal intensity, whereas cysts had different T2-WI signal intensities depending on fluid viscosity. Tamura et al. [17] analyzed 18 cases of struma ovarii, and their MRI study revealed a solid contrast-accumulating area that corresponded to a malignant variant of the tumor only in 54% of cases; meanwhile, restricted diffusion was established only in 11% of cases.

In the present study, restricted diffusion was heterogeneous but indicated malignant features, given the perfusion parameters in the tumor. Data similar to ours were reported by Yamauchi et al. [7]: the solid component in the malignant struma ovarii was characterized by the increased MR signal in diffusion-weighted imaging and a reduced signal in apparent diffusion coefficient maps. Thus, when compared with a pathomorphological study, the areas of the papillary carcinoma in struma ovarii corresponded to the area of true diffusion restriction in MRI.

Herein, we compared recurrent lesions of malignant struma and serous ovarian cancer. The recurrent lesions of malignant struma were similar in structure to serous ovarian cancer and had an isohypoechoic structure; however, US angiography and US-CT did not record blood flow in 4–5 mm lesions of the serous ovarian cancer. In this case, we did not register blood flow in the 4-mm lesion of serous ovarian cancer in the pelvic peritoneum. Moreover, Ranade et al. [19] reported peritoneal strumosis (struma peritonei) by US in a patient 6 years after surgical treatment of stroma ovarii, and the lesion had a mixed structure with calcifications.

Brogsitter et al. [20] reported a case of peritoneal strumosis and highlighted the role of histological examination of conditions similar to those of ovarian carcinoma. Many aspects of peritoneal strumosis remain unexplored; however, the authors suggest a connection with either rupture of mature ovarian teratoma or ovarian resection for mature ovarian teratoma. In addition, the authors noted a "slow" course of peritoneal strumosis [20]. In our case, the patient's somatic condition did not worsen for 3 years from the detection of multiple peritoneal lesions, despite the insignificant positive effect of radioiodine therapy. In the databases studied, no up-to-date observations of recurrence of malignant struma ovarii—peritoneal strumosis—were found based on MRI data.

CONCLUSION

Preoperative diagnosis of malignant struma ovarii is quite challenging. Although struma ovarii is difficult to differentiate from ovarian adenocarcinoma, US and MRI may be instrumental for the differential diagnosis.

In summary, the combination of the thyroid tissue and areas of restricted diffusion in the solid tumor component visualized in MRI may be a sign of malignant stroma ovarii. Compared with serous ovarian cancer, small (up to 4–5 mm) recurrent lesions of malignant struma ovarii along the pelvic peritoneum are even well vascularized and can be detected using US volumetric imaging in the angio mode.

ADDITIONAL INFORMATION

Funding source. This article was not supported by any external sources of funding.

Competing interests. The authors declare that they have no competing interests.

Authors' contribution. All authors made a substantial contribution to the conception of the work, acquisition, analysis, interpretation of data for the work, drafting and revising the work, final approval of the version to be published and agree to be accountable for all aspects of the work. Nudnov N.V. — concept and design of the work; agreement on the final version of the text; Ivashina S.V. — writing the text of the article, analysis of the results, preparation of illustrations; Aksenova S.P. — writing the text of the article, analysis the results, preparing illustrations; manuscript editing.

Consent for publication. Written consent was obtained from the patient for publication of relevant medical information and all of accompanying images within the manuscript in Digital Diagnostics journal.

REFERENCES

1. Female Genital Tumours. WHO Classification of Tumours, 5th Edition, vol. 4. WHO Classification of Tumours Editorial Board; 2020. Available from: https://publications.iarc.fr/Book-And-Report-Series/Who-Classification-Of-Tumours/Female-Genital-Tumours-2020. Accessed: 15.04.2023.

2. Li S, Yang T, Li X. FIGO stage IV and age over 55 years as prognostic predicators in patients with metastatic malignant struma ovarii. *Front Oncol*. 2020;(10):1983. doi: 10.3389/fonc.2020.584917

3. Roth LM, Karseladze AI. Highly differentiated follicular carcinoma arising from struma ovarii: A report of 3 cases, a review of the literature, and a reassessment of so-called peritoneal strumosis. *Int J Gynecol Pathol*. 2008;27(2):213–222. doi: 10.1097/PGP.0b013e318158e958

4. Ayhan S, Kilic F, Ersak B, et al. Malignant struma ovarii: From case to analysis *J Obstet Gynaecol Res*. 2021;47(9):3339–3351. doi: 10.1111/jog.14902

5. Kanasugi M, Nishiyama H, Sanpei M, et al. Ovarian strumal carcinoid: A case report. *Fukushima J Med Sci*. 2023;69(1):51–55. doi: 10.5387/fms.2022-22

6. Smith LP, Brubaker LW, Wolsky RJ. It does exist! Diagnosis and management of thyroid carcinomas originating in struma ovarii. *Surg Pathol Clin*. 2023;16(1):75–86. doi: 10.1016/j.path.2022.09.008

7. Yamauchi S, Kokabu T, Kataoka H, et al. Computed tomography, magnetic resonance imaging, and positron emission tomography/computed tomography findings for the diagnosis of malignant struma ovarii: A case report. *J Obstet Gynaecol Res*. 2023;49(5):1456–1461. doi: 10.1111/jog.15619
8. Yazawa R, Yazawa H, Fukuda K, Ohara M. Struma ovarii with massive ascites mimicking ovarian carcinoma treated with conservative laparoscopic surgery: A case report. *Fukushima J Med Sci*. 2023;69(1):37–43. doi: 10.5387/fms.2022-30
9. Shou L, Lu J, Yang J, et al. Follicular carcinoma originating from struma ovarii: A case report. *Medicine (Baltimore)*. 2023;102(1):e32658. doi: 10.1097/MD.0000000000032658
10. Elshafie O, Hussein S, Al Kalbani M, et al. Papillary follicular variant thyroid cancer in a malignant struma ovarii: A report of a rare case. *Endocrinol Diabetes Metab Case Rep*. 2022;2022:21-0169. doi: 10.1530/EDM-21-0169
11. Antonova IB, Fomin DK, Babaeva NA, et al. Malignant ovarian stroma. Literature review and own observation of a rare variant of the tumor. *Difficult Patient*. 2018;16(8-9):16–18. (In Russ).
12. Giovannopoulou E, Saliaris K, Kavoura E, et al. Highly differentiated follicular carcinoma of ovarian origin: A systematic review of the literature. *Curr Oncol*. 2022;29(12):9105–9116. doi: 10.3390/curroncol29120712
13. ResearchGate GmbH [Internet]. Alt C, Bharwani N, Brunesch L, et al.; ESUR Female Pelvis Imaging Working Group. Esur quick guide to female pelvis imaging [cite July 2019]. Available from: https://www.esur.org/fileadmin/content/2019/ESUR_2019_ESUR_Quick_Guide_to_Female_Pelvis_Imaging.pdf. Accessed: 15.04.2023.
14. Gil R, Cunha TM, Rolim I. Mature cystic teratoma with high proportion of solid thyroid tissue: A controversial case with unusual imaging findings. *J Radiol Case Rep*. 2017;11(7):20–30. doi: 10.3941/jrcr.v11i7.2853
15. Ozerskaya IA, Chekalova MA, Ivanov VA, Kazaryan GG. Ultrasound signs of ovarian tumors according to a standardized protocol. *Medical Imaging*. 2023;27(2):110–124. (In Russ). doi: 10.24835/1607-0763-1144
16. Fujiwara S, Tsuyoshi H, Nishimura T, et al. Precise preoperative diagnosis of struma ovarii with pseud-Meigs' syndrome mimicking ovarian cancer with the combination of ^{131}I scintigraphy and 18F-FDG PET: Case report and review of the literature. *J Ovarian Res*. 2018.11(1):11. doi: 10.1186/s13048-018-0383-2
17. Savelli L, Testa AC, Timmerman D, et al. Imaging of gynecologic disease (4): Clinical and ultrasound characteristics of struma ovarii. *Ultrasound Obstet Gynecol*. 2008;32(2):210–219. doi: 10.1002/uog.5396
18. Tamura N, Murakami K, Ozaki R, et al. Current state of management of struma ovarii and preoperative imaging features: A retrospective case series study of 18 patients at a single institution. *J Obstet Gynaecol Res*. 2023;49(3):1007–1011. doi: 10.1111/jog.15545
19. Ranade R, Rachh S, Basu S. Late Manifestation of struma peritonei and widespread functioning lesions in the setting of struma ovarii simulating highly differentiated follicular carcinoma. *J Nucl Med Technol*. 2015;43(3):231–233. doi: 10.2967/jnmt.114.149294
20. Brogsitter C, Wonsak A, Würl K, Kotzerke J. Peritoneal strumosis. *Eur J Nucl Med Mol Imaging*. 2004;31(7):1057. doi: 10.1007/s00259-004-1548-3

СПИСОК ЛИТЕРАТУРЫ

1. Female Genital Tumours. WHO Classification of Tumours, 5th Edition, vol. 4. WHO Classification of Tumours Editorial Board, 2020. Режим доступа: https://publications.iarc.fr/Book-And-Report-Series/Who-Classification-Of-Tumours/Female-Genital-Tumours-2020. Дата обращения: 15.04.2023.
2. Li S., Yang T., Li X. FIGO stage IV and age over 55 years as prognostic predicators in patients with metastatic malignant struma ovarii // Front Oncol. 2020. N 10. P. 584917. doi: 10.3389/fonc.2020.584917
3. Roth L.M., Karseladze A.I. Highly differentiated follicular carcinoma arising from struma ovarii: A report of 3 cases, a review of the literature, and a reassessment of so-called peritoneal strumosis // Int J Gynecol Pathol. 2008. Vol. 27, N 2. P. 213–222. doi: 10.1097/PGP.0b013e318158e958
4. Ayhan S., Kilic F., Ersak B., et al. Malignant struma ovarii: From case to analysis // J Obstet Gynaecol Res. 2021. Vol. 47, N 9. P. 3339–3351. doi: 10.1111/jog.14902
5. Kanasugi M., Nishiyama H., Sanpei M., et al. Ovarian strumal carcinoid: A case report // Fukushima J Med Sci. 2023. Vol. 69, N 1. P. 51–55. doi: 10.5387/fms.2022-22
6. Smith L.P., Brubaker L.W., Wolsky R.J. It does exist! Diagnosis and management of thyroid carcinomas originating in struma ovarii // Surg Pathol Clin. 2023. Vol. 16, N 1. P. 75–86. doi: 10.1016/j.path.2022.09.008
7. Yamauchi S., Kokabu T., Kataoka H., et al. Computed tomography, magnetic resonance imaging, and positron emission tomography/computed tomography findings for the diagnosis of malignant struma ovarii: A case report // J Obstet Gynaecol Res. 2023. Vol. 49, N 5. P. 1456–1461. doi: 10.1111/jog.15619
8. Yazawa R., Yazawa H., Fukuda K., Ohara M. Struma ovarii with massive ascites mimicking ovarian carcinoma treated with conservative laparoscopic surgery: A case report // Fukushima J Med Sci. 2023. Vol. 69, N 1. P. 37–43. doi: 10.5387/fms.2022-30
9. Shou L., Lu J., Yang J., et al. Follicular carcinoma originating from struma ovarii: A case report // Medicine (Baltimore). 2023. Vol. 102, N 1. P. e32658. doi: 10.1097/MD.0000000000032658
10. Elshafie O., Hussein S., Al Kalbani M., et al. Papillary follicular variant thyroid cancer in a malignant struma ovarii: A report of a rare case // Endocrinol Diabetes Metab Case Rep. 2022. Vol. 2022. P. 21-0169. doi: 10.1530/EDM-21-0169
11. Антонова И.Б., Фомин Д.К., Бабаева Н.А., и др. Злокачественная струма яичников. Обзор литературы и собственное наблюдение редкого варианта опухоли // Трудный пациент. 2018. Т. 16, № 8-9. С. 16–18.
12. Giovannopoulou E., Saliaris K., Kavoura E., et al. Highly differentiated follicular carcinoma of ovarian origin: A systematic review of the literature // Curr Oncol. 2022. Vol. 29, N 12. P. 9105–9116. doi: 10.3390/curroncol29120712
13. ResearchGate GmbH [интернет]. Alt C., Bharwani N., Brunesch L., et al.; ESUR Female Pelvis Imaging Working Group. Esur quick guide to female pelvis imaging [cite July 2019]. Режим доступа: https://www.esur.org/fileadmin/content/2019/ESUR_2019_ESUR_Quick_Guide_to_Female_Pelvis_Imaging.pdf. Дата обращения: 15.04.2023.

14. Gil R., Cunha T.M., Rolim I. Mature cystic teratoma with high proportion of solid thyroid tissue: A controversial case with unusual imaging findings // J Radiol Case Rep. 2017. Vol. 11, N 7. P. 20–30. doi: 10.3941/jrcr.v11i7.2853
15. Озерская И.А., Чекалова М.А., Иванов В.А., Казарян Г.Г. Ультразвуковые признаки опухолей яичников по стандартизованному протоколу // Медицинская визуализация. 2023. Т. 27, № 2. С. 110–124. doi: 10.24835/1607-0763-1144
16. Fujiwara S., Tsuyoshi H., Nishimura T., et al. Precise preoperative diagnosis of struma ovarii with pseud-Meigs' syndrome mimicking ovarian cancer with the combination of ^{131}I scintigraphy and 18F-FDG PET: Case report and review of the literature // J Ovarian Res. 2018. Vol. 11, N 1. P. 11. doi: 10.1186/s13048-018-0383-2
17. Savelli L., Testa A.C., Timmerman D., et al. Imaging of gynecologic disease (4): Clinical and ultrasound characteristics of struma ovarii. *Ultrasound Obstet Gynecol.* 2008. Vol. 32, N 2. P. 210–219. doi: 10.1002/uog.5396
18. Tamura N., Murakami K., Ozaki R., et al. Current state of management of struma ovarii and preoperative imaging features: A retrospective case series study of 18 patients at a single institution // J Obstet Gynaecol Res. 2023. Vol. 49, N 3. P. 1007–1011. doi: 10.1111/jog.15545
19. Ranade R., Rachh S., Basu S. Late manifestation of struma peritonei and widespread functioning lesions in the setting of struma ovarii simulating highly differentiated follicular carcinoma // J Nucl Med Technol. 2015. Vol. 43, N 3. P. 231–233. doi: 10.2967/jnmt.114.149294
20. Brogsitter C., Wonsak A., Würl K., Kotzerke J. Peritoneal strumosis // Eur J Nucl Med Mol Imaging. 2004. Vol. 31, N 7. P. 1057. doi: 10.1007/s00259-004-1548-3

AUTHORS' INFO

*** Nikolai V. Nudnov,** MD, Dr. Sci. (Med), Professor;
address: 86 Profsoyuznaya street, 117997 Moscow, Russia;
ORCID: 0000-0001-5994-0468;
eLibrary SPIN: 3018-2527;
e-mail: nudnov@rncrr/ru

Svetlana V. Ivashina, MD, Cand. Sci. (Med),
Senior Research Associate;
ORCID: 0000-0002-9287-2636;
eLibrary SPIN: 7829-2899;
e-mail: s.ivashina@bk.ru

Svetlana P. Aksenova, MD, Cand. Sci. (Med), Research Associate;
ORCID: 0000-0003-2552-5754;
eLibrary SPIN: 4858-4627;
e-mail: fabella@mail.ru

ОБ АВТОРАХ

*** Нуднов Николай Васильевич,** д-р мед. наук, профессор;
адрес: Россия, 117997, Москва, ул. Профсоюзная, д. 86;
ORCID: 0000-0001-5994-0468;
eLibrary SPIN: 3018-2527;
e-mail: nudnov@rncrr/ru

Ивашина Светлана Вячеславовна, к.м.н.,
ст. науч. сотр.;
ORCID: 0000-0002-9287-2636;
eLibrary SPIN: 7829-2899;
e-mail: s.ivashina@bk.ru

Аксенова Светлана Павловна, к.м.н., науч. сотр.;
ORCID: 0000-0003-2552-5754;
eLibrary SPIN: 4858-4627;
e-mail: fabella@mail.ru

* Corresponding author / Автор, ответственный за переписку

DOI: https://doi.org/10.17816/DD289714

Мальформация Абернети: клинический случай

А.В. Панюкова[1], В.Е. Синицын[1], Е.А. Мершина[1], Н.А. Ручьёва[2]

[1] Московский государственный университет имени М.В. Ломоносова, Медицинский научно-образовательный центр, Москва, Российская Федерация
[2] Национальный медицинский исследовательский центр трансплантологии и искусственных органов имени академика В.И. Шумакова, Москва, Российская Федерация

АННОТАЦИЯ

Врождённые портокавальные шунты — редкие сосудистые аномалии, связанные с частичным или полным отведением портальной крови в системный кровоток. Врождённые внепечёночные портокавальные шунты называются мальформацией Абернети. Ввиду низкой частоты встречаемости и разнообразия клинических проявлений выявление данной патологии представляет диагностическую проблему.

В статье описан клинический случай мальформации Абернети типа Ib у 15-летнего пациента с длительным анамнезом повышенного артериального давления, рецидивирующими носовыми кровотечениями, болью в груди, головокружением, одышкой, низкой толерантностью к физической нагрузке, эпизодами крови в стуле, болью в эпигастральной области, тошнотой и зудом. В результате проведённого комплексного обследования у пациента была диагностирована аномалия развития портальной системы: расширенный кондуит воротной вены, впадающий непосредственно в нижнюю полую вену. Выявлены также множественные узлы в паренхиме печени, расширение камер сердца, гипертрофия миокарда и лёгочная гипертензия. Учитывая выраженность симптомов, размеры и тип шунта, междисциплинарным консилиумом рекомендована трансплантация печени.

В статье рассматриваются алгоритмы диагностики и другие возможные варианты лечения аномалий развития портальной системы.

Ключевые слова: клинический случай; сосудистые мальформации; врождённые внепечёночные портосистемные шунты; мальформация Абернети; КТ-ангиография.

Как цитировать

Панюкова А.В., Синицын В.Е., Мершина Е.А., Ручьёва Н.А. Мальформация Абернети: клинический случай // *Digital Diagnostics*. 2023. Т. 4, № 2. С. 226–237. DOI: https://doi.org/10.17816/DD289714

Рукопись получена: 06.03.2023 **Рукопись одобрена:** 03.04.2023 **Опубликована:** 12.05.2023

DOI: https://doi.org/10.17816/DD289714

Abernethy malformation: A case report

Alexandra V. Panyukova[1], Valentin E. Sinitsyn[1], Elena A. Mershina[1], Natalia A. Rucheva[2]

[1] Lomonosov Moscow State University, Medical Research and Educational Center, Moscow, Russian Federation
[2] V.I. Shumakov National Medical Research Center of Transplantology and Artificial Organs, Moscow, Russian Federation

ABSTRACT

Congenital portosystemic shunts are rare congenital vascular anomalies associated with partial or complete portal blood diversion into the systemic circulation. Congenital extrahepatic portosystemic shunts, termed Abernethy malformation, are a diagnostic challenge owing to its low incidence and clinical presentations. We report a case of Abernethy malformation type Ib in a 15-year-old male with a history of chronic epigastric pain and nausea, high arterial blood pressure, recurrent nose bleeds, chest pain, dizziness, dyspnea, low exercise tolerance, hematochezia, and itching. Imaging studies revealed a dilated portal vein conduit flowing into the inferior vena cava, bypassing the porta hepatis. Other findings included multiple liver nodules, heart chamber dilatation, myocardial hypertrophy, and pulmonary hypertension. Because of the severity of the patient's symptoms and shunt anatomy, liver transplantation was recommended after multidisciplinary panel consultations. Further, diagnostic algorithms and other treatment options are discussed.

Keywords: Case report; vascular malformations; congenital extrahepatic portosystemic shunt; Abernethy malformation; computed tomography angiography.

To cite this article

Panyukova AV, Sinitsyn VE, Mershina EA, Rucheva NA. Abernethy malformation: A case report. *Digital Diagnostics.* 2023;4(2):226–237.
DOI: https://doi.org/10.17816/DD289714

Received: 06.03.2023 **Accepted:** 03.04.2023 **Published:** 12.05.2023

DOI: https://doi.org/10.17816/DD289714

Abernethy畸形：临床病例

Alexandra V. Panyukova[1], Valentin E. Sinitsyn[1], Elena A. Mershina[1], Natalia A. Rucheva[2]

[1] Lomonosov Moscow State University, Medical Research and Educational Center, Moscow, Russian Federation
[2] V.I. Shumakov National Medical Research Center of Transplantology and Artificial Organs, Moscow, Russian Federation

简评

先天性肝外门腔分流是与部分或全部门静脉血转入全身血液有关的罕见血管异常。先天性肝外门腔分流被称为Abernethy畸形。由于发病率低并临床表现多样，这种病理的识别是一个诊断问题。

本文描述了一个15岁患者的Ib型Abernethy畸形的临床病例，该患者长期有高血压、反复鼻出血、胸痛、头晕、呼吸困难、运动耐力低下、便血、上腹痛、恶心和瘙痒等病史。经过全面检查，患者被诊断为门静脉系统异常：门静脉导管扩张，直接流入下腔静脉。还发现了肝实质中的多个结节、扩张的心腔、心肌肥厚和肺动脉高压。鉴于症状的严重性以及分流的大小和类型，一个多学科科联合会诊建议进行肝移植。

我们在本文中讨论了门静脉系统异常的诊断算法和其他可能的治疗方案。

关键词：临床病例；血管畸形；先天性肝外门腔分流；Abernethy畸形；CT血管造影。

To cite this article
Panyukova AV, Sinitsyn VE, Mershina EA, Rucheva NA. Abernethy畸形：临床病例. *Digital Diagnostics.* 2023;4(2):226–237.
DOI: https://doi.org/10.17816/DD289714

收到： 06.03.2023 **接受：** 03.04.2023 **发布日期：** 12.05.2023

INTRODUCTION

Congenital portosystemic shunts (CPSS) are rare congenital anomalies associated with partial or complete portal blood diversion into the systemic circulation. The estimated CPSS incidence is 1:30,000 births and 1:50,000 for those that persist beyond early life [7]. The classification of CPSS is complex because of the significant variability of vascular anatomy. All CPSSs are divided into intra- and extrahepatic shunts with partial or complete portal blood deprivation [27]. Congenital extrahepatic portosystemic shunts (CEPSS) are termed Abernethy malformation, first documented in 1793 by John Abernethy [1]. However, reported CEPSS cases are limited.

DESCRIPTION OF THE CASE

A 15-year-old male was admitted to the hospital for evaluation of chronic epigastric pain and nausea. He also had episodes of high arterial blood pressure (reaching 160/90 mmHg), recurrent nose bleeds, episodes of chest pain, dizziness, shortness of breath, low exercise tolerance, hematochezia, and long history of itching. His medical history was limited: 12 years prior to admission, portal hypertension was diagnosed (no medical records provided).

Liver function tests showed a mild increase in alanine aminotransferase (59.8 U/L (normal range, 13–50 IU/L)) and increased aspartate aminotransferase (67.1 U/L (15–46 IU/L)), gamma-glutamyl transferase (91 U/L (2–42 U/L)), alkaline phosphatase (316 U/L (52–171 U/L)), total bilirubin (39.2 μmol/L (3.4–17.1 μmol/L)), and direct bilirubin (12.5 μmol/L (0–5 μmol/L)); albumin was slightly decreased (40.2 g/L (41–55 g/L)). Routine blood tests and coagulation studies were normal. Further, his serum BUN, and creatinine were within reference ranges.

Transthoracic echocardiogram revealed heart chamber dilatation, myocardial hypertrophy (left ventricular wall thickness, 1.6 cm), and systolic pulmonary hypertension (pulmonary artery systolic pressure [PASP], 40 mmHg). Aortic ectasia (diameter at the level of the fibrous ring, 3.4 cm; sinuses of Valsalva, 5.1 cm; and ascending aorta, 4.0 cm) was observed. No left ventricular outflow tract stenosis or ventricular wall hypokinesia were found; left ventricular function was preserved.

Abdominal ultrasound (US) showed an enlarged liver with multiple nodules, changes in parenchymal structure, and signs of fibrosis. No prominent portal venous trunk or branches at the porta hepatis were noted. The hepatic vascular pattern was deformed with stenosis of the hepatic veins. Further findings were portal hypertension and moderate spleen enlargement.

To evaluate liver nodules, alpha-fetoprotein (AFP) tumor marker test was ordered. The AFP concentration was normal (1.72 IU/ml). Additional imaging studies were performed to confirm the diagnosis and to clarify the vascular anatomy.

Contrast-enhanced abdominal computed tomography (CT) with multiplanar reconstruction revealed that the splenic (12 mm in diameter (Figure 1)) and superior mesenteric veins fused together, forming a portal vein conduit dilated to 28 mm in diameter (Figures 2 and 3), flowing directly into the inferior vena cava (IVC), bypassing the porta hepatis (Figure 4). Moreover, moderate liver and spleen enlargement and weak heterogeneous contrast enhancement of the liver parenchyma were noted. The findings were consistent with Abernethy malformation type Ib.

CT pulmonary angiogram showed no abnormal vascular shunts, but confirmed pulmonary trunk dilatation (diameter, 40 mm) (Figure 5), heart chamber dilatation, and myocardial hypertrophy (Figure 6).

Owing to the low effectiveness of conservative treatment, severity of symptoms, and shunt anatomy, liver transplantation was recommended after multidisciplinary panel consultations. Currently, the patient is waiting for surgical intervention.

DISCUSSION

Mechanisms

The etiology and development of congenital and acquired portosystemic shunts differ significantly. CEPSSs occur because of abnormal formation or involution of the fetal

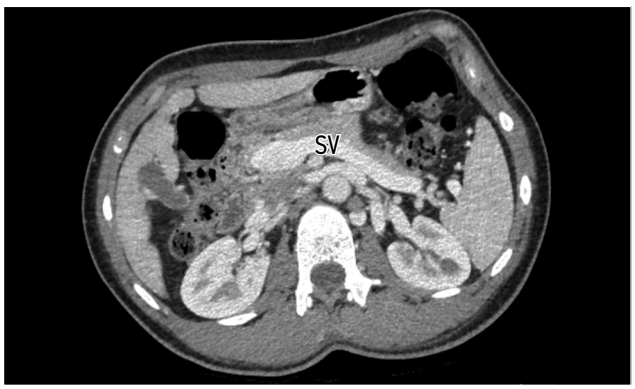

Fig. 1. Contrast-enhanced CT, portal phase, axial view. Dilated splenic vein (SV).

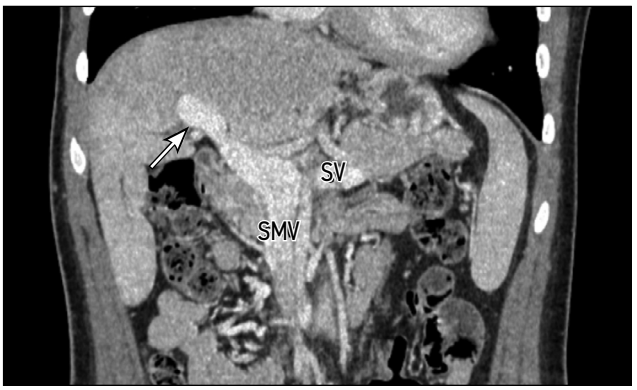

Fig. 2. Contrast-enhanced CT, portal phase, coronal view. Splenic (SV) and superior mesenteric (SMV) veins fused together, forming a portal vein conduit (white arrow).

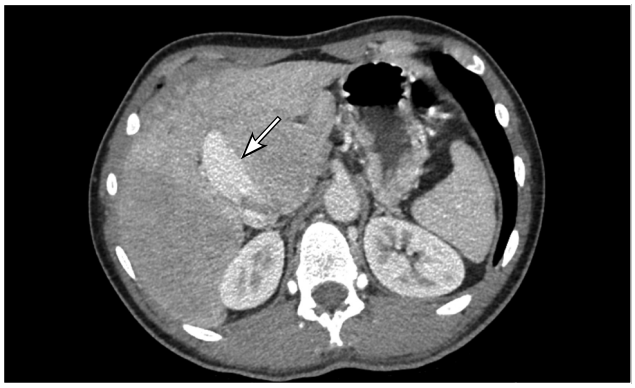

Fig. 3. Contrast-enhanced CT, portal phase, axial view. Portal vein conduit (white arrow).

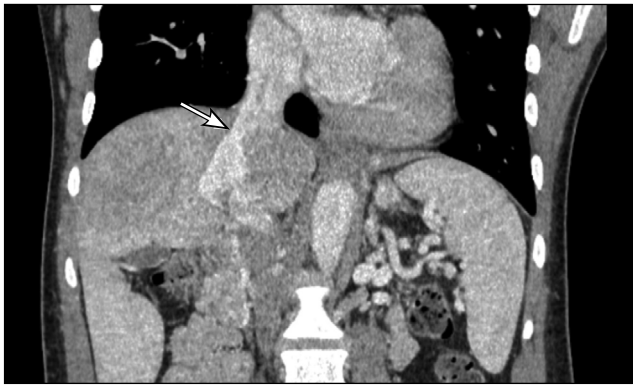

Fig. 4. Contrast-enhanced CT, portal phase, coronal view. Portal vein conduit flowing directly into the IVC (white arrow), enlarged liver with heterogeneous parenchymal enhancement.

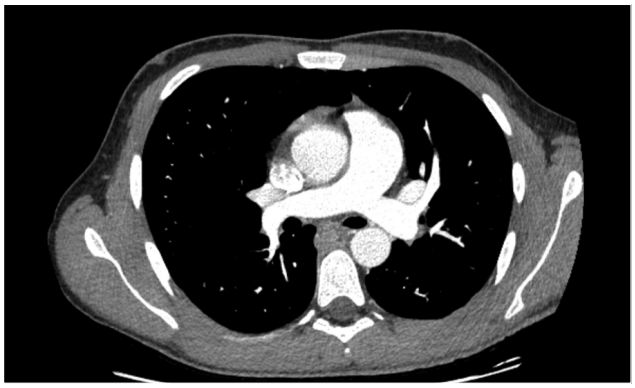

Fig. 5. CT pulmonary angiography, axial view. Pulmonary trunk dilatation.

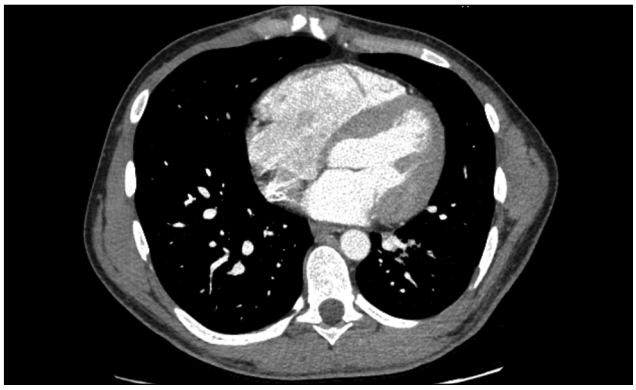

Fig. 6. CT pulmonary angiography, axial view. Myocardial hypertrophy.

vasculature; acquired shunts are secondary to liver diseases [27]. In the literature, there are two dominant theories of CEPSS formation: congenital malformations and anomalies of the ductus venosus.

The development of the portal system is complex and occurs between weeks 4 and 10 of embryonic life. The systemic venous system results from the embryonic anterior and posterior cardinal veins. The portal venous system forms from the vitelline veins, which carry blood from the yolk sac to the sinus venosus [13]. If portal system development is disrupted, CEPSS occurs. This variant is closely associated with combined congenital pathologies. According to the study of Bernard et al., congenital heart disease was the most frequently observed concomitant pathology (in 45/265 cases); other recorded malformations included abnormalities of the kidneys, bile ducts (including biliary atresia), digestive system, bones, and brain [7].

Another discussed mechanism is the absence of the functioning fetal ductus venosus due to anatomical defects or occlusion. In a normal fetus, the ductus venosus shunts blood from the umbilical vein to the IVC, bypassing the liver. Naturally, functional closure occurs within the first minutes of birth and structural closure during the first weeks of life in most full-term neonates [8]. The umbilical vein and ductus venosus anatomically close during the first months of life and become the ligamentum teres and ligamentum venosum, respectively [13]. Pathologies of the ductus venosus in the fetus can stimulate the formation of abnormal vessels. These abnormal vessels may persist and develop into abnormal shunts, resulting in hypoplasia of the portal venous system. The absence of the ductus venosus has been reported in some cases of CEPSS [5,12].

Classification

A widely used classification of CEPSS is the classification system introduced by Morgan and Superina in 1994 (Table 1) [23]. According to this classification, Abernethy malformation is divided into two types depending on the patency of the intrahepatic portal system. Type 1 is defined as a complete portosystemic shunt, whereas type 2 is described as partial blood shunting to systemic veins with a certain degree of portal system development (Figure 7). Different treatment options are available depending on the CEPSS type [35].

Clinical manifestations and complications

Clinical presentations are variable and depend on the ratio of blood flow through the shunt. Manifestations vary from accidental findings in asymptomatic adult patients [26,32] to complex congenital malformations [36], severe

Table 1. Classification System for portasystemic anomalies by Morgen and Superina [23].

Type I	**Liver not perfused with portal blood — total shunt**
	Ia: SMV and splenic vein do not joint to form confluence
	Ib: SMV and splenic vein join to form confluence
Type II	**The liver perfused with portal blood — partial shunt** (e.g., portal-hepatic venous anastomoses)
	IIa: congenital
	IIb: acquired

Note. SMV — superior mesenteric vein.

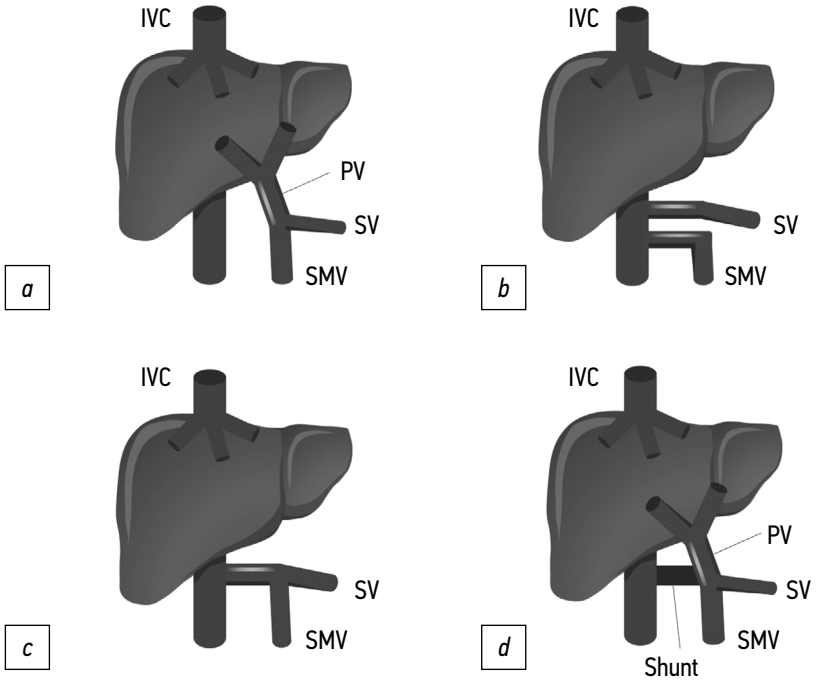

Fig. 7. Normal portal vein anatomy and shunt classification. IVC — inferior vena cava; PV – portal vein; SV — splenic vein; SMV — superior mesenteric vein; *a* — normal PV anatomy; *b* — CEPSS type Ia; *c* — CEPSS type Ib; and *d* — CEPSS type II.

hypoxemia [31], encephalopathy [21, 22], or liver tumors [33]. Most patients present with nonspecific symptoms, such as acute hepatic decompensation or cirrhosis. According to Lin et al., data of 703 patients with CEPSS extracted from 451 articles revealed that majority of the reported patients with Abernethy malformation were children or young adults <18 years old [20]. Severe congenital pathologies with a higher degree of blood shunting are usually diagnosed at a younger age, whereas patients with partial blood shunting can remain asymptomatic till adulthood.

In the early neonatal period, galactosemia, diagnosed during routine screening, can be the first sign of CEPSS. Galactose is metabolized in the liver by the GALT enzyme to glucose. However, in children with CEPSS, galactose bypasses the liver, resulting in increased levels in the systemic circulation [14, 29]. According to several researchers, hypergalactosemia is present in up to 70% of newborns with CPSS [7]. Other potential symptoms in the early neonatal period are growth restriction, neonatal cholestasis, and hepatic encephalopathy [28].

In patients with milder pathology, CEPSS can go unnoticed until adulthood. The presentation may be due to symptoms related to hepatic encephalopathy, liver masses, or pulmonary hypertension.

Subclinical hepatic encephalopathy is observed in up to 30% of patients with CEPSS [11]. Portal blood shunting causes increased ammonium levels in the systemic blood flow. Blood ammonia produced in the gastrointestinal tract bypasses the liver and flows directly into the IVC. Astrocytes metabolize ammonium to glutamine, which has toxic effects on the brain [21]. Hyperammonemia may present without encephalopathy, particularly at younger ages. Clinical encephalopathy is more common in older patients, probably due to lower compensatory abilities [22]. Diagnosis in such cases can be difficult because of the low specificity of symptoms [2,3,21]. Elevated serum ammonia concentration without evidence of liver cirrhosis should prompt further investigations for extrahepatic shunts.

Patients with CPSS are prone to developing multiple liver tumors. The literature on histological changes in the liver

parenchyma in patients with CPSS is limited. De Vito et al. described a case series of 22 patients with CPSS, including 19 patients with CEPSS, who were diagnosed and managed in their institution for 15 years [10]. According to their results, the most characteristic histological findings in peripheral liver parenchyma included the presence of portal prominent thin-walled channels, arterial-biliary dyads, increased arterial profiles in the portal tracts and lobule, and frequent lack of the physiological periportal-vacuolated hepatocytes in children.

The pathophysiology of hepatic tumor in patients with CEPSS remains unclear. One of the mechanisms is attributed to reduced liver regeneration abilities. Low portal blood flow leads to a decrease in the delivery of insulin and glucagon to hepatocytes, making them more vulnerable to damage and neoplasm development [17]. Moreover, increased hepatic arterial blood flow can be associated with parenchymal cell de-differentiation [33].

Nodular liver lesions are common findings in different types of Abernethy malformation. In most cases, liver nodules are benign, and include focal nodular hyperplasia, hepatic adenomas, and regenerative nodules. Most patients are asymptomatic, although some patients present with an abdominal mass. In our case, liver nodules were accidentally found during abdominal US.

However, not all liver masses are benign. Type I Abernethy malformation is associated with hepatoblastoma and hepatocellular carcinoma (HCC) [9,16]. Hepatoblastoma is a rare tumor seen in children with CEPSS. These tumors have an unfavorable prognosis. Majority of the described cases were lethal [9,17]. Hepatocellular carcinomas more often develop in adults, although Benedict et al. published a case of a 12-month-old male with histologically and immunohistochemically confirmed HCC [6]. Diagnosis can be complicated as some of the reported lesions have controversial radiological features and can be mistaken for benign masses [32]; biopsy is usually required. Liver transplant is a treatment option [25].

In some CEPSS cases, patients present with signs of pulmonary hypertension: shortness of breath and dyspnea [19, 24]. Severe pulmonary hypertension can lead to cardiogenic syncope due to decreased preload and low cerebral perfusion [20]. In our case, pulmonary hypertension was diagnosed.

Hepatopulmonary syndrome occurs in patients with liver disease accompanied by portal hypertension. Vasoactive mediators from the intestine bypass the hepatic circulation through the portosystemic shunt, flowing directly to the pulmonary vascular bed, causing imbalance between vasodilation and vasoconstriction substances, inducing pulmonary hypertension [35]. The correction of hepatic vascular anomalies is curative.

Diagnosis and treatment

There are currently no published guidelines for the diagnosis and treatment of CEPSS. Based on the results of the multicenter international study that included 66 patients, Baiges et al. have proposed a management algorithm for patients with CEPSS (Figure 8) [4].

In our case, Abernethy malformation was suspected in the abdominal US. Generally, US signs of CEPSS include portal trunk absence or hypoplasia, solid focal lesions in the liver parenchyma, deficiencies of the intrahepatic portal

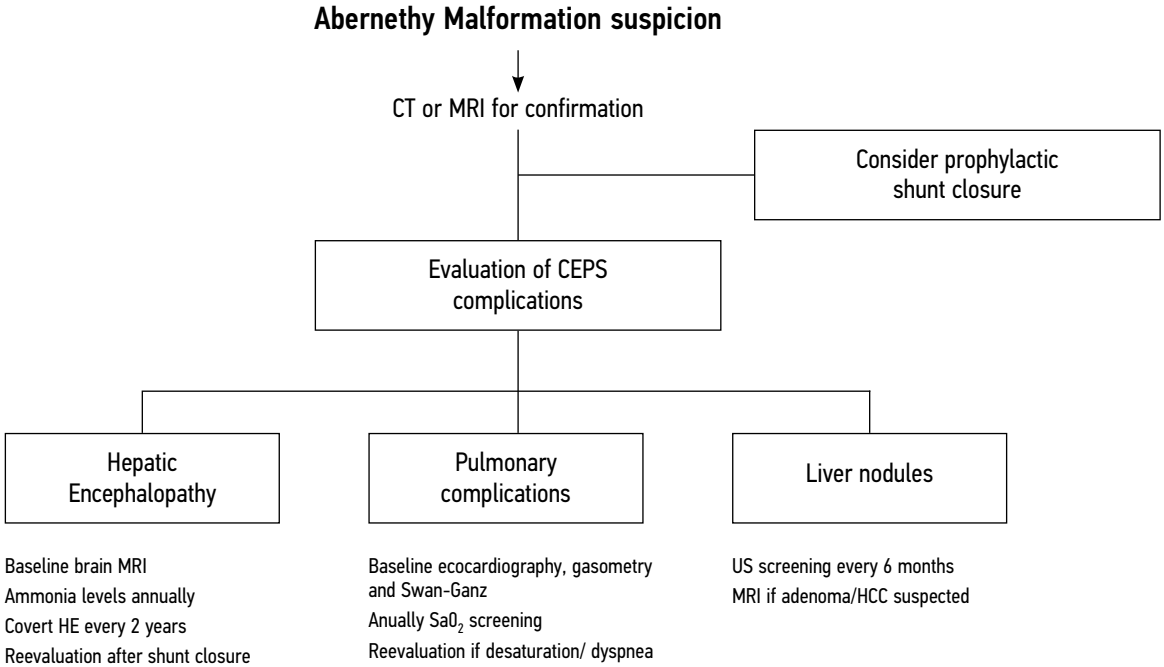

Fig. 8. A congenital extrahepatic portosystemic shunt management algorithm proposed by Baiges et al. [4]. CEPS — congenital extrahepatic portosystemic; CT — computed tomography; HCC — hepatocellular carcinoma; HE — hepatic encephalopathy; MRI — magnetic resonance imaging; US — ultrasound.

vessels and flow signals, and hepatic artery hypertrophy [30]. Anomalies identified by the US should be further confirmed with other imaging modalities, such as CT, or MR angiography. Contrast-enhanced CT provides essential information about shunt size, orientation, and type, which helps in choosing the most suitable treatment approach for each patient. Further, it allows to visualize and evaluate concomitant anomalies, including liver masses. MR angiography is a reliable and noninvasive modality for visualizing hepatic vascular anatomy. It is radiation-free and has better soft tissue contrast than CT. Moreover, diffusion-weighted sequences and hepatocyte-specific contrast agents can provide additional valuable information for the evaluation of nodular liver lesions and decision-making.

The therapeutic approach depends on the shunt type and size, severity of symptoms, coexisting anomalies, and related complications. Asymptomatic patients could be medically followed. Given the complication development risks, Kwapisz et al. recommended routine clinical assessments, regular blood work, including liver enzyme and liver function tests, and annual liver imaging for patients with CEPSS [16].

Experience in the treatment of patients with Abernethy malformation remains limited. Based on the reported cases, current treatment options include interventional or surgical shunt closure and liver transplantation. Type I long-term treatment options are limited to the liver transplant with supportive therapy while waiting for surgery. Patients with Type II CEPSS have more therapeutic options depending on the developed complications and associated anomalies. It is possible to ligate or close the portosystemic shunt using interventional angiography (with coils or plugs) [34]. However, interventional closure may cause recurrent hyperammonemia, as has been reported [18].

It may be beneficial to perform the balloon shunt occlusion test to assess the intrahepatic portal system (IHPS) in patients with both types of CEPSS [18]. This test allows to visualize small portal vein branches which cannot be seen on US. Kanazawa et al. proposed a new IHPS classification (mild, moderate, and severe) based on the results of the shunt occlusion test [15]. The IHPS classification correlates with the portal venous pressure under shunt occlusion, histopathological findings, postoperative portal venous flow, and liver regeneration, and is useful for decision-making whether to perform single-stage or two-stage shunt closure or liver transplantation.

CONCLUSION

Abernethy malformation is a rare pathology associated with severe complications and poor outcomes. Owing to the low incidence, unspecific symptoms, involvement of different organ systems, and variable presentations, diagnosis of CEPSS is a challenge. Imaging plays a critical role in the diagnosis and treatment planning. Early identification and individualized treatment approaches are crucial in preventing complications. Long-term follow-up and monitoring for malignancy are required.

ADDITIONAL INFORMATION

Funding source. This study was not supported by any external sources of funding.

Competing interests. The authors declare that they have no competing interests.

Authors' contribution. All authors made a substantial contribution to the conception of the work, acquisition, analysis, interpretation of data for the work, drafting and revising the work, final approval of the version to be published and agree to be accountable for all aspects of the work.

Consent for publication. Written consent was obtained from the patient's parents for publication of relevant medical information and all of accompanying images within the manuscript in Digital Diagnostics journal.

REFERENCES

1. Bernard O, Franchi-Abella S, Branchereau S, et al. Congenital portosystemic shunts in children: Recognition, evaluation, and management. *Seminars Liver Dis*. 2012;32(4):273–287. doi: 10.1055/s-0032-1329896

2. Papamichail M, Pizanias M, Heaton N. Congenital portosystemic venous shunt. *Eur J Pediatrics*. 2018;177(3):285–294. doi: 10.1007/s00431-017-3058-x

3. Abernethy J. Account of two instances of uncommon formation in the viscera of the human body: From the philosophical transactions of the royal society of London. *Med Facts Observations*. 1797;(7):100–108.

4. Guérin F, Blanc T, Gauthier F, et al. Congenital portosystemic vascular malformations. *Seminars Pediatric Sur*. 2012;21(3):233–244. doi: 10.1053/j.sempedsurg.2012.05.006

5. Born M. The ductus venosus. *RoFo Fortschritte Gebiet Rontgenstrahlen Bildgebenden Verfahren*. 2021;193(5):521–526. doi: 10.1055/a-1275-0984

6. Baller SE, Reinehr M, Haslinger C, et al. Case report of neonatal ductus venosus atresia. *J Neonatal-Perinatal Med*. 2021;14(2):307–312. doi: 10.3233/NPM-190398

7. Franchi-Abella S, Branchereau S, Lambert V, et al. Complications of congenital portosystemic shunts in children: Therapeutic options and outcomes. *J Pediatric Gastroenterol Nutrition*. 2010;51(3):322–330. doi: 10.1097/MPG.0b013e3181d9cb92

8. Morgan G, Superina R. Congenital absence of the portal vein: Two cases and a proposed classification system for portasystemic vascular anomalies. *J Pediatric Sur*. 1994;29(9):1239–1241. doi: 10.1016/0022-3468(94)90812-5

9. Tang H, Song P, Wang Z, et al. A basic understanding of congenital extrahepatic portosystemic shunt: Incidence, mechanism, complications, diagnosis, and treatment. *Intractable Rare Dis Res*. 2020;9(2):64–70. doi: 10.5582/irdr.2020.03005

10. Păcurar D, Dijmărescu I, Dijmărescu AD, et al. A case report on an incidental discovery of congenital portosystemic shunt. *Medicine*. 2019;98(31):e16679. doi: 10.1097/MD.0000000000016679
11. Shah A, Aziz A, Awwad A, et al. Incidental radiological diagnosis of asymptomatic Abernethy malformations: Two case reports. *BJR|Case Reports*. 2017;3(1):20150496. doi: 10.1259/bjrcr.20220059
12. Yangín-Ergon E, Ermis N, Colak R, et al. Abernethy malformation type 2 and biliary atresia coexistence: A rare cause of infantile liver transplant. *Euroasian J Hepatogastroenterol*. 2018;8(2):163–166. doi: 10.5005/jp-journals-10018-1283
13. Sahu MK, Bisoi AK, Chander NC, et al. Abernethy syndrome, a rare cause of hypoxemia: A case report. *Ann Pediatric Cardiol*. 2015;8(1):64–66. doi: 10.3389/fcvm.2021.784739
14. Lux D, Naito A, Harikrishnan S. Congenital extrahepatic portosystemic shunt with progressive myelopathy and encephalopathy. *Practical Neurol*. 2019;19(4):368–371. doi: 10.1136/practneurol-2018-002111
15. Merola E, Cao M, La Starza S. et al. Portosystemic encephalopathy in an 86-year-old patient: A clinical challenge. *Acta Gastro-Enterologica Belgica*. 2016;79(1):58–59.
16. Sharma R, Suddle A, Quaglia A, et al. Congenital extrahepatic portosystemic shunt complicated by the development of hepatocellular carcinoma. *Hepatobiliary Pancreatic Dis Int*. 2015;14(5):552–557. doi: 10.1016/S1499-3872(15)60418-0
17. Lin X, Rao J, Xiang Y, et al. Case report: A rare syncope case caused by abernethy II and a review of the literature. *Frontiers Cardiovascular Med*. 2022;8:2050. doi: 10.3389/fcvm.2021.784739
18. Hasegawa T, Sato T, Ishii T, et al. Oral sodium phenylbutyrate for hyperammonemia associated with congenital portosystemic shunt: A case report. *J Pediatric Endocrinol Metabolism*. 2021;34(3):407–410. doi: 10.1515/jpem-2020-0603
19. Peček J, Fister P, Homan M. Abernethy syndrome in Slovenian children: Five case reports and review of literature. *World J Gastroenterol*. 2020;26(37):5731–5744. doi: 10.3748/wjg.v26.i37.5731
20. Pathak A, Agarwal N, Mandliya J, et al. Abernethy malformation: a case report. *BMC Pediatrics*. 2012;12(1):1. doi: 10.1186/1471-2431-12-57
21. Duarte-Mesquita R, Sousa M, Vilaverde F, Cardoso R. Abernethy malformation : beware in cases of unexplained hepatic encephalopathy in adults. *BJR| Case Reports*. 2017;4(1):20170054. doi: 10.1259/bjrcr.20170054
22. Allegritti M, Enrico B, Basile E, et al. Non-cirrhotic extra-hepatic porto-systemic shunt causing adult-onset encephalopathy treated with endovascular closure. *Digestive Dis Sci*. 2020;65(4):946–951. doi: 10.1007/s10620-019-06024-4
23. Alvi AA, Pichardo J, Gupta S, et al. An interesting case of congenital intrahepatic porto-hepatic shunt as a cause of unexplained encephalopathy. *Cureus*. 2020;12(4):e7639. doi: 10.14309/01.ajg.0000598392.71372.f2
24. De Vito C, Tyraskis A, Davenport M, et al. Histopathology of livers in patients with congenital portosystemic shunts (Abernethy malformation): A case series of 22 patients. *Virchows Archiv*. 2019;474(1):47–57. doi: 10.1007/s00428-018-2464-4
25. Lautz TB, Shah SA, Superina RA. Hepatoblastoma in children with congenital portosystemic shunts. *J Pediatric Gastroenterology Nutrition*. 2016;62(4):542–545. doi: 10.1097/MPG.0000000000001012
26. Correa C, Luengas JP, Howard SC, Veintemilla G. Hepatoblastoma and abernethy malformation type I: Case report. *J Pediatric Hematology/Oncology*. 2017;39(2):e79–e81. doi: 10.1097/MPH.0000000000000650
27. Kwapisz L, Wells MM, Judaibi BA. Abernethy malformation: Congenital absence of the portal vein. *Can J Gastroenterol Hepatol*. 2014;28(11):587–588. doi: 10.1155/2014/675812
28. Benedict M, Rodriguez-Davalos M, Emre S, et al. Congenital extrahepatic portosystemic shunt (abernethy malformation type Ib) with associated hepatocellular carcinoma: Case report and literature review. *Pediatric Developmental Pathology*. 2017;20(4):354–362. doi: 10.1177/1093526616686458
29. Özden İ, Yavru A, Güllüoğlu M, et al. Transplantation for large liver tumors in the setting of abernethy malformation. *Exp Clin Transplantation*. 2017;15(Suppl 2):82–85. doi: 10.6002/ect.TOND16.L23
30. Lin KY, Chen H, Yu L. Pulmonary arterial hypertension caused by congenital extrahepatic portocaval shunt: A case report. *BMC Cardiovascular Disorders*. 2019;19(1):1–5. doi: 10.1186/s12872-019-1124-1
31. Osorio MJ, Bonow A, Bond GJ, et al. Abernethy malformation complicated by hepatopulmonary syndrome and a liver mass successfully treated by liver transplantation. *Pediatric Transplantation*. 2011;15(7):149–151. doi: 10.1111/j.1399-3046.2010.01337.x
32. Baiges A, Turon F, Simón-Talero M, et al. Congenital extrahepatic portosystemic shunts (Abernethy malformation): An international observational study. *Hepatology*. 2020;71(2):658–669. doi: 10.1002/hep.30817
33. Ponziani FR, Faccia M, Zocco MA, et al. Congenital extrahepatic portosystemic shunt: description of four cases and review of the literature. *J Ultrasound*. 2019;22:349–358. doi: 10.1007/s40477-018-0329-y
34. Sheth R, Sivakumar K. The Abernethy malformation with inferior caval vein hypoplasia: A tailored technique for transcatheter closure and an insight into embryological perspective. *Cardiology Young*. 2018;28(9):1169–1171. doi: 10.1017/S1047951118000884
35. Li H, Ma Z, Xie Y, Tian F. Recurrent hyperammonemia after abernethy malformation type 2 closure: A case report. *Ann Hepatol*. 2017;16(3):460–464. doi: 10.5604/01.3001.0009.8603
36. Kanazawa H, Nosaka S, Miyazaki O, et al. The classification based on intrahepatic portal system for congenital portosystemic shunts. *J Pediatric Sur*. 2015;50(4):688–695. doi: 10.1016/j.jpedsurg.2015.01.009

СПИСОК ЛИТЕРАТУРЫ

1. Bernard O., Franchi-Abella S., Branchereau S., et al. Congenital portosystemic shunts in children: Recognition, evaluation, and management // Seminars Liver Dis. 2012. Vol. 32, N 4. P. 273–287. doi: 10.1055/s-0032-1329896
2. Papamichail M., Pizanias M., Heaton N. Congenital portosystemic venous shunt // Eur J Pediatrics. 2018. Vol. 177, N 3. P. 285–294. doi: 10.1007/s00431-017-3058-x
3. Abernethy J. Account of two instances of uncommon formation in the viscera of the human body: From the philosophical transactions of the royal society of London // Med Facts Observations. 1797. N 7. P. 100–108.
4. Guérin F., Blanc T., Gauthier F., et al. Congenital portosystemic vascular malformations // Seminars Pediatric Sur. 2012. Vol. 21, N 3. P. 233–244. doi: 10.1053/j.sempedsurg.2012.05.006

5. Born M. The ductus venosus // RoFo Fortschritte Gebiet Rontgenstrahlen Bildgebenden Verfahren. 2021. Vol. 193, N 5. P. 521–526. doi: 10.1055/a-1275-0984
6. Baller S.E., Reinehr M., Haslinger C., et al. Case report of neonatal ductus venosus atresia // J Neonatal-Perinatal Med. 2021. Vol. 14, N 2. P. 307–312. doi: 10.3233/NPM-190398
7. Franchi-Abella S., Branchereau S., Lambert V., et al. Complications of congenital portosystemic shunts in children: Therapeutic options and outcomes // J Pediatric Gastroenterol Nutrition. 2010. Vol. 51, N 3. P. 322–330. doi: 10.1097/MPG.0b013e3181d9cb92
8. Morgan G., Superina R. Congenital absence of the portal vein: Two cases and a proposed classification system for portasystemic vascular anomalies // J Pediatric Sur. 1994. Vol. 29, N 9. P. 1239–1241. doi: 10.1016/0022-3468(94)90812-5
9. Tang H., Song P., Wang Z., et al. A basic understanding of congenital extrahepatic portosystemic shunt: Incidence, mechanism, complications, diagnosis, and treatment // Intractable Rare Dis Res. 2020. Vol. 9, N 2. P. 64–70. doi: 10.5582/irdr.2020.03005
10. Păcurar D., Dijmărescu I., Dijmărescu A.D., et al. A case report on an incidental discovery of congenital portosystemic shunt // Medicine. 2019. Vol. 98, N 31. P. e16679. doi: 10.1097/MD.0000000000016679
11. Shah A., Aziz A., Awwad A., et al. Incidental radiological diagnosis of asymptomatic Abernethy malformations: Two case reports // BJR|Case Reports. 2017. Vol. 3, N 1. P. 20150496. doi: 10.1259/bjrcr.20220059
12. Yangín-Ergon E., Ermis N., Colak R., et al. Abernethy malformation type 2 and biliary atresia coexistence: A rare cause of infantile liver transplant // Euroasian J Hepatogastroenterol. 2018. Vol. 8, N 2. P. 163–166. doi: 10.5005/jp-journals-10018-1283
13. Sahu M.K., Bisoi A.K., Chander N.C., et al. Abernethy syndrome, a rare cause of hypoxemia: A case report // Ann Pediatric Cardiol. 2015. Vol. 8, N 1. P. 64–66. doi: 10.3389/fcvm.2021.784739
14. Lux D., Naito A., Harikrishnan S. Congenital extrahepatic portosystemic shunt with progressive myelopathy and encephalopathy // Practical Neurology. 2019. Vol. 19, N 4. P. 368–371. doi: 10.1136/practneurol-2018-002111
15. Merola E., Cao M., La Starza S., et al. Portosystemic encephalopathy in an 86-year-old patient: A clinical challenge // Acta Gastro-Enterologica Belgica. 2016. Vol. 79, N 1. P. 58–59.
16. Sharma R., Suddle A., Quaglia A., et al. Congenital extrahepatic portosystemic shunt complicated by the development of hepatocellular carcinoma // Hepatobiliary Pancreatic Dis Int. 2015. Vol. 14, N 5. P. 552–557. doi: 10.1016/S1499-3872(15)60418-0
17. Lin X., Rao J., Xiang Y., et al. Case report: A rare syncope case caused by abernethy ii and a review of the literature // Front Cardiovascul Med. 2022. Vol. 8. P. 2050. doi: 10.3389/fcvm.2021.784739
18. Hasegawa T., Sato T., Ishii T., et al. Oral sodium phenylbutyrate for hyperammonemia associated with congenital portosystemic shunt: A case report // J Pediatric Endocrinology Metabolism. 2021. Vol. 34, N 3. P. 407–410. doi: 10.1515/jpem-2020-0603
19. Peček J., Fister P., Homan M. Abernethy syndrome in Slovenian children: Five case reports and review of literature // World J Gastroenterol. 2020. Vol. 26, N 37. P. 5731–5744. doi: 10.3748/wjg.v26.i37.5731
20. Pathak A., Agarwal N., Mandliya J., et al. Abernethy malformation: A case report // BMC Pediatrics. 2012. Vol. 12, N 1. P. 1. doi: 10.1186/1471-2431-12-57
21. Duarte-Mesquita R., Sousa M., Vilaverde F., Cardoso R. Abernethy malformation: Beware in cases of unexplained hepatic encephalopathy in adults // BJR| Case Reports. 2017. Vol. 4, N 2. P. 20170054. doi: 10.1259/bjrcr.20170054
22. Allegritti M., Enrico B., Basile E., et al. Non-cirrhotic extra-hepatic porto-systemic shunt causing adult-onset encephalopathy treated with endovascular closure // Digestive Diseases and Sciences. 2020. Vol. 65, N 4. P. 946–951. doi: 10.1007/s10620-019-06024-4
23. Alvi A.A., Pichardo J., Gupta S., et al. An interesting case of congenital intrahepatic porto-hepatic shunt as a cause of unexplained encephalopathy // Cureus. 2020. Vol. 12, N 4. P. e7639. doi: 10.14309/01.ajg.0000598392.71372.f2
24. De Vito C., Tyraskis A., Davenport M., et al. Histopathology of livers in patients with congenital portosystemic shunts (Abernethy malformation): A case series of 22 patients // Virchows Archiv. 2019. Vol. 474, N 1. P. 47–57. doi: 10.1007/s00428-018-2464-4
25. Lautz T.B., Shah S.A., Superina R.A. Hepatoblastoma in children with congenital portosystemic shunts // J Pediatric Gastroenterology Nutrition. 2016. Vol. 62, N 4. P. 542–545. doi: 10.1097/MPG.0000000000001012
26. Correa C., Luengas J.P., Howard S.C., Veintemilla G. Hepatoblastoma and abernethy malformation type I: Case report // J Pediatric Hematology/Oncology. 2017. Vol. 39, N 2. P. e79–e81. doi: 10.1097/MPH.0000000000000650
27. Kwapisz L., Wells M.M., Judaibi B. Al Abernethy malformation: Congenital absence of the portal vein // Can J Gastroenterol Hepatol. 2014. Vol. 28, N 11. P. 587–588. doi: 10.1155/2014/675812
28. Benedict M., Rodriguez-Davalos M., Emre S., et al. Congenital extrahepatic portosystemic shunt (abernethy malformation type Ib) with associated hepatocellular carcinoma: Case report and literature review // Pediatric Developmental Pathology. 2017. Vol. 20, N 4. P. 354–362. doi: 10.1177/1093526616686458
29. Özden İ., Yavru A., Güllüoğlu M., et al. Transplantation for large liver tumors in the setting of abernethy malformation // Experimental Clin Transplantation. 2017. Vol. 15, Suppl. 2. P. 82–85. doi: 10.6002/ect.TOND16.L23
30. Lin K. Y., Chen H., Yu L. Pulmonary arterial hypertension caused by congenital extrahepatic portocaval shunt: A case report // BMC Cardiovascular Disorders. 2019. Vol. 19, N 1. P. 1–5. doi: 10.1186/s12872-019-1124-1
31. Osorio M.J., Bonow A., Bond G.J., et al. Abernethy malformation complicated by hepatopulmonary syndrome and a liver mass successfully treated by liver transplantation // Pediatric Transplantation. 2011. Vol. 15, N 7. P. 149–151. doi: 10.1111/j.1399-3046.2010.01337.x
32. Baiges A., Turon F., Simón-Talero M., et al. Congenital extrahepatic portosystemic shunts (Abernethy malformation): An international observational study // Hepatology. 2020. Vol. 71, N 2. P. 658–669. doi: 10.1002/hep.30817
33. Ponziani F.R., Faccia M., Zocco M.A., et al. Congenital extrahepatic portosystemic shunt: Description of four cases and review of the literature // J Ultrasound. 2019. N 22. P. 349–358. doi: 10.1007/s40477-018-0329-y
34. Sheth R., Sivakumar K. The Abernethy malformation with inferior caval vein hypoplasia: A tailored technique for transcatheter closure and an insight into embryological perspective // Cardiology Young. 2018. Vol. 28, N 9. P. 1169–1171. doi: 10.1017/S1047951118000884

35. Li H., Ma Z., Xie Y., Tian F. Recurrent hyperammonemia after abernethy malformation Type 2 closure: A case report // Ann Hepatol. 2017. Vol. 16, N 3. P. 460–464. doi: 10.5604/01.3001.0009.8603

36. Kanazawa H., Nosaka S., Miyazaki O., et al. The classification based on intrahepatic portal system for congenital portosystemic shunts // J Pediatric Sur. 2015. Vol. 50, N 4. P. 688–695. doi: 10.1016/j.jpedsurg.2015.01.009

AUTHORS' INFO

*** Alexandra V. Panyukova,** MD;
address: 27/10 Lomonosovsky prospekt, 119192 Moscow, Russia;
ORCID: 0000-0002-5367-280X;
e-mail: panyukovaalexandra@gmail.com

Valentin E. Sinitsyn, MD, Dr. Sci. (Med); Professor;
ORCID: 0000-0002-5649-2193;
eLibrary SPIN: 8449-6590;
e-mail: vsini@mail.ru

Elena A. Mershina, MD, Cand. Sci. (Med.), Assistant Professor;
ORCID: 0000-0002-1266-4926;
eLibrary SPIN: 6897-9641;
e-mail: elena_mershina@mail.ru

Natalia A. Rucheva, MD, Cand. Sci. (Med.);
ORCID: 0000-0002-8063-4462;
e-mail: rna1969@yandex.ru

ОБ АВТОРАХ

*** Панюкова Александра Вадимовна;**
адрес: Россия, 119192, Москва, Ломоносовский пр-т, д. 27, кор. 10;
ORCID: 0000-0002-5367-280X;
e-mail: panyukovaalexandra@gmail.com

Синицын Валентин Евгеньевич, д-р мед. наук, профессор;
ORCID: 0000-0002-5649-2193;
eLibrary SPIN: 8449-6590;
e-mail: vsini@mail.ru

Мершина Елена Александровна, канд. мед. наук, доцент;
ORCID: 0000-0002-1266-4926;
eLibrary SPIN: 6897-9641;
e-mail: elena_mershina@mail.ru

Ручьёва Наталья Александровна, канд. мед. наук;
ORCID: 0000-0002-8063-4462;
e-mail: rna1969@yandex.ru

* Corresponding author / Автор, ответственный за переписку

DOI: https://doi.org/10.17816/DD121368

Проверка гипотез исследования с использованием языка R

И.А. Блохин[1], М.Р. Коденко[1, 2], Ю.Ф. Шумская[1, 3], А.П. Гончар[1], Р.В. Решетников[1]

[1] Научно-практический клинический центр диагностики и телемедицинских технологий, Москва, Российская Федерация
[2] Московский государственный технический университет имени Н.Э. Баумана (национальный исследовательский университет), Москва, Российская Федерация
[3] Первый Московский государственный медицинский университет имени И.М. Сеченова (Сеченовский Университет), Москва, Российская Федерация

АННОТАЦИЯ

Для современных учёных становятся всё более важными компетенции в области статистической обработки данных. Очевидными преимуществами открытого программного обеспечения (open-source software) для статистического анализа являются доступность и многофункциональность. Наиболее широкими возможностями среди бесплатных решений обладают язык программирования и соответствующее программное обеспечение R, доступное в виде минималистичного консольного интерфейса или полноценной среды разработки RStudio/Posit.

Предлагаем вашему вниманию практическое руководство по сравнению двух групп с помощью инструментов языка R на примере сопоставления эффективной дозы, полученной при проведении стандартной компьютерной и низкодозной компьютерной томографии при COVID-19, в котором кратко обобщены теоретические подходы к обработке медицинских данных, а также рекомендации по корректной формулировке задач исследования и выбора оптимальных методов статистического анализа.

Основная задача практического руководства — познакомить читателя с интерфейсом Posit и базовым функционалом языка R на практическом примере решения реальной медицинской задачи. Представленный материал может быть полезен на начальном этапе освоения статистического анализа с помощью инструментов языка R.

Ключевые слова: R; RStudio; Posit; статистический анализ; медицинские данные; практическое руководство.

Как цитировать

Блохин И.А., Коденко М.Р., Шумская Ю.Ф., Гончар А.П., Решетников Р.В. Проверка гипотез исследования с использованием языка R // *Digital Diagnostics*. 2023. Т. 4, № 2. С. 238–247. DOI: https://doi.org/10.17816/DD121368

Рукопись получена: 11.01.2023 **Рукопись одобрена:** 18.01.2023 **Опубликована:** 10.04.2023

DOI: https://doi.org/10.17816/DD121368

Hypothesis testing using R

Ivan A. Blokhin[1], Maria R. Kodenko[1, 2], Yuliya F. Shumskaya[1, 3], Anna P. Gonchar[1], Roman V. Reshetnikov[1]

[1] Moscow Center for Diagnostics and Telemedicine, Moscow, Russian Federation
[2] Bauman Moscow State Technical University, Moscow, Russian Federation
[3] The First Sechenov Moscow State Medical University, Moscow, Russian Federation

ABSTRACT

Competencies in statistical data processing are becoming increasingly important for modern scientists. The apparent advantages of open-source software for statistical analysis are its accessibility and adaptability. The programming language and the corresponding software R, available as a minimalistic console interface or a complete development environment RStudio/Posit, have the widest possibilities among free solutions.

We present a practical guide for comparing two groups using the software R. This study compares the effective doses of standard computed tomography with low-dose computed tomography for COVID-19 patients. The practical guide summarizes theoretical approaches to medical data processing and recommendations for correctly formulating research tasks and selecting optimal statistical analysis methods.

The main goal of the practical guide is to introduce the reader to the Posit interface and the basic functionality of the R language by using a practical example of treating a real medical problem. The presented material can be useful as an introduction to statistical analysis using the programming language R.

Keywords: medical data, Posit, R, RStudio, statistical analysis, tutorial

To cite this article

Blokhin IA, Kodenko MR, Shumskaya YuF, Gonchar AP, Reshetnikov RV. Hypothesis testing using R. *Digital Diagnostics.* 2023;4(2):238–247.
DOI: https://doi.org/10.17816/DD121368

Received: 11.01.2023 **Accepted:** 18.01.2023 **Published:** 10.04.2023

DOI: https://doi.org/10.17816/DD121368

使用R语言进行研究假设检验

Ivan A. Blokhin[1], Maria R. Kodenko[1, 2], Yuliya F. Shumskaya[1, 3], Anna P. Gonchar[1], Roman V. Reshetnikov[1]

[1] Moscow Center for Diagnostics and Telemedicine, Moscow, Russian Federation
[2] Bauman Moscow State Technical University, Moscow, Russian Federation
[3] The First Sechenov Moscow State Medical University, Moscow, Russian Federation

简评

对于现代科学家来说，统计数据处理的能力越来越重要。用于统计分析的开源软件（open-source software）的明显优势是可用性和多功能性。在免费的解决方案中，R语言和相关软件大有可为，可作为一个最简控制台界面或作为一个完全合格的开发环境RStudio/Posit。

我们提供一份使用R语言工具比较两组数据的实用指南，以COVID-19的标准电子计算机断层扫描和低剂量电脑断层扫描的有效剂量比较为例。本指南简略地总结了医学数据处理的理论方法，以及正确制定研究目标和选择最佳统计分析方法的建议。

本实用指南的主要目的是通过一个解决真实医学问题的实际例子向读者介绍Posit界面和R语言的基本功能。所介绍的材料在借助R语言工具掌握统计分析的初始阶段可以有益处。

关键词： R；RStudio；Posit；统计分析；医学数据；实用手册。

To cite this article
Blokhin IA, Kodenko MR, Shumskaya YuF, Gonchar AP, Reshetnikov RV. 使用R语言进行研究假设检验. *Digital Diagnostics.* 2023;4(2):238–247.
DOI: https://doi.org/10.17816/DD121368

收到： 11.01.2023 **接受：** 18.01.2023 **发布日期：** 10.04.2023

INTRODUCTION

For modern researchers, statistical data processing has become an increasingly important competency. In 1983, understanding two-thirds of the 760 scientific papers in the esteemed New England Journal of Medicine only required basic knowledge of descriptive statistics (such as percentage, mean, and standard deviation) and one method of statistical hypothesis testing (Student's *t*-test) [1]. However, over time, the scientific community has identified some limitations of this approach for data analysis. In 2014, the Journal of American Medical Association announced a special series describing the methods of statistical analysis for clinicians.[1] Currently, open access review papers are available not only on the basic aspects of data analysis [2], but also on the choice of an appropriate data processing method [3]. Moreover, a detailed Statistical Analysis Method in the Biomedical Research checklist was published in 2019 [4]. However, the practical use of data analysis methods remains a sophisticated problem if programs for its automation are not actively developed.

Because there are many paid statistical analysis programs and commercial services for end-to-end data processing, open-source software has some obvious advantages, such as accessibility and versatility [5]. The most powerful free solution is the programming language and associated software R [6], which is available as a minimalist console interface [7] or as a full-fledged development environment RStudio/Posit [8].

The aim of this paper is to present some basic operations in R based on a real-life problem as follows: comparing the effective dose received by patients during standard computed tomography (CT) and low-dose computed tomography (LDCT) for COVID-19. The relevance of this task is based on the need to monitor radiation exposure [9], considering the increased number of imaging studies [10] resulting in the importance of developing [11] and clinical testing [12, 13] LDCT protocols.

Statistical analysis should include some fundamental steps.

Setting a task and generating a null hypothesis for the analysis

The null hypothesis is the starting point in the statistical analysis. When comparing two groups, the null hypothesis (H_0) is generated as "no statistically significant differences." In our case, the effective patient doses were compared when performing two types of CT scans (full and low dose) for COVID-19. Therefore, the H_0 for this task would state that "radiation exposure levels for CT and LDCT are comparable."

In addition, it is necessary to consider the "alternative hypothesis" (H_1), which presents an antagonistic hypothesis for H_0. These are meant to be mutually exclusive. In our case, the alternative hypothesis would state that "there is a statistically significant difference between effective radiation doses when using CT and LDCT in patients with COVID-19."

In statistics, testing of the null hypothesis yields the *p*-value, which represents the probability of incorrectly rejecting H_0. This parameter can be interpreted as follows: "If we repeat the experiment many times and reject the null hypothesis, we will make a mistake in the *p*-value cases of 100%." For example, a *p*-value of 0.03 implies that we incorrectly reject H_0 in favor of H_1 in 3% of cases. A predetermined threshold helps to determine whether this value is high or low. According to Ronald Fischer, the threshold *p*-value is commonly set to 0.05 [14]. In our case, using a threshold value of 0.05, with a *p*-value of 0.03, we can confidently conclude that the compared samples are different.

Raw data analysis

The choice of the statistical analysis method for raw data processing depends on the type and distribution. Data can be quantitative and qualitative.[2] Quantitative data characterize the magnitude of an event or the number of objects, e.g., the radiation exposure in millisieverts (mSv) during a chest CT. Qualitative or categorical data describe the association between the studied event and a particular group, e.g., patient gender or KT0-4 category.

In data analysis, it is essential to test not only the main null hypothesis, but also one more H_0, which should be "data are normally distributed." Normal distribution is one of the most important statistical phenomena, because it often characterizes naturally occurring parameters, including height, weight, shoe size, and many other population characteristics. The normal distribution is described by two parameters: the mean value and standard deviation. This assumption is the basis for statistical hypothesis testing methods.

There is no single solution for each distribution test case for normality. X. Romão et al. [15] compared 33 methods and suggested optimal solutions depending on the data type. The choice of method also depends on the size of the study sample [16]. The Kolmogorov–Smirnov and Shapiro–Wilk tests are the most important [17].

Null hypothesis testing for the study

For the correct choice of statistical analysis method, we should consider not only the data type in compared samples but also the number of compared groups and the

[1] JAMA guide to statistics and methods [Electronic resource]. Available from: https://jamanetwork.com/collections/44042/jama-guide-to-statistics-and-methods.

[2] Medical statistics [electronic resource]. General issues of statistics. Available from: https://medstatistic.ru/statistics/statistics3.html.

presence of the association between them, e.g., whether CT and LDCT data were obtained from the same or different patients. More than 50 different statistical tests have already been developed, and there are special online resources for choosing the optimal method.[3]

In our case, samples were paired because CT and LDCT data were obtained sequentially from the same patients. It is recommended to use a paired Student's *t*-test for normal distribution and a Wilcoxon test for non-normal distribution.

CASE STUDY

Statistical analysis was performed using R software package (version 4.2.2, https://cloud.r-project.org/) and Posit interface (version 353, https://posit.co/download/rstudio-desktop/, ex-RStudio).

1. The basic Posit interface can be divided into the console, environment, and files (Fig. 1).

Data were imported using the File-Import Dataset. In our case, we imported an Excel spreadsheet containing data on the effective doses of CT and LDCT.

After import, the program interface changes; a "data" variable is displayed in the environment block (Fig. 2). A new area also appeared in the upper left quadrant. This is a data-view block with the loaded table displayed. The comparison columns in the table are named as "Effective Dose (CT)" and "Effective Dose (LDCT)." Latin was used in the column names to avoid problems with encoding and incorrect display of characters in Posit.

For convenience, we created a separate variable for each of these columns by performing the commands shown in Fig. 3.

A "$" operator (see Fig. 3) displays a drop-down menu of imported table columns to facilitate command entry. After creating the variables, they are displayed in the upper right quadrant of the interface as "values" (Fig. 4).

2. The distribution of the loaded data was checked for normality using the Shapiro–Wilk test by the shapiro.test command (Fig. 5).

The resulting *p*-values for both variables were significantly less than the established threshold *p*-value of 0.05, so the distribution of the effective dose data for both CT and LDCT was non-normal. Therefore, the null hypothesis of this study was tested using the Wilcoxon test.

3. For null hypothesis testing of paired quantitative samples with non-normal data distribution, the wilcox.test command was used (Figs. 6, 7).

The resulting *p*-value was significantly less than the selected threshold *p*-value of 0.05; therefore, H_0 could be rejected in favor of H_1. This means that for CT and LDCT, the radiation exposure levels were statistically significantly different.

CONCLUSION

The main aim of this paper is to present the Posit interface and basic functions of the R language using a real-life medical case.

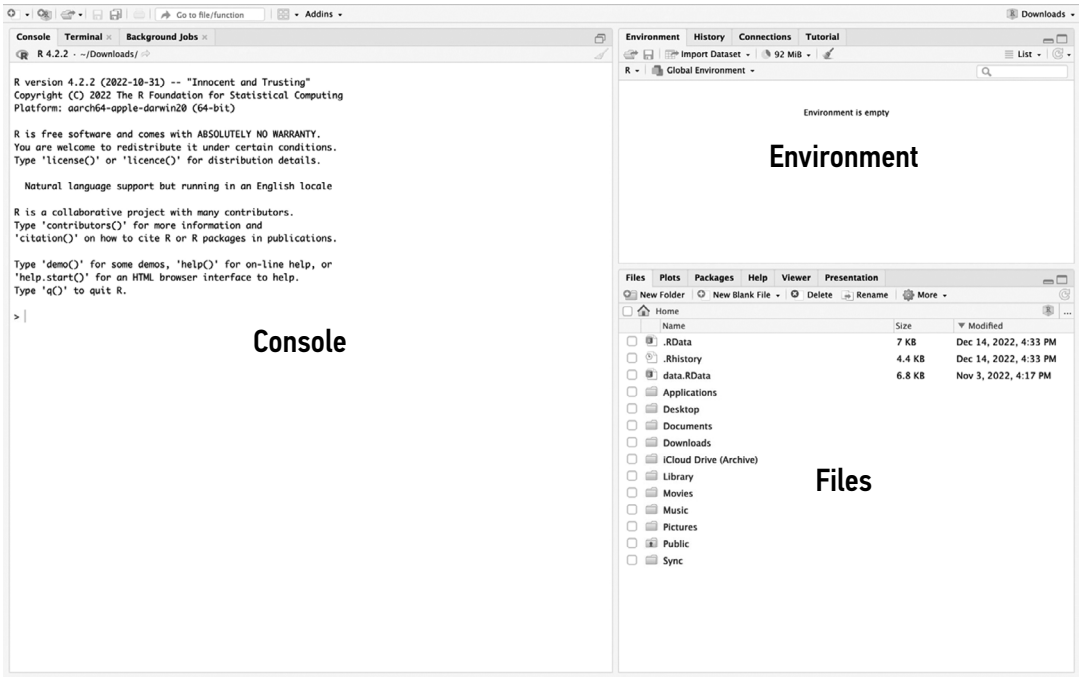

Fig. 1. The Posit interface shows areas of the console, environment, and files.

[3] Statistics online--checks assumptions, interprets results (https://www.statskingdom.com/); Medical statistics. Choice of statistical analysis method (https://medstatistic.ru/calculators/calcchoice.html).

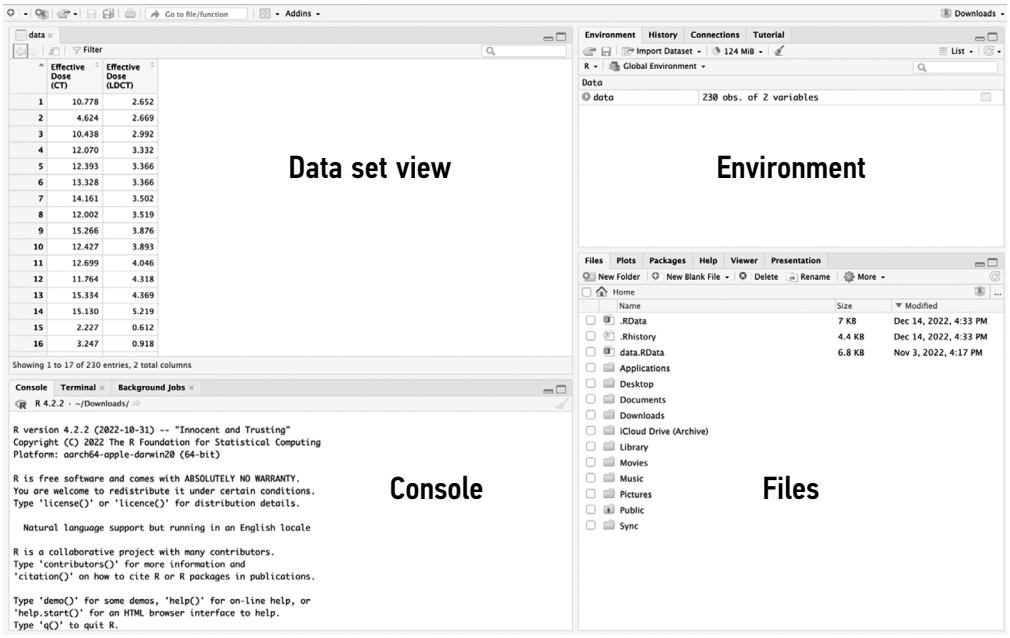

Fig. 2. The Posit interface after importing the file. In the upper-left quadrant of the screen, a window with loaded columns of the data set. In the upper-right quadrant, the number of columns (variables) and rows (obs., observations).

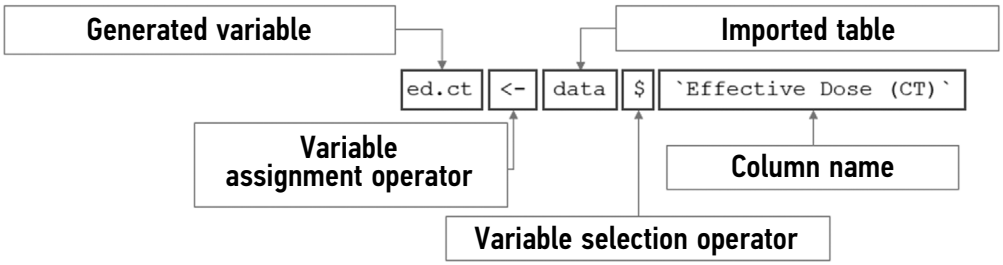

Fig. 3. Generating a separate variable for the effective dose of computed tomography with the functions of each command element is indicated.

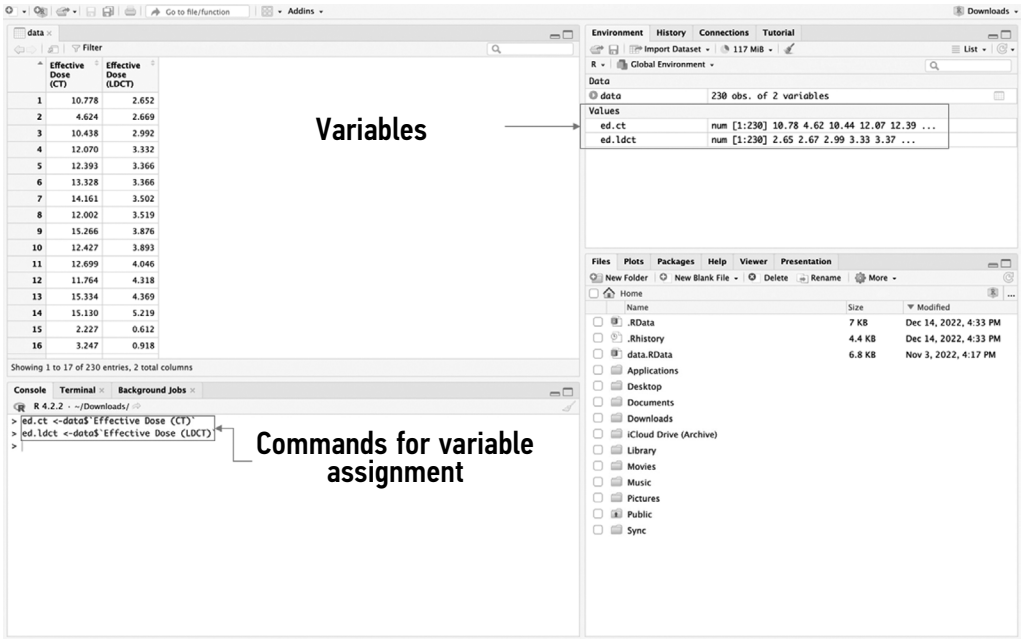

Fig. 4. The Posit window after importing the file and assigning values to the variables. In the upper-right quadrant, new variables with preview of the first five values in each. In the lower-left quadrant, a console interface for commands.

DOI: https://doi.org/10.17816/DD121368

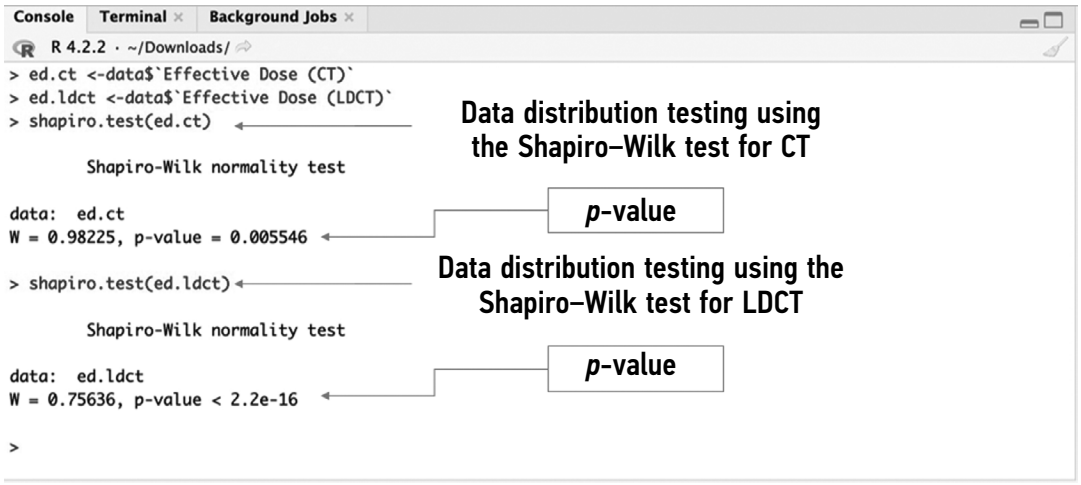

Fig. 5. Area with Posit console interface. Testing for normal data distribution using the Shapiro–Wilk test.

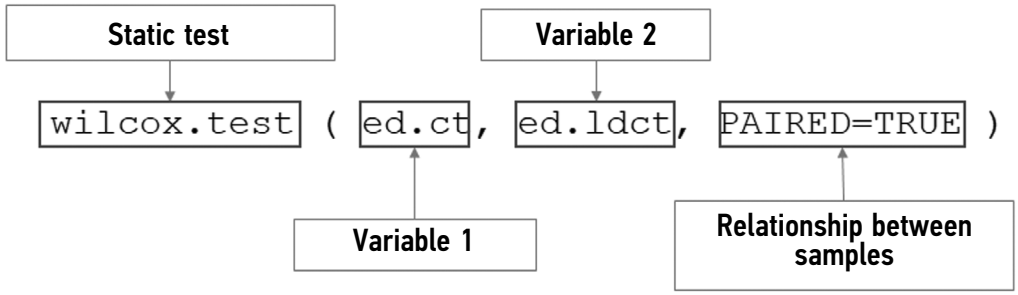

Fig. 6. Using a Wilcoxon with functions of each command element indicated.

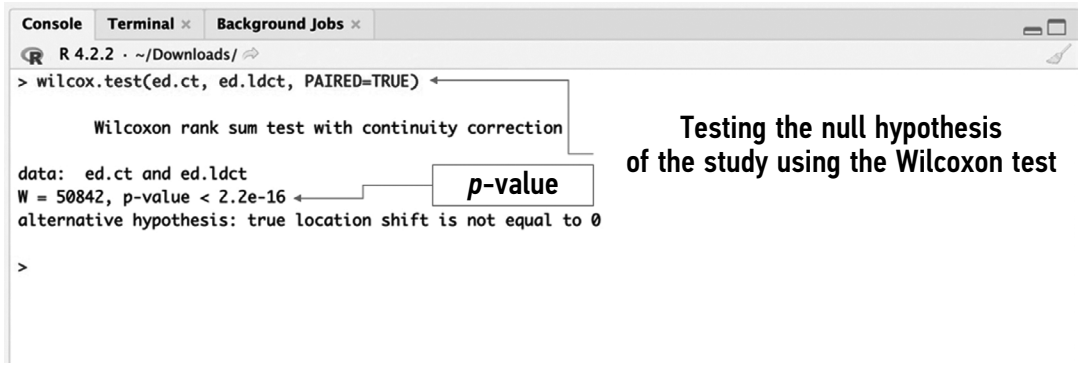

Fig. 7. Testing the null hypothesis of the study using the Wilcoxon test.

This paper summarizes theoretical approaches to medical data processing as well as recommendations for generating correct research tasks and selecting optimal methods for statistical analysis.

The presented material can be useful in the early stages of exploring statistical analysis methods using R language tools.

ADDITIONAL INFORMATION

Funding source. This article was prepared by a group of authors as a part of the medical research project (No. USIS [in the Unified State Information System for Accounting of Research, Development, and Technological Works]: 123031500005-2) «Scientific rationale for diagnostic radiology in oncology using radiomics».

Competing interests. The authors declare that they have no competing interests.

Authors' contribution. All authors made a substantial contribution to the conception of the work, acquisition, analysis, interpretation of data for the work, drafting and revising the work, final approval of the version to be published and agree to be accountable for all aspects of the work. I.A. Blokhin — writing the text of the article, editing and approval of the final version of the text of the manuscript; M.R. Kodenko, Yu.F. Shumskaya, A.P. Gonchar — editing and approval of the final version of the text of the manuscript; R.V. Reshetnikov — editing and approval of the final version of the text of the manuscript, advisory support.

REFERENCES

1. Emerson J, Colditz GA. Use of statistical analysis in the New England Journal of Medicine. *New Engl J Med*. 1983;309(12):709–713. doi: 10.1056/NEJM198309223091206
2. Ali Z, Bhaskar SB. Basic statistical tools in research and data analysis. *Indian J Anaesth*. 2016;60(9):662–669. doi: 10.4103/0019-5049.190623
3. Mishra P, Pandey CM, Singh U, et al. Selection of appropriate statistical methods for data analysis. *Ann Card Anaesth*. 2019;22(3):297–301. doi: 10.4103/aca.ACA_248_18
4. Dwivedi AK, Shukla R. Evidence-based statistical analysis and methods in biomedical research (SAMBR) checklists according to design features. *Cancer Rep (Hoboken)*. 2020;3(4):e1211. doi: 10.1002/cnr2.1211
5. Rigby PC, German DM, Cowen L, et al. Peer review on open-source software projects: Parameters, statistical models, and theory. *ACM Trans Softw Eng Methodol*. 2014;23(4):35.
6. Culpepper SA, Aguinis H. R is for revolution: A cutting-edge, free, open source statistical package. *Organizational Research Methods*. 2011;14(4):735–740.
7. Ihaka R, Gentleman R. R: A language for data analysis and graphics. *J Computational Graphical Statistics*. 1996;5(3):299–314. doi: 10.1080/10618600.1996.10474713
8. Niu G, Segall RS, Zhao Z, et al. A survey of open source statistical software (OSSS) and their data processing functionalities. *Int J Open Source Software Processes*. 2021;12(1):1–20. doi: 10.4018/IJOSSP.2021010101
9. Shatenok MP, Ryzhov SA, Lantukh ZA, et al. Patient dose monitoring software in radiology. *Digital Diagnostics*. 2022;3(3):212–230. (In Russ). doi: 10.17816/DD106083
10. Druzhinina UV, Ryzhov SA, Vodovatov AV, et al. Coronavirus Disease-2019: Changes in computed tomography radiation burden across Moscow medical facilities. *Digital Diagnostics*. 2022;3(1):5–15. (In Russ). doi: 10.17816/DD87628
11. Gombolevskiy V, Morozov S, Chernina V, et al. A phantom study to optimise the automatic tube current modulation for chest CT in COVID-19. *Eur Radiol Exp*. 2021;5(1):21. doi: 10.1186/s41747-021-00218-0
12. Blokhin I, Gombolevskiy V, Chernina V, et al. Inter-observer agreement between low-dose and standard-dose CT with soft and sharp convolution kernels in COVID-19 pneumonia. *J Clin Med*. 2022;11(3):669. doi: 10.3390/jcm11030669
13. Blokhin IA, Gonchar AP, Kodenko M, et al. Impact of body mass index on the reliability of the CT0–4 grading system: A comparison of computed tomography protocols. *Digital Diagnostics*. 2022;3(2):108–118. (In Russ). doi: 10.17816/DD104358
14. Kennedy-Shaffer L. Before p<0.05 to beyond p<0.05: Using history to contextualize p-values and significance testing. *Am Stat*. 2019;73(Suppl. 1):82–90. doi: 10.1080/00031305.2018.1537891
15. Romão X, Delgado R, Costa A. An empirical power comparison of univariate goodness-of-fit tests for normality. *J Statist Computation Simulat*. 2010;80(5):545–591. doi: 10.1080/00949650902740824
16. Lumley T, Diehr P, Emerson S, Chen L. The Importance of the normality assumption in large public health data sets. *Ann Rev Pub Health*. 2002;23(1):151–169. doi: 10.1146/annurev.publhealth.23.100901.140546
17. Mishra P, Pandey CM, Singh U, et al. Descriptive statistics and normality tests for statistical data. *Ann Card Anaesth*. 2019;22(1):67–72. doi: 10.4103/aca.ACA_157_18

СПИСОК ЛИТЕРАТУРЫ

1. Emerson J.D., Colditz G.A. Use of statistical analysis in the New England Journal of Medicine // New Engl J Med. 1983. Vol. 309, N 12. P. 709–713. doi: 10.1056/NEJM198309223091206
2. Ali Z., Bhaskar S.B. Basic statistical tools in research and data analysis // Indian J Anaesth. 2016. Vol. 60, N 9. P. 662–669. doi: 10.4103/0019-5049.190623
3. Mishra P., Pandey C.M., Singh U., et al. Selection of appropriate statistical methods for data analysis // Ann Card Anaesth. 2019. Vol. 22, N 3. P. 297–301. doi: 10.4103/aca.ACA_248_18
4. Dwivedi A.K., Shukla R. Evidence-based statistical analysis and methods in biomedical research (SAMBR) checklists according to design features // Cancer Rep (Hoboken). 2020. Vol. 3, N 4. P. e1211. doi: 10.1002/cnr2.1211
5. Rigby P.C., German D.M., Cowen L,. et al. Peer review on open-source software projects: Parameters, statistical models, and theory // ACM Trans Softw Eng Methodol. 2014. Vol. 23, N 4. P. 35.
6. Culpepper S.A., Aguinis H. R is for revolution: A cutting-edge, free, open source statistical package // Organizational Research Methods. 2011. Vol. 14, N 4. P. 735–740.
7. Ihaka R., Gentleman R. R: A language for data analysis and graphics // J Computational Graphical Statistics. 1996. Vol. 5, N 3. P. 299–314. doi:10.1080/10618600.1996.10474713
8. Niu G., Segall R.S., Zhao Z., et al. A survey of open source statistical software (OSSS) and their data processing functionalities // Int J Open Source Software Processes. 2021. Vol. 12, N 1. P. 1–20. doi: 10.4018/IJOSSP.2021010101
9. Shatenok M.P., Ryzhov S.A., Lantukh Z.A., et al. Patient dose monitoring software in radiology // Digital Diagnostics. 2022. Vol. 3, N 3. P. 212–230. doi: 10.17816/DD106083
10. Druzhinina U.V., Ryzhov S.A., Vodovatov A.V., et al. Coronavirus Disease-2019: Changes in computed tomography radiation burden across Moscow medical facilities // Digital Diagnostics. 2022. Vol. 3, N 1. P. 5–15. doi: 10.17816/DD87628
11. Gombolevskiy V., Morozov S., Chernina V., et al. A phantom study to optimise the automatic tube current modulation for chest CT in COVID-19 // Eur Radiol Exp. 2021. Vol. 5, N 1. P. 21. doi: 10.1186/s41747-021-00218-0
12. Blokhin I., Gombolevskiy V., Chernina V., et al. Inter-observer agreement between low-dose and standard-dose CT with soft and sharp convolution kernels in COVID-19 pneumonia // J Clin Med. 2022. Vol. 11, N 3. P. 669. doi: 10.3390/jcm11030669
13. Blokhin I.A., Gonchar A.P., Kodenko M., et al. Impact of body mass index on the reliability of the CT0–4 grading system: A comparison of computed tomography protocols: 2 // Digital Diagnostics. 2022. Vol. 3, N 2. P. 108–118. doi: 10.17816/DD104358
14. Kennedy-Shaffer L. Before p<0.05 to beyond p<0.05: Using history to contextualize p-values and significance testing // Am Stat. 2019. Vol. 73, Suppl. 1. P. 82–90. doi: 10.1080/00031305.2018.1537891

15. Romão X., Delgado R., Costa A. An empirical power comparison of univariate goodness-of-fit tests for normality // J Statist Computation Simulat. 2010. Vol. 80, N 5. P. 545–591. doi: 10.1080/00949650902740824
16. Lumley T., Diehr P., Emerson S., Chen L. The importance of the normality assumption in large public health data sets // Ann Rev Pub Health. 2002. Vol. 23, N 1. P. 151–169. doi: 10.1146/annurev.publhealth.23.100901.140546
17. Mishra P., Pandey C.M., Singh U., et al. Descriptive statistics and normality tests for statistical data // Ann Card Anaesth. 2019. Vol. 22, N 1. P. 67–72. doi: 10.4103/aca.ACA_157_18

AUTHORS' INFO

*** Ivan A. Blokhin;**
address: 24/1 Petrovka street, 127051 Moscow, Russia;
ORCID: 0000-0002-2681-9378;
eLibrary SPIN: 3306-1387;
e-mail: BlokhinIA@zdrav.mos.ru

Maria R. Kodenko;
ORCID: 0000-0002-0166-3768;
eLibrary SPIN: 5789-0319;
e-mail: KodenkoMR@zdrav.mos.ru

Yuliya F. Shumskaya;
ORCID: 0000-0002-8521-4045;
eLibrary SPIN: 3164-5518;
e-mail: ShumskayaYF@zdrav.mos.ru

Anna P. Gonchar;
ORCID: 0000-0001-5161-6540;
eLibrary SPIN: 3513-9531;
e-mail: GoncharAP@zdrav.mos.ru

Roman V. Reshetnikov, Cand. Sci. (Phys-Math);
ORCID: 0000-0002-9661-0254;
eLibrary SPIN: 8592-0558;
e-mail: r.reshetnikov@gmail.com

ОБ АВТОРАХ

*** Блохин Иван Андреевич;**
адрес: Россия, 127051, Москва, ул. Петровка, д. 24, стр. 1;
ORCID: 0000-0002-2681-9378;
eLibrary SPIN: 3306-1387;
e-mail: BlokhinIA@zdrav.mos.ru

Коденко Мария Романовна;
ORCID: 0000-0002-0166-3768;
eLibrary SPIN: 5789-0319;
e-mail: KodenkoMR@zdrav.mos.ru

Шумская Юлия Федоровна;
ORCID: 0000-0002-8521-4045;
eLibrary SPIN: 3164-5518;
e-mail: ShumskayaYF@zdrav.mos.ru

Гончар Анна Павловна;
ORCID: 0000-0001-5161-6540;
eLibrary SPIN: 3513-9531;
e-mail: GoncharAP@zdrav.mos.ru

Решетников Роман Владимирович, к.ф.-м.н.;
ORCID: 0000-0002-9661-0254;
eLibrary SPIN: 8592-0558;
e-mail: r.reshetnikov@gmail.com

* Corresponding author / Автор, ответственный за переписку